ADVANCES IN THE FLUORINE CHEMISTRY OF TRANSITION METALS AND N-HETEROCYCLIC CARBENES: UNDERSTANDING PERFLUOROALKYL AND FLUOROALKENE REACTIVITY

by

Matthew Leclerc

Thesis submitted to the

Faculty of Graduate & Postdoctoral Studies

University of Ottawa

in partial fulfillment of the requirements for the

Doctor of Philosophy

Ottawa-Carleton Chemistry Institute

Faculty of Science

University of Ottawa

Abstract

The importance of fluorine in a wide array of different areas within chemistry and biochemistry has been demonstrated time and time again. Fluorine-containing products range from essential substituents in pharmaceuticals and relatively long-lived tracers for PET imagining, to fluoropolymers with outstanding properties, to essential components in most of the strongest acids available to chemists today. Fluorine's extreme electronegativity makes it a truly unique element, but its acute toxicity in its elemental F_2 form makes it difficult to handle, prompting researchers to explore different options for incorporating this important element into a variety of different molecular scaffolds.

Due to the remarkable thermodynamic and kinetic stabilities of C-F bonds, methods for forming and breaking these cleanly, and under relatively mild conditions, are in high demand. Fortunately, transition metals have greatly aided in this process. However, fluoroorganometallic chemistry is much less developed than transition metal chemistry involving hydrocarbons, and certainly less understood. One of the primary reasons for this relative dearth of fluoroorganometallic complexes is the difficulty associated with their synthesis. In this work, important steps towards perfluoroalkyl chain-growth within the coordination sphere of a transition metal will be presented, stemming in part from the synthesis and characterization of novel cobalt fluoride and bis(perfluoroalkyl) complexes.

As important electrophiles, fluoroalkenes have primarily been used as monomers for the formation of important fluoropolymers. However, their direct reactivity with organics remains rare and is usually difficult to control, with limited substrate scopes. Herein, the formation of stable N-heterocyclic fluoroalkene adducts as versatile synthons for the incorporation of fluoroalkene fragments into various chemical environments will be introduced. By forming these adducts, the inconvenience of manipulating fluorinated gases in further reactions can be avoided, and the N-heterocyclic fragment is shown to aid in directing substitutions involving polyfluoroalkenyl imidazolium salts and organic nucleophiles to form a variety of C-E (E = C, N, O, S) and C-M bonds (M = Mn, Mo).

The ease with which C-F bonds are manipulated in these systems is quite remarkable, as the substitution reactions occur cleanly and efficiently at room temperature, to form a variety of new bonds without the need for a transition metal. By expanding on the fundamental reactivity between N-heterocyclic carbenes and fluoroalkenes, attempts were made to correlate the observed reactivity with certain electronic and steric parameters unique to the utilized carbenes. Although a correlation has not yet been established, the effects of atypical steric constraints in a cyclic (alkyl)(amino)carbene were demonstrated, wherein the initial point of attack by the carbene on the fluoroalkene was modified. It is hoped that this work will eventually lead to new roles for organocatalysts in fluoroalkene transformations.

Acknowledgements

The entirety of the work presented in this thesis, but more importantly everything that will remain buried in lab books and never be published, would simply not have been possible without the incredible guidance and support of my supervisor Professor R. Tom Baker. It can be quite difficult to remain motivated during the natural ups and downs of a PhD, but his constant excitement and genuine desire to understand how and why chemistry does what it does is quite simply astonishing. He taught me to never be satisfied simply by the result, but to be curious about the process. He is an incredible scientist, as well as an inspiring person, and I am very grateful to have had the privilege to be one of his students. Baker, thank you for everything, and for always making time.

To Graham and Daniels, sharing lab space with you both has been quite the experience. I can't imagine getting to this point without having been able to discuss chemistry and non-chemistry related things with you. You've helped me maintain my sanity throughout this process. Daniels, I've never seen a human being ingest larger volumes of Diet Coke per day than you do, and that should scare you. To everyone in the Baker Group, past and present (there are simply too many to name), with special mentions to Kaitie, Uttam, Mehdi, Cassandra, Nick and Sicard, you've all contributed to making this lab an exciting place to work, as well as a place to have fun and not take yourselves too seriously. A special thank you to Julia, Yardley and Jason; I could not have been asked to mentor better students, you were all incredible to work with, and I sincerely thank you for all your hard work. Dan, your work ethic and incredible talent as a chemist and a mentor have influenced me more than you could know, thank you for everything.

During my tenure at the University of Ottawa, I have had the immense pleasure of working with incredibly dedicated and important people. All the X-ray crystallography presented in this work was performed by Ilia and Bulat, whose anxiously awaited e-mails were either the highlights of my day, or my cue to go home and question my motives for doing a PhD. All forms of mass spectrometry were performed by Yardley and Sharon, quite often with the promise of fascinating headaches. All the weird

and unconventional NMR experiments were made possible by Glenn and Eric, without whom many of the secrets of this technique would still be foreign to me.

To friends I've made in grad school, including Jen, Katie, Gabe and Nathan, as well as those I've known since undergrad and continue to cherish, here's looking at you Bianca, Mr. Tom and Michel, thank you all for your support. A special thank you to Brad & Ranjita, who have nothing to do with chemistry, but are simply incredible in every way. To Ken, Deb and Sheri, as well as my entire family, thank you for your endless generosity and for constantly reminding me of how much more there is to life than grad school.

À mes parents, il n'y a rien à dire sauf merci. Merci de m'avoir déménagé, merci de m'avoir supporté sans cesse et sans hésitation, merci de toujours avoir répondu au téléphone, merci de m'avoir écouté et de ne jamais m'avoir laissé lâcher, merci d'être venu me voir, merci pour votre sourire et merci de toujours comprendre.

To Solls, you have brought the most unexpected joy and excitement to my life, and you've been a trooper throughout the late nights and the long weekends. Thank you for hanging in there.

Becky, you are quite simply everything.

Table of Contents

List of Figures

List of Schemes

List of Tables

List of Abbreviations

6-Mes	1,3-bis-(2,4,6-trimethylphenyl)hexahydropyrimidin-2-ylidene
7-Mes	1,3-bis-(2,4,6-trimethylphenyl)hexahydro-1*H*-diazepin-2-ylidene
[^{18}F]FDG	2-[^{18}F]fluoro-2-deoxyglucose
BDE	bond dissociation energy
BTB	1,3-bis(trifluoromethyl)benzene
CAAC	cyclic (alkyl)(amino)carbene
CFC	chlorofluorocarbon
$(CO)_2$SIMes	4,5-dioxo-1,3-bis-(2,4,6-trimethylphenyl)imidazolidin-2-ylidene
Cp	cyclopentadienyl
DBU	1,8-diazabicyclo[5.4.0]undec-7-ene
DCE	1,2-dichloroethane
DCM	dichloromethane
DEE	diethyl ether
DFT	density functional theory
Dipp	2,6-diisopropylphenyl
DMAP	4-dimethylaminopyridine
DMF	dimethylformamide
DMSO	dimethyl sulfoxide
EA	elemental analysis
ESI-MS	electrospray ionization mass spectrometry
ESP	electrostatic potential
FT-IR	Fourier transform infrared spectroscopy
FW	formula weight
GIAO	gauge-independent atomic orbital

HCFC	hydrochlorofluorocarbon
HFA	hydrofluoroalkene
HFC	hydrofluorocarbon
HFP	hexafluoropropene
HTFE	trifluoroethylene
HOESY	heteronuclear Overhauser effect spectroscopy
HOMO	highest occupied molecular orbital
IAd	1,3-bis(adamantyl)imidazol-2-ylidene
ICy	1,3-bis(cyclohexyl)imidazol-2-ylidene
I^iPr	1,3-bis(isopropyl)imidazol-2-ylidene
IMe_4	1,3,4,5-tetramethylimidazol-2-ylidene
IMes	1,3-bis(2,4,6-trimethylphenyl)imidazol-2-ylidene
IPr	1,3-bis(2,6-diisopropylphenyl)imidazol-2-ylidene
IR	infrared
I^tBu	1,3-bis(*tert*-butyl)imidazol-2-ylidene
KHMDS	potassium bis(trimethylsilyl)amide
LDA	lithium diisopropylamide
LLCT	ligand-to-ligand charge transfer
LMCT	ligand-to-metal charger transfer
LUMO	lowest unoccupied molecular orbital
Me_2Dipp(CAAC)	1-[2,6-bis(diisopropylphenyl)]-3,3,5,5-tetramethyl-2-pyrrolidinylidene
Me_2ThiaDipp	3-(2,6-diisopropylphenyl)thiazol-2-ylidene
Mes	2,4,6-trimethylphenyl
MLCT	metal-to-ligand charge transfer
MO	molecular orbital

mp	melting point
MPA	Mulliken population analysis
MS	mass spectrometry
NaHMDS	sodium bis(trimethylsilyl)amide
NFSI	*N*-fluorobenzenesulfonimide
NHC	N-heterocyclic carbene
NHCA	N-heterocyclic alkene
NMR	nuclear magnetic resonance
NOESY	nuclear Overhauser effect spectroscopy
PCTFE	polychlorotrifluoroethylene
PET	positron emission tomography
PFOA	perfluorooctanoic acid
PTFE	polytetrafluoroethylene
PXRD	powder X-ray diffraction
R^F	perfluoroalkyl
Selectfluor	1-chloromethyl-4-fluoro-1,4-diazoniabicyclo[2.2.2]octane bis(tetrafluoroborate)
SIMes	1,3-bis(2,4,6-trimethylphenyl)imidazolidin-2-ylidene
SIPr	1,3-bis(2,6-diisopropylphenyl)imidazolidin-2-ylidene
TCNE	tetracyanoethylene
TD-DFT	time-dependent density functional theory
TEP	Tolman electronic parameter
TFE	tetrafluoroethylene
THF	tetrahydrofuran
TMS	trimethylsilyl
ToF	time of flight

UV	ultraviolet
VDF	vinylidene fluoride
$\%V_{bur}$	percent buried volume

Published Contributions

(6) **Leclerc, M. C.**; Da Gama, J. G.; Gabidullin, B. M.; Baker, R. T. *J. Fluorine Chem.* **2017**, doi: 10.1016/j.jfluchem.2017.05.012.

(5) **Leclerc, M. C.**; Gabidullin, B. M.; Da Gama, J. G.; Daifuku, S. L.; Iannuzzi, T. E.; Neidig, M. L.; Baker, R. T. *Organometallics* **2017**, *36*, 849-857.

(4) **Leclerc, M. C.**; Gorelsky, S. I.; Gabidullin, B. M.; Korobkov, I.; Baker, R. T. *Chem. Eur. J.* **2016**, *22,* 8063-8067.

(3) **Leclerc, M. C.**; Bayne, J. M.; Lee, G. M.; Gorelsky, S. I.; Vasiliu, M.; Korobkov, I.; Harrison, D. J.; Dixon, D. A.; Baker, R. T. *J. Am. Chem. Soc.* **2015**, *137*, 16064-16073.

(2) Fuller, J. T.; Harrison, D. J.; **Leclerc, M. C.**; Baker, R. T.; Ess, D. H.; Hughes, R. P. *Organometallics* **2015**, *34*, 5210-5213.

(1) Harrison, D. J.; Lee, G. M.; **Leclerc, M. C.**; Korobkov, I.; Baker, R. T. *J. Am. Chem. Soc.* **2013**, *135*, 18296-18299.

Chapter 1

Introduction

1.1 Fluorine

As the most electronegative element in the periodic table, fluorine has long fascinated chemists for its ability to impart unique and desirable properties to molecules and materials. Fluorinated molecules are known to exhibit enhanced chemical and thermal stabilities,[1] and pharmaceuticals containing fluorine have demonstrated increased lipophilicity and delayed metabolism.[2,3] As a potential bioisostere for hydrogen, replacing even a single hydrogen by a fluorine atom can introduce desirable properties to target compounds, while maintaining the overall topology and molecular structure of the initial molecule. In fact, approximately 20% of all commercialized pharmaceutical compounds contain at least one fluorine atom, including several of the highest-selling products on the market (Figure 1.1).[4–6]

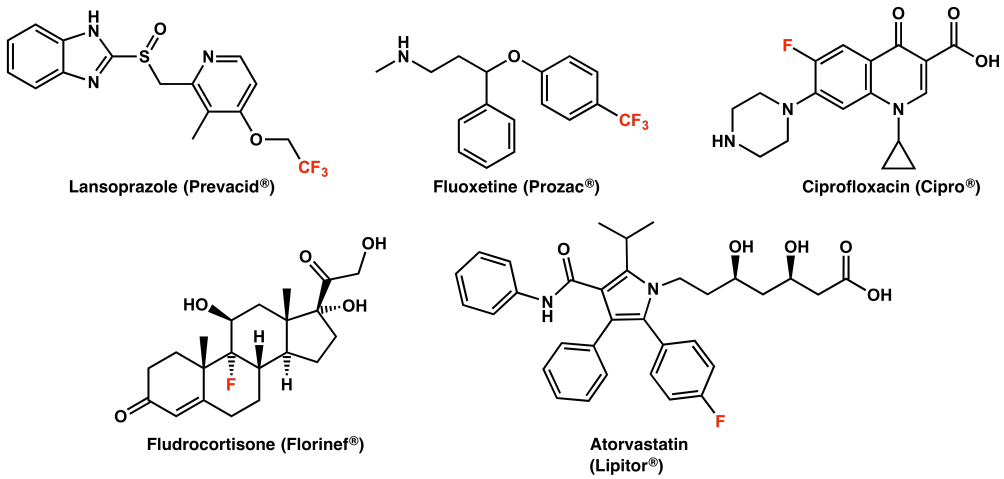

Figure 1.1. Important pharmaceutical compounds containing at least one fluorine atom.

Fluorine exhibits a marked inductive effect when incorporated into a molecule, and this becomes especially important when multiple fluorine atoms are involved. This effect becomes evident when comparisons to hydrocarbon analogues are made, such as examples involving acids.[7] The ability of the fluorine substituents in trifluoroacetic acid to stabilize the negative charge present in the conjugate base renders this acid approximately 34,000 times stronger than normal acetic acid. Many important Lewis acids, such as BF_3 and Me_3SiOTf (OTf = SO_3CF_3), and a significant number of known superacids, such as H_2FSbF_6, contain one or more fluorine atoms.[8] Due to the extremely reactive and oxidative nature of F_2, fluorine's elemental state, compounds of fluorine are known for every element in the periodic table except for helium and neon. Except in very rare instances, fluorine always adopts an oxidation state of -1 when forming compounds with various elements. Many elements, including a variety of transition metals, have been isolated and characterized in their highest known oxidation states only when forming fluoride compounds.[9]

1.1.1 Difficulties in manipulating C-F bonds

There are very few naturally occurring compounds containing C-F bonds,[10] and as invaluable targets they must thus be synthesized. The most important source of fluorine on our planet is fluorite, CaF_2, and it is from this mineral that almost all HF is prepared, either as a gas or as hydrofluoric acid when dissolved in water.[11,12] Almost every fluorine-containing compound or material available to chemists is directly or indirectly produced from this mildly acidic, but highly corrosive and toxic reagent.[13] Although synthetically useful, safety and selectivity concerns during reactivity have prompted a push towards mild and easy to handle alternatives. The formation and manipulation[14] of C-F bonds, however, are rendered difficult owing to their large

thermodynamic and kinetic stabilities.[7,15] Fluorine forms the strongest single bond to carbon of any other element, in part due to the significant ionic character present in the bond, as a result of fluorine's extreme electronegativity. The presence of increasing numbers of fluorine atoms on the same carbon leads to even shorter (and stronger) bonds. As such, the bond dissociation energy (BDE) of a C-F bond can be as large as ~545 kJ/mol,[7] and polymers or materials containing a large number of these bonds often exhibit exceptional thermal stability, as well as significant resistance towards decomposition by various solvents.[16,17] Fluorine also exhibits low polarizability, being a small atom with significant charge density, and this further contributes to the stability of its compounds. Due to these factors, forming and breaking C-F bonds is quite challenging, and harsh conditions are often required, sometimes leading to issues with regards to selectivity and to the use of inconvenient reagents, such as HF. In trying to move away from these limiting reaction conditions and in attempting to expand on the available substrate scope for the introduction of fluorine into molecular systems, researchers have taken advantage of the various oxidation states that transition metals can access, and their ability to mediate bond-forming and bond-breaking reactions, in order to develop catalytic systems involving fluorine and fluorinated substrates.

1.2 Fluoroorganometallic chemistry

Transition metals have been used to facilitate a wide array of difficult transformations, and, in many cases, have enabled reactions to be performed that were previously thought to simply be inaccessible. These include reactions such as, but not limited to: hydrogenation and dehydrogenation, isomerization, polymerization, cross-coupling, cross-metathesis, reduction and oxidation, as well as hydroformylation.[18–20] This barely scratches the surface of what transition

metals have allowed researchers to perform, and to say that the development of transition metal catalysis over the last century has revolutionized the way we produce fine chemicals and materials would be an incredible understatement. Truly, almost every industrial chemical process utilizes a metal catalyst, if not several, throughout the course of production. The formation of plastics and many other everyday items would simply not be feasible on their current production scales without the key role catalysis plays in these processes.[21]

Similarly, fluorine chemistry has been aided tremendously using transition metals, whether in stoichiometric, or ideally in catalytic reactions.[22] These reactions include the introduction of various fluorinated groups, such as fluorine, fluoromethyl, difluoromethyl, trifluoromethyl, and perfluoroalkyls into organic molecules, as well as the production of trifluoromethyl ethers, sulfides and amines.[23–27] In these transformations, sp^3 and sp^2 carbon centers have been activated, including olefins, epoxides and aryl groups. In a few instances, direct C-H bond activation has even been demonstrated.[28–31] Although significant advances have been made over the last several years with regards to fluoroorganometallic chemistry, this field is not nearly as developed, and certainly not as well understood, as typical organometallic chemistry involving hydrocarbons.

1.2.1 Metal fluoride and perfluoroalkyl complexes

There are countless examples of transition metal fluorides, with each metal in a variety of different geometries, oxidation states, and phases.[32] The simplest method for synthesizing the large majority of binary metal fluorides, i.e., complexes that contain only the metal and various fluoride ligands, remains the direct oxidation of the metal of choice with pure fluorine gas, where variations in the temperatures and pressures enable the isolation of different complexes.

Alternatively, if the hexafluoride of a metal can be obtained, step-wise reduction of the complex can lead to the lower metal fluorides.[9] When aiming to introduce a fluoride ligand into a metal complex that features a more elaborate ligand environment, however, fluorine gas ceases to be a very effective technique due to its incredible oxidation potential. Typically, a much gentler method such as halide metathesis will be utilized. As a ligand, fluoride behaves similarly to the other halides, but the M-F bond demonstrates much more pronounced ionic character, and these bonds can be much stronger than with other halides. Typically, this leads to complexes exhibiting enhanced thermal and chemical stabilities, and in many cases a significant increase in the volatility of these complexes has been observed. [33]

Similarly, the challenges associated with the study of transition metal perfluoroalkyls are primarily based on difficulties relating to their synthesis. A wide array of examples has been presented and discussed in detail, however, methods that have proven effective for the synthesis of analogous hydrocarbon complexes often fail when attempting to obtain the fluorinated variants.[34,35] Although there are now several methods by which these types of species can be synthesized, issues with the generality of these transformations are still problematic. Due to the strength of C-F and C-C bonds in perfluoroalkyls, these do not typically undergo oxidative addition when exposed to transition metals.[34] As such, alternative and sometimes roundabout methods are routinely employed and will be discussed briefly.

The first trifluoromethyl transition metal complex, wherein the CF_3 is bound directly to the metal, was isolated by Stone *et al*. via decarbonylation of the trifluoromethyl acyl substituent in $(OC)_5Mn(C(O)(CF_3)$ to afford $(OC)_5MnCF_3$.[36] Since then, a large variety of perfluoroalkyl complexes have been characterized, and this decarbonylation method has provided a useful route towards many of these systems.[37,38] Unfortunately, this method provides some limitations as not

all complexes can accommodate a trifluoromethyl acyl ligand, and some are unable to promote the decarbonylation reaction.

A very important class of precursors, perfluoroalkyl iodides, was thus explored as a more direct route to these types of complexes.[39] These have been shown to be capable of C-I bond oxidative addition, most commonly with low-valent d^8 and d^{10} metals, to form [M](R^F)(I) complexes.[40,41] Many perfluoroalkyl groups are known to possess similar properties to halogens and can often exhibit similar reactivity, such that a molecule like CF_3CF_2I can be compared to I_2, for example. This is well represented in early studies with perfluoroalkyl iodides, wherein metals that were known to undergo oxidative addition with I_2 were shown to be capable of the same transformations with perfluoroalkyl iodides. Once a complex of the type M(R^F)(I) is obtained, the relative lability of the iodide ligand allows for further transformations and some degree of freedom.

Also noteworthy is the use of group 12 elements (Zn,[42–45] Cd[43,44,46,47] and Hg[48–50]) as effective perfluoroalkyl transfers agents from their M(R^F)$_2$ complexes, allowing for the isolation of many novel main-group and transition metal perfluoroalkyls. Finally, silicon-based reagents have been used extensively to transfer fluorinated groups to organic molecules, and to transition metals.[51–53] The driving force of these reactions is almost always the formation of the strongest single bond between two elements in chemistry, namely the Si-F bond (~582 kJ/mol).[54] The Ruppert-Prakash reagent, Me_3SiCF_3, is the most widely used of these reagents, capable of transferring CF_3 when exposed to a fluoride source, which leads to the formation of Me_3SiF.[53]

Transition metal fluorides and perfluoroalkyls have been used to fluorinate various molecules and systems via nucleophilic, electrophilic and radical methods. The introduction of fluorinated substituents into organic molecules is an extensive area of research and has been

covered in detail elsewhere.[23–27,55,56] Although these transformations are very important, they are beyond the direct scope of this work and will only be introduced briefly. The reactivity of nucleophilic F^- with electrophilic carbon groups in organic molecules is conceptually simple, but issues with solubility and the significant reduction of nucleophilicity caused by strong hydrogen bonding in certain systems can hinder the reactivity.[27] Transition metals have helped with these issues, in some cases by enhancing the solubility of these species, and in others by offering control and selectivity over the fluorination sites. Due to the significant electronegativity of the fluorine atom, it is counter-intuitive to ponder its reactivity with carbon-based nucleophiles, termed electrophilic fluorination. Nonetheless, this reactivity has been successfully exploited and is in large part possible due to the development of stable, easy-to-handle reagents capable of formally transferring F^+ to organic substrates.[57] The oxidizing potential of electrophilic fluorinating sources is important to consider when developing these molecules, due to the functional group restrictions that can be imposed. For example, xenon difluoride (XeF_2) is a potent electrophilic fluorinating agent, but its uses are limited by its tendency to oxidize several functional groups.[58] As such, researchers have focused on the development of selective, mildly oxidizing reagents. Commonly, these contain N-F bonds, and special focus is placed on removing electron density from nitrogen by introducing adjacent electron withdrawing groups.[57] In doing so, fluorine will donate some of its electrons to nitrogen and become susceptible to nucleophilic attack. Two of the most widely used compounds for these transformations are commercially available *N*-fluorobenzenesulfonimide (NFSI)[59] and 1-chloromethyl-4-fluoro-1,4-diazoniabicyclo[2.2.2]octane bis(tetrafluoroborate) (Selectfluor)[60] (Figure 1.2).

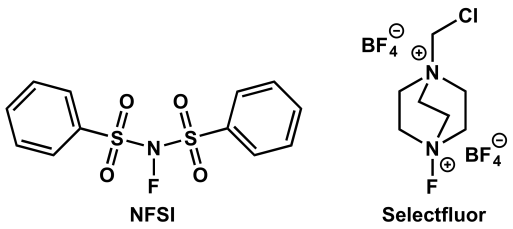

Figure 1.2. Two commercially available electrophilic fluorinating agents, available as stable and easy-to-handle solids.

Late-stage fluorination has also attracted significant interest from researchers, especially within the context of positron emission tomography (PET) imaging.[61] Of fluorine's radioisotopes, fluorine-18 (^{18}F) has the most stable half-life (109.77 minutes), and is a significant source of positrons, which makes it very appealing for use in this technique. In fact, ^{18}F is the most commonly used isotope for PET imaging, with the majority of scans using the 2-[^{18}F]fluoro-2-deoxyglucose ([^{18}F]FDG) tracer. However, methods for the introduction of ^{18}F into the appropriate radiotracer must be efficient and selective, due to the necessity of producing ^{18}F in a cyclotron and the time constraints that must be taken into consideration throughout the entire process.[27]

1.2.2 Difficulties associated with metal catalyzed metathesis and polymerization of fluoroalkenes

Transition metals have afforded unparalleled control and selectivity over the formation of hydrocarbon polymers, allowing researchers to produce materials with precise tacticities and molecular weights. Unfortunately, the polymerization of fluoroalkenes has not yet been achieved within the coordination sphere of a transition metal. The generally accepted pathway for transition-metal catalyzed alkene polymerization, the Cossee-Arlman mechanism,[62–67] is not

feasible for systems involving fluoroalkenes.[68] Specifically, the strength of [M]-R^F (R^F = perfluoroalkyl) bonds renders the insertion of a perfluoroalkyl into a fluoroalkene very difficult on a transition metal (Figure 1.3).

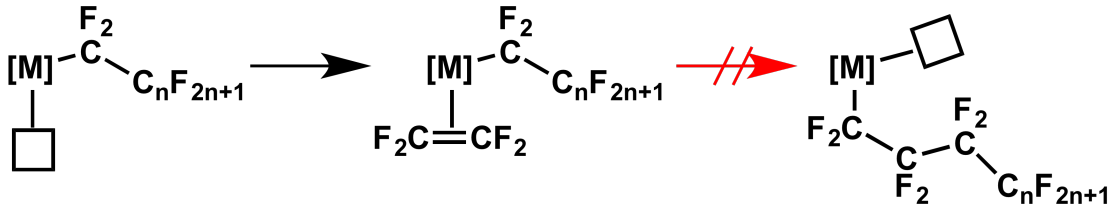

Figure 1.3. Schematic representation of the Cossee-Arlman mechanism. In perfluorinated systems, the problematic step is represented by the red dashed arrow.

Our group has recently proposed a fluoro-variant of the Green-Rooney mechanism as a potential pathway towards the polymerization of fluoroalkenes mediated by a transition metal.[69] This route was once put forth as the potential operating pathway in the polymerization of regular alkenes, but was ultimately disproved in an elegant study by Grubbs and coworkers.[67] However, this method may still prove valuable for fluoroalkenes, as it avoids the problematic insertion step of a perfluoroalkyl into a fluoroalkene (Figure 1.4). Starting with a transition metal fluorocarbene complex, [M](=CF(R^F)) (M = transition metal, R^F = perfluoroalkyl), a [2+2] cycloaddition could lead to a perfluorometallacyclobutane complex, [M](κ^2-CF(R^F)CF_2CF_2-), which could undergo a retro [2+2] cycloaddition and provide metathesis products. Alternatively, a 1,3-F shift would form a new fluorocarbene complex, capable of an additional cycloaddition reaction with a fluoroalkene and leading to chain growth.

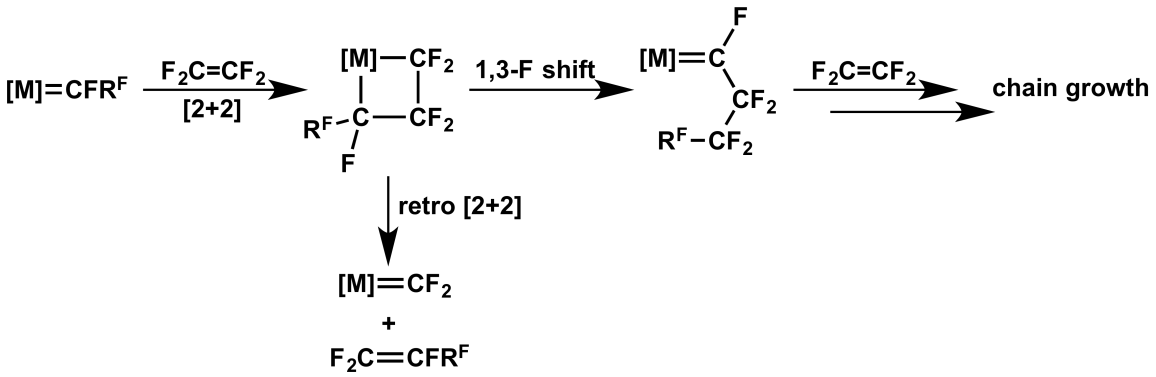

Figure 1.4. Proposed fluoro-variant of the Green-Rooney mechanism for the potential metathesis or polymerization of fluoroalkenes.

Importantly, this proposed pathway requires the synthesis of terminal *nucleophilic* transition metal fluorocarbene complexes, in order to react with *electrophilic* fluoroalkenes. Isolated and stable examples of fluorocarbene complexes are still very limited (see Section 1.2.3). Carbene ligands have the potential to be viewed as either singlet or triplet state species (Figure 1.5), and this has a significant impact on their binding modes to metals, as well as their reactivity.[70]

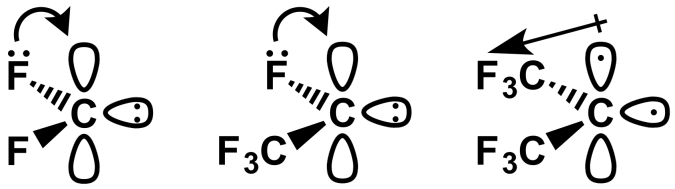

Figure 1.5. Fischer-type singlet fluorocarbenes focused on within this work (left and middle) and an example of a Schrock-type triplet fluorocarbene (right).

Singlet state carbenes, often termed Fischer carbenes[71,72] when bound to metals, are neutral two-electron donors, which bond to metals via σ-type donation from the carbene lone pair into an empty d-orbital on the metal. Additionally, π-backbonding from the metal into the empty p-orbital on the carbene can help stabilize the interaction. The singlet state is often stabilized by

the presence of π-donor groups on the carbon center, which can help fill the empty carbene p-orbital. Fischer carbenes do not affect the oxidation state of the metal, and are often observed on middle to late transition metals with lower oxidation states. Conversely, triplet carbenes, often termed Schrock carbenes[73] or alkylidenes when bound to metals, are ionic two-electron donors and will increase the oxidation state of the metal by +2 upon bonding. Schrock carbenes are often observed on early transition metals with high oxidation states. This type of carbene is commonly stabilized by the presence of electron withdrawing groups on the carbon center, which can interact with the unpaired electron in the half-filled carbene p-orbital.

1.2.3 Metal fluorocarbene complexes

There are relatively few examples of stable transition metal terminal fluorocarbene complexes,[68,74] such that it appears warranted to try and present them all here and briefly discuss their common structural and chemical characteristics. A thorough overview of metal fluorocarbene complexes reported in the literature is presented in Figure 1.6. Typically, metal perfluoroalkyl complexes act as precursors to perfluorocarbenes. By taking advantage of the activated fluorine atoms present on a carbon bound directly to a transition metal,[34,75] fluoride abstraction by a Lewis acid or reduction reactions have provided most of the fluorocarbene complexes in the literature.

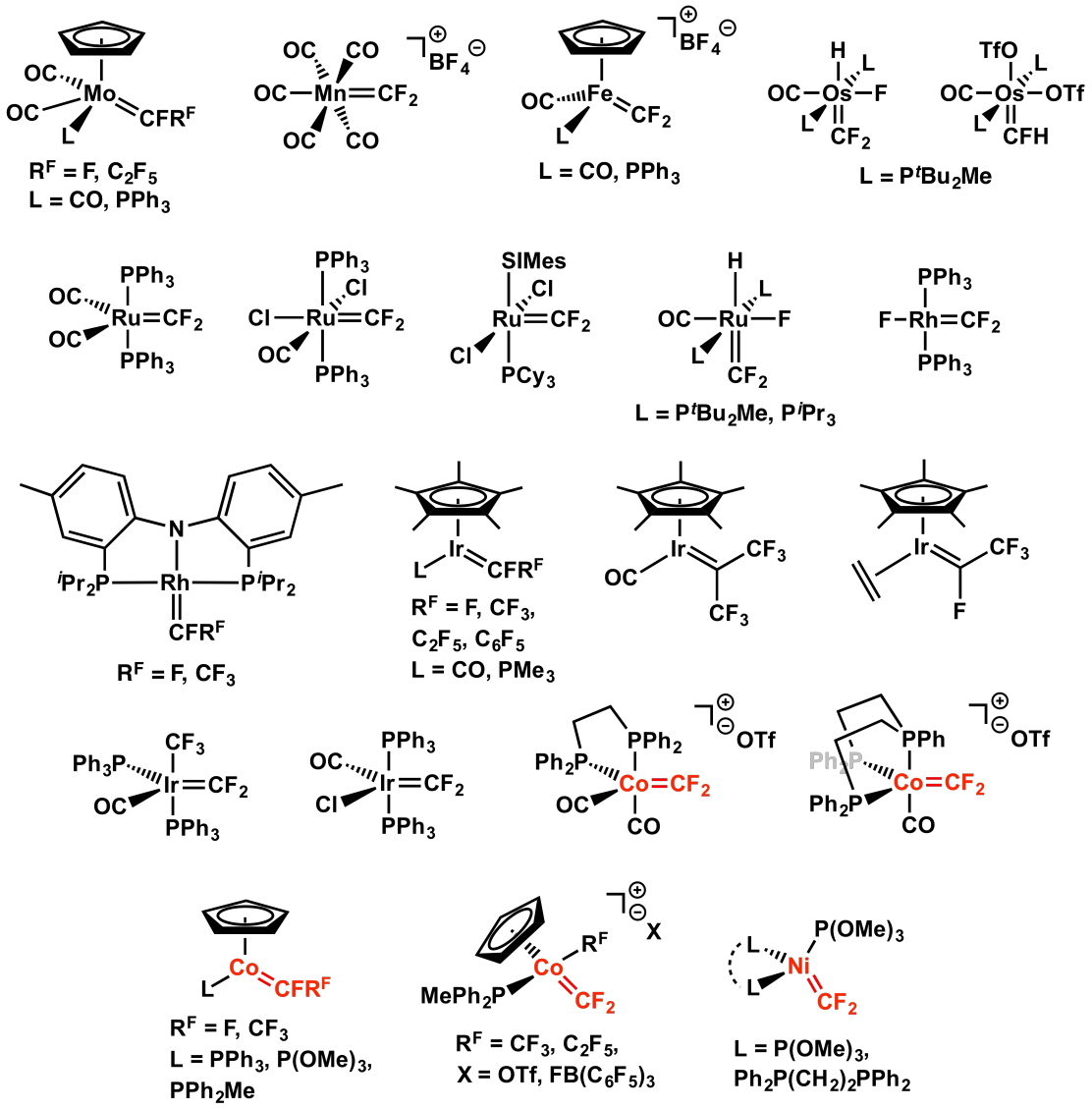

Figure 1.6. Overview of isolated terminal metal fluorocarbenes reported in the literature. Examples from our group are shown in red.

To date, examples featuring Mo,[76,77] Mn,[78] Fe,[79–81] Ru,[82–85] Os,[82] Ir,[86–89] Rh,[90,91] have emerged, and our group has been responsible for the first examples featuring Co[92–96] and Ni.[97] It is noteworthy that the majority of these complexes feature the metal in its +1 oxidation state, with a few examples of the metal in its +2 oxidation state, and both a Ru and a Co example in their

neutral oxidation state. The only example of a metal in the +3 oxidation state bearing a fluorocarbene ligand was reported by our group for a Co complex,[95] but these species quickly reacted by way of an insertion reaction with the remaining perfluoroalkyl fragment on cobalt, which is discussed at length in Chapter 2. Fischer carbenes are known to often exhibit electrophilic character at carbon, and fluorocarbenes can be very sensitive to moisture, affording two equivalents of HF and transforming the fluorocarbene ligand into a carbonyl. This reactivity is very well known, and is observed with a large amount of reported transition metal fluorocarbene complexes,[74,76,77,81,98] while only a few examples demonstrate a resistance to hydrolysis, and at least some degree of nucleophilic character. Specifically, the group 9 metals have demonstrated this when in their formal d^8 states, such as has been observed with Co(I),[92–94,96] Rh(I)[90,91] and half-sandwich Ir(I)[87,88,88,89] systems. A similar trend has been observed for the only stable group 10 fluorocarbenes isolated to date, featuring d^{10} complexes of Ni(0).[97] For the group 8 metals, the nucleophilic nature of a d^8 fluorocarbene complex of Ru(0) has also been reported.[83] Finally, a unique d^6 example with Ru(II), formed by cross-metathesis of vinylidene fluoride with Grubbs' 2nd generation catalyst, was reported.[85] Although the nucleophilic nature of this fluorocarbene complex was not explicitly demonstrated, the product was worked up in air using column chromatography, a process that would lead to facile hydrolysis of the fluorocarbene if it were susceptible to this type of transformation.

1.2.4 Cobalt fluorocarbene complexes and their reactivity with tetrafluoroethylene

---

The work presented in this section has been published:

(2) Fuller, J. T.; Harrison, D. J.; **Leclerc, M. C.**; Baker, R. T.; Ess, D. H.; Hughes, R. P. *Organometallics* **2015**, *34*, 5210-5213.

(1) Harrison, D. J.; Lee, G. M.; **Leclerc, M. C.**; Korobkov, I.; Baker, R. T. *J. Am. Chem. Soc.* **2013**, *135*, 18296-18299.

The first examples of stable terminal cobalt fluorocarbene complexes were synthesized and fully characterized by our group,[92] and their nucleophilic character was demonstrated by their reactivity with $LutH^+Br^-$ (Lut = 2,6-lutidine), wherein the H^+ was found to end up on the carbene carbon and the Br^- on the metal. Additional support stems from the lack of reactivity these complexes exhibit with 20 equiv. of water in acetonitrile.

With these nucleophilic fluorocarbene complexes in hand, we theorized that they might be active towards electron deficient tetrafluoroethylene (TFE). Indeed, when complexes featuring PPh_2Me as a ligand were exposed to TFE in various solvents and allowed to react under pressure over several days, a clean transformation arising from formal [2+2] cycloaddition between the fluorocarbene and the fluoroalkene was observed (Scheme 1.1).[94] The complexes are thermally stable and represent the first example of this type of cycloaddition with a metal fluorocarbene in the literature, and the resulting perfluorometallacyclobutane complex is one of only five known examples of its kind, three of which are derivatives of the same system. An Fe-based perfluorometallacyclobutane complex was formed by Karel *et al.*[99] via successive decarbonylation of a bis(acyl) complex, and a recent report by Vicic *et al.*[100] introduces three novel Pt-based perfluorometallacyclobutane complexes.

Scheme 1.1. Reactivity of cobalt fluorocarbene complexes in a [2+2] cycloaddition fashion with TFE and subsequent reactivity of the perfluorometallacyclobutane products

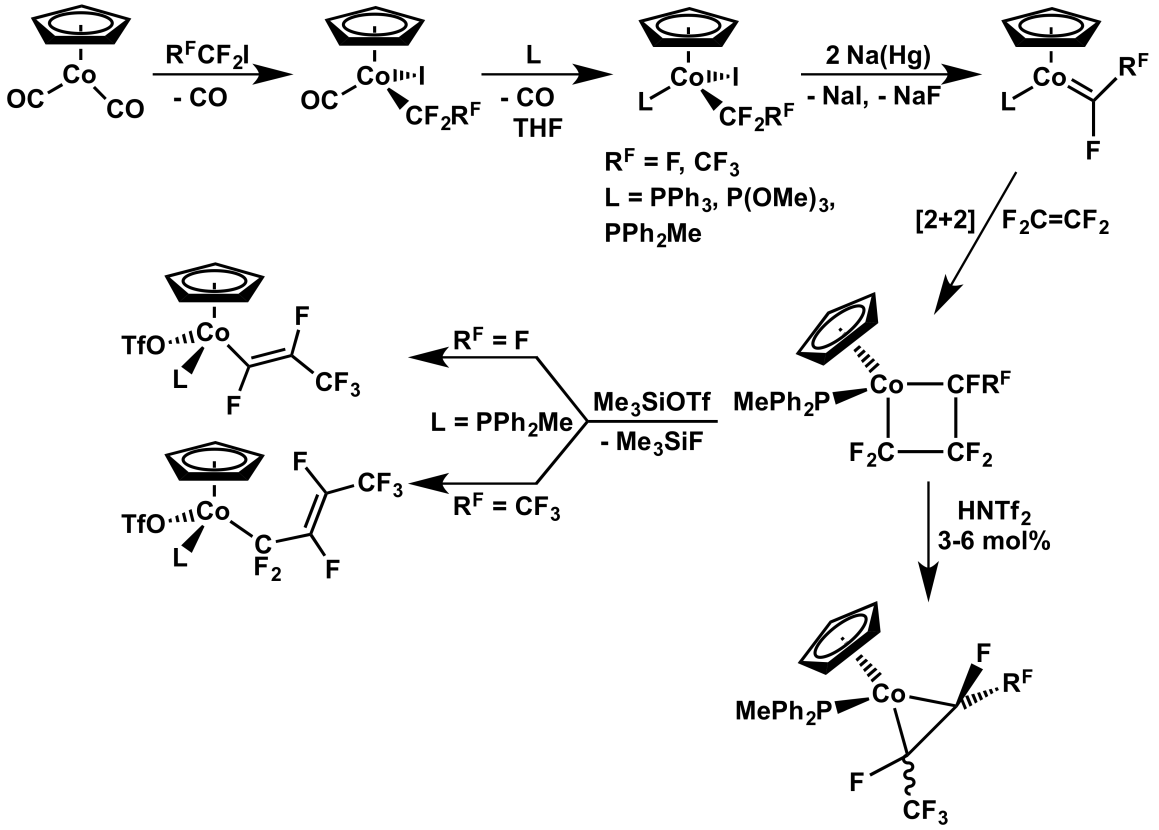

The cobalt perfluorometallacyclobutane complexes were shown to further react with catalytic amounts of $HNTf_2$, a Brønsted acid, to afford clean isomerization/ring-contraction products. When treated with Me_3SiOTf, a Lewis acid, abstraction of a fluoride led to the corresponding perfluoro-*trans*-vinyl and perfluoro-*trans*-allyl complexes. When the perfluorometallacycle was allowed to react with $[HPPh_2Me][NTf_2]$, a β-phosphonium-substituted metallacycle was obtained, shedding insight into the reactivity of this system (Scheme 1.2). The isolation of this complex strongly suggests that the activation of these perfluorometallacycles by fluoride abstraction occurs at the β position of the metallacycle,[101] as opposed to the expected α

position.[68,74,102–104] Typically, fluorines on carbons bound directly to the metal are activated due in part to donation from filled metal d-orbitals into the C-F σ* orbital, weakening that bond.[34,75] There is some precedence for this type of proposed allyl intermediate on Fe, wherein nucleophilic attack by PMe_3 and F^- was demonstrated to occur on an η^3-perfluoroallyl, providing support for the proposed intermediate with Co.[105,106]

Scheme 1.2. Evidence for C_β-F activation in a cobalt perfluorometallacyclobutane

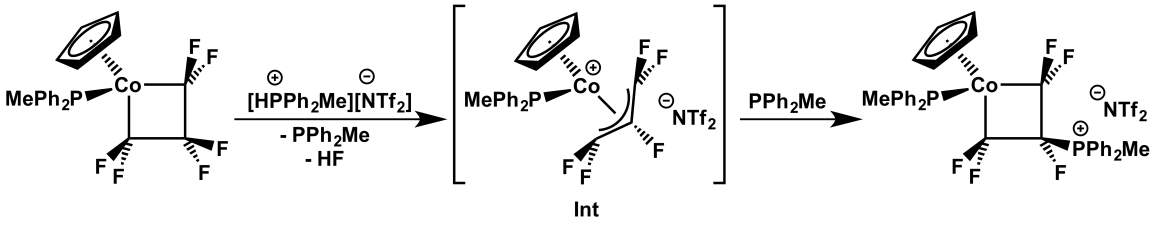

The novelty of the [2+2] cycloaddition reaction between a metal fluorocarbene and TFE was investigated computationally, to provide additional insight into the reaction pathway and probe the feasibility of fluoroalkene metathesis with this system.[107] The results of these studies demonstrated that the [2+2] cycloaddition was likely occurring via a 1,4-singlet diradical intermediate (Scheme 1.3).[108–110] Unfortunately, the stability of the perfluorometallacyclobutanes, resulting in part from the considerable strength of the fluorinated C-C and M-C bonds, especially as compared to the relatively weak C=C bonds in the starting materials, implies that perfluoroalkene metathesis with this system is likely not feasible in its current form. Nonetheless, a very important step was demonstrated and valuable insight was gained, and we hope that this will provide us with the ability to better design a system capable of reversible fluoroalkene addition, perhaps even with another transition metal.

Scheme 1.3. Proposed computed 1,4-singlet diradical reaction pathway for cobalt fluorocarbenes reacting in a [2+2] cycloaddition fashion with TFE

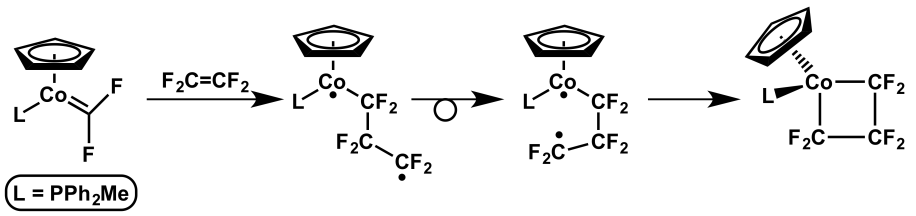

1.3 Fluoroalkenes

Fluoroalkenes are known to react with various types of reagents, but often with little to no selectivity, and in a manner that can sometimes be difficult to predict.[1] Many of the examples demonstrating clean reactivity are not general, and focus on a specific reagent with limitations on both substrate scope and reaction conditions, which impose a lack of variability within this context. However, fluoroalkenes are very important and industrially relevant examples of electron deficient alkenes. Their main uses are as building blocks for very important fluoropolymers[17] and as valuable refrigerants.[111] As such, methods for their manipulation in a selective manner, and the ability to synthesize new fluoroalkenes from existing ones with potentially novel and desirable chemical properties, are desired and actively being explored. Fluorinated materials have long played a key role in refrigeration. Initially, chlorofluorocarbons (CFCs)[112] were heavily utilized as refrigerants, but were eventually phased out for hydrochlorofluorocarbons (HCFCs) and hydrofluorocarbons (HFCs) with rising stratospheric ozone depletion concerns.[111] A newer generation of refrigerants, including hydrofluoroalkenes (HFAs), are actively being developed in hopes of further reducing our emission of species that contribute heavily to global warming.[113]

1.3.1 Fluoropolymers

Since the discovery of the first fluoropolymer, polychlorotrifluoroethylene (PCTFE) in 1934 at IG Farber and the accidental discovery of the first perfluorinated polymer, polytetrafluoroethylene (PTFE, Teflon) in 1938 at DuPont, these high value-added materials now include numerous examples with various exceptional properties.[17,114] Commonly, these include chemical inertness, low friction coefficients, resistance to UV and aging, thermal stability, and both hydro- and lipophobicity, among others.[16,115–118] It is thus somewhat unsurprising that they have been used for a wide variety of applications, which include but are certainly not limited to: coatings for various surfaces (including non-stick cookware), elastomers, seals, membranes, resins, gaskets, lubricants, insulators, etc.[119–125] As such, methods for their production have been studied and developed for several decades. Unfortunately, these still include the use of harmful reagents, such as HF, Cr(VI) species and SbF_5,[17] or environmentally persistent surfactants, such as perfluorooctanoic acid (PFOA).[126] Additionally, the formation of fluoropolymers often proceeds via difficult to control radical pathways.[115] Typically, fluoropolymers are derived from the polymerization of fluoroalkenes, the most common of which are presented in Figure 1.7.

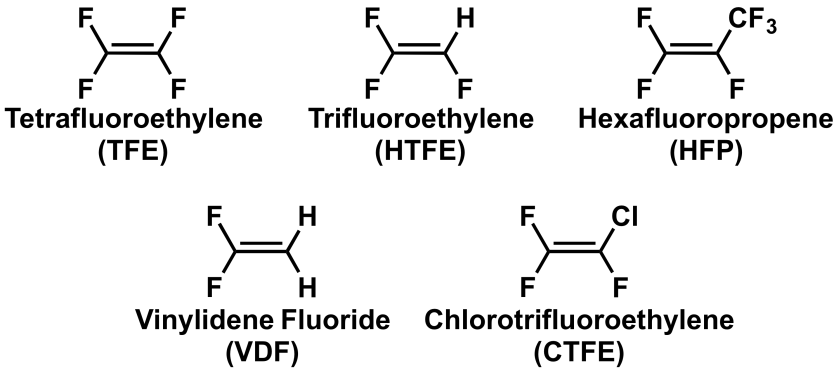

Figure 1.7. Common fluoroalkenes used as building blocks to produce fluoropolymers.

1.3.2 Reactivity of fluoroalkenes with nucleophiles, electrophiles, radicals and dienes

Typically, the attack of a nucleophile on a fluoroalkene will lead to the formation of a carbanion, which must be trapped immediately due to its relatively unstable nature.[127] The presence of fluorine atoms on a carbon β to a carbanion is somewhat stabilizing due to the inductive nature of these substituents, which serves to stabilize the negative charge. However, the anionic species is destabilized if fluorine atoms are directly bound to the carbon bearing the negative charge, due to the repulsion of adjacent electron pairs.[7] As such, these species will often be trapped by electrophiles in the hopes of obtaining stable or easier to manipulate products.[128,129] A representative example featuring the cyanide ion reacting with TFE is illustrated in Scheme 1.4, wherein the carbanion is trapped by CO_2 and again by dimethyl sulfate.[127]

Scheme 1.4. Representative example of reactivity between fluoroalkenes and nucleophiles[127]

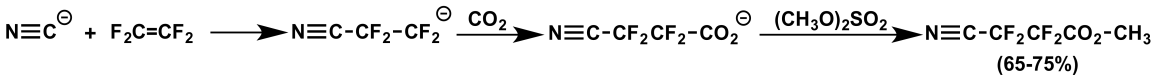

It should be noted that although this is an isolated example, similar reactivity is obtained in most cases, where a nucleophile attacks the electrophilic fluoroalkene and the resulting carbanion is trapped by varying types of electrophiles, such as a proton or a fluoro-ester, among others.[1]

Due to the electrophilic nature of fluoroalkenes, it is somewhat unsurprising that their direct reactivity with other electrophiles is much less developed than their reactivity with nucleophiles. In fact, perfluorinated alkenes are quite resistant to electrophilic attack, but hydro- and chlorofluoroalkenes have demonstrated an appreciable range of reactivity with reagents often viewed as electrophilic in nature.[130] However, these reactions often involve corrosive and dangerous mixtures of HF/HNO_3[131,132] or H_2SO_4/HNO_3,[133] and in some cases, give rise to modest

yields and a mixture of products. Partly due to the harsh conditions necessary to drive these reactions and the poor selectivity often observed, the reactivity of fluoroalkenes with electrophiles is not commonly explored.

The reactivity of fluoroalkenes with radicals is well established,[116,134–136] and the stability of the intermediates formed in these reactions is somewhat analogous to that of fluorinated carbanions.[7] That is, the presence of fluorine atoms on a carbon bearing a radical has a destabilizing effect, whereas fluorines or perfluorinated substituents bound to the carbon β to the radical center will have a stabilizing effect. The radical reactivity of fluoroalkenes can be difficult to control at times, especially if polymerization is not the desired outcome. The tendency of radical species formed in these reactions to react with another equivalent of the fluoroalkene instead of the desired organic fragment can sometimes lead to unwanted by-products, as demonstrated in Scheme 1.5.

Scheme 1.5. Reactivity of fluoroalkenes with radicals, demonstrating the competing role that polymerization can play[137]

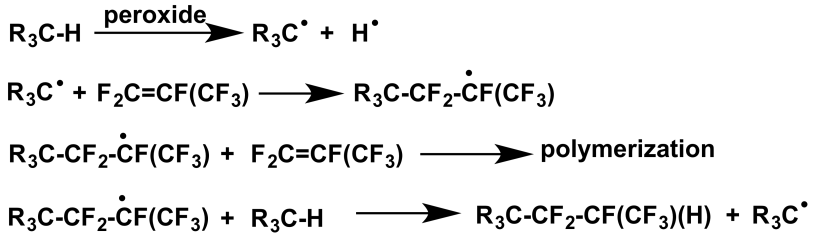

Although this type of reactivity is rare, exotic fluoroalkene dienophiles have been shown to react in Diels-Alder [4+2] cycloaddition-type reactions with dienes.[138–140] Two examples are presented in Scheme 1.6, demonstrating the unique nature of the fluoroalkene starting material in these reactions.

Scheme 1.6. Reactivity of fluoroalkenes with dienes in a Diels-Alder [4+2] cycloaddition fashion[140]

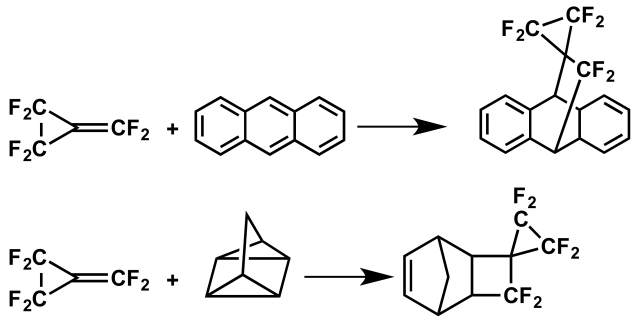

1.4 N-heterocyclic carbenes

Carbenes are neutral species (i.e., the carbon bears no formal charge), which feature a two-coordinate carbon atom possessing two non-bonding electrons.[141,142] As quintessential examples of stable, singlet-state carbenes, N-heterocyclic carbenes (NHCs) have found widespread usage in many different areas of chemistry and have been featured as ancillary ligands on early-, late- and post-transition metals.[143–146] They have also been utilized to stabilize low-valent *p*-block element compounds.[147–149] These highly-tunable reagents are featured in the 2nd generation of Grubbs' catalyst, a potent alkene metathesis catalyst, which introduces an NHC ligand in replacement of the phosphine originally found in the 1st generation of catalysts, rendering the complex more active and stable to air and moisture.[150] As very strong σ-donors and relatively weak π-acceptors, NHCs are often compared to phosphines, especially as ligands.[141] In general, NHCs are better electron donors than phosphines, and tend to form stronger metal-ligand bonds.[143,145]

1.4.1 Nature of NHC stability

Since the first report of a stable and isolable NHC by Arduengo *et al*. in 1991,[151] a staggering number of examples featuring varying steric and electronic parameters have been synthesized and characterized. This first example, 1,3-di(adamantyl)imidazol-2-ylidene (IAd),[151] was proposed to benefit from the presence of very bulky adamantyl substituents on the nitrogen atoms, providing sufficient kinetic shielding for this carbene to be completely stable under an inert atmosphere. However, it became apparent that electronic stabilization also plays a considerable role in the stability of these molecules when much less sterically demanding NHCs, like IMe_4, were shown to be stable with very limited steric hindrance being provided by the methyl substituents on the nitrogen atoms.[152] The electronic stabilization of NHCs stems from a mixture of σ and π factors, as illustrated in Figure 1.8, and it is important to consider them both when attempting to rationalize the stability of these molecules.[153] The σ stabilization is due to the presence of the more electronegative nitrogen atoms next to the carbon bearing the non-bonding lone pair. This effect mediates the nucleophilicity of the carbene and renders them less likely to react via undesired pathways. The stability imparted by π interactions arises from the donation of the nitrogen lone pairs into the empty out-of-plane p-orbital of the carbon. The combined σ and π effects increase the singlet-triplet gap of the carbene, and in doing so the less reactive singlet state is favoured.[154,155]

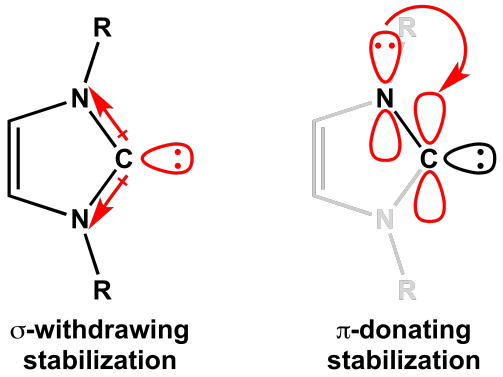

Figure 1.8. Representation of the σ and π stabilizing effects present within NHCs, which are responsible for their stability.

1.4.2 Types of NHCs

The most common examples of NHCs are surely the N,N'-diaryl-heterocyclic type, which can feature various types of substituted aryl groups on either nitrogen atom.[142] The aryl groups can rotate in and out of plane to accommodate or restrict certain bonding arrangements and are thus surprisingly flexible. Two common examples are 1,3-bis-(2,4,6-trimethylphenyl)imidazolidin-2-ylidene (SIMes)[156] and 1,3-bis-(2,4,6-trimethylphenyl)imidazol-2-ylidene (IMes),[152] the only difference being the saturation or unsaturation of the two-carbon backbone. When referring to NHCs with their shorthand names, it is common to utilize "S" at the beginning to denote a saturated backbone, the omission of which implies that it will be unsaturated. Next, "I" is used to denote that the main structure is based on an imidazole. Finally, terms such as "Mes" and "Ad" are employed to represent the nature of the nitrogen substituents. On occasion, such as with IMe_4, this term can also be used to denote substituents on the backbone. Although this nomenclature can be relatively arbitrary at times, it is widely used by most researchers and will be employed throughout this document. A few common NHCs are presented in Figure 1.9, intending to demonstrate a fraction of the variety of stable carbenes that

have been isolated and characterized to date. NHCs with a saturated backbone are generally slightly less basic than their unsaturated counterparts, owing in part to the aromatic stability imparted to the molecule by the imidazolium fragment upon reaction.[141]

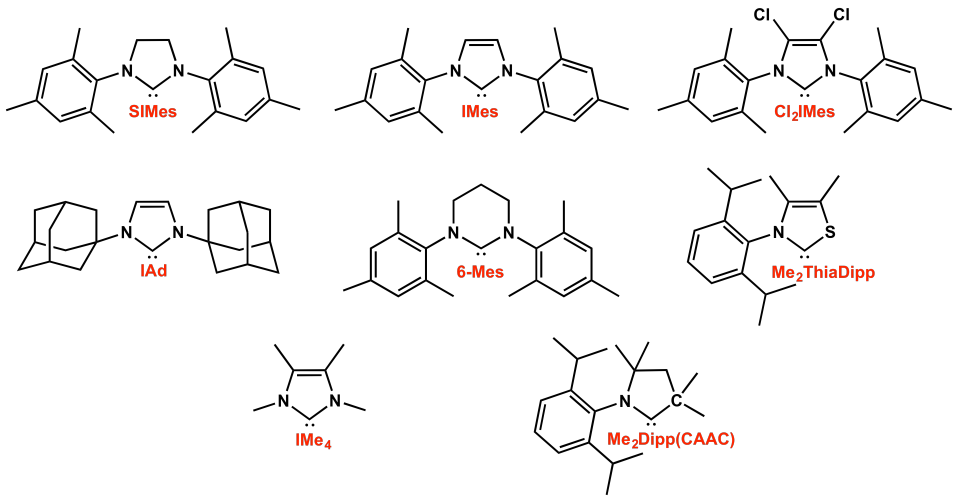

Figure 1.9. Examples of NHCs featuring different substituents and with saturated, unsaturated or substituted backbones.

The most common method for probing the electronic properties of NHCs remains the Tolman electronic parameter (TEP).[157] This metric was initially developed to determine the electronic properties of tertiary phosphines as ligands to transition metals. Most of these values are obtained by reacting a metal carbonyl complex, such as $Ni(CO)_4$, with the appropriate ligand to obtain $Ni(CO)_3(L)$. The infrared spectrum of this complex is then recorded and the electron donating abilities of the ligand are evaluated by observing the shift in the stretching frequency of the carbonyl ligands. A potent electron donating ligand will increase electron density at the metal, and this will in turn increase the strength of the M-C bond by donation from filled metal d-orbitals into the π^* C-O anti-bonding orbital. This effectively weakens the C-O bond and leads to a lower stretching frequency, as observed by IR spectroscopy. More recently, researchers have

chosen to focus on Ir- and Rh-based complexes of the form $M(Cl)(CO)_2(L)$ to obtain these values, opting to move away from Ni due to greater ease of handling and decreased safety concerns. Linear regression analysis has allowed these systems to be compared on the original Ni scale, allowing for easier comparisons.[158,159] The TEP values of many NHCs have been collected over the years, and this has allowed researchers to compare their bonding to metals with phosphines.[160] The TEP values for some common NHCs introduced in Figure 1.9 are presented in Table 1.1. Unfortunately, the range of TEP values for phosphines only span a range of *ca*. 60 cm^{-1}, and this range is even smaller with NHCs, spanning *ca*. 10 cm^{-1}.

Table 1.1. TEP (cm^{-1}) and $\%V_{bur}$ values for the common NHCs introduced in Figure 1.9

NHC	TEP (cm^{-1})[a]	$\%V_{bur}$[b]
SIMes	2050.8	36.9
IMes	2049.6	36.5
Cl_2IMes	2054.2	32.7[c]
IAd	2048.3	39.8
6-Mes	2042.6[c]	42.2
Me_2ThiaDipp	2053.6	32.4[f]
IMe_4	2051.7[d]	26.2
Me_2Dipp(CAAC)	2046.0[e]	38.0[e]

[a]Obtained from $Ir(Cl)(CO)_2(NHC)$ complexes. [b]Obtained from (NHC)AuCl complexes. [c]Obtained from $Rh(Cl)(CO)_2(NHC)$ complexes. [d]Obtained from DFT calculations. [e]Obtained from $Ni(CO)_3(NHC)$ complexes. [f]Obtained from the corresponding $HClO_4$ salt.

An important downside of TEP values as a measure of the electronic properties of NHCs is their inability to provide any accurate information about the π-acidity of these species. In fact, for many years, NHCs were viewed solely as σ-donors. It is now accepted that a more complete description of their bonding must include at least some mention of their π-accepting capabilities.[161–165] There are two primary methods for establishing or quantifying the degree of π-acidity of NHCs, which involve the formation of carbene-phosphinidene[161,163] and carbene-selenium[162,164] complexes. By collecting the ^{31}P and ^{77}Se NMR spectra of these complexes, a

trend can be observed between the chemical shifts and the degree of π-backbonding from P or Se into the NHC fragment (Figure 1.10).

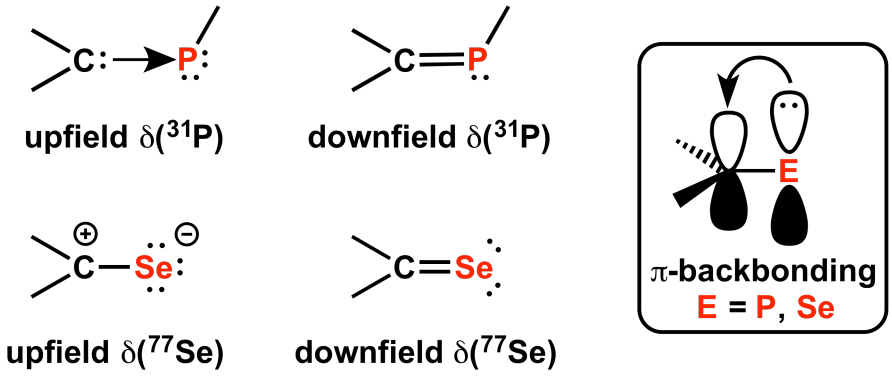

Figure 1.10. Carbene-phosphinidene and carbene-selenium complexes for the determination of the relative π-acidity of various NHCs, based on ^{31}P and ^{77}Se chemical shifts.

Like the TEP, the Tolman cone angle[157] remains the most common way of evaluating the steric impact of a wide variety of phosphines and phosphites. However, this model was shown to be an inefficient metric to evaluate NHCs and related carbenes. A more thorough overview of this parameter can be obtained by invoking the percent buried volume ($\%V_{bur}$) as a measure of this effect.[166–170] Briefly, the $\%V_{bur}$ is described as the percentage of a sphere with r = 3.5 Å around a metal centre being occupied by a chosen ligand (Figure 1.11). The metal-ligand bond length is typically set to either 2.00 Å or 2.28 Å. The $\%V_{bur}$ values for some common NHCs introduced in Figure 1.9 are presented in Table 1.1.

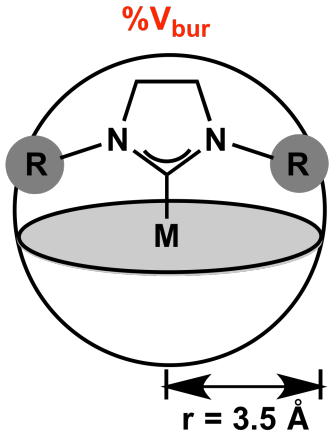

Figure 1.11. Schematic representation of the percent buried volume ($\%V_{bur}$) of an NHC coordinated to a metal. Adapted from reference 171.

A staggering number of NHCs and other persistent carbenes has been published over the last 25 years, however, this description will focus on those classes that are relevant to the work presented in this thesis. As such, it is important to introduce N,N'-dialkyl NHCs, and bring attention to the fact that, unlike the N,N'-diaryl analogues, they impose a very different type of steric environment. Although it is tempting to initially view the alkyl substituents as being inherently smaller and less sterically demanding than aryl substituents, it is important to consider the three-dimensional nature of many of these groups. For example, a *tert*-butyl group occupies a significant amount of space when viewed as a sphere with a limited ability to offer relief to hindered systems, like that which an aryl group could provide by rotating out of plane. Another, less common type of NHCs are so-called expanded ring carbenes.[172] These typically contain aryl substituents on the nitrogen atoms, but feature larger central fragments as opposed to the typical imidazole. The most common examples are of six- and seven-membered ring NHCs. These expanded ring carbenes have been shown to be even more basic than unsaturated NHCs.[173–175] This, combined with their twisted structures, makes them quite unique as carbenes. They have

almost exclusively been studied for their uses as ligands on transition metal catalysts. Finally, there are several classes of carbenes featuring variations on the typical "two nitrogen" arrangement. These types of carbenes can be difficult to manipulate due to the loss in stability that is otherwise provided by having two nitrogen atoms present. Nonetheless, notable examples feature thiazole-based carbenes, wherein one nitrogen atom has been replaced by sulfur.[176] This class of carbenes is typically less basic than the more common ones. Conversely, cyclic (alkyl)(amino)carbenes (CAACs), pioneered by Bertrand *et al*., are among the most basic carbenes that have been reported thus far.[177–180] These contain a carbon atom instead of one nitrogen, and they impose unique steric constraints (Figure 1.12). Specifically, the carbon fragment can have substituents pointing in and out of the plane of the main carbene-containing fragment.

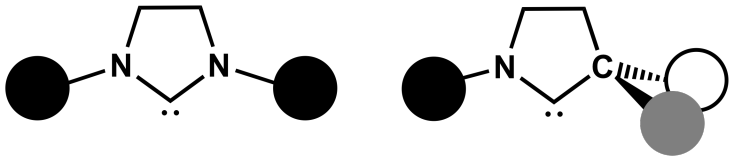

Figure 1.12. Demonstration of the different steric environments present in NHCs (left) and CAACs (right). Adapted from reference 177.

There are several extremely thorough, recent and informative reviews about NHCs,[141,142,145,146] including in-depth studies by Nolan *et al*. on both their electronic[160] and steric[171] parameters. The reader is encouraged to read these reports if a more in-depth discussion about this remarkable class of molecules is desired.

1.4.3 NHCs in organocatalysis and the Breslow intermediate

The significant nucleophilic nature of NHCs makes them attractive candidates for reactivity with species containing electrophilic carbon centers, and this has led to them being used as very effective organocatalysts.[142,181] Commonly, this type of reaction will lead to an umpolung of the initially electrophilic substrate carbon, rendering it nucleophilic in nature due to the ability of the imidazole fragment to delocalize the positive charge and donate electrons from the nitrogen atoms.[182] This effect is best viewed when considering the reaction between an NHC and an aldehyde (Figure 1.13), wherein the acyl anion-like Breslow intermediate is obtained. This transient intermediate, proposed by Ronald Breslow in 1958,[183] was finally successfully isolated and characterized in 2012 by Berkessel *et al.*[184] This intermediate is crucial in almost all organocatalytic reactions involving NHCs, and its reactivity stems from the presence of the acyl anion-like carbon, which can react with an incredible variety of electrophiles. This has allowed for countless examples demonstrating the catalytic coupling, via C-C bond formation, of two electrophilic substrates, such as aldehydes, which could not be achieved easily utilizing other methods due to unfavorable charge interactions.[141,181,182]

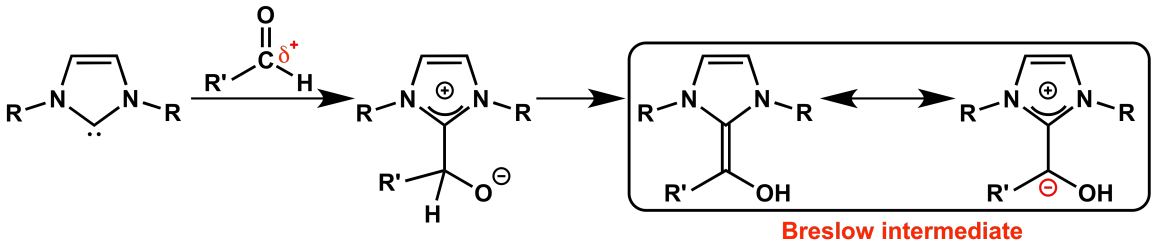

Figure 1.13. Typical reactivity between an NHC and an aldehyde leading to the formation of the Breslow intermediate, which features an umpolung of the initially electrophilic carbon.

Although the reactivity of NHCs with aldehydes is very well established, their reactivity with additional classes of reagents is also noteworthy (Figure 1.14). The acyl azolium species

resulting from the attack of an NHC on an ester leads to enhanced electrophilic character on carbon, encouraging nucleophilic attack by alcohols and effectively promoting transesterification.[141]

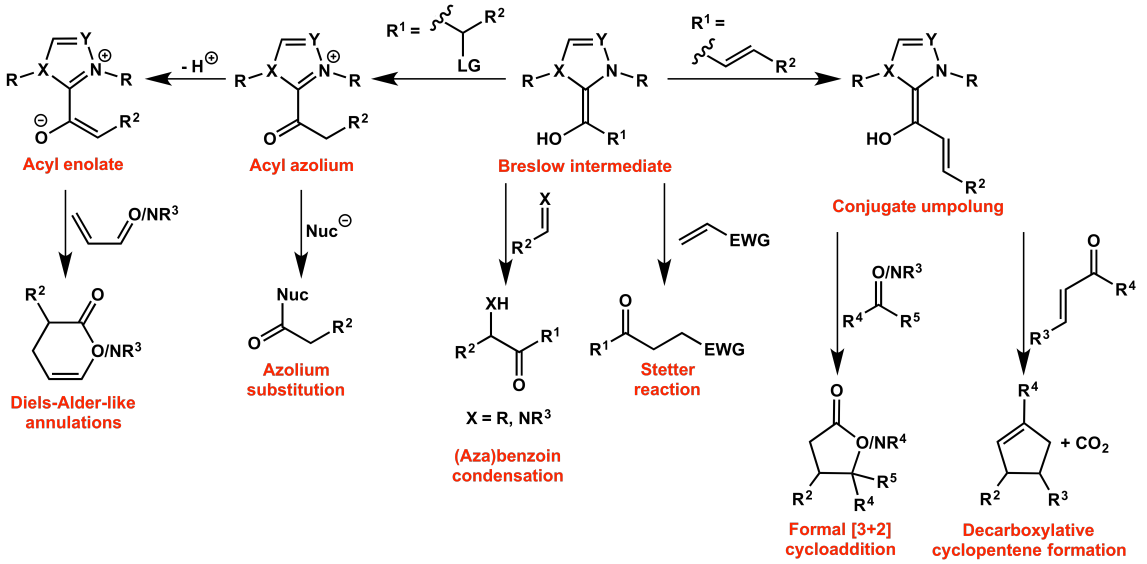

Figure 1.14. Selected examples of reactivity involving the Breslow intermediate, demonstrating its versatility. Adapted from reference 141.

The Breslow intermediate is also involved in reactions with Michael acceptors[185,186] via the Stetter reaction, and has been shown to form unique "conjugate umpolung" systems.[187] These arise from the reactivity of the Breslow intermediate with α,β-unsaturated aldehydes, affording a conjugated π-system capable of reactions leading to annulated products. These types of ring-forming reactions, especially in an organocatalytic fashion, are extremely important transformations in organic chemistry, and NHCs have rendered a large amount of these possible.[188] As organocatalysts, NHCs have also been used successfully in polymerization chemistry, an area of research that continues to receive much attention due to the diminished

toxicity and price benefits that could be gained by being able to synthesize certain polymers without the need for a transition metal or harsh conditions.[189]

1.5 Summary and thesis outline

The importance of fluorine and the desirable properties it can impart to systems within the context of pharmaceuticals, PET imaging, polymers, refrigerants, and much more, has been introduced. Additionally, the numerous challenges and difficulties inherent to the manipulation of C-F bonds have been presented, underlining a need for a deeper fundamental understanding of these systems. The polymerization of fluoroalkenes within the coordination sphere of a transition metal has not yet been achieved. However, work within our group has been presented, with special focus on Co(I) fluorocarbene complexes and their reactivity with TFE to demonstrate the first steps of a proposed fluoro-variant on a Rooney-Green-type mechanism. The [2+2] cycloaddition reactions were studied computationally and shown to proceed via a unique 1,4-singlet diradical pathway. Additionally, NHCs were introduced as a truly versatile class of reagents, and their different subclasses were explored and elaborated upon. Their importance as organocatalysts was illustrated by way of the Breslow intermediate, and their rich reactivity with electrophilic substrates was also presented. Chapter 2 will focus on the fluoroorganometallic chemistry of Co(III) fluoride and bis(perfluoroalkyl) complexes, and entirely different reactivity than what has been observed for Co(I) systems will be presented. This includes: the synthesis and characterization of several new cobalt complexes featuring fluorinated ligands, the selective formation of new cobalt fluorocarbene complexes capable of insertion into a metal perfluoroalkyl, and the most upfield ^{19}F NMR shifts reported to date. Chapter 3 will introduce pioneering studies on the reactivity between NHCs and fluoroalkenes to form novel NHC

fluoroalkene molecules. From these, the formation of polyfluoroalkenyl imidazolium salts will be demonstrated, and both fluoride substitution and nucleophilic addition reactions on these new molecules will be shown. Chapter 4 will elaborate on the substitution chemistry of polyfluoroalkenyl imidazolium salts, with formation of C-E bonds (E = C, N, O, S) and C-M bonds (M = Mn, Mo) by facile C-F bond activation. Chapter 5 will feature an in-depth reactivity scope study between a large number of NHCs with varying electronic and steric requirements, and several fluoroalkenes. This will serve to gain a deeper understanding of the fundamental reactivity between these two species, as relatively little is known about this type of reactivity thus far. Finally, Chapter 6 will summarize the previous chapters and include an outlook for the future of the projects detailed in this thesis.

Chapter 2

2.1 Context

Having previously established the potential of cobalt fluoroorganometallic chemistry as a platform for C-F bond forming and breaking (section 1.2.4), including the reactivity of cobalt fluorocarbene complexes with tetrafluoroethylene (TFE) in a [2+2] cycloaddition fashion to form novel cobalt perfluorometallacyclobutanes,[95,107] we sought to explore what effects a change in oxidation state might have on this reactivity. Initially, nucleophilic Co(I) fluorocarbene complexes were synthesized specifically for reactivity with electrophilic TFE by reductions with sodium,[92] but the chemistry of Co(III) with multiple fluorinated ligands remains largely unexplored. This chapter aims to expand on this area, and key differences in reactivity between the Co(I)/Co(III) systems will be highlighted.

Transition metal complexes bearing two perfluorinated ligands are very uncommon,[43,48,190–194] in large part due to the difficulties associated with their synthesis. Unlike typical hydrocarbons, oxidative addition of a C-F or C-C bond in a perfluoroalkane is typically not feasible, due to the very stable nature of these compounds.[34] An alternative synthetic route, involving oxidative addition of a perfluoroalkyl iodide followed by transmetalation with F or CF_3 will be described in Chapter 2. In total, 6 novel Co(III) fluoride and bis(perfluoroalkyl) complexes were synthesized and fully characterized, providing us with a foundation for studying Co(III) fluoroorganometallic chemistry, as opposed to our previous work focusing primarily on Co(I).

The fluoride complexes in this work were shown to exhibit the most extreme upfield ^{19}F NMR shifts reported to date, the nature of which was determined computationally. Additionally,

these Co(III) complexes demonstrated potential towards catalytic fluorination at relatively low catalyst loadings (5 mol%). The catalytic fluorination chemistry of Co(III) systems has since been the subject of a high-throughput study in our group.[195]

From Co(III) bis(perfluoroalkyl) complexes, novel Co(III) difluorocarbenes were prepared. These carbenes exhibited marked electrophilic character, contrary to the Co(I) analogues, which manifested itself in its immediate reactivity with trace moisture. The reactivity of these difluorocarbenes further distinguished itself from their nucleophilic counterparts by undergoing rapid insertion into the remaining cobalt perfluoroalkyl bond, effectively growing the perfluoroalkyl fragment by one CF_2 unit. To the best of our knowledge, this represents the only example for this type of reactivity besides previous work by Burton *et al.* on a copper system.[196,197]

2.1.1 Published contributions

(1) **Leclerc, M. C.**; Bayne, J. M.; Lee, G. M.; Gorelsky, S. I.; Vasiliu, M.; Korobkov, I.; Harrison, D. J.; Dixon, D. A.; Baker, R. T. *J. Am. Chem. Soc.* **2015**, *137*, 16064-16073.

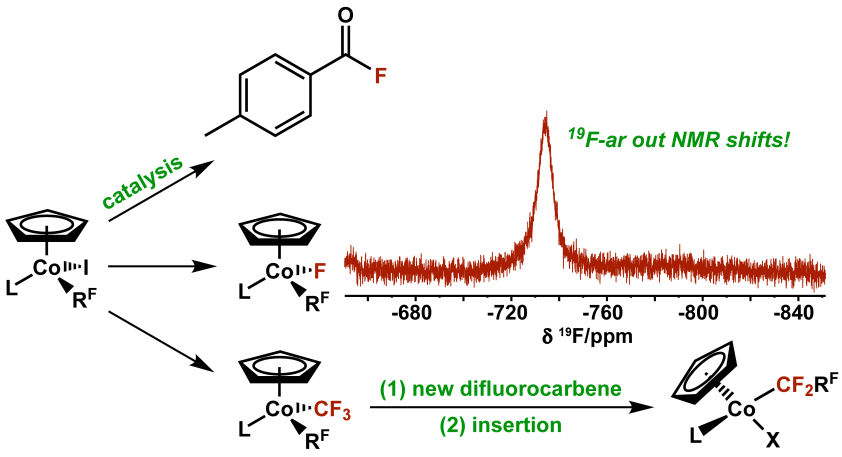

Four perfluoroalkyl cobalt(III) fluoride complexes have been synthesized and characterized by elemental analysis, multinuclear NMR spectroscopy, X-ray crystallography, and powder X-ray diffraction. The remarkable cobalt fluoride ^{19}F NMR chemical shifts (−716 to −759 ppm) were studied computationally, and the contributing paramagnetic and diamagnetic factors were extracted. Additionally, the complexes were shown to be active in the catalytic fluorination of *p*-toluoyl chloride. Furthermore, two examples of cobalt(III) bis(perfluoroalkyl)complexes were synthesized and their reactivity studied. Interestingly, abstraction of a fluoride ion from these complexes led to selective formation of cobalt difluorocarbene complexes derived from the trifluoromethyl ligand. These electrophilic difluorocarbenes were shown to undergo insertion into the remaining perfluoroalkyl fragment, demonstrating the elongation of a perfluoroalkyl chain arising from a difluorocarbene insertion on a cobalt metal center. The reactions of both the fluoride and bis(perfluoroalkyl) complexes provide insight into the potential catalytic applications of these model systems to form small fluorinated molecules as well as fluoropolymers.

Author contributions: The manuscript was written in equal parts by MCL and GML. MCL was responsible for the synthesis and characterization of complexes **5**, **7** and **9**. GML was responsible for the synthesis and characterization of complexes **6**, **8** and **10**. Preliminary experiments involving complexes **5-8** were performed by JMB, under the supervision of MCL. The catalytic fluorination chemistry was developed by MCL. The formation of **Int 1-4** was established by GML, and finalizing characterization work was performed by MCL. SIG, MV, and DAD performed the DFT calculations. IK performed the crystallography.

2.2 Perfluoroalkyl Cobalt(III) Fluoride and Bis(perfluoroalkyl) Complexes: Catalytic Fluorination and Selective Difluorocarbene Formation

2.2.1 Introduction

Transition metal complexes bearing fluoride or fluorocarbon ligands have attracted considerable interest because they are used to mediate/catalyze C–F or C–R^F bond-forming reactions, which are highly important in the pharmaceutical, agrochemical, and advanced materials industries.[34,198] Despite this widespread interest, the fundamental chemistry of these species is considerably less developed than that of analogous hydrocarbon compounds. In particular, reports of complexes bearing two fluorinated ligands (i.e., one perfluoroalkyl and one fluoride, or two perfluoroalkyls) are very rare, with most examples belonging to second or third row metals.[43,48,190,191] Recently, examples of Ni complexes bearing two perfluoroalkyl ligands have been reported.[192–194] There are synthetic challenges associated with preparing such complexes: The most direct approach would be via oxidative addition of the C–F or C–C bond of a perfluoroalkane (CF_4, C_2F_6, C_3F_8, etc.) to a low-valent metal, but the inert nature of perfluoroalkanes makes this route inaccessible.[34] Here, we use alternative synthetic routes to access the products of the hypothetical oxidative addition reaction between perfluoroalkanes and first row metals. Our general strategy is to utilize the oxidative addition of iodoperfluoroalkanes (R^F–I) to install the first perfluoroalkyl group on the metal, followed by exchange of the iodide ligand for either a fluoride or a trifluoromethyl group (Scheme 2.1).

Scheme 2.1. Alternative synthetic route to transition metal fluorides and perfluoroalkyls

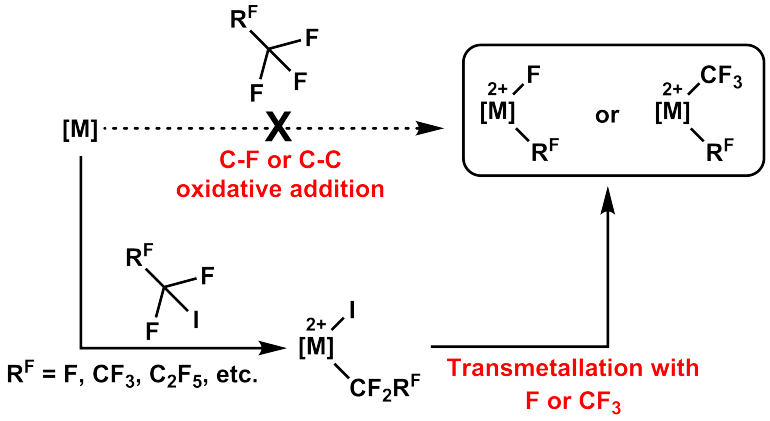

Oxidative addition of R^F–I to metal complexes has been shown to proceed for group 9 metals,[199,200] and methods for converting [M]–X (X = halide) to [M]–F[102,201] or to [M]–CF_3[198,202–206] are known. Reactions between the inexpensive and commercially available cobalt(I) complex $CpCo(CO)_2$ (Cp = η^5-cyclopentadienyl) and R^F–I (R^F = CF_3 and CF_2CF_3) furnish cobalt(III) complexes $CpCo(R^F)(I)(CO)$.[40] Substitution of the carbonyl ligand with a phosphine is facile and leads to the series of isolable starting materials $CpCo(R^F)(I)(L)$ (**1**–**4**), as shown in Scheme 2.2.[207]

Scheme 2.2. Synthetic scheme for phosphine substitutions

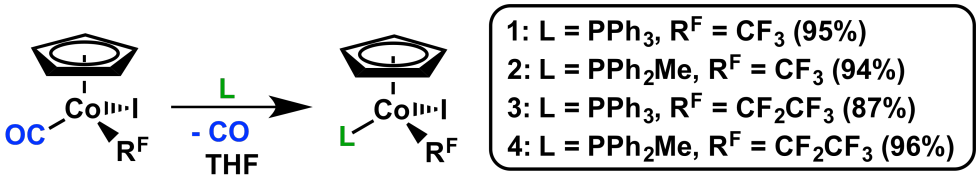

In recent reports, we described the two-electron reduction of complexes **1**–**4** with sodium to furnish a series of nucleophilic Co^I perfluorocarbene complexes, and demonstrated [2 + 2] cycloaddition reactions with tetrafluoroethylene.[92,94] The resulting cobalt(III) perfluorometallacyclobutane complexes reacted with both Lewis and Brønsted acids to give ring-

opening/isomerization products. However, the chemistry of cobalt(III) systems with multiple perfluorinated ligands remains largely unexplored, and herein we expand that area.

2.2.2 Results and discussion

2.2.2.1 Synthesis and characterization of perfluoroalkyl cobalt fluorides

Seeking to isolate the hypothetical products that would arise from the oxidative addition of perfluoroalkanes to a cobalt center, we opted for a pathway involving the substitution of iodide for fluoride, using a method previously reported by Hughes et al. to afford analogous perfluoroalkyl Ir^{III} fluorides. Reactions of complexes **1**–**4** with 3 equiv of AgF in dichloromethane at room temperature over 20 h in the absence of light afforded perfluoroalkyl Co^{III} fluoride complexes of the general formula $CpCo(R^F)(F)(L)$ (Cp = η^5-cyclopentadienyl, R^F = CF_3 and CF_2CF_3, L = PPh_3 and PPh_2Me) (**5**–**8**) in 68–91% isolated yield as dark-green solids (Scheme 2.3). Complexes **5**–**8** were characterized spectroscopically and structurally, and the results were further analyzed by density functional theory (DFT)[208] calculations with the B3LYP[209,210] and PW91[211,212] exchange-correlation functionals and polarized double- and triple-ζ basis sets. Structurally, complexes **5** and **6** represent the expected products arising from the oxidative addition of perfluoromethane to cobalt, whereas complexes **7** and **8** are those that would arise from the same type of reaction with perfluoroethane. As previously mentioned, these oxidative addition reactions are not feasible; thus, it is necessary to utilize other synthetic methods to obtain such complexes.

Scheme 2.3. Synthetic scheme for cobalt(III) fluorides

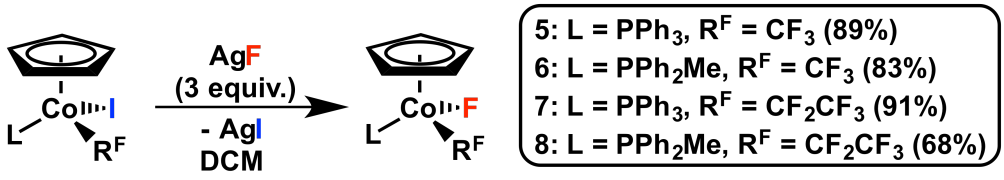

Cobalt fluorides are uncommon in the literature, and the few that have been presented mostly feature cobalt in either the +1 or the +2 oxidation state.[213,214] There are only three examples featuring cobalt in the +3 oxidation state: cobaltocenium fluoride, CoF_3, and an example from Klein et al. with a cyclometalated complex featuring azine as an anchoring group.[215] Cobaltocenium fluoride was synthesized by Richmond et al. in 1994,[216] and has been applied to several stoichiometric fluorination reactions. This extremely hygroscopic reagent is formed from the reaction of the one-electron reductant cobaltocene with an excess of perfluorodecalin in toluene at low temperature. CoF_3 is commercially available, although it is often too reactive to promote transformations in a selective manner. Of these three systems, only cobaltocenium fluoride and the cyclometalated cobalt fluoride are truly organometallic complexes, but they do not offer any opportunity for varying the ligand environment on cobalt because their scaffolds are limited as a result of the conditions of forming the fluorides, contrary to complexes **5**–**8**, which offer the ability to modify both the nature of the phosphine ligands and the perfluoroalkyl ligands on cobalt.

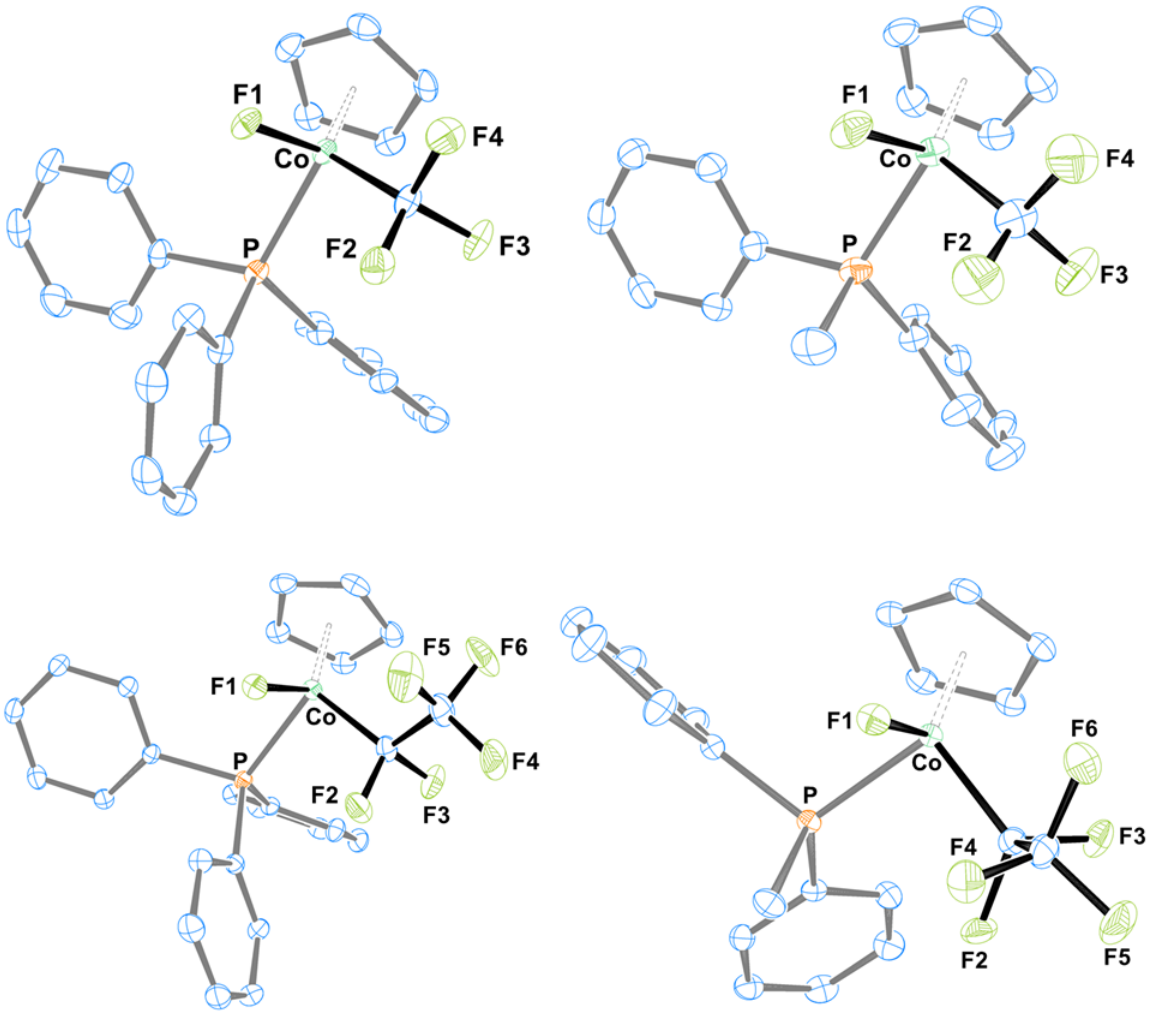

Figure 2.1. Crystallographic representations of **5** (top left), **6** (top right), **7** (bottom left), and **8** (bottom right) with 30% probability thermal ellipsoids. Hydrogen atoms are omitted for clarity. One molecule of acetonitrile has been removed from **5**. Sample of **6** crystallized with two molecules in the unit cell. Selected bond lengths and angles are presented in the Supporting Information of the original publication.[95]

X-ray structural studies confirm that complexes **5**–**8** are well-defined monomeric Co^{III} fluorides featuring cyclopentadienyl, phosphine, and perfluoroalkyl ligands (Figure 2.1). The Co–F bond distances in complexes **5**–**8** range from 1.86 to 1.88 Å, similar to the value of

1.89 Å found in CoF_3.[217,218] For perfluoroethyl complexes **7** and **8**, the C_α–F bond distances (avg. 1.378(2) and 1.393(2) Å) are significantly longer than C_β–F (avg. 1.326(2) and 1.333(2) Å) as observed previously for an Ir analogue.[102] The Co–P distances are approximately 0.04 Å shorter with PPh_2Me as compared to PPh_3 because the former is known to be a slightly more basic donor ligand. Moreover, the Co–C bond distances are shorter for the trifluoromethyl ligand versus the perfluoroethyl fragment by 0.2 Å for the PPh_3 derivatives and 0.4 Å for the PPh_2Me examples. Seminal work by Stone et al. has established that [M]–C bonds are shorter with perfluoroalkyls than with analogous hydrocarbons, an effect observed in this system as well.[219] Recently, another example of a transition metal simultaneously bearing a fluoride and a perfluoroalkyl was reported that features a bis(trifluoromethyl) nickel dimer with bridging fluoride ligands.[220]

DFT calculations were used to gain insight into the electronic structure of **5** as a representative example. TD-DFT calculations at the B3LYP/TZVP level with the SMD solvent model[221] reproduced the electronic absorption spectrum in CH_2Cl_2 well, with two principal experimental bands at 16 300 cm^{-1} (263 M^{-1} cm^{-1}, calcd = 15 600 cm^{-1}) and 21 800 cm^{-1} (1190 M^{-1} cm^{-1}, calcd = 21 700 cm^{-1}) (See Figure B.1 and the band assignments in Appendix B).[95] Relative to typical Co^{III} octahedral inorganic complexes,[222] the high intensities of these two absorption bands indicate significant charge-transfer character in the corresponding electron excitations. Calculated Mayer bond orders[223] for **5** provide values for Co–Cp (2.37), Co–PPh_3 (0.98), and Co–CF_3 bonds (0.91) that are unsurprising. However, the value for the Co–F bond (0.61) indicates significant ionic character in this metal–ligand interaction and that the Co–F is the least covalent among the metal–ligand bonds.

The ^{19}F NMR spectra of **5**–**8** exhibit extreme upfield resonances for the fluoride ligands ranging from δ −716 to −759 ppm. These shifts are significantly upfield from the analogous Ir

complexes previously reported by both Hughes et al.[102] ($\delta(^{19}F)$ = −437 to −446 ppm) and Bergman et al.[224] ($\delta(^{19}F)$ = −413 to −415 ppm). To the best of our knowledge, these represent the most upfield resonances reported for a ^{19}F NMR signal. The resonances at half-height are very broad (900–1900 Hz) and featureless, presumably because of the fluorides being bound to ^{59}Co, a nuclide with a spin of $^{7}/_{2}$, a natural abundance of 100%, and a large quadrupolar coupling constant of 42.0×10^{-30} m^2, all of which contribute to a significant broadening of the fluoride signal. The addition of molecular sieves to an NMR sample of **5**–**8** did not affect the broadness of the fluoride signals, indicating that the signal is not broadened artificially by the presence of moisture.

From the results of DFT computational studies, we are now able to understand the unique nature of these chemical shifts. The results for all the calculated Co–F chemical shifts and their diamagnetic and paramagnetic tensor components are shown in Appendix B. There are minor quantitative differences between the three sets of chemical calculations but not qualitative differences. There is reasonable agreement with experiment for the CF_3 and CF_2 chemical shifts with differences of up to 30 ppm, which is typical of such fluorine NMR calculations. The differences between the experimental and the calculated shifts for the F bonded to the Co are larger by 30–100 ppm depending on the method, with the BLYP/TZVP2 results being the closest to experiment for this shift. The magnitudes of the calculated shifts for the Co–F were found to be very sensitive to the bond distance, suggesting why the difference between the calculated and experimental values for this shift can be large. For L = PPh_3 and R = CF_3, the calculations predict a small value for the ^{19}F shift of the CF_3 group (ca. −20 ppm as compared to the experimental value of −2 ppm), so the difference in the diamagnetic and paramagnetic components are comparable to those of the standard $CFCl_3$ (BLYP/TZ2P σ(standard) = 118.8 ppm) with the

diamagnetic component larger than the paramagnetic component. The ^{19}F chemical shift for the F bonded to the Co is large and negative, resulting from the fact that the diamagnetic and paramagnetic components have the same sign, both shielding. The paramagnetic component is larger than the diamagnetic component. We note that the diamagnetic shielding component for the F bonded to C and of the F bonded to Co are very similar, within ~10 ppm, so the large changes are due to the differences in the paramagnetic components between the "normal" value for the F in the CF_3 group and the value predicted for the F bonded to Co.

The fact that the paramagnetic component tensor has the same sign as the diamagnetic component tensor has been noted previously for ClF because of mixing of the appropriate π orbitals with the σ* orbital in the presence of a magnetic field.[225–227] Although F_2 has the same mixing interactions, the presence of symmetry prevents the paramagnetic component from being shielding. The high-lying occupied and low-lying unoccupied molecular orbitals (HOMO and LUMO, respectively) for $CpCo(CF_3)(F)(PH_3)$ and $CpCo(CF_3)(F)(PPh_3)$ (**5**) are shown in Appendix B. The orbitals are essentially the same for both compounds. The HOMO, HOMO-1, and HOMO-2 are lone pairs on the F bonded to Co interacting with different d orbitals on the Co. For the Co contribution, the HOMO is the $d_{x^2y^2}$, the HOMO-1 is the d_{z^2}, and the HOMO-2 is the d_{xy}. The LUMO is the Co–F σ* orbital with the d_{xz} on the Co, and the LUMO+1 is predominantly the Co–C σ*. Thus, the HOMO, HOMO-1, and HOMO-2 serve as the equivalent to the π-type orbitals in ClF, and the LUMO is the equivalent of the ClF σ*. It is the interaction of these orbitals in the presence of a magnetic field that leads to the paramagnetic component being shielding, similar to what is found for ClF.

2.2.2.2 Reactivity of fluoride complexes

The importance of fluorinated organic substrates has been amply demonstrated.[35] Efficient, reliable techniques for the introduction of fluorine into such products have been the subject of widespread research for many years.[24] Consequently, and encouraged by the ionic character of the Co–F bonds in our system, we sought to determine the ability of these cobalt systems to fluorinate simple organic compounds. Reactions with *p*-toluoyl chloride were explored as a potential route toward fluorination to form *p*-toluoyl fluoride. Gray et al. have recently demonstrated this reaction in stoichiometric fashion, proceeding through halide metathesis with cyclometalated iridium fluoride complexes.[228] Stoichiometric reactions with complex **6** in C_6D_6 showed clean and essentially complete conversion of the starting substrate within 2 h and formation of the *p*-toluoyl fluoride product, proceeding through overall halide metathesis with the cobalt fluoride complex. Prompted by the initial results of these stoichiometric reactions, we aimed to develop a catalytic process whereby, starting with the iodide complex **2**, the fluoride complex **6** could be generated *in situ* by the presence of an excess of AgF.

Table 2.1. Catalytic fluorination reactions

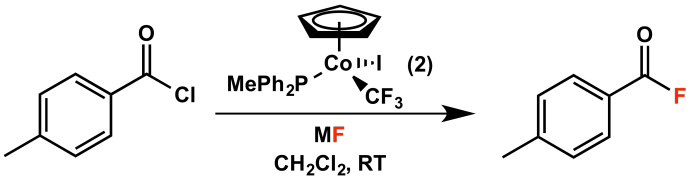

entry	MF (equiv.)	catalyst loading (mol %)	*t* (h)	yield (%)
1	AgF (1.0)	-	16	2
2	CsF (1.0)	-	16	5
3	KF (1.0)	-	16	<1
4	CoF_3 (1.0)	-	16	2
5	AgF (3.0)	10	4	99
6	**AgF (3.0)**	**5**	**4**	**99**
7	AgF (3.0)	1	4	47
8	AgF (3.0)	0.1	4	26

Control experiments convincingly demonstrated that stoichiometric reactions between *p*-toluoyl chloride and the fluoride sources AgF, CsF, KF, and CoF_3 gave minimal conversion of the starting reagent to the target compound overnight in dichloromethane (<5% in all cases). Optimized reaction conditions led to essentially quantitative conversion of the starting chloride to the fluoride within 4 h, using 5 mol % of **2** and 3 equiv of AgF. (See Table 2.1 for selected control experiments and Table B.4 for a full list.) This catalytic fluorination occurs cleanly, affording an approximately 1:1 mixture of the Co–F and Co–Cl complexes upon completion. Relatively few methods of producing *p*-toluoyl fluoride exist in the literature, and they feature either exotic or potentially harmful reagents such as cyanuric fluoride,[229] cesium fluoroxysulfate,[230] potassium bifluoride,[231] and hydrogen fluoride.[232] Furthermore, this substrate is not commercially available, but Pd-based systems are used to produce it catalytically.[233] Two stoichiometric reactions were run in parallel, one of them containing excess PPh_2Me (5 equiv), and analyzed at the same time. Both reactions provided the same amount of conversion to the target product. It thus appears unlikely that the reaction proceeds through a dissociative

mechanism, wherein the phosphine could dissociate from the metal and vacate a coordination site for the acyl chloride to bind.

Scheme 2.4. Proposed catalytic cycle for the fluorination of *p*-toluoyl chloride

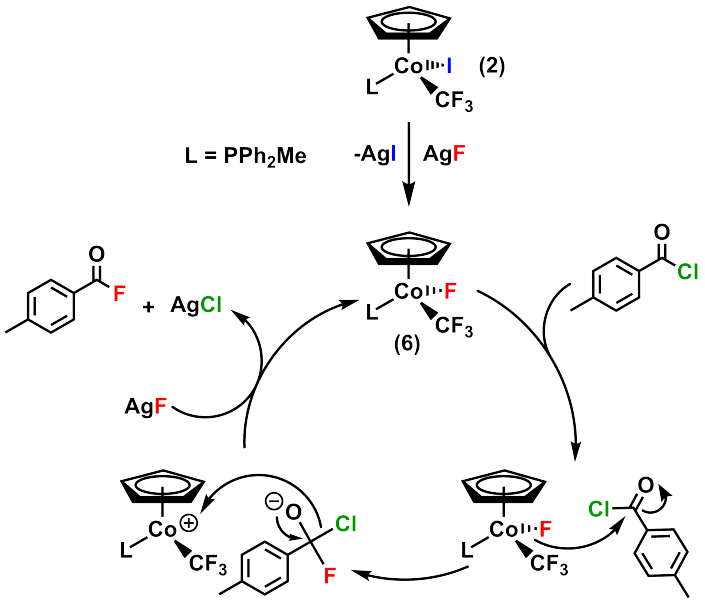

With this information in hand, a proposed catalytic cycle is shown in Scheme 2.4. Starting from iodide complex **2**, fluoride analogue **6** is first formed using AgF as the fluoride source. The ionic nature of the Co–F bond provides a latent source of fluoride, which can react readily with the electrophilic carbon center of the acyl chloride. Expulsion of the chloride from the organic substrate gives the target compound, generating a cobalt chloride complex, which can react with AgF to regenerate the catalytically active complex **6** and form the inactive AgCl. Many examples of electrophilic fluorination of organic substrates have been explored over recent years,[55] and efficient catalytic nucleophilic fluorination has more recently made major strides as well.[27] Importantly, transition metals have been used to prepare a variety of alkyl fluorides,[234–236] alkenyl fluorides,[237–239] and aryl fluorides[240–244] via nucleophilic fluorination. Alkyl fluorides

have been synthesized by Toste et al. from gold(III)[234] systems and by Sanford et al. from palladium(IV)[236,240] systems. Electrophilic gold(I)[237,238] complexes have been used almost exclusively for the synthesis of alkenyl fluorides, affording good yields and regioselectivity. Aryl fluorides have been synthesized by the groups of Sanford et al. and Gagné et al. through the use of palladium(IV)[240] and platinum(IV),[241] respectively, as well as certain silver salts[242–244] and some copper complexes.[245–247] Additionally, Grushin et al. have reported various fluorination examples with palladium(II) and rhodium(I) systems.[248–250] Of these examples, only copper stands out as a nonprecious, first row transition metal. Catalytic systems incorporating these types of abundant and nontoxic metals are very important and are active areas of research as the search for renewable and efficient methods of producing target fluorinated reagents continues. Moreover, the catalytic formation of sp^2 C–F bonds has mostly been limited to examples with palladium[246,251,252] as well as a few with copper[245] and gold.[237,238]

The tendency of third row transition metals to form weaker bonds to fluorine than most first row transition metals has made them useful for catalytic reactions,[34,253] but it is essential to develop methods that utilize inexpensive, nontoxic, and abundant metals such as cobalt. Interestingly, it appears that the significant ionic character of the Co–F bond in this system, as demonstrated by the calculated Mayer bond orders, might be a major contributing factor to its catalytic potential. Furthermore, this reaction does not require the use of extravagant reagents and represents a step toward the potential uses of cobalt in additional catalytic fluorination reactions.

2.2.2.3 Synthesis and characterization of cobalt bis(perfluoroalkyls)

The isolation of perfluoroalkyl cobalt(III) halide complexes **1**–**8** motivated efforts to generate bis(perfluoroalkyl) complexes via transmetalation of the halide group with CF_3. Converting [M]–X complexes to [M]–CF_3 is an established process, first presented by Fuchikami et al.[254] using a copper system and Me_3SiCF_3 and subsequently by other groups.[52,205] We initiated our investigation by studying the reactivity of the Co^{III} perfluoroalkyl halide complexes with Me_3SiCF_3, using CsF as the initiator and DMF as solvent. Reactions with PPh_3 derivatives mostly resulted in decomposition and very low yields of the desired products. However, reactions with PPh_2Me derivatives (**2**, **4**, **6**, and **8**) led to the desired bis(perfluoroalkyl) products (**9** and **10**) in good yields (**9** = 71% and **10** = 75% from [Co]–F, **9** = 57% and **10** = 52% from [Co]–I) after only 2 h as stable yellow-orange powders (Scheme 2.5). Although the relative yields are lower when starting from [Co]–I complexes, it is an overall more direct approach to complexes **9** and **10**.

Scheme 2.5. Synthetic scheme for cobalt(III) bis(perfluoroalkyls)

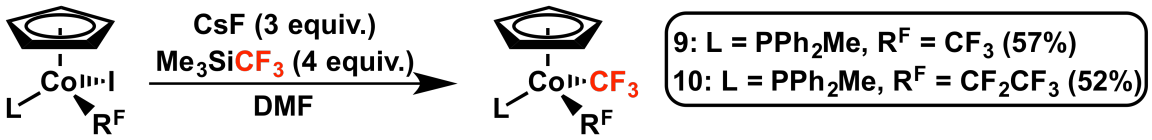

It has been demonstrated previously that Me_3SiCF_3 undergoes activation by fluoride to liberate CF_3^-. Important studies by Yagupolskii et al.[255] and Röschenthaler et al.[256] independently demonstrated that this activation involves the *in situ* formation of pentacoordinate silicate anions, either $[Me_3SiF(CF_3)]^-$ or $[Me_3Si(CF_3)_2]^-$, which extrude $[CF_3]^-$ to form Me_3SiF or Me_3SiCF_3, respectively. We propose that in our system, CsF reacts with Me_3SiCF_3 to produce the cesium salts of the aforementioned pentacoordinate silicates, which then effect the transmetalation with [Co]–X. This is in contrast to a report by Wang et al.,[257] where the reaction between AgF and

Me_3SiCF_3 forms a proposed [$AgCF_3$] species that can effect transmetalation. It is important to note that for [Co]–I complexes **2** and **4**, CsI is formed during the course of the reaction. In addition, experiments in our lab show the following: (1) When CsI is used in the place of CsF, no transmetalation takes place. (2) [Co]–I complexes **2** and **4** do not react with CsF in DMF to produce [Co]–F complexes **6** and **8**. These observations are consistent with the lower yield of products **9**/**10** when starting from [Co]–I (**2**/**4**) rather than [Co]–F (**6**/**8**).

Complexes **9** and **10** were studied through X-ray crystallography (Figure 2.2). The Co–C bond distance of 1.940 Å in **9** is significantly longer than the Ni–C bond distances in analogous nickel bis(trifluoromethyl) complexes: The (bipy)Ni$(CF_3)_2$ complex from Vicic et al.[192] has a distance of 1.88 Å, and an example from Mirica et al.[193] has a distance of 1.91 Å with the Ni^{II} complex. However, the latter's bond lengths increase to 1.97 Å when the metal is oxidized to Ni^{III}. A recent report by Sanford et al. features an octahedral Ni^{IV} complex, TpNi(Ph)$(CF_3)_2$ (Tp = trispyrazolylborate), with Ni–C bond distances of 1.99 Å.[194] It is interesting to compare this complex with **9** because they are both d^6 systems, and the Ni^{IV} complex was proven capable of promoting Aryl–CF_3 coupling through reductive elimination.

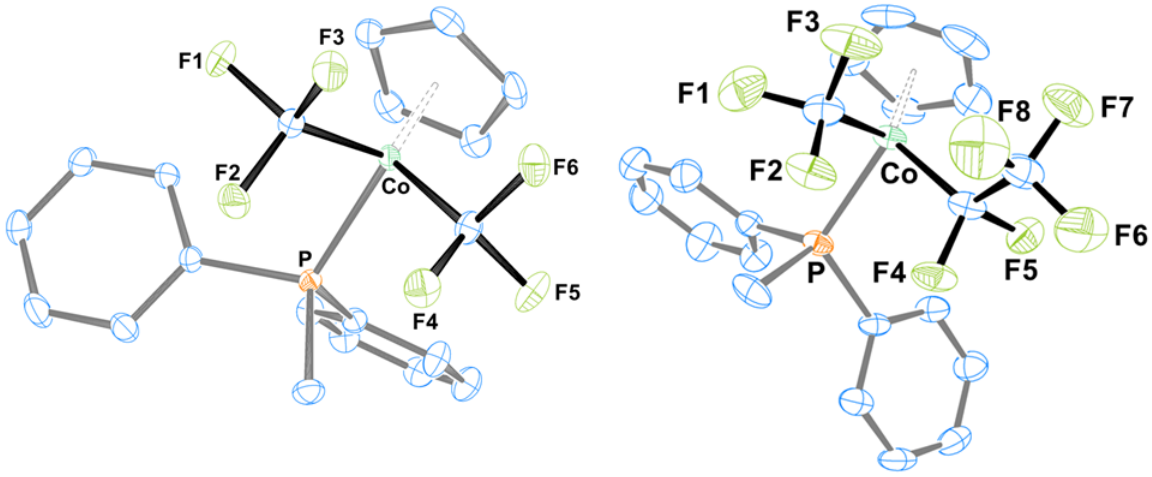

Figure 2.2. Crystallographic representations of **9** (left) and **10** (right) with 30% probability thermal ellipsoids. Hydrogen atoms are omitted for clarity. One molecule of toluene has been removed from both **9** and **10**. Selected bond lengths and angles are presented in the Supporting Information of the original publication.[95]

DFT calculations were used to obtain insight into the electronic structure of **9**. TD-DFT calculations at the B3LYP/TZVP level reproduce the electronic absorption spectrum well (Figure B.1). The absorption bands in **9** are blue-shifted relative to the spectrum of **5**. The assignment of two bands at 23 000 cm^{-1} (shoulder) and 25 800 cm^{-1} (730 M^{-1} cm^{-1}) is shown in Appendix B. Calculated Mayer bond orders for **9** are 2.31 for the Co–Cp bond, 1.01 for Co–PPh_2Me, and 0.93 and 0.95 for the two Co–CF_3 bonds. These bond orders are almost identical to those in **5**. Thus, replacement of the fluoride ligand in **5** with the more strongly covalently bound CF_3 ligand does not affect the covalency of other Co–ligand interactions.

Full NMR characterization of these complexes was obtained, and assignment of the nonequivalent methylene fluorine resonances in the various ^{19}F spectra was achieved. A 1D ^{1}H–^{19}F HOESY experiment allowed the selective pulsing of each of the three different fluorine resonances to determine the relative spatial proximity to the three closest protons in the structure

(Figure 2.3). Additionally, a $^{19}F–^{19}F$ NOESY was collected to observe how the trifluoromethyl ligand correlated through space to the different methylene fluorines of the perfluoroethyl ligand (Figure B.7). These experiments indicate that the relative orientation of the ligands is essentially the same in solution as in the solid state.

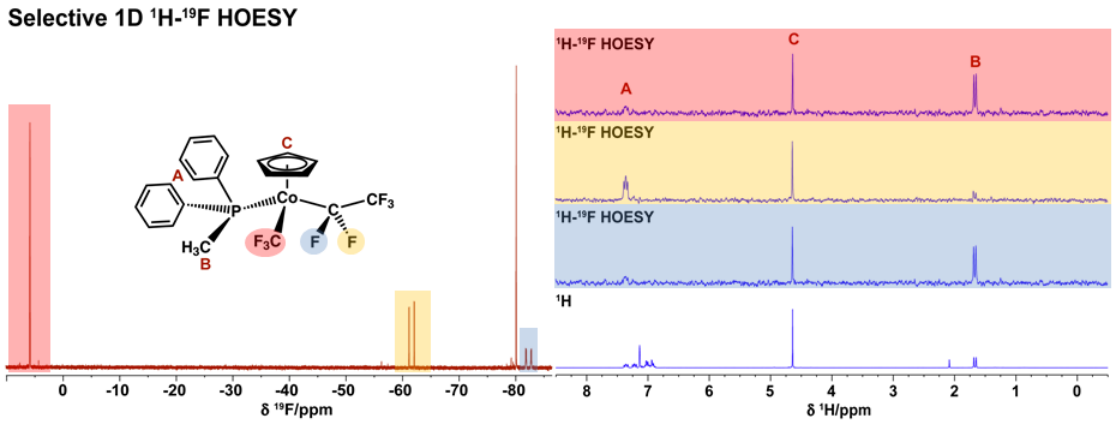

Figure 2.3. Selective 1D ^{1}H-^{19}F HOESY experiment in C_6D_6 to help in the assignment of the two [Co]-CF_2CF$_3$ fluorine signals is shown. The Cp signals were set to equal intensity for clarity. Coloured boxes above the ^{1}H spectrum demonstrate the effect of selective saturation of the appropriate fluorine signal and showing which signals are correlated by a through-space interaction.

The 1D ^{1}H-^{19}F HOESY experiment has been utilized recently by Claridge et al.[258] in the analysis of fluorinated pyrrolidines. This experiment offers the advantage of being much faster than the more prevalent 2D ^{19}F-^{19}F NOESY experiments found in the literature. In our case, by taking advantage of two nuclides in ^{1}H and ^{19}F that each have essentially 100% natural abundance, the 1D method offers the possibility to obtain similar conformational information in a matter of minutes, as opposed to several hours for the traditional 2D method.

2.2.2.4 Reactivity of bis(perfluoroalkyl) complexes

Transition metal perfluoroalkyl complexes can be precursors to metal fluorocarbenes. We previously reported the two-electron reduction of perfluoroalkyl Co^{III} iodide complexes **1**–**4** to afford Co^{I} fluorocarbene complexes, which exhibit nucleophilic type reactivity at the carbene carbon.[92,94] We are interested in preparing analogous Co^{III} fluorocarbenes in order to probe the effect that changing the oxidation state of cobalt will have on carbene reactivity, with the expectation that Co^{III} fluorocarbenes might react as electrophiles. This concept was previously demonstrated in an elegant study by Roper et al., where they showed that Ru^{0} and Ru^{II} fluorocarbenes differed by having nucleophilic and electrophilic reactivity at the carbene carbon, respectively.[84]

Our strategy to prepare Co^{III} fluorocarbenes consisted of abstracting a fluoride from a perfluoroalkyl ligand using a Lewis acid, similar to the preparation of other fluorocarbene complexes in the literature. Our initial attempts to abstract a fluoride from perfluoroalkyl Co^{III} iodides **1**–**4** were unsuccessful because reactions with the Lewis acids Me_3SiOTf and $B(C_6F_5)_3$ did not result in the formation of fluorocarbenes, presumably as a result of a preference by the Lewis acid to abstract the iodide ligand. However, bis(perfluoroalkyl) complexes **9**–**10** were attractive precursors for fluorocarbene formation because they both eliminate the possibility of an undesirable metal halide abstraction. Indeed, reactions of **9** and **10** with Lewis acids (Me_3SiOTf and $B(C_6F_5)_3$) in DCM led to fluoride abstraction and formation of cobalt difluorocarbene complexes (**Int 1**–**4**, Scheme 2.6). Addition of the Lewis acid to a solution of the bis(perfluoroalkyl) precursors led to a colour change from yellow-orange to deep red over the course of 1 h at room temperature, and NMR analysis demonstrated that quantitative conversion was achieved. The ^{19}F NMR resonances for the difluorocarbene ligand in complexes **Int 1**–**4** are

highly characteristic, with downfield chemical shifts ranging between δ 178 and 180 ppm.[79,85] This is in contrast to the difluorocarbene ligand of previously reported Co^{I} complexes, with resonances for the two unique fluorine environments at δ 63 and 94 ppm.[92,94]

Scheme 2.6. Formation of cobalt(III) difluorocarbenes

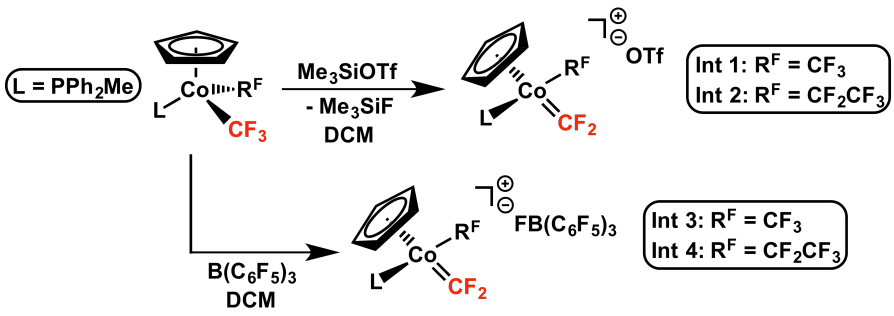

Both Lewis acids provided selective fluoride abstraction from complex **10** because only abstraction from the trifluoromethyl ligand was observed, leaving the perfluoroethyl fragment untouched (Scheme 2.7). This is supported by ^{19}F NMR, where the only fluorocarbene signal that is observed is the one associated with the difluorocarbene fragment and not that of the fluoro(trifluoromethyl) carbene. The selectivity of fluoride abstraction from CF_3 and not CF_2CF_3 can be rationalized by comparing the π-donating ability of F and CF_3 fragments. Metal carbene bonds are typically stabilized by contributions of d orbital electrons from the metal. However, because the Co^{III}carbene complexes here have two fewer d electrons compared to the Co^{I} carbenes we reported previously (d^6 vs d^8), the M=C bond is likely more reliant on donation from the other carbene substituents for stabilization. Therefore, because F is a better π-donating substituent than CF_3, fluoride abstraction from CF_3 rather than CF_2CF_3 is preferred. Efforts to increase electron density around the metal by utilizing PMe_3 in the hopes of promoting some amount of fluoride abstraction from the perfluoroethyl ligand were unsuccessful.

Scheme 2.7. Selectivity of fluoride abstraction

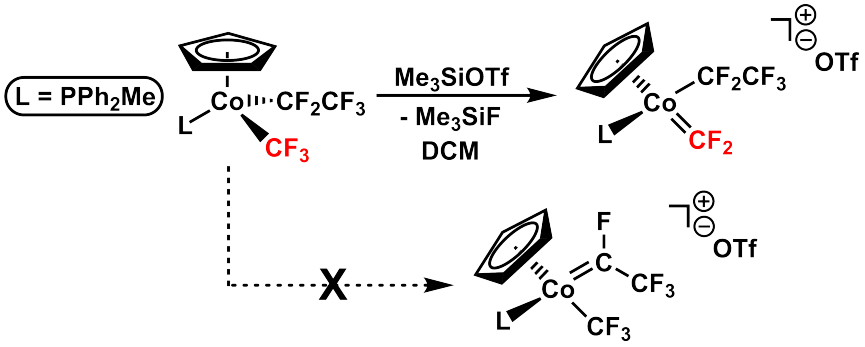

The newly formed difluorocarbene complexes underwent two primary reactions in solution, which prevented their isolation in pure form. One involves the insertion of difluorocarbene into the remaining perfluoroalkyl fragment, effectively increasing the length of the perfluoroalkyl chain on the transition metal center by one CF_2 unit (Scheme 2.8, top). These products are clearly identified using ^{19}F NMR because the resulting perfluoroethyl and perfluoropropyl ligands have highly characteristic chemical shifts and splitting patterns, which are identical to those of previously isolated Co^{III} complexes.[259] Previous work by Burton et al.[196,197] on copper demonstrated a rare example of this type of perfluoroalkyl chain growth from CF_2 insertion on a transition metal. This reaction demonstrates a step toward potential perfluoroalkene polymerization using a transition metal catalyst, a sought-after process that has been stunted at least in part by the difficulties involved in promoting such insertion reactions,[260] in large part due to the strength of various [M]–R^F bonds. Attaining better control of this reaction is an area of ongoing study within our group.

Scheme 2.8. Reactivity of cobalt(III) difluorocarbenes (see Experimental Section (2.2.4) for product yields)

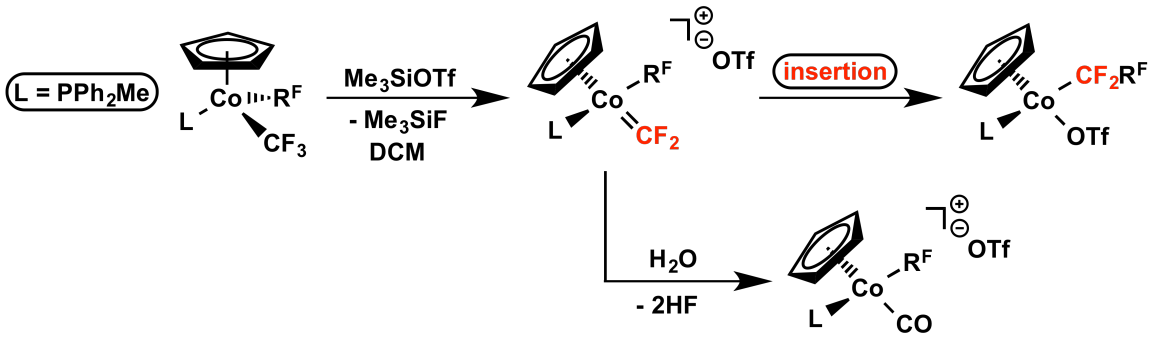

The second reaction is the well-known hydrolysis of the difluorocarbene ligand by trace H_2O to furnish a carbonyl ligand and 2 equiv of HF (Scheme 2.8, bottom).[261] This reaction occurs almost instantaneously and is a common reaction with metal difluorocarbenes that have formal d^6 metal centers.[74,84] Although the hydrolysis of difluorocarbene ligands is undesirable, the observation of electrophilic reactivity by our Co^{III} fluorocarbenes further highlights a key difference from our previously reported Co^{I} fluorocarbenes, which did not react with 20 equiv of H_2O in acetonitrile solutions.

2.2.3 Conclusions

We have isolated and characterized four perfluoroalkyl Co^{III} fluoride complexes. These complexes exhibit remarkable ^{19}F NMR shifts, largely due to an unusual paramagnetic component that is shielding. Additionally, these complexes were shown to be active in the catalytic fluorination of *p*-toluoyl chloride. Furthermore, both the fluoride and iodide complexes could be used in the synthesis of Co^{III} bis(perfluoroalkyl) complexes, potential precursors in the development of catalytically relevant systems. These complexes were shown to react with

different Lewis acids to form electrophilic Co^{III} difluorocarbenes. The insertion of these difluorocarbenes into the remaining perfluoroalkyl fragment on the metal demonstrated the elongation of a perfluoroalkyl chain on a transition metal by one carbon. Further studies on the catalytic activity of these complexes are currently underway in our laboratory.

2.2.4 Experimental section

2.2.4.1 General considerations

All manipulations were carried out using standard Schlenk techniques or in an MBraun glovebox. All glassware was oven-dried at >150 °C for a minimum of 2 h prior to use or flame-dried using a torch. Toluene, hexanes, tetrahydrofuran (THF), diethyl ether (DEE), and dimethylformamide (DMF) were dried on columns of activated alumina using a J. C. Meyer (formerly Glass Contour) solvent purification system. Dichloromethane (DCM), chloroform-*d* ($CDCl_3$), and acetonitrile-d_3 (CD_3CN) were dried by refluxing over calcium hydride under a nitrogen flow, followed by distillation and filtration through a column of activated alumina (ca. 10 wt %). Benzene-d_6 (C_6D_6) was dried by standing over activated alumina (ca. 10 wt %) overnight followed by filtration. The following chemicals were used as purchased, without further purification: $CpCo(CO)_2$ (Cp = η^5-cyclopentadienyl) (Strem, 95%), CF_3I (SynQuest, 99%), CF_3CF_2I (SynQuest, 98%), PPh_3 (Strem, 99%), PPh_2Me (Strem, 99%), Me_3SiOTf (OTf = SO_3CF_3) (Aldrich, 98%), AgF (Strem, 98%), CsF (Strem, 99+%), KF (Aldrich 99+%), CoF_3 (Aldrich, 98%), and *p*-toluoyl chloride (Aldrich, 98%). Starting complexes $CpCo(R^F)(I)(CO)$ (Cp = η^5-cyclopentadienyl; R^F = CF_3 and CF_2CF_3) were synthesized according to slightly modified literature procedures from $CpCo(CO)_2$.[40] From these complexes, facile substitution of the CO ligands provided the phosphine analogues according to a slightly modified

literature procedure[207] (see the Supporting Information of the original publication for complete details on isolation of these complexes).[95] ^{1}H, ^{19}F, $^{19}F\{^{1}H\}$, and $^{31}P\{^{1}H\}$ NMR spectra were recorded on either a Bruker Avance 300 or Bruker Avance II 300 spectrometer at room temperature. ^{1}H NMR spectra were referenced to the residual proton peaks associated with the deuterated solvents (C_6D_6 = 7.16 ppm, $CDCl_3$ = 7.26 ppm, CD_3CN = 1.94 ppm). ^{19}F and $^{19}F\{^{1}H\}$ NMR spectra were referenced to internal 1,3-bis(trifluoromethyl)benzene (BTB) (Aldrich, 99%, deoxygenated by purging with nitrogen and stored over 4 Å molecular sieves), set to −63.5 ppm. $^{31}P\{^{1}H\}$ NMR spectra were referenced to external H_3PO_4 (85% aqueous solution), set to 0.0 ppm. The ^{19}F NMR signals corresponding to the different [Co]–CF_2CF_3 complexes are labeled as A and A′. For labeling information, see Supporting Information of the original publication.[95] Assignments were derived from 2D experiments with $CpCo(CF_2CF_3)(CF_3)(PPh_2Me)$ and applied to the other complexes because instrumental constraints did not permit the same experiments to be undertaken with the various fluoride complexes. Throughout this manuscript, F^{A} refers to the more upfield resonance and $F^{A'}$ refers to the more downfield resonance. UV–vis spectra were recorded on a Cary 100 instrument, using sealable quartz cuvettes (1.0 cm path length). Elemental analyses were performed by the Laboratoire d'Analyse Élémentaire de l'Université de Montréal (Montréal, Québec, Canada) and the G. G. Hatch Stable Isotope Laboratory at the University of Ottawa (Ottawa, Ontario, Canada). A Micromass Q-ToF 1 (positive mode) was used for electrospray ionization (ESI), with samples diluted to ca. 5 μg/mL in methanol. Infrared spectroscopy was carried out on a Thermo Nicolet NEXUS 670 FTIR instrument. Powder X-ray diffraction (PXRD) experiments were performed using a RIGAKU Ultima IV, equipped with a Cu Kα radiation source (λ = 1.541836 Å), and a graphite monochromator. Scanning of the 2θ range was performed from 5 to 40°. PXRD pattern was consistent in 2θ values with the generated

pattern from XRD, with slight discrepancies in some intensities of peaks attributed to preferred crystallite orientation.

2.2.4.2 Synthesis and characterization

General Procedure for the Synthesis of CpCo(R^F)(F)(L) (R^F = CF_3 or CF_2CF_3; L = PPh_3 or PPh_2Me). A 100 mL round-bottomed Schlenk flask was charged with CpCo(R^F)(I)(L) (0.58 mmol) dissolved in CH_2Cl_2 (ca. 15 mL). AgF (1.74 mmol) was added, and the resulting solution/suspension was stirred at room temperature for approximately 20 h in the absence of light. After this time, a colour change form dark yellow-brown to dark green was observed. The resulting mixture was filtered through a plug of Celite, and the volatiles were removed in vacuo. The crude product was recrystallized from a concentrated solution of CH_2Cl_2 and hexanes at −35 °C. Pure product was collected via filtration, washed with cold (−35 °C) hexanes, and dried in vacuo. The products were obtained as dark-green powders. Crystals suitable for X-ray crystallography were obtained by diffusion of hexanes into a concentrated solution of the appropriate complex in toluene. Complexes **5** and **7** were not viable for elemental analysis (approximately 1–2% off) due to the suspected presence of a small amount of unidentified paramagnetic impurity. The latter also potentially contributes to the broadness of the ^{1}H NMR spectra for these complexes. The use of various solvents and variable temperature NMR were unsuccessful in diminishing the broadening. Sublimation, additional recrystallizations, and column chromatography were attempted to purify these complexes. Column chromatography with a solvent mixture of THF/MeOH (8:2), followed by recrystallization from a concentrated solution of toluene proved most effective, but a small amount of impurity still remained. Additionally, THF inserts within the crystal lattice and cannot be removed under high vacuum

(ca. 10^{-3} mtorr), even with heating. As such, PXRD patterns were compared with the calculated pattern from XRD in order to confirm the bulk-phase purity of complex **7** (Figure B.10). The patterns were in excellent agreement with one another, thus confirming the crystalline-phase purity of the sample. The same comparison with complex **5** was unsuccessful because of the presence of solvent within the unit cell of the crystallographic data.

CpCo(CF$_3$)(F)(PPh$_3$) (5). Yield: 245 mg, 89% based on CpCo(CF$_3$)(I)(PPh$_3$). UV–vis (1.0 mM in CH_2Cl_2) $\lambda_{max}(\varepsilon)$ = 459 (1190), 615 (263). ^{1}H NMR (300 MHz, C_6D_6) δ 4.60 (s, 5H, Cp), 6.98 (m, 6H, *m*- and *p*-C*H*(PPh)), 7.89 (m, 4H, *o*-CH(PPh)). ^{19}F NMR (282 MHz, C_6D_6) δ −2.0 (d, $^3J_{FF} \approx 8$ Hz, 3F, CF_3), −734 (br, $\omega_{1/2} \approx 1900$ Hz, 1F, Co–*F*). ^{31}P{^{1}H} NMR (121 MHz, C_6D_6) δ 29.8 (br, $\omega_{1/2} \approx 65$ Hz). Elemental analysis for $C_{24}H_{20}F_4PCo$ Calcd: C, 60.77; H, 4.25. Found: C, 58.73; H, 4.36.

CpCo(CF$_3$)(F)(PPh$_2$Me) (6). Yield: 198 mg, 83% based on CpCo(CF$_3$)(I)(PPh$_2$Me). UV–vis (0.5 mM in CH_2Cl_2) $\lambda_{max}(\varepsilon)$ = 450 (1640), 604 (347). ^{1}H NMR (300 MHz, C_6D_6) δ 1.57 (d, $^2J_{HP} \approx 13$ Hz, 3H, CH_3), 4.60 (s, 5H, Cp), 7.05 (m, 6H, *m*- and *p*-C*H*(PPh)), 7.52 (dt, $^3J_{HH} \approx 8$ Hz, $^3J_{HP} \approx 78$ Hz, 4H, *o*-C*H*(PPh)). ^{19}F NMR (282 MHz, C_6D_6) δ −3.3 (d, $^3J_{FF} \approx 9$ Hz, 3F, CF_3), −716 (br, $\omega_{1/2} \approx$ 1300 Hz, 1F, Co–*F*). ^{31}P{^{1}H} NMR (121 MHz, C_6D_6) δ 33.7 (br, $\omega_{1/2} \approx 130$ Hz). Elemental analysis for $C_{19}H_{18}F_4PCo$ Calcd: C, 55.36; H, 4.40. Found: C, 54.98; H, 4.69.

CpCo(CF$_2$CF$_3$)(F)(PPh$_3$) (7). Yield: 277 mg, 91% based on CpCo(CF$_2$CF$_3$)(I)(PPh$_3$). UV–vis (0.5 mM in CH_2Cl_2) $\lambda_{max}(\varepsilon)$ = 473 (1420), 621 (340). ^{1}H NMR (300 MHz, $CDCl_3$) δ 4.61 (s, 5H, Cp), 7.40 (m, 6H, *m*- and *p*-C*H*(PPh)), 7.79 (m, 4H, *o*-C*H*(PPh)). ^{19}F NMR (282 MHz, $CDCl_3$) δ −68.6 (d, $^2J_{FF} \approx 240$ Hz, 1F, $CF^AF^{A'}$; $F^{A'}$), −79.8 (d, $^4J_{FF} \approx 10$ Hz, 3F, CF_3), −81.0 (ddd, $^3J_{FF} \approx 8$ Hz, $^3J_{FP} \approx 46$ Hz, 1F, $CF^AF^{A'}$; F^A), −759 (br, $\omega_{1/2} \approx 1000$ Hz, 1F, Co–*F*). ^{31}P{^{1}H} NMR (121

MHz, $CDCl_3$) δ 26.3 (br, $\omega_{1/2} \approx 95$ Hz). Elemental analysis for $C_{25}H_{20}F_6PCo$ Calcd: C, 57.27; H, 3.84. Found: C, 55.93; H, 3.97.

CpCo(CF_2CF_3)(F)(PPh_2Me) (8). Yield: 268 mg, 68% based on CpCo(CF_2CF_3)(I)(PPh_2Me). UV–vis (0.25 mM in CH_2Cl_2) $\lambda_{max}(\varepsilon)$ = 461 (3140), 605 (680). ^{1}H NMR (300 MHz, C_6D_6) δ 1.51 (d, $^2J_{HP} \approx 13$ Hz, 3H, CH_3), 4.60 (s, 5H, Cp), 7.07 (m, 6H, *m*- and *p*-C*H*(PPh)), 7.45 (dt, $^3J_{HH} \approx 7$ Hz, $^3J_{HP} \approx 55$ Hz, 4H, *o*-C*H*(PPh)). ^{19}F NMR (282 MHz, C_6D_6) δ −70.8 (d, $^2J_{FF} \approx 248$ Hz, 1F, $CF^AF^{A'}$; $F^{A'}$), −79.7 (d, $^4J_{FF} \approx 12$ Hz, 3F, CF_3), −80.7 (dd, $^3J_{FP} \approx 43$ Hz, 1F, $CF^AF^{A'}$; F^A), −734 (br, $\omega_{1/2} \approx 900$ Hz, 1F, Co–*F*). ^{31}P{^{1}H} NMR (121 MHz, C_6D_6) δ 31.9 (br, $\omega_{1/2} \approx 130$ Hz). Elemental analysis for $C_{20}H_{18}F_6PCo$ Calcd: C, 51.97; H, 3.93. Found: C, 51.45; H, 4.06.

General Procedure for the Synthesis of CpCo(R^F)(CF_3)(PPh_2Me) (R^F = CF_3 or CF_2CF_3). CpCo(R^F)(I)(PPh_2Me) (0.877 mmol) was dissolved in DMF (15 mL), and CsF (2.63 mmol) was added as a solid. The resulting solution was stirred at room temperature for 5 min. To this solution was added dropwise Me_3SiCF_3 (4.22 mmol) in toluene (5 mL) over 3 min, and the reaction was stirred at room temperature for approximately 3 h. During this time, the colour of the reaction mixture changed from dark green to bright orange. The mixture was then filtered through a pad of Celite, washed with ~10 mL of toluene, and the filtrate was evaporated under vacuum to dryness. The resulting residue was triturated with DEE (4 × 10 mL). The orange solid was dissolved in minimal toluene and mounted on a silica-gel column. DEE was used as the eluent and pushed through the column until the washings were clear. The solvent was again removed under vacuum to afford pure product as a yellow-orange powder. Crystals suitable for X-ray crystallography were obtained from a concentrated solution of the appropriate complex in toluene cooled to −35 °C.

$CpCo(CF_3)_2(PPh_2Me)$ (9). Yield: 231 mg, 57% based on $CpCo(CF_3)(I)(PPh_2Me)$. UV–vis (0.5 mM in CH_2Cl_2) $\lambda_{max}(\varepsilon)$ = 388 (1335), 430 (shoulder of the principal band). ^{1}H NMR (300 MHz, C_6D_6) δ 1.70 (d, $^2J_{HP} \approx$ 11 Hz, 3H, CH_3), 4.63 (s, 5H, Cp), 7.01 (m, 6H, *m*- and *p*-C*H*(PPh)), 7.34 (m, 4H, *o*-C*H*(PPh)). ^{19}F NMR (282 MHz, C_6D_6) δ 3.6 (d, $^3J_{FP} \approx$ 3 Hz, 6F, CF_3). ^{31}P{^{1}H} NMR (121 MHz, C_6D_6) δ 40.3 (br, $\omega_{1/2} \approx$ 150 Hz). Elemental analysis for $C_{20}H_{18}F_6PCo$ Calcd: C, 51.97; H, 3.93. Found: C, 51.83; H, 3.99.

$CpCo(CF_2CF_3)(CF_3)(PPh_2Me)$ (10). Yield: 235 mg, 52% based on $CpCo(CF_2CF_3)(I)(PPh_2Me)$. UV–vis (0.75 mM in CH_2Cl_2) $\lambda_{max}(\varepsilon)$ = 375 (730), 450 (shoulder of the principal band). ^{1}H NMR (300 MHz, CD_3CN) δ 1.69 (d, $^2J_{HP} \approx$ 11 Hz, 3H, CH_3), 4.67 (s, 5H, Cp), 6.99 (m, 6H, *m*- and *p*-C*H*(PPh)), 7.31 (dt, $^3J_{HH} \approx$ 9 Hz, $^3J_{HP} \approx$ 40 Hz, 4H, *o*-C*H*(PPh)). ^{19}F NMR (282 MHz, CD_3CN) δ 5.2 (m, 3F, Co–CF_3), −62.3 (dd, $^2J_{FF} \approx$ 258 Hz, $^3J_{FP} \approx$ 16 Hz, 1F, $CF^AF^{A'}$; $F^{A'}$), −80.7 (m, 3F, Co–CF_2CF_3), −82.9 (dm, $^2J_{FF} \approx$ 258 Hz, 1F, $CF^AF^{A'}$; F^A). ^{31}P{^{1}H} NMR (121 MHz, CD_3CN) δ 37.2 (br, $\omega_{1/2} \approx$ 140 Hz). Elemental analysis for $C_{21}H_{18}F_8PCo$ Calcd: C, 49.24; H, 3.54. Found: C, 49.16; H, 3.70.

General Procedure for the Determination of NMR Yields in the Formation of $[CpCo(R^F)(=CF_2)(PPh_2Me)](X)$ (R^F = CF_3 or CF_2CF_3; X = OTf^- or $[FB(C_6F_5)_3]^-$) and the Products Derived from These Intermediates. Note that as the difluorocarbene complexes form they react either with any trace quantities of water present (immediately) or in an insertion reaction (over a period of several hours). Furthermore, the reactions involving the difluorocarbene intermediates occur more quickly when using Me_3SiOTf as compared to $B(C_6F_5)_3$. Because of the enhanced stability of the difluorocarbenes formed by using $B(C_6F_5)_3$, yields for these complexes are reported for a certain reaction time. Because of the nature of these reactions, yields for the

products deriving from the reactions with water and the insertion reactions will be presented for an elapsed reaction time with Me_3SiOTf and when possible with $B(C_6F_5)_3$.

Method A. $CpCo(R^F)(CF_3)(PPh_2Me)$ (0.043 mmol) was dissolved in DCM (0.8 mL), and BTB (0.043 mmol) was added. The solution was transferred to an NMR tube, and Me_3SiOTf (0.043 mmol) was added with a microliter syringe. The NMR tube was sealed and shaken vigorously. The ^{19}F NMR yields were determined by integration of signals with respect to BTB. Complete conversion of starting material was observed within 60 min.

Method B. $CpCo(R^F)(CF_3)(PPh_2Me)$ (0.043 mmol) was dissolved in DCM (0.4 mL), and BTB (0.043 mmol) was added. The solution was transferred to an NMR tube, and a solution of $B(C_6F_5)_3$ (0.043 mmol) in DCM (0.4 mL) was added. The NMR tube was sealed and shaken vigorously. The ^{19}F NMR yields were determined by integration of signals with respect to BTB. Complete conversion of starting material was observed within 30 min.

[CpCo(CF$_3$)(=CF$_2$)(PPh$_2$Me)][OTf] (Int 1). ^{19}F NMR (282 MHz, CH_2Cl_2 with C_6D_6 capillary) δ 180.0 (br, 2F, Co=CF_2), 9.0 (br, Co–CF_3), −78.9 (br, 3F, C$F_3SO_3^-$). $^{31}P\{^1H\}$ NMR (121 MHz, CH_2Cl_2 with C_6D_6 capillary) δ 40.1 (br, $\omega_{1/2} \approx 136$ Hz).

[CpCo(CF$_2$CF$_3$)(=CF$_2$)(PPh$_2$Me)][OTf] (Int 2). Yield: 68% based on Co = CF_2 after 30 min (20% after 4 h). ^{19}F NMR (282 MHz, CH_2Cl_2 with C_6D_6 capillary) δ 179.5 (br, 2F, Co=CF_2), −58.4 (d, $^2J_{FF} \approx 228$ Hz, 1F, $CF^AF^{A'}$; $F^{A'}$), −75.3 (dd, $^2J_{FF} \approx 228$ Hz, $^3J_{FP} \approx 36$ Hz 1F, $CF^AF^{A'}$; F^A), −80.9 (br, 3F, Co–CF_2CF_3). $^{31}P\{^1H\}$ NMR (121 MHz, CH_2Cl_2 with C_6D_6 capillary) δ 35.6 (br, $\omega_{1/2} \approx 142$ Hz).

[CpCo(CF_3)(=CF_2)(PPh_2Me)][$FB(C_6F_5)_3$] (Int 3). ^{19}F NMR (282 MHz, CH_2Cl_2 with C_6D_6 capillary) δ 178.8 (br, 2F, Co=CF_2), 9.4 (br, Co–CF_3), −134.4 (d, br, $^3J_{FF} \approx 18$ Hz, 6F, FB(*o*-C_6F_5)$_3$), −159.1 (s, br, 3F, FB(*o*-C_6F_5)$_3$), −165.8 (m, br, 6F, FB(*m*-C_6F_5)$_3$), −188.8 (s, br, 1F, *F*B(C_6F_5)$_3$). $^{31}P\{^1H\}$ NMR (121 MHz, CH_2Cl_2 with C_6D_6 capillary) δ 37.6 (br, $\omega_{1/2} \approx 136$ Hz).

[CpCo(CF_2CF_3)(=CF_2)(PPh_2Me)][$FB(C_6F_5)_3$] (Int 4). Yield: 75% based on Co=CF_2 after 30 min (60% after 4 h). ^{19}F NMR (282 MHz, CH_2Cl_2 with C_6D_6capillary) δ 178.2 (t, br, $^4J_{FF} \approx 7$ Hz, 2F, Co=CF_2), −57.2 (dm, $^2J_{FF} \approx 225$ Hz, 1F, $CF^AF^{A'}$; $F^{A'}$), −74.6 (dd, $^2J_{FF} \approx 225$ Hz, $^3J_{FP} \approx 35$ Hz 1F, $CF^AF^{A'}$; F^A), −80.8 (br, 3F, Co–CF_2CF_3), −189.0 (s, br, 1F, *F*B(C_6F_5)$_3$). $^{31}P\{^1H\}$ NMR (121 MHz, CH_2Cl_2 with C_6D_6 capillary) δ 37.5 (br, $\omega_{1/2} \approx 148$ Hz).

Analysis of the Proposed Products Derived from Int 1–4 by ^{19}F NMR and Mass Spectrometry

[CpCo(CF_3)(CO)(PPh_2Me)][OTf] (from Int 1). Yield: 14% based on Co–CF_3 after 60 min. ^{19}F NMR (282 MHz, CH_2Cl_2 with C_6D_6 capillary) δ 2.79 (br, 3F, Co–CF_3), −78.3 (br, 3F, C$F_3SO_3^-$). $^{31}P\{^1H\}$ NMR (121 MHz, CH_2Cl_2 with C_6D_6capillary) δ 35.8 (br, $\omega_{1/2} \approx 75$ Hz). IR: 2241 cm^{-1} (s, br, Co–*CO*).

CpCo(CF_2CF_3)(OTf)(PPh_2Me) (from Int 1). Yield: 18% based on Co–CF_2CF_3 after 60 min. ^{19}F NMR (282 MHz, CH_2Cl_2 with C_6D_6 capillary) δ −74.7 (dm, $^2J_{FF} \approx 247$ Hz, 1F, $CF^AF^{A'}$; $F^{A'}$), −78.1 (br, 3F, C$F_3SO_3^-$), −80.3 (br, 3F, Co–CF_2CF_3), −83.9(dd, $^2J_{FF} \approx 247$ Hz,$^3J_{FP} \approx 30$ Hz 1F, $CF^AF^{A'}$; F^A). $^{31}P\{^1H\}$ NMR (121 MHz, CH_2Cl_2 with C_6D_6capillary) δ 30.0 (br, $\omega_{1/2} \approx 97$ Hz). MS [ESI (positive mode), solvent: MeOH] Calcd *m*/*z* (% intensity) for [CpCo(CF_2CF_3)(PPh_2Me)$^+$] 443.04 (100), 444.04 (22), 445.05 (2). Found: 443.04 (100), 444.04 (23).

[CpCo(CF_2CF_3)(CO)(PPh_2Me)][OTf] (from Int 2). Yield and NMR assignments could not be obtained because of peak overlap. IR: 2243 cm^{-1} (s, br, Co–*CO*).

CpCo($CF_2CF_2CF_3$)(OTf)(PPh_2Me) (from Int 2). Yield: 13% based on Co–$CF_2CF_2CF_3$ after 4 h. Only the F_β signals of the perfluoropropyl fragment could be assigned with certainty because of peak overlap. ^{19}F NMR (282 MHz, CH_2Cl_2 with C_6D_6capillary) δ −115.1 (d, $^2J_{FF}$ = 282 Hz, 1F, Co–$CF_2CF_2CF_3$), −116.8 (d, $^2J_{FF}$ = 282 Hz, 1F, Co–$CF_2CF_2CF_3$). MS [ESI (positive mode), solvent: MeOH] Calcd *m*/*z* (% intensity) for [CpCo($CF_2CF_2CF_3$)(PPh_2Me)$^+$]: 493.04 (100), 494.04 (23), 495.05 (3). Found: 493.04 (100), 494.04 (24). Calcd *m*/*z* (% intensity) for [$CF_3CF_2CF_2^+$]: 168.99 (100), 169.99 (3). Found: 168.99 (100), 169.99 (3).

[CpCo(CF_3)(CO)(PPh_2Me)][$FB(C_6F_5)_3$] (from Int 3). Yield: 60% based on CpCo(CF_3)$_2$(PPh_2Me) after 4 h. ^{19}F NMR (282 MHz, CH_2Cl_2 with C_6D_6capillary) δ 12.1 (d, $^3J_{FP}$ = 4 Hz, 3F, Co–CF_3). $^{31}P\{^1H\}$ NMR (121 MHz, CH_2Cl_2 with C_6D_6capillary) δ 33.0 (br, $\omega_{1/2} \approx 60$ Hz).

CpCo(CF_2CF_3)($FB(C_6F_5)_3$)(PPh_2Me) (from Int 3). Yield: 35% based on CpCo(CF_3)$_2$(PPh_2Me) after 4 h. ^{19}F NMR (282 MHz, CH_2Cl_2 with C_6D_6capillary) δ −76.7 (dd, $^2J_{FF} \approx 251$ Hz, $^3J_{FP} \approx 14$ Hz, 1F, $CF^AF^{A'}$; $F^{A'}$), −80.5 (br, 3F, Co–CF_2CF_3), −86.6 (dd, $^2J_{FF} \approx 251$ Hz, $^3J_{FP} \approx 35$ Hz 1F, $CF^AF^{A'}$; F^A). $^{31}P\{^1H\}$ NMR (121 MHz, CH_2Cl_2 with C_6D_6 capillary) δ 25.2 (br, $\omega_{1/2} \approx 96$ Hz).

[CpCo(CF_2CF_3)(CO)(PPh_2Me)][$FB(C_6F_5)_3$] (from Int 4). Yield and NMR assignments could not be obtained because of peak overlap.

CpCo($CF_2CF_2CF_3$)($FB(C_6F_5)_3$)(PPh_2Me) (from Int 4). Yield: 10% based on Co–$CF_2CF_2CF_3$ after 24 h. Only the F_β signals of the perfluoropropyl fragment could be assigned with

certainty because of peak overlap. ^{19}F NMR (282 MHz, $CH_2Cl_2$with C_6D_6 capillary) δ −112.6 (d, $^2J_{FF}$ = 284 Hz, 1F, Co–$CF_2CF_2CF_3$), −114.3 (d, $^2J_{FF}$ = 284 Hz, 1F, Co–$CF_2CF_2CF_3$).

General Procedure for the Catalytic Formation of *p*-Toluoyl Fluoride. The formation of *p*-toluoyl fluoride could be easily established by the growth of a sharp singlet at δ(^{19}F) = 16.5 ppm. The only other signals observed via ^{19}F NMR were a mixture of $CpCo(CF_3)(Cl)(PPh_2Me)$ and $CpCo(CF_3)(F)(PPh_2Me)$ (**6**). Yields for the formation of the target compound were established by integration to BTB. See Table 2.1 for yields and selected control experiments and Table B.4 for a full list.

Control Reactions with Various Fluoride Sources. To 0.8 mL of DCM in a vial was added AgF (92 mg, 0.72 mmol), CsF (110 mg, 0.72 mmol), KF (42 mg, 0.72 mmol), or CoF_3 (84 mg, 0.72 mmol). To this suspension were added *p*-toluoyl chloride (32 μL, 0.24 mmol) and BTB (18.6 μL, 0.12 mmol). The reaction was stirred vigorously (in the absence of light in the case of AgF) for 16 h and then transferred to an NMR tube with a C_6D_6 capillary.

Catalytic Reactions with Varying Catalyst Loadings. A stock solution (0.0152 M) was prepared for the reactions involving 5, 1, and 0.1 mol % $CpCo(CF_3)(I)(PPh_2Me)$ (**2**). The complex (40 mg, 0.076 mmol) was dissolved in DCM (5 mL), affording a dark-yellow-brown solution.

10 mol % Loading. $CpCo(CF_3)(I)(PPh_2Me)$ (**2**) (13 mg, 0.024 mmol) was added to a vial, along with AgF (92 mg, 0.72 mmol) and DCM (0.8 mL). To this dark-yellow-brown solution were added *p*-toluoyl chloride (32 μL, 0.24 mmol) and BTB (18.6 μL, 0.12 mmol). The reaction was

stirred vigorously (in the absence of light) for 4 h and then transferred to an NMR tube with a C_6D_6 capillary.

5 mol % Loading. $CpCo(CF_3)(I)(PPh_2Me)$ (**2**) (0.79 mL, 0.012 mmol) was added to a vial, along with AgF (92 mg, 0.72 mmol). To this dark-yellow-brown solution were added *p*-toluoyl chloride (32 μL, 0.24 mmol) and BTB (18.6 μL, 0.12 mmol). The reaction was stirred vigorously (in the absence of light) for 4 h and then transferred to an NMR tube with a C_6D_6 capillary.

1 mol % Loading. $CpCo(CF_3)(I)(PPh_2Me)$ (**2**) (0.16 mL, 0.0024 mmol) was added to a vial, along with AgF (92 mg, 0.72 mmol) and DCM (0.64 mL). To this pale-yellow-brown solution were added *p*-toluoyl chloride (32 μL, 0.24 mmol) and BTB (18.6 μL, 0.12 mmol). The reaction was stirred vigorously (in the absence of light) for 4 h and then transferred to an NMR tube with a C_6D_6 capillary.

0.1 mol % Loading. To 0.8 mL of DCM in a vial was added $CpCo(CF_3)(I)(PPh_2Me)$ (**2**) (79 μL, 0.0012 mmol) and AgF (92 mg, 0.72 mmol). To this pale-yellow-brown solution were added *p*-toluoyl chloride (32 μL, 0.24 mmol) and BTB (18.6 μL, 0.12 mmol). The reaction was stirred vigorously (in the absence of light) for 4 h and then transferred to an NMR tube with a C_6D_6 capillary.

Chapter 3

3.1 Context

As potent nucleophiles, it is somewhat surprising how little work has been published featuring the reactivity between N-heterocyclic carbenes (NHCs) and electrophilic alkenes. In fact, most of the reactivity analogous to this involves aldehydes and proceeds via the famed Breslow intermediate.[142,181–184] Fluoroalkenes are a very important class of electrophilic alkenes, having been featured in many different areas of chemistry (section 1.3). The presence of fluorinated substituents makes this class of alkenes very electron deficient, and this property makes them appealing candidates for reactions with nucleophiles, such as NHCs.

In Chapter 3, this reactivity will be explored and a total of 6 NHC fluoroalkene adducts with tetrafluoroethylene (TFE), hexafluoropropene (HFP) and trifluoroethylene (HTFE) will be presented. These adducts are easily prepared, in excellent yields, and stand out as a novel platform for C-F bond manipulation. Reactivity with vinylidene fluoride (VDF) also affords insight on the reaction pathway of this unique transformation. My pioneering studies within this area of research have led us to perform a more in-depth and fundamental study of the reactivity between NHCs and fluoroalkenes, and this is the subject of Chapter 5.

The NHC fluoroalkene adducts presented in Chapter 3 share certain structural characteristics with the Breslow intermediate, but their reactivity is markedly different. Specifically, the fluorine atoms on C_β were shown to be highly activated, and reacted readily with a Lewis acid to yield polyfluoroalkenyl imidazolium salts, the first examples of their kind. The ability of NHCs to activate fluoroalkenes towards direct substitution with organic nucleophiles via sp^2 C-F bond activation was demonstrated with pyrrolidine, to form a C_β-substituted enamine

and 4-dimethylaminopyridine (DMAP), to form a Cα-substituted pyridinium product. This facile sp^2 C-N bond formation, reminiscent of a Buchwald-Hartwig-type amination, was the basis for the entirety of the work presented in Chapter 4.

3.1.1 Published contributions

(1) **Leclerc, M. C.**; Gorelsky, S. I.; Gabidullin, B. M.; Korobkov, I.; Baker, R. T. *Chem. Eur. J.* **2016**, *22,* 8063-8067.

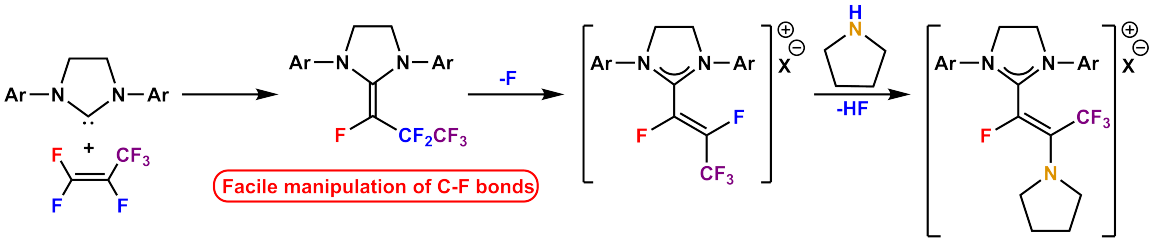

Selective reactions between nucleophilic N,N′-diaryl-heterocyclic carbenes (NHCs) and electrophilic fluorinated alkenes afford NHC fluoroalkenes in high yields. These stable compounds undergo efficient and selective fluoride abstraction with Lewis acids to give polyfluoroalkenyl imidazolium salts. These salts react at C_β with pyrrolidine to give ammonium fluoride-substituted salts, which give rise to conjugated imidazolium-enamine salts through loss of HF. Alternatively, reaction with 4-dimethylaminopyridine provides a C_α-pyridinium-substituted NHC fluoroalkene. These compounds were studied using multinuclear NMR spectroscopy, mass spectrometry, and X-ray crystallography. Insight into their electronic structure and reactivity was gained through the use of DFT calculations.

Author contributions: The manuscript was written by MCL. All compounds were synthesized and characterized by MCL. SIG performed the DFT calculations, BMG and IK performed the crystallography.

3.2 Selective Activation of Fluoroalkenes with N-Heterocyclic Carbenes: Synthesis of N-Heterocyclic Fluoroalkenes and Polyfluoroalkenyl Imidazolium Salts

3.2.1 Introduction

As quintessential examples of singlet carbenes, N-heterocyclic carbenes (NHCs) have been featured as ancillary ligands on early-, late-, and post-transition metals[262,263] and serve as key stabilizing elements for novel low-valent *p*-block element compounds.[146,147] The nucleophilicity of the carbon center, increased in part by the ability of nitrogen to π-donate into the empty *p*-orbital on carbon, makes this class of compounds especially useful for a variety of applications. Whereas metal NHC complexes serve as effective catalysts for alkene metathesis and C−C bond formation,[141] NHCs are themselves effective organocatalysts for a number of different processes including selective polymerization.[181,264] Since the isolation of the first stable NHC in 1991,[151] a variety of derivatives have been successfully synthesized and their nucleophilic character has made them attractive reaction partners with electrophiles.

Fluorine-containing compounds and materials have found numerous useful applications, ranging from non-stick polymers and refrigerants to solvents and lubricants.[265] Unfortunately, many of the methods still used to produce them employ toxic reagents such as HF, Cr^{VI}, and SbF_5[17] or environmentally persistent additives such as perfluorooctanoic acid.[126] The manipulation of C−F bonds is challenging owing to their large thermodynamic and kinetic stabilities.[14,15] As such, desirable methods for achieving controlled transformations of fluorinated organics are in great demand, particularly if these can be achieved without the use of synthetically complex reagents. Fluoroalkenes are an important class of electrophilic substrates, owing to the electron-withdrawing effects of various fluorinated substituents. Thus, the unique nucleophilic nature of NHCs makes them attractive candidates for reactions with electron deficient

fluoroalkenes. Herein, I demonstrate the utility of NHCs for the selective and efficient manipulation of fluoroalkene C−F bonds.

3.2.2 Results and discussion

3.2.2.1 Synthesis and characterization of NHC fluoroalkenes

We report on the formation and facile isolation of a variety of NHC fluoroalkene compounds. When common NHCs such as SIPr [1,3-bis-(2,6-diisopropylphenyl)imidazolidin-2-ylidene] or SIMes [1,3-bis-(2,4,6-trimethylphenyl)imidazolidin-2-ylidene] are treated with a variety of fluorinated alkenes, the corresponding NHC fluoroalkenes are easily obtained and isolated (Scheme 3.1). The first report of this reaction was mentioned in the Supporting Information of work performed by Ogoshi et al.,[266] wherein the product derived from the reaction of IPr [1,3-bis-(2,6-diisopropylphenyl)imidazol-2-ylidene] and tetrafluoroethylene (TFE) was a by-product of their organometallic reactions. During the preparation of this manuscript, work by Arduengo et al. demonstrating the reactivity between imidazol(in)-2-ylidenes and fluoroalkenes was published, including the study of compound **2a**.[267]

Scheme 3.1. Synthetic scheme for N-heterocyclic fluoroalkenes

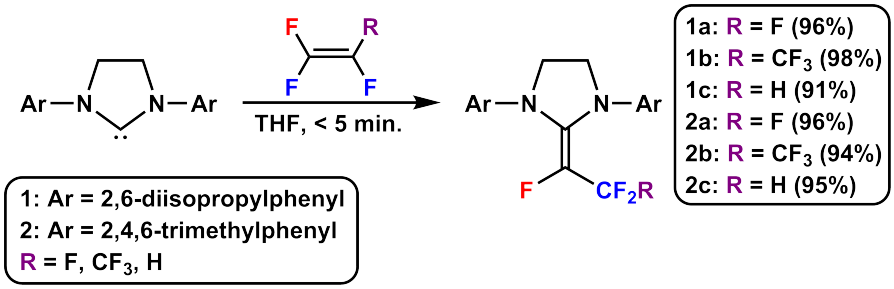

The reactions introduced here proceed at room temperature in THF or toluene and afford a single product, except when using vinylidene fluoride (VDF), which gives rise to two products, one of which has not yet been identified. The other product has been characterized as the salt formed between the fluoroalkenyl cation and a fluoride counteranion (Scheme 3.2, **Int 1**).

Scheme 3.2. Proposed reaction pathway for NHC fluoroalkene formation from HFP (red) and VDF (blue). See Experimental Section (3.2.4) for more information on the observation of Int 1 through ^{1}H and ^{19}F NMR analysis

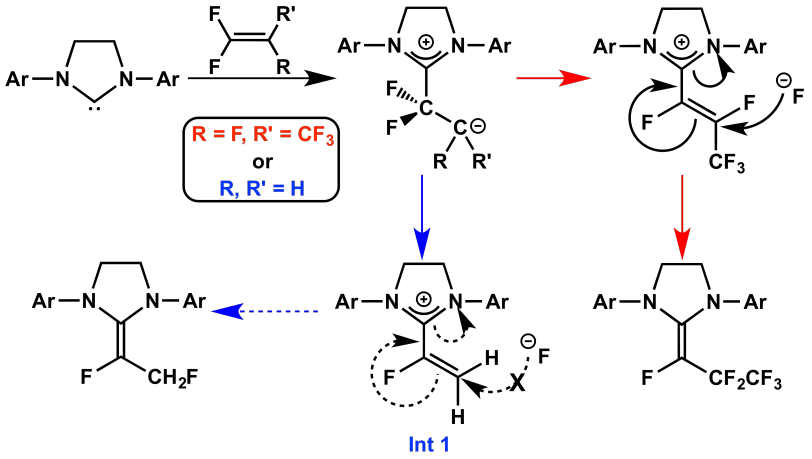

The direct observation of **Int 1** through ^{1}H and ^{19}F NMR spectroscopy supports the previously proposed mechanistic pathway.[267] TFE, hexafluoropropene (HFP), and trifluoroethylene (HTFE) derivatives have been isolated in high yields and characterized by ^{1}H, ^{13}C{^{1}H}, and ^{19}F NMR spectroscopy, as well as mass spectrometry. Additionally, compound **1b** has been studied through X-ray crystallography (Figure 3.1).

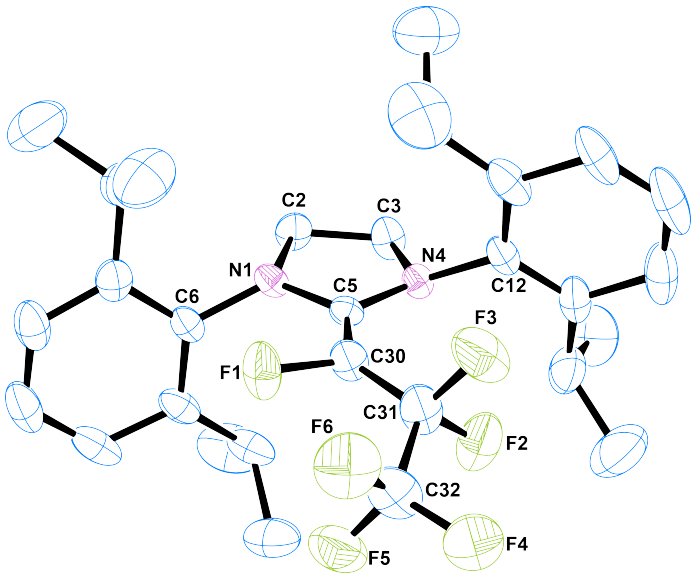

Figure 3.1. Crystallographic representation of **1b** with 30% probability thermal ellipsoids. H atoms and a second molecule within the unit cell are omitted for clarity. Selected bond lengths and angles are presented in the Supporting Information of the original publication.[268]

These products can be thought of as fluorinated variations on the Breslow intermediate (Figure 3.2), an important product arising from the reaction between an NHC and an aldehyde.[182] First proposed in 1958,[183] and successfully isolated in 2012,[184] this enamine-like compound, along with its many variations, represents an important example of umpolung in organic chemistry[182] and has demonstrated rich reactivity towards electrophilic substrates, such as aldehydes, esters, and Michael acceptors.[141] These results have provided systems capable of transesterification and transition metal-free polymerization.[181] Contrary to the classic Breslow intermediate, the compounds presented here do not react with benzaldehyde as might be expected, even with heating. Instead, the fluorine atoms on the carbon directly bound to the alkene are activated. Indeed, the average C−F bond length of the difluoromethylene group in **1b** is 1.37 Å, compared to the average C−F bond length of the trifluoromethyl group of 1.33 Å. Additionally, the C=C

bond in **1b** is the same length (1.35 Å) as the analogous bond in the crystallographically studied IMes=CH(OMe) and SIMes=CH(OMe), supporting the lack of a major contribution from a zwitterionic/azolium form.[184] Finally, the lack of symmetry observed through ^{1}H NMR for all derivatives of **1** and **2** supports the alkene form being favoured. Variable temperature NMR experiments using [D_8]toluene with heating up to 100 °C, coupled with NOESY experiments, demonstrated that there was no appreciable rotation around the C=C bond, and the appearance of symmetry was not observed.

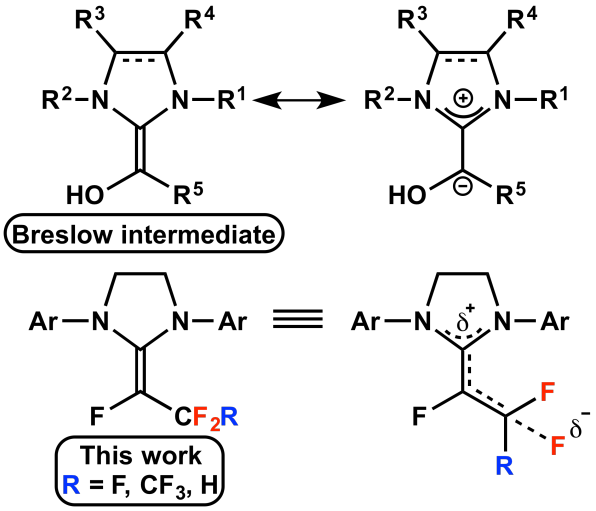

Figure 3.2. Comparison between NHC fluoroalkenes presented in this work and the Breslow intermediate.

There are only a few examples of analogous hydrocarbon N-heterocyclic alkenes (NHCAs) and their reactivity in the literature.[269] Since the first report by Kaska et al. in 1979,[270] further work has established the ability of NHCAs to perform organic transformations,[271–274] including organocatalysis[275] and transition metal-free polymerization,[276–278] as well as their reactivity towards main-group elements,[279–282] transition metal complexes,[283–286] and

lanthanides.[287] Additionally, it has been shown that NHCs react with dimethyl fumarate to form stable NHCAs, proposed to occur through a 1,2-H shift.[288,289]

It is interesting to note that these addition reactions do not proceed with all fluoroalkenes; no reaction was observed with *cis*-1,2-difluoroethylene, even upon heating for extended periods of time. It is probable that the latter lacks a sufficiently electrophilic carbon center; the reactive gases all have at least one electrophilic CF_2 fragment, which is presumably where the initial attack occurs.

On addition of the gas to a solution of the free NHC, an immediate and vivid colour change from the initial pale yellow solution occurs and persists for approximately 15 seconds before changing to the final colour of the respective products (see Experimental Section (3.2.4) for more details on the colour changes for the different reactions). This phenomenon is proposed to arise from a short-lived zwitterionic intermediate, leading to a delocalized cation within the N-C-N fragment of the heterocycle, and a terminal carbanion on the remaining fragment (Scheme 3.2). Subsequent expulsion of a fluoride to form the corresponding alkenyl salt, followed by attack of the fluoride on the electrophilic terminal fragment affords the final product. Presumably, the vinyl fragment formed in the reaction with VDF is not sufficiently electrophilic for the fluoride to attack, bearing two hydrogen substituents and lacking the fluorine or trifluoromethyl substituents present in the other systems. Attempts to observe the proposed zwitterion intermediates by low-temperature NMR spectroscopy have not yet been successful.[290]

Interestingly, of the gases used in this study, only TFE reacts cleanly with the unsaturated IPr, as demonstrated previously.[266] Reactions with HFP and HTFE led to a multitude of different products. The importance of the electronic and steric properties of the NHC in these reactions is also apparent. Reactions with smaller and electronically different alkyl NHCs (IMe_4 and I^iPr) led

to NHC decomposition and complex mixtures that were not studied further.[291] When a bulkier alkyl NHC was used (I^{t}Bu), no reaction whatsoever was observed. Heating to 65 °C led to decomposition of the NHC. The TFE derivatives (**1a** and **2a**) are stable in the presence of water (20 equiv in CD_3CN), but the HFP derivatives (**1b** and **2b**) and the HTFE derivatives (**1c** and **2c**) react quickly under the same conditions to form several different products that have not yet been fully characterized.

3.2.2.2 Synthesis and characterization of polyfluoroalkenyl imidazolium salts

I next examined the C−F bond reactivity of these NHC fluoroalkenes. Treatment with a Lewis acid, boron trifluoride (diethyl etherate), in diethyl ether at room temperature leads to the formation of novel polyfluoroalkenyl imidazolium salts in high yields within 2 h (Scheme 3.3). These compounds can be readily isolated as off-white powders due to their insolubility in diethyl ether. Selective abstraction of a fluoride occurs in all cases, leading to a single product. These reactions also occur cleanly and in high yields using Me_3SiOTf (OTf = SO_3CF_3) as a Lewis acid in DCM. The selective activation of alkyl C−F bonds by Lewis acids has previously been demonstrated through the use of silylium-carborane-,[292] boron-,[293] and aluminium-based[294] catalysts.

Scheme 3.3. Synthetic scheme for polyfluoroalkenyl imidazolium salts

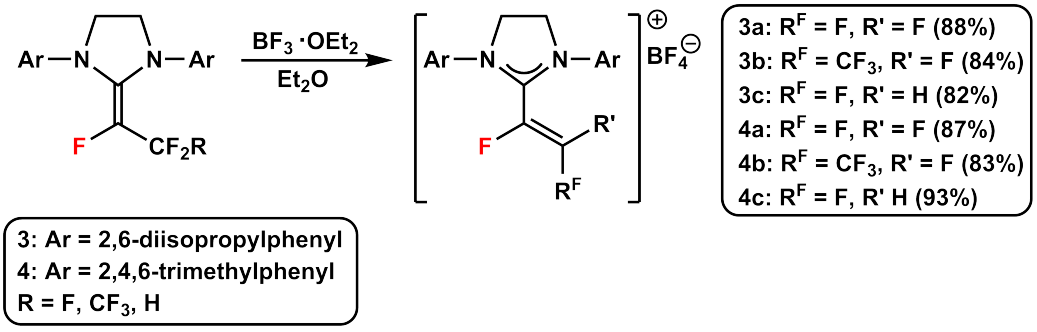

The molecular structure of **3b** (Figure 3.3, left) clearly demonstrates the importance of aryl ring rotation away from the alkenyl fragment, as well as the bending of the isopropyl groups to relieve further steric strain. Furthermore, the CF_3 substituent is located *trans* with respect to the NHC fragment. This phenomenon is also present in solution, where a single isomer is observed through NMR analysis, and the orientation is further corroborated by convincing coupling constant values. To the best of our knowledge, there is only one analogous compound in the literature, formed by the presence of adventitious water.[267] Additionally, Lehmann et al.[284] have characterized a boron adduct that shares certain structural characteristics to these polyfluoroalkenyl systems. This fluoride abstraction leads to several decomposition products when the previously reported IPr derivative of the TFE adduct undergoes reaction.[266] Importantly, there does not appear to be any formation of the corresponding polyfluoroalkenyl imidazolium salt.

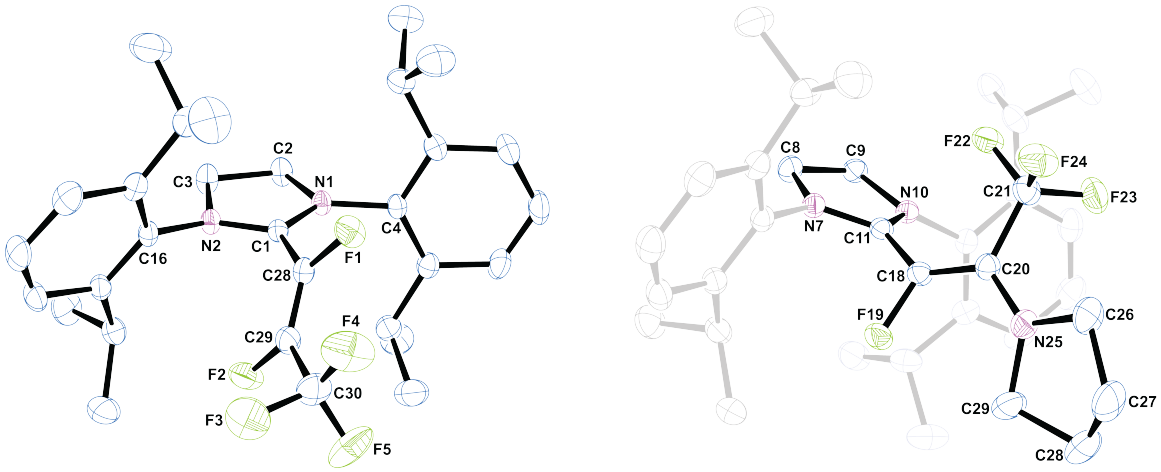

Figure 3.3. Crystallographic representation of **3b** (left) and **6** (right) with 30% probability thermal ellipsoids. H atoms and tetrafluoroborate anions are omitted for clarity. There is disorder within the tetrafluoroborate and trifluoromethyl fragments due to rotation of **3b**. One molecule each of toluene, dichloromethane and pentane was removed from **6**. Selected bond lengths and angles are presented in the Supporting Information of the original publication.[268]

3.2.2.3 Reactivity of polyfluoroalkenyl imidazolium salts with nitrogen-based nucleophiles

The polyfluoroalkenyl imidazolium salts are likely to exhibit rich reactivity with nucleophiles. In fact, reaction of **3b** with pyrrolidine in DCM or MeCN leads to the selective substitution of one fluorine on C_β with an ammonium fluoride fragment (Scheme 3.4, compound **5**). Further treatment with DBU affords the pyrrolidine-containing species **6**. The alkenyl fragment is retained, as supported by the symmetry observed through ^{1}H and ^{19}F NMR analysis, which persists from the initial salts. Furthermore, NMR coupling constants and crystal structure studies (Figure 3.3, right) convincingly demonstrate that the pyrrolidine substituent is oriented *trans* with respect to the N-heterocyclic fragment, presumably for steric relief, and only one isomer is observed using NMR spectroscopy.

Scheme 3.4. Reaction of 3b with pyrrolidine to form ammonium fluoride derivative 5 and further reaction with 1,8-diazabicyclo[5.4.0]undec-7-ene (DBU) to form enamine product 6 (iminium resonance form is also shown). The reaction of 4b with DMAP is also shown.

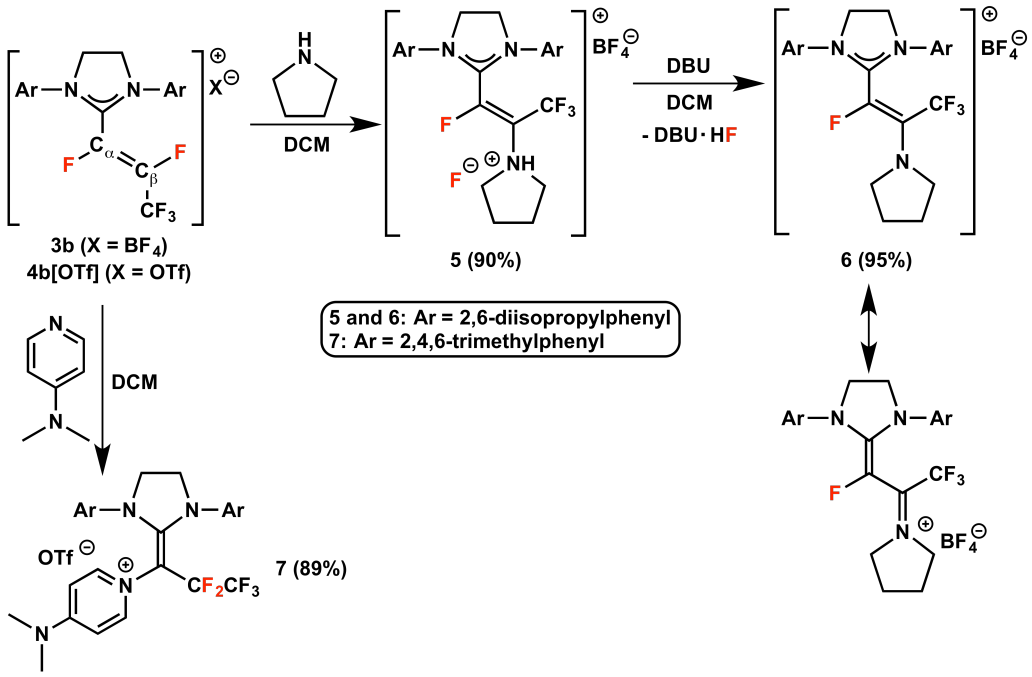

Alternatively, reaction between the triflate salt of **4 b**, (**4 b[OTf]**)[295] and 4-dimethylaminopyridine (DMAP) in dichloromethane affords a novel C_α-pyridinium-substituted N-heterocyclic fluoroalkene (Scheme 3.4, compound **7**) in high yield. The perfluoroethyl fragment obtained with the original HFP adduct is reformed and net substitution at C_α occurs. Without the option of HF loss, it is possible that, following an initial nucleophilic attack of the DMAP on C_β, a [1,2] fluoride shift occurs from C_α to C_β and the DMAP is finally able to bind to C_α. Alternatively, it is possible that nucleophilic attack of DMAP on C_β is reversible, and occasional nucleophilic attack on C_α, followed by expulsion of fluoride and a subsequent attack of this fluoride at the electrophilic C_β could lead to **7**. Although reactivity with HFP derivatives is demonstrated as an example, the different derivatives presented in this work also give rise to analogous products under the same conditions.

It is interesting to note that, although DMAP is very reactive towards **4 b[OTf]**, closely related substrates do not react under the same conditions, or with added heating. Specifically, triethylamine, pyridine, and *N,N*-dimethylaniline are not reactive, presumably due to the fact that their respective pK_b values are all larger than those of DMAP, and thus less basic.[296] It appears unlikely that steric hindrance plays a role with these structurally related compounds, and so relative basicity is seemingly the governing factor.

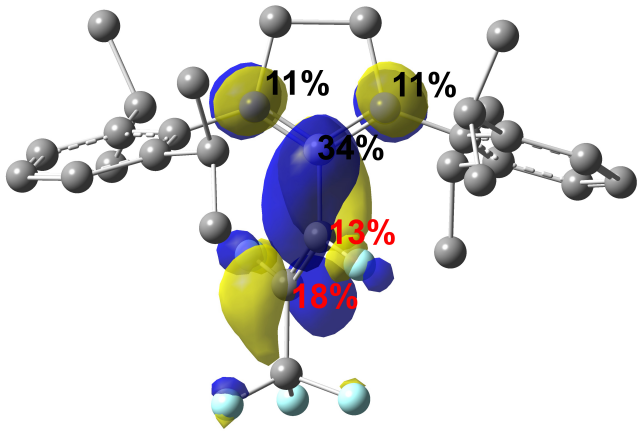

Figure 3.4. LUMO of **3b** with % atomic contributions (alkenyl atom contributions are shown in red). H atoms are omitted for clarity.

DFT[208] calculations at the B3LYP[209,210]/TZVP[297] level were used to study the electronic structure of neutral **1b**, and cationic **3b** and **6**, as well as to better understand the selectivity observed in the reactivity of **3b** with pyrrolidine. The single-point calculations of the geometries corresponding to the X-ray structures with C−H bond lengths adjusted to 1.08 Å were conducted to evaluate the electron density distribution, the bond orders, and the electrostatic potential (ESP). The HOMO of **1b** is localized on the NHC C=C bond coupled with the lone pairs of the nitrogen atoms (Figure C.1a). The LUMO of **1b** is localized on the aryl group (Figure C.1b). The Mayer bond order[223] for the formally double C=C bond is 1.66. The ESP of **1b** (Figure C.1c) indicates a polarization of the molecule, where the positive area is located near the backbone of the NHC and the negative area is located near the F and CF_2CF_3 groups.

The HOMO of **3b** is localized on the aryl group (Figure C.2a). The LUMO of **3b**, which is responsible for reactivity of **3b** with nucleophiles, is localized on the FC=CF bond, coupled with the π orbitals of the N-C-N atoms of the NHC (Figure 3.4). The alkenyl carbon bonded to the NHC, C_α, has a contribution of 13 % to the LUMO, whereas the other alkenyl carbon, C_β, has

a larger contribution of 18 %. This makes C_β a preferential site for a nucleophilic attack. As such, DFT supports the selectivity observed experimentally in this work with pyrrolidine. The nature of the DMAP reactivity is currently under study in our laboratory, but direct attack at C_α is still being considered as a possible reaction pathway due to the relatively small difference between the C_α and C_β contributions to the LUMO (*ca*. 5%). The Mayer bond order for the FC=CF bond is 1.70, which indicates a fairly weak delocalization of the double-bond character in **3b**. The ESP of **3b** (Figure C.2c) indicates that the positive potential (attractive to a negative charge) is located around the outside surface of the cation. The HOMO and the LUMO of **6** are localized on the FC=C(CF_3) bond (Figure C.3), with the LUMO showing stronger coupling with the π orbitals of the N-C-N atoms of the NHC (Figure C.3a). Relative to **3b**, the π orbitals of the C(4)=C(5) bond in **6** are more strongly coupled with the adjacent bonds and, as a result, the Mayer bond order for the formal double C(4)=C(5) bond is only 1.43. Similar to the ESP of **3**, that of cationic **6** (Figure C.3c) indicates that the positive potential (attractive to a negative charge) is located around the outside surface of the cation.

3.2.3 Conclusions

In conclusion, I have synthesized and fully characterized six N-heterocyclic fluoroalkenes, and demonstrated that their exposure to Lewis acids leads to the clean, selective, and high-yielding formation of six polyfluoroalkenyl imidazolium salts. Initial studies demonstrate the importance of an electrophilic carbon center on the fluoroalkenes for the initial attack of the NHC to occur. These polyfluoroalkenyl imidazolium salts react cleanly with pyrrolidine at C_β to afford ammonium fluoride derivatives, which can be further deprotonated to their enamine forms. Additionally, reaction with DMAP generates a pyridinium-substituted N-

heterocyclic fluoroalkene through formal C_α substitution. Insight into the electronic structure and the reactivity of these new compounds was gained through DFT calculations. Studies on the reactivity of these compounds are currently underway in our laboratory.

3.2.4 Experimental

3.2.4.1 General considerations

All manipulations were carried out using standard Schlenk techniques or in an MBraun glove box. All glassware was oven-dried at >150 °C for a minimum of 2 hours prior to use, or flame-dried using a torch. Toluene, hexanes, 1,2-dichloroethane (DCE), tetrahydrofuran (THF) and diethyl ether (DEE) were dried on columns of activated alumina using a J. C. Meyer (formerly Glass Contour®) solvent purification system. Dichloromethane (DCM) and chloroform-d ($CDCl_3$) were dried by refluxing over calcium hydride under a nitrogen flow, followed by distillation and filtration through a column of activated alumina (ca. 10 wt. %). Benzene-d6 (C_6D_6) was dried by standing over activated alumina (ca. 10 wt. %) overnight, followed by filtration. All solvents were stored over activated (heated at 250 °C for >6 h under vacuum) 4Å molecular sieves. The following chemicals were used as purchased, without further purification: 2,6-diisopropylaniline (Alfa Aesar, 90+%), 2,4,6-trimethylaniline (Alfa Aesar, 98%), triethyl orthoformate (Alfa Aesar, 98%), glacial acetic acid (Alfa Aesar, 99+%), *N,N*-diisopropylethylamine (Alfa Aesar, 99%), boron trifluoride diethyl etherate (Strem Chemicals, 47-48% boron trifluoride), trimethylsilyl trifluoromethanesulfonate (Sigma Aldrich, 98+%), 1,3-diisopropylimidazolium chloride (Strem Chemicals, 97%), 1,3-di-tert-butylimidazol-2-ylidene (Strem Chemicals, 98%), 1-hexanol (Sigma Aldrich, 98%), 3- hydroxy-2-butanone (Sigma Aldrich, 98+%), *N,N*'-dimethylthiourea (Sigma Aldrich, 99%), potassium (Sigma Aldrich, 98%),

potassium *tert*-butoxide (Strem Chemicals, 98%), sodium hydride (Strem Chemicals, 60% in oil), hexafluoropropene (HFP) (SynQuest Labs, 98.5%), trifluoroethylene (HTFE) (SynQuest Labs, 98%), 1,1-difluoroethylene (VDF) (SynQuest Labs, 99%), cis-1,2-difluoroethylene (SynQuest Labs, 95%). Tetrafluoroethylene (TFE) was made by pyrolysis of polytetrafluoroethylene (PTFE) (Scientific Polymer Products, powdered) under vacuum, using a slightly modified literature procedure [10-20 mTorr, 650 °C, 15 g scale, product stabilized with (*R*)-(+)-limonene (Aldrich, 97%), giving TFE of ≥ 97% purity]. The following imidazolium chloride salts were prepared according to literature procedure: 1,3-bis(2,6-diisopropylphenyl)imidazol-2-ylidene ([SIPr][HCl]),[298] 1,3-bis(2,4,6- trimethylphenyl)imidazol-2-ylidene ([SIMes][HCl]),[298] 1,3,4,5-tetramethylimidazol-2-ylidene (IMe_4).[299] Free N-heterocyclic carbenes were synthesized from the appropriate imidazolium chloride salts by reaction with sodium hydride (2 equiv) and catalytic potassium *tert*-butoxide (5 mol%) in THF overnight with vigorous stirring. The resulting solution was filtered through Celite with THF washings and the solvent removed in vacuo to afford flaky white solid of pure free N-heterocyclic carbene in high yields (>95%). The free N-heterocyclic carbenes were stored in a glove box freezer at -35 °C. ^{1}H, $^{13}C\{^{1}H\}$, ^{19}F and $^{19}F\{^{1}H\}$ NMR spectra were recorded on either a Bruker Avance 300 or Bruker Avance II 300 spectrometer at room temperature. ^{1}H NMR spectra were referenced to the residual proton peaks associated with the deuterated solvents (C_6D_6 = 7.16 ppm, $CDCl_3$ = 7.26 ppm). ^{13}C NMR spectra were referenced to the signal associated with $CDCl_3$ (77.16 ppm). It is important to note that ^{13}C NMR signals coupled to ^{19}F nuclei are broadened out significantly, and although coupling constant values and multiplicity can sometimes be extracted it is often impossible to do so. As such, the data is presented to the best of our ability and all efforts are made to avoid any ambiguity in the presentation of the data. ^{19}F and $^{19}F\{^{1}H)$ NMR spectra were referenced to internal 1,3-

bis(trifluoromethyl)benzene (BTB) (Aldrich, 99%, deoxygenated by purging with nitrogen and stored over 4Å molecular sieves), set to - 63.5ppm. ^{1}H NMR data for BTB: (300 MHz, C_6D_6) δ 6.60 (m, 1H, Ar-5-H), 7.12 (m, 2H, Ar-4,6-H), 7.76 (m, 1H, Ar-2-H). A Micromass Q- ToF 1 (positive mode) was used for electrospray ionization (ESI), with samples diluted to ca. 5 μg/mL in acetonitrile. A Mel-Temp II was used for the determination of melting points.

3.2.4.2 Synthesis and characterization

Synthesis of N-heterocyclic fluoroalkenes. In a glove box, SIPr or SIMes (1.00 g) was dissolved in THF (10 mL) and transferred to a 100 mL tubular Schlenk flask with a stir bar. On a Schlenk line, the flask was degassed with three freeze-pump-thaw cycles. The appropriate gas was added to a pressure of 10 psig (set on a gas regulator fitted to the cylinder) and the flask was sealed under pressure. The solution was stirred for 1 hour and the solvent was then removed *in vacuo*. The vessel was transferred to a glove box and DEE (*ca.* 15 mL) was used to dissolve the product. The solution was filtered through Celite® with DEE washings until washings came out clear (*ca.* 10 mL). The filtrate was pumped down to dryness to afford pure product as a solid. Note that a small amount of unidentified crystalline precipitate forms in all reactions during the synthesis of **1-2**. The solid was isolated on a frit without Celite® during separate runs and weighed out to determine its impact on the overall yield.

SIPr=CF(CF_3) (1a). TFE was used as the reaction gas. Upon TFE addition, the colour of the solution changed from colourless to pale pink-red. The colour persisted for approximately 15 seconds before changing to dark yellow-brown. A small amount of unidentified crystalline precipitate could be seen in the reaction flask, accounting for *ca.* 2% of the yield loss. The product was isolated as an off-white solid. Yield: 1.21 g, 96% based on SIPr. mp: 114 °C. ^{1}H

NMR (300 MHz, C_6D_6) δ 1.17 (d, $^3J_{HH}$ ≈ 6.9 Hz, 6H, CH(CH_3)$_2$), 1.24 (d, $^3J_{HH}$ ≈ 6.9 Hz, 6H, CH(CH_3)$_2$), 1.35 (d, $^3J_{HH}$ ≈ 6.8 Hz, 6H, CH(CH_3)$_2$) 1.37 (d, $^3J_{HH}$ ≈ 6.7 Hz, 6H, CH(CH_3)$_2$), 3.24-3.50 (ov m, 8H, N-CH_2CH_2-N and CH(CH$_3$)$_2$), 7.05-7.21 (ov m, 6H, Ar-*H*). ^{13}C{^{1}H} NMR (101 MHz, C_6D_6) δ 22.96, 23.90, 24.75, 26.01, 28.49, 28.77, 51.89, 53.66, 118.57 (dq, $^1J_{CF}$ ≈ 45 Hz, $^2J_{CF}$ ≈ 200 Hz, SIPr=CF(*C*F$_3$)), 121.82 (d, $^1J_{CF}$ ≈ 34 Hz, SIPr=*C*F(CF$_3$)), 124.08, 124.35, 128.07, 128.36, 137.44 (d, $^2J_{CF}$ ≈ 4 Hz, SIPr(*C*)=CF(CF$_3$)), 138.96 (br), 146.57 (br dm), 147.17 (br), 147.20, 147.23. ^{19}F NMR (282 MHz, C_6D_6) δ -60.8 (d, $^3J_{FF}$ ≈ 16 Hz, 3F, SIPr=CF(C*F*$_3$)), -203.1 (q, $^3J_{FF}$ ≈ 16 Hz, 1F, SIPr=C*F*(CF$_3$)). MS [ESI (positive mode), solvent: MeCN] Calc. *m/z* (% intensity) for [SIPr=CF(CF$_3$) + H$^+$]: 491.30 (100), 492.31 (31), 493.21 (3). Found *m/z* (% intensity): 491.3049 (100), 492.3103 (34), 493.3164 (5).

SIPr=CF(CF$_2$CF$_3$) (1b). HFP was used as the reaction gas. Upon HFP addition, the colour of the solution changed from colourless to deep purple. The colour persisted for approximately 5 seconds before changing to orange. A small amount of unidentified crystalline precipitate could be seen in the reaction flask, accounting for *ca.* 1% of the yield loss. The product was isolated as an orange solid. Yield: 1.36 g, 98% based on SIPr. mp: 146-147 °C. ^{1}H NMR (300 MHz, C_6D_6) δ 1.16 (d, $^3J_{HH}$ ≈ 6.9 Hz, 6H, CH(CH_3)$_2$), 1.22 (d, $^3J_{HH}$ ≈ 7.0 Hz, 6H, CH(CH_3)$_2$), 1.35 (ov dd, 12H, CH(CH_3)$_2$), 3.31-3.50 (ov m, 8H, N-CH_2CH_2-N and CH(CH$_3$)$_2$), 7.01-7.19 (ov m, 6H, Ar-*H*). ^{13}C{^{1}H} NMR (101 MHz, C_6D_6) δ 22.86, 23.20, 23.52, 23.69, 24.9, 25.22, 26.07, 26.27, 28.56, 28.74, 29.11, 29.41, 51.83, 53.16, 53.64, 56.44, 123.99, 124.29, 124.41, 125.56, 128.01, 128.41, 129.12, 132.14, 137.24 (d, $^2J_{CF}$ ≈ 4 Hz, SIPr(*C*)=CF(CF$_2$CF$_3$)), 145.64, 146.10, 147.07, 147.28, 157.62 (d). ^{19}F NMR (282 MHz, C_6D_6) δ -83.1 (dt, $^3J_{FF}$ ≈ 4 Hz, $^4J_{FF}$ ≈ 15 Hz, 3F, SIPr=CF(CF$_2$C*F*$_3$)), -106.7 (dq, $^3J_{FF}$ ≈ 4 Hz, $^3J_{FF}$ ≈ 19 Hz, 2F, SIPr=CF(C*F*$_2$CF$_3$)), -206.3 (tq, $^3J_{FF}$ ≈ 19 Hz, $^4J_{FF}$ ≈ 15 Hz, 1F, SIPr=C*F*(CF$_2$CF$_3$)). ESI-MS for this compound consistently provided

a m/z value of 528.29, which is 12 less than the expected product ion mass of $[SIPr{=}CF(CF_2CF_3)]^+$. The same result was obtained for compound **2b**.

SIPr=CF(CF$_2$H) (1c). HTFE was used as the reaction gas. Upon HTFE addition, the colour of the solution changed from colourless to pale brown. The colour persisted for approximately 5 seconds before changing to a very dark brown. A small amount of unidentified crystalline precipitate could be seen in the reaction flask, accounting for *ca.* 4% of the yield loss. The product was isolated as a brown solid. Yield: 1.10 g, 91% based on SIPr. mp: 162-165 °C. ^{1}H NMR (300 MHz, C_6D_6) δ 1.15 (d, $^3J_{HH}$ ≈ 6.8 Hz, 6H, CH(CH_3)$_2$), 1.27 (d, $^3J_{HH}$ ≈ 7.0 Hz, 6H, CH(CH_3)$_2$), 1.34 (d, $^3J_{HH}$ ≈ 6.9 Hz, 6H, CH(CH_3)$_2$) 1.39 (d, $^3J_{HH}$ ≈ 6.9 Hz, 6H, CH(CH_3)$_2$), 3.22-3.42 (ov m, 4H, CH(CH$_3$)$_2$), 3.32 (ov s, 4H, N-CH_2CH_2-N), 5.51 (dt, $^2J_{FH}$ ≈ 52 Hz, $^3J_{FH}$ ≈ 22 Hz, 1H, SIPr=CF(CF$_2$$H$)), 6.98-7.27 (ov m, 6H, Ar-H). ^{13}C{^{1}H} NMR (101 MHz, C_6D_6) δ 23.99, 25.11, 29.39, 55.05, 125.98, 130.19, 132.15, 136.14 (dd), 145.42, 147.66 (dd), 156.83 (dd). ^{19}F NMR (282 MHz, C_6D_6) δ -113.6 (dd, $^2J_{FH}$ ≈ 52 Hz, $^3J_{FF}$ ≈ 18 Hz, 1F, SIPr=CF(CF_2H)), -207.6 (dt, $^3J_{FH}$ ≈ 22 Hz, $^3J_{FF}$ ≈ 18 Hz, 1F, SIPr=CF(CF$_2$H)). ^{19}F{^{1}H} NMR (282 MHz, C_6D_6) δ -113.6 (d, $^3J_{FF}$ ≈ 18 Hz, 1F, SIPr=CF(CF_2H)), -207.6 (t, $^3J_{FF}$ ≈ 18 Hz, 1F, SIPr=CF(CF$_2$H)). This compound was not viable for ESI-MS but the analogous **2c** gave excellent high resolution ESI-MS results.

SIMes=CF(CF$_3$) (2a). TFE was used as the reaction gas. Upon TFE addition, the colour of the solution changed from pale yellow to pale brown. The colour persisted for approximately 30 seconds before changing to dark brown. A small amount of unidentified crystalline precipitate could be seen in the reaction flask, accounting for *ca.* 2% of the yield loss. The product was isolated as a brown solid. Yield: 1.27 g, 96% based on SIMes. mp: 175 °C. ^{1}H NMR (300 MHz, C_6D_6) δ 2.09 (s, 3H, Ar-*p*-CH_3), 2.11 (s, 3H, Ar-*p*-CH_3), 2.26 (s, 6H, Ar-*o*-CH_3), 2.27 (s, 6H, Ar-

o-CH_3), 3.06 (s, 4H, N-CH_2CH_2-N), 6.73 (s, 2H, Ar-*H*), 6.76 (s, 2H, Ar-*H*). ^{13}C{^{1}H} NMR (101 MHz, C_6D_6) δ 18.09, 18.19, 21.04, 21.09, 50.16, 51.90, 118.94(dq, $^2J_{CF}$ ≈ 196 Hz, SIMes=CF(*C*F_3)), 123.48 (dq, $^1J_{CF}$ ≈ 264 Hz, SIMes=*C*F(CF_3)), 129.32, 129.56, 135.87 (br), 136.09 (d), 136.67, 136.99, 137.95 (d), 138.82 (br), 144.20 (dq, $^2J_{CF}$ ≈ 17 Hz, $^3J_{CF}$ ≈ 2 Hz, SIMes(*C*)=CF(CF_3)). ^{19}F NMR (282 MHz, C_6D_6) δ -61.9 (d, $^3J_{FF}$ ≈ 15 Hz, 3F, SIMes=CF(C*F*$_3$)), -206.6 (q, $^3J_{FF}$ ≈ 15 Hz, 1F, SIMes=C*F*(CF_3)). MS [ESI (positive mode), solvent: MeCN] Calc. *m/z* (% intensity) for [SIMes=CF(CF_3) + H^+]: 407.21 (100), 408.21 (25), 409.22 (3). Found *m/z* (% intensity): 407.2073 (100), 408.2138 (28), 409.2218 (5).

SIMes=CF(CF_2CF_3) (2b). HFP was used as the reaction gas. Upon HFP addition, the colour of the solution changed from pale yellow to pink. The colour persisted for approximately 5 seconds before changing to deep orange-red. A small amount of unidentified crystalline precipitate could be seen in the reaction flask, accounting for *ca.* 3% of the yield loss. The product was isolated as a red-brown solid. Yield: 1.40 g, 94% based on SIMes. mp: 151 °C. ^{1}H NMR (300 MHz, C_6D_6) δ 2.07 (s, 3H, Ar-*p*-CH_3), 2.08 (s, 3H, Ar-*p*-CH_3), 2.27 (ov s, 12H, Ar-*o*-CH_3), 3.05 (s, 4H, N-CH_2CH_2-N), 6.73 (s, 2H, Ar-*H*), 6.76 (s, 2H, Ar-*H*). ^{13}C{^{1}H} NMR (101 MHz, C_6D_6) δ 17.70, 17.99, 20.80, 20.86, 50.05, 51.78, 114.20 (dq, SIMes=CF(CF_2*C*F_3)), 118.38 (dt, $^1J_{CF}$ ≈ 193 Hz, $^2J_{CF}$ ≈ 37 Hz, SIMes=*C*F(CF_2CF_3)), 120.56 (td, $^1J_{CF}$ ≈ 40 Hz, SIMes=CF(*CF2*CF*3*)), 129.07, 129.36, 135.55 (t), 135.73 (d), 136.46, 136.78, 137.69 (d), 138.98 (t), 146.18 (d, $^2J_{CF}$ ≈ 17 Hz, SIMes(*C*)=CF(CF_2CF_3). ^{19}F NMR (282 MHz, C_6D_6) δ -83.1 (dt, $^3J_{FF}$ ≈ 5 Hz, $^4J_{FF}$ ≈ 15 Hz, 3F, SIMes=CF(CF_2C*F*$_3$)), -108.9 (dq, $^3J_{FF}$ ≈ 5 Hz, $^3J_{FF}$ ≈ 20 Hz, 2F, SIMes=CF(C*F*$_2$$CF_3$)), -208.9 (tq, $^3J_{FF}$ ≈ 20 Hz, $^4J_{FF}$ ≈ 15 Hz, 1F, SIMes=C*F*(CF_2CF_3)). ESI-MS for this compound consistently provided a m/z value of 444.20, which is 12 less than the expected product ion mass of [SIMes=CF(CF_2CF_3)]$^+$. The same result was obtained for compound **1b**.

SIMes=CF(CF_2H) (2c). HTFE was used as the reaction gas. Upon HTFE addition, the colour of the solution changed from colourless to dark brown. The colour persisted for approximately 15 seconds before changing to bright yellow. A small amount of unidentified crystalline precipitate could be seen in the reaction flask, accounting for *ca.* 3% of the yield loss. The product was isolated as a pale brown solid. Yield: 1.20 g, 95% based on SIMes. mp: 145 °C. ^{1}H NMR (300 MHz, C_6D_6) δ 2.02 (s, 3H, Ar-*p*-CH_3), 2.13 (s, 3H, Ar-*p*-CH_3), 2.18 (s, 6H, Ar-*o*-CH_3), 2.30 (s, 6H, Ar-*o*-CH_3), 3.09 (m, 4H, N-CH_2CH_2-N), 6.67 (m, 2H, Ar-*H*), 5.51 (dt, $^2J_{FH} \approx 53$ Hz, $^3J_{FH} \approx 21$ Hz, 1H, SIMes=CF(CF_2H)) 6.76 (m, 2H, Ar-*H*). ^{13}C{^{1}H} NMR (101 MHz, C_6D_6) δ 17.78, 17.92, 21.05, 21.19, 50.08, 50.26, 111.08 (br d), 129.11, 129.55, 130.15, 130.30, 131.07, 136.21, 136.60, 136.82, 136.94, 137.55, 138.07, 139.99, 142.49 (br d), 172.13 (d). ^{19}F NMR (282 MHz, C_6D_6) δ -112.8 (dd, $^2J_{FH} \approx 53$ Hz, $^3J_{FF} \approx 17$ Hz, 1F, SIMes=CF(CF_2H)), -210.9 (dt, $^3J_{FH} \approx 21$ Hz, $^3J_{FF} \approx 17$ Hz, 1F, SIMes=C*F*(CF_2H)). ^{19}F{^{1}H} NMR (282 MHz, C_6D_6) δ -112.8 (d, $^3J_{FF} \approx 17$ Hz, 1F, SIMes=CF(CF_2H)), -210.9 (t, $^3J_{FF} \approx 17$ Hz, 1F, SIMes=C*F*(CF_2H)). MS [ESI (positive mode), solvent: MeCN] Calc. *m/z* (% intensity) for [SIMes=CF(CF_2H) + H^+]: 389.22 (100), 390.22 (25), 391.23 (3). Found *m/z* (% intensity): 389.2180 (100), 390.2393 (25), 391.2745 (12).

Observation of [SIPr-CF=CH_2][F] (Int 1). In a glove box, SIPr (20 mg, 0.051 mmol) was dissolved in THF (0.8 mL) and transferred to a septum cap NMR tube. Using a syringe, 3 mL of gas was removed from the headspace in the NMR tube. From a regulator fitted with a septum, 3 mL of VDF was added via syringe to the NMR tube. Upon VDF addition, the colour of the solution changed from pale yellow to bright yellow, and formation of precipitate was observed. The NMR tube was shaken vigorously and left to sit for 30 minutes. The solvent was decanted, and the NMR tube washed with THF (*ca*. 2 mL). The off-white solid in the NMR tube was

dissolved in $CDCl_3$ to give a pale yellow solution, containing [SIPr-CF=CH_2][F] (**Int 1**). Note that the THF-soluble product that was decanted from the NMR tube is still unidentified. ^{1}H NMR (300 MHz, $CDCl_3$) δ 1.21 (d, $^3J_{HH}$ ≈ 6.8 Hz, 12H, CH(CH_3)$_2$), 1.36 (d, $^3J_{HH}$ ≈ 6.8 Hz, 12H, CH(CH_3)$_2$), 3.22-3.42 (ov m, 4H, CH(CH$_3$)$_2$), 2.95 (sep, $^3J_{HH}$ ≈ 6.8 Hz, 4H, CH(CH$_3$)$_2$), 4.73 (dd, $^2J_{HH}$ ≈ 5.2 Hz, $^3J_{HF}$ ≈ 46.1 Hz, 1H, SIPr-CF=CH_2, *trans*), 4.76 (s, 4H, N-CH_2CH_2-N), 5.34 (dd, $^2J_{HH}$ ≈ 5.2 Hz, $^3J_{HF}$ ≈ 17.8 Hz, 1H, SIPr-CF=CH_2, *cis*), 7.21-7.47 (ov m, 6H, Ar-*H*). ^{19}F NMR (282 MHz, $CDCl_3$) δ -106.0 (dd, $^3J_{FH}$ ≈ 17.8 Hz (*cis*), $^3J_{FH}$ ≈ 46.18 Hz (*trans*), 1F, SIPr-C*F*=CH_2), -160.7 (br, 1F, [SIPr-CF=CH_2][*F*]). ^{19}F{^{1}H} NMR (282 MHz, $CDCl_3$) δ -106.0 (s, 1F, SIPr-C*F*=CH_2), -160.7 (br, 1F, [SIPr-CF=CH_2][*F*]).

Synthesis of polyfluoroalkenyl imidazolium salts. In a glove box, the corresponding N-heterocyclic fluoroalkene (1.00 mmol) was dissolved in DEE (10 mL) in a vial with a stir bar. To this stirring solution was added BF_3·OEt_2 (124 μL, 1.00 mmol). Formation of precipitate is observed immediately upon addition, as the resulting polyfluoroalkenyl imidazolium salts are completely insoluble in DEE. The suspension was stirred for 1 hour and the product was isolated as a fine powder by filtration on a frit and washing with DEE (*ca.* 10 mL). Note that in the ^{19}F NMR analysis of these compounds, the -*cis* and -*trans* labels are used with respect to the fluorine geminal to the N-heterocylic carbene fragment.

[SIPr-CF=CF_2][BF_4] (3a). The product was isolated as a white powder. Yield: 491 mg, 88% based on SIPr=CF(CF_3). mp: 203-205 °C. ^{1}H NMR (300 MHz, $CDCl_3$) δ 1.21 (d, $^3J_{HH}$ ≈ 6.8 Hz, 12H, CH(CH_3)$_2$), 1.32 (d, $^3J_{HH}$ ≈ 6.8 Hz, 12H, CH(CH_3)$_2$), 2.87 (sep, $^3J_{HH}$ ≈ 6.8 Hz, 4H, CH(CH$_3$)$_2$), 4.66 (s, 4H, N-CH_2CH_2-N), 7.19-7.50 (ov m, 6H, Ar-*H*). ^{13}C{^{1}H} NMR (101 MHz, $CDCl_3$) δ 23.41, 25.98, 29.48, 55.12, 125.70, 125.83, 127.80 (d, $^1J_{CF}$ ≈ 117 Hz, SIPr-*C*F=CF_2),

129.18, 132.07, 132.50, 132.84, 145.89, 146.24 (d), 147.25 (d). ^{19}F NMR (282 MHz, $CDCl_3$) δ -81.6 (dd, $^2J_{FF}$ ≈ 25 Hz, $^3J_{FF}$ ≈ 36 Hz, 1F, SIPr-CF=C*F*$_2$, *cis*), -96.1 (dd, $^2J_{FF}$ ≈ 25 Hz, $^3J_{FF}$ ≈ 118 Hz, 1F, SIPr-CF=C*F*$_2$, *trans*), -154.2 (br, 4F, B*F*$_4^-$), -182.7 (dd, $^3J_{FF}$ ≈ 36 Hz, $^3J_{FF}$ ≈ 118 Hz, 1F, SIPr-C*F*=CF$_2$). MS [ESI (positive mode), solvent: MeCN] Calc. *m/z* (% intensity) for [SIPr-CF=CF$_2^+$ + HF]: 491.30 (100), 492.31 (31), 493.31 (3). Found *m/z* (% intensity): 491.0821 (100), 492.0813 (30), 493.0872 (5).

[SIPr-CF=CF(CF$_3$)][BF$_4$] (3b). The product was isolated as a light pink powder. Yield: 511 mg, 84% based on SIPr=CF(CF$_2$CF3). mp: 248-249 °C. ^{1}H NMR (300 MHz, $CDCl_3$) δ 1.24 (d, $^3J_{HH}$ ≈ 6.8 Hz, 12H, CH(C*H*$_3$)$_2$), 1.35 (d, $^3J_{HH}$ ≈ 6.8 Hz, 12H, CH(C*H*$_3$)$_2$), 2.89 (sep, $^3J_{HH}$ ≈ 6.8 Hz, 4H, C*H*(CH$_3$)$_2$), 4.77 (s, 4H, N-C*H*$_2$C*H*$_2$-N), 7.20-7.53 (ov m, 6H, Ar-*H*). ^{13}C{^{1}H} NMR (101 MHz, $CDCl_3$) δ 23.20, 26.28, 29.46, 55.49, 125.73, 128.33, 132.40, 146.13, 155.83 (dd). ^{19}F NMR (282 MHz, $CDCl_3$) δ -69.0 (dd, $^3J_{FF}$ ≈ 8 Hz, $^4J_{FF}$ ≈ 19 Hz, 3F, SIPr-CF=CF(C*F*$_3$), *cis*), -148.9 (dq, $^3J_{FF}$ ≈ 8 Hz, $^3J_{FF}$ ≈ 142 Hz, 1F, SIPr-CF=C*F*(CF$_3$), *trans*), -150.1 (dq, $^3J_{FF}$ ≈ 8 Hz, $^4J_{FF}$ ≈ 142 Hz, 1F, SIPr-C*F*=CF(CF$_3$)), -154.1 (br, 4F, B*F*$_4^-$). MS [ESI (positive mode), solvent: MeCN] Calc. *m/z* (% intensity) for [SIPr-CF=CF(CF$_3$)$^+$]: 521.29 (100), 522.30 (32), 523.30 (5). Found *m/z* (% intensity): 521.2903 (100), 522.3006 (36), 523.1482 (7).

[SIPr-CF=CF(H)][BF$_4$] (3c). The product was isolated as a grey powder. Yield: 443 mg, 82% based on SIPr=CF(CF$_2$H). mp: 201-206 °C. ^{1}H NMR (300 MHz, $CDCl_3$) δ 1.26 (d, $^3J_{HH}$ ≈ 6.8 Hz, 12H, CH(C*H*$_3$)$_2$), 1.42 (d, $^3J_{HH}$ ≈ 6.8 Hz, 12H, CH(C*H*$_3$)$_2$), 2.98 (sep, $^3J_{HH}$ ≈ 6.8 Hz, 4H, C*H*(CH$_3$)$_2$), 4.67 (s, 4H, N-C*H*$_2$C*H*$_2$-N), 6.23 (dd, $^2J_{FH}$ ≈ 68 Hz, $^3J_{FH}$ ≈ 15 Hz, 1H, SIPr-CF=CF(*H*), *trans*), 7.30-7.58 (ov m, 6H, Ar-*H*). ^{13}C{^{1}H} NMR (101 MHz, $CDCl_3$) δ 23.99, 25.12, 29.39, 55.05, 125.99, 130.20 (d), 132.15, 136.08 (dd), 145.43, 147.74 (dd), 156.84 (dd,

$^{2}J_{CF} \approx 22$ Hz, $^{3}J_{CF} \approx 5$ Hz, SIPr(*C*)-CF=CF(H)). ^{19}F NMR (282 MHz, $CDCl_3$) δ -128.4 (dd, $^{2}J_{FH} \approx 68$ Hz, $^{3}J_{FF} \approx 13$ Hz, 1F, SIPr-CF=C*F*(H), *cis*), -148.4 (ov dd, $^{3}J_{FH} \approx 15$ Hz, $^{3}J_{FF} \approx 13$ Hz, 1F, SIPr-C*F*=CF(H)), -154.2 (br, 4F, BF_4^-). ^{19}F{^{1}H} NMR (282 MHz, $CDCl_3$) δ -128.4 (d, $^{3}J_{FF} \approx 13$ Hz, 1F, SIPr-CF=C*F*(H), *cis*), -148.4 (d, $^{3}J_{FF} \approx 13$ Hz, 1F, SIPr-C*F*=CF(H)), -154.2 (br, 4F, BF_4^-). MS (from [SIPr-CF=CF(H)][OTf] [ESI (positive mode), solvent: MeCN] Calc. *m/z* (% intensity) for [SIPr-CF=CF(H)$^+$ - 2H$^+$]: 451.29 (100), 452.30 (31), 453.30 (3). Found *m/z* (% intensity): 451.2992 (100), 452.3190 (18), 453.3185 (2).

[SIMes-CF=CF$_2$][BF$_4$] (4a). The product was isolated as a pale brown powder. Yield: 413 mg, 87% based on SIMes=CF(CF_3). mp: 148-151 °C. ^{1}H NMR (300 MHz, $CDCl_3$) δ 2.31 (s, 6H, Ar-*p*-CH_3), 2.33 (s, 12H, Ar-*o*-CH_3), 4.69 (s, 4H, N-CH_2CH_2-N), 6.98 (s, 4H, Ar-*H*). ^{13}C{^{1}H} NMR (101 MHz, $CDCl_3$) δ 17.36, 21.18, 52.54, 129.91, 130.53, 134.97, 141.40, 156.73 (br d). ^{19}F NMR (282 MHz, $CDCl_3$) δ -80.8 (dd, $^{2}J_{FF} \approx 29$ Hz, $^{3}J_{FF} \approx 37$ Hz, 1F, SIMes-CF=CF_2, *cis*), -97.6 (dd, $^{2}J_{FF} \approx 29$ Hz, $^{3}J_{FF} \approx 118$ Hz, 1F, SIMes-CF=CF_2, *trans*), -153.6 (br, 4F, BF_4^-), -185.5 (dd, $^{3}J_{FF} \approx 37$ Hz, $^{3}J_{FF} \approx 118$ Hz, 1F, SIMes-C*F*=CF_2). MS [ESI (positive mode), solvent: MeCN] Calc. *m/z* (% intensity) for [SIMes-CF=CF_2^+]: 387.20 (100), 388.21 (25), 389.21 (3). Found *m/z* (% intensity): 387.2048 (100), 388.1945 (18), 389.2458 (2).

[SIMes-CF=CF(CF$_3$)][BF$_4$] (4b). The product was isolated as an orange-brown powder. Yield: 435 mg, 83% based on SIMes=CF(CF_2CF_3). mp: 146-147 °C. ^{1}H NMR (300 MHz, $CDCl_3$) δ 2.31 (s, 6H, Ar-*p*-CH_3), 2.35 (s, 12H, Ar-*o*-CH_3), 4.78 (s, 4H, N-CH_2CH_2-N), 6.99 (s, 4H, Ar-*H*).^{13}C{^{1}H} NMR (101 MHz, $CDCl_3$) δ 17.17, 21.09, 52.82, 116.46 (ddd), 129.04, 130.45, 135.09, 136.94 (ddq), 141.64, 144.6 (br dm), 155.56 (dd, $^{2}J_{CF} \approx 25$ Hz, $^{3}J_{CF} \approx 4$ Hz, SIMes(*C*)-CF=CF(CF_3)). ^{19}F NMR (282 MHz, $CDCl_3$) δ -69.0 (dd, $^{3}J_{FF} \approx 9$ Hz, $^{4}J_{FF} \approx 20$ Hz, 1F, SIMes-

CF=CF(CF_3), *cis*), -149.9 (dq, $^3J_{FF}$ ≈ 9 Hz, $^3J_{FF}$ ≈ 142 Hz, 1F, SIMes-CF=C*F*(CF_3), *trans*), -151.9 (dq, $^3J_{FF}$ ≈ 142 Hz, $^4J_{FF}$ ≈ 20 Hz, 1F, SIMes-C*F*=CF(CF_3)), -153.5 (br, 4F, BF_4^-). MS (from [SIMes-CF=CF(CF_3)][OTf] [ESI (positive mode), solvent: MeCN] Calc. *m/z* (% intensity) for [SIMes-CF=CF(CF_3)$^+$]: 437.20 (100), 438.20 (27), 439.21 (3). Found *m/z* (% intensity): 437.2016 (100), 438.2048 (28), 439.2081 (4).

[SIMes-CF=CF(CF_3)][OTf] (4b[OTf]). In a glove box, **2b** (1.00 g, 2.18 mmol) was dissolved in DCM (10 mL) in a vial with a stir bar. To this stirring solution was added Me_3SiOTf (400 µL, 2.18 mmol). A slight colour change from dark red to a slightly more red-orange was observed immediately. The reaction was stirred for 1 hour and DEE (10 mL) was added, causing immediate precipitation of the product. The vial was kept in the freezer (-35 °C) for 1 hour and the product was isolated as a pale red powder by filtration on a frit and washing with DEE (*ca.* 10 mL). Yield: 1.06 g, 91% based on SIMes=CF(CF_2CF_3). mp: 190 °C. ^{1}H NMR (300 MHz, $CDCl_3$) δ 2.32 (s, 6H, Ar-*p*-CH_3), 2.35 (s, 12H, Ar-*o*-CH_3), 4.84 (s, 4H, N-CH_2CH_2-N), 7.00 (s, 4H, Ar-*H*). ^{19}F NMR (282 MHz, $CDCl_3$) δ -69.0 (dd, $^3J_{FF}$ ≈ 9 Hz, $^4J_{FF}$ ≈ 20 Hz, 1F, SIMes-CF=CF(CF_3), *cis*), 78.7 (s, 3F, $SO_3CF_3^-$), -149.9 (dq, $^3J_{FF}$ ≈ 9 Hz, $^3J_{FF}$ ≈ 142 Hz, 1F, SIMes-CF=C*F*(CF_3), *trans*), -152.0 (dq, $^3J_{FF}$ ≈ 142 Hz, $^4J_{FF}$ ≈ 20 Hz, 1F, SIMes-C*F*=CF(CF_3)).

[SIMes-CF=CF(H)][BF_4] (4c). The product was isolated as an off-white powder. Yield: 423 mg, 93% based on SIMes=CF(CF_2H). mp: 206-208 °C. ^{1}H NMR (300 MHz, $CDCl_3$) δ 2.31 (s, 6H, Ar-*p*-CH_3), 2.34 (s, 12H, Ar-*o*-CH_3), 4.59 (s, 4H, N-CH_2CH_2-N), 6.42 (dd, $^2J_{FH}$ ≈ 67 Hz, $^3J_{FH}$ ≈ 15 Hz, 1H, SIMes-CF=CF(*H*), *trans*) 6.99 (s, 4H, Ar-*H*). ^{13}C{^{1}H} NMR (101 MHz, $CDCl_3$) δ 17.42, 21.17, 52.19, 130.66, 130.68 (ov s), 134.73, 135.20 (dd), 141.34, 146.13 (dd), 156.56 (dd, $^2J_{CF}$ ≈ 24 Hz, $^3J_{CF}$ ≈ 6 Hz, SIMes(*C*)-CF=CF(H)). ^{19}F NMR (282 MHz, $CDCl_3$) δ -130.1 (dd, $^2J_{FH}$ ≈ 67

Hz, $^{3}J_{FF}$ ≈ 14 Hz, 1F, SIMes-CF=C*F*(H), *cis*), -152.6 (ov dd, $^{3}J_{FF}$ ≈ 14 Hz, $^{3}J_{FH}$ ≈ 15 Hz, 1F, SIMes-C*F*=CF(H)), -153.9 (br, 4F, BF_4^-). $^{19}F\{^{1}H\}$ NMR (282 MHz, $CDCl_3$) δ -130.1 (d, $^{3}J_{FF}$ ≈ 14 Hz, 1F, SIMes-CF=C*F*(H), *cis*), -152.6 (d, $^{3}J_{FF}$ ≈ 14 Hz, 1F, SIMes-C*F*=CF(H)), -153.9 (br, 4F, BF_4^-). MS (from [SIMes-CF=CF(H)][OTf] [ESI (positive mode), solvent: MeCN] Calc. *m/z* (% intensity) for [SIMes-CF=CF(H)$^+$ - 2H$^+$]: 367.20 (100), 368.20 (25), 369.20 (3). Found *m/z* (% intensity): 367.2069 (100), 368.2139 (37), 369.2231 (5).

Synthesis of [SIPr-CF=C(CF_3)(pyrrolidine)][BF_4][HF] (5). In a glove box, [SIPr-CF=CF(CF_3)][BF_4] (**3b**) (300 mg, 0.49 mmol) was dissolved in DCM (4 mL) in a vial with a stir bar. To this stirring solution was added pyrrolidine (41 µL, 0.49 mmol). A colour change from light yellow to bright yellow was observed within seconds. The reaction was stirred for 1 hour and hexanes (10 mL) were added, causing precipitation of the product. The mixture was placed in the freezer (-35 °C) for 30 minutes and the product was isolated as a crystalline, bright-yellow solid by filtration on a frit and washing with hexanes (*ca.* 10 mL). Yield: 300 mg, 90% based on [SIPr-CF=CF(CF_3)][BF_4]. Note that in the ^{19}F NMR analysis of these compounds, the -*cis* and -*trans* labels are used with respect to the fluorine geminal to the N-heterocylic carbene fragment. mp: 206-207 °C. ^{1}H NMR (300 MHz, $CDCl_3$) δ 1.26 (br, 6H, CH(CH_3)$_2$), 1.29 (br, 6H, CH(CH_3)$_2$), 1.31 (br, 6H, CH(CH_3)$_2$), 1.34 (br, 6H, CH(CH_3)$_2$), 1.72 (m, 4H, pyrrolidine N-CH_2-CH_2), 3.00 (sep, $^{3}J_{HH}$ ≈ 7.3 Hz, 4H, C*H*(CH_3)$_2$, 3.10 (m, 4H, imidazole N-CH_2CH_2-N), 3.36 (br, 1H, pyrrolidine N-*H*), 4.62 (dm, 4H, pyrrolidine N-CH_2-CH_2), 7.20-7.49 (ov m, 6H, Ar-*H*). $^{13}C\{^{1}H\}$ NMR (101 MHz, $CDCl_3$) δ 22.8, 22.9, 25.0, 26.4, 26.6, 28.9, 29.5, 51.4, 54.1, 124.9, 125.5, 130.7, 131.3, 145.7, 146.9, 161.2 (d, $^{2}J_{CF}$ ≈ 26 Hz, SIPr-*C*F=C(CF_3)(pyrrolidine)). ^{19}F NMR (282 MHz, $CDCl_3$) δ - 63.6 (br d, $^{4}J_{FF}$ ≈ 4 Hz, 3F, SIPr-CF=C(CF_3)(pyrrolidine), *cis*), -133.4 (br, 1F, *F*), -148.0 (br, 1F, SIPr-C*F*=C(CF_3)(pyrrolidine)), -154.5 (br, 4F, BF_4^-). $^{19}F\{^{1}H\}$

NMR (282 MHz, $CDCl_3$) δ - 63.6 (d, $^4J_{FF}$ ≈ 4 Hz, 3F, SIPr-CF=C(C*F*$_3$)(pyrrolidine), *cis*), -133.4 (br, 1F, *F*), -148.0 (q, $^4J_{FF}$ ≈ 4 Hz, 1F, SIPr-C*F*=C(CF_3)(pyrrolidine)), -154.5 (br, 4F, B*F*$_4^-$). MS [ESI (positive mode), solvent: MeCN] Calc. *m/z* (% intensity) for [SIPr-CF=C(CF_3)(pyrrolidine)$^+$ - H^+]: 572.36 (100), 573.37 (37), 574.37 (7). Found *m/z* (% intensity): 572.3575 (100), 573.3724 (44), 574.3568 (8).

Synthesis of [SIPr-CF=C(CF_3)(pyrrolidine)][BF_4] (6). In a glove box, [SIPr-CF=C(CF_3)(pyrrolidine)][BF_4][HF] (**5**) (100 mg, 0.15 mmol) was dissolved in DCM (2 mL) in a vial with a stir bar. To this stirring solution was added 1,8-diazabicyclo[5.4.0]undec-7-ene (DBU) (23 μL, 0.15 mmol). A colour change from bright yellow to orange-yellow was observed within several minutes. The reaction was stirred for 1 hour and the solvent was removed in vacuo. The orange residue was dissolved in a minimal amount of DCM (2 mL) and filtered through a Celite pipette. Hexanes (10 mL) were added to the filtered solution, causing precipitation of the product. The mixture was placed in the freezer (-35 °C) for 30 minutes and the product was isolated as an orange powder by filtration on a frit and washing with hexanes (*ca.* 10 mL). Yield: 94 mg, 95% based on [SIPr-CF=C(CF_3)(pyrrolidine)][BF_4][HF]. Note that in the ^{19}F NMR analysis of these compounds, the -*cis* and -*trans* labels are used with respect to the fluorine geminal to the N-heterocylic carbene fragment. mp: 163-165 °C (decomposition). ^{1}H NMR (300 MHz, $CDCl_3$) δ 1.16-1.39 (ov d, 24H, CH(C*H*$_3$)$_2$), 1.72 (m, 4H, pyrrolidine N-C*H*$_2$-CH_2), 3.00 (ov sep, 4H, C*H*(CH_3)$_2$, 3.10 (m, 4H, imidazole N-C*H*$_2$C*H*$_2$-N), 4.62 (dm, 4H, pyrrolidine N-CH_2-C*H*$_2$), 7.20-7.49 (ov m, 6H, Ar-*H*). ^{19}F NMR (282 MHz, $CDCl_3$) δ -63.6 (d, $^4J_{FF}$ ≈ 4 Hz, 3F, SIPr-CF=C(C*F*$_3$)(pyrrolidine), *cis*), -147.8 (br q, 1F, SIPr-C*F*=C(CF_3)(pyrrolidine)), -154.5 (br, 4F, B*F*$_4^-$).

Synthesis of [SIMes=C(DMAP)(CF_2CF_3)][OTf] (7). In a glove box, [SIMes-CF=CF(CF_3)][OTf] (100 mg, 0.17 mmol) was dissolved in DCM (2 mL) in a vial with a stir bar. To this stirring solution was added 4-dimethylaminopyridine (DMAP) (21 mg, 0.17 mmol). A slight colour change from dark red to a slightly lighter red was observed over 10 minutes. The reaction was stirred for 1 hour and DEE (6 mL) was added, causing precipitation. The product was isolated as a yellow powder by filtration on a frit and washing with DEE (*ca*. 10 mL). Yield: 110 mg, 89% based on [SIMes-CF=CF(CF_3)][OTf]. mp: 127 °C. ^{1}H NMR (300 MHz, $CDCl_3$) δ 2.18 (s, 6H, Ar-*p*-CH_3), 2.23 (s, 3H, Ar-*p*-CH_3), 2.28 (s, 3H, Ar-*o*-CH_3), 2.37 (s, 6H, Ar-*o*-CH_3), 3.18 (s, 6H, N(CH_3)$_2$), 3.81 (dm, 4H, N-CH_2CH_2-N), 6.41 (m, 2H, Ar-*m*-H (N-CH-C*H*-C)), 6.78 (s, 2H, Ar-*H*), 6.92 (s, 2H, Ar-*H*), 7.29 (m, 2H, Ar-*o*-H (N-C*H*-CH-C)). ^{13}C{^{1}H} NMR (101 MHz, $CDCl_3$) δ 18.3, 18.6, 20.9, 21.0, 40.5, 50.1. 52.4, 106.8, 129.7, 130.2, 135.5, 135.8, 136.6, 137.3, 138.0, 138.7, 147.1, 155.9, 157.1 (t, $^3J_{CF}$ ≈ 2 Hz, [SIMes(*C*)=C(DMAP)(CF_2CF_3)][OTf]. ^{19}F NMR (282 MHz, $CDCl_3$) δ -78.6 (s, 3F, $SO_3CF_3^-$), -82.6 (t, $^3J_{FF}$ ≈ 4 Hz, 3F, [SIMes=C(DMAP)(CF_2CF_3)][OTf], -100.7 (q, $^3J_{FF}$ ≈ 4 Hz, 2F, [SIMes=C(DMAP)(CF_2CF_3)][OTf]. MS [ESI (positive mode), solvent: MeCN] Calc. *m/z* (% intensity) for [SIMes=C(DMAP)(CF_2CF_3)$^+$ + Na]: 582.28 (100), 583.28 (34), 584.28 (5). Found *m/z* (% intensity): 582.2758 (100), 583.2789 (36), 584.2820 (5).

Chapter 4

4.1 Context

Due to the difficulties involved in manipulating C-F bonds (section 1.1.1), new methods enabling these transformations with relative ease are very desirable. Specifically, platforms capable of achieving this without the need for a transition metal or harsh conditions are preferred. Fluoroalkenes have the potential to be a particularly useful synthon for building larger molecules incorporating fluorine,[300] but their direct reactivity with organics remains relatively difficult to control and selectivity is a primary concern (section 1.3.2). These issues, coupled with the obvious limitations involved in manipulating fluorinated gases, have hindered this area of research. As such, N-heterocyclic fluoroalkenes emerge as conveniently synthesized and stable building blocks for the indirect incorporation of fluoroalkenes into larger organic fragments.

Having established the formation of polyfluoroalkenyl imidazolium salts in Chapter 3, I sought to expand on the substitution chemistry observed with pyrrolidine and 4-dimethylaminopyridine (DMAP). Previous insight from TD-DFT studies indicated that the C_β position in these salts should be the preferred sight of a nucleophilic attack. As such, Chapter 4 will feature facile, transition-metal-free substitution reactions to form C-E bonds (E = C, N, O, S) and C-M bonds (M = Mn, Mo), further establishing the ability of an NHC to direct and control substitutions on fluoroalkenes. In all cases, a single isomer of the C_β-substituted product was obtained, the formation of which is seemingly governed by sterics.

Reactivity with 1-methylimidazole provides an imidazolium product, analogous to the one previously observed with DMAP. Trace moisture was found to induce double C-F bond activation, leading to the formation of an α,β-unsaturated trifluoromethyl ketone. Although the

reverse reaction is known, this type of transformation had not been demonstrated before this report. This double C-F bond activation was also observed in the reactivity between an HTFE-derived fluoroalkene adduct and sodium cyclopentadienide. The use of manganese- and molybdenum-based nucleophiles led to the formation of transition metal complexes featuring fluorovinyl-imidazolium ligands, a unique scaffold that might prove to possess interesting properties within the context of push-pull alkenes.

4.1.1 Published contributions

(1) **Leclerc, M. C.**; Gabidullin, B. M.; Da Gama, J. G.; Daifuku, S. L.; Iannuzzi, T. E.; Neidig, M. L.; Baker, R. T. *Organometallics* **2017**, *36*, 849-857.

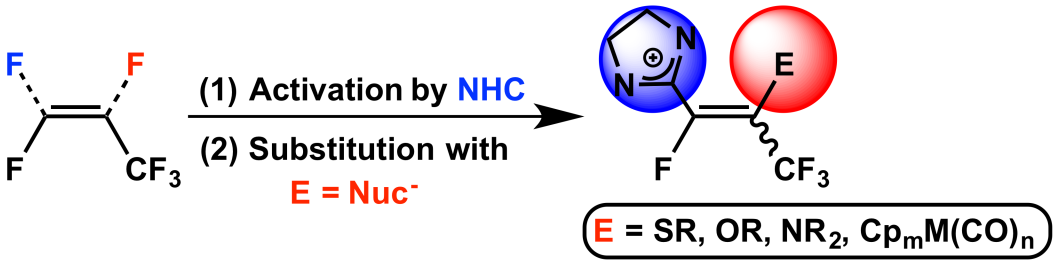

Herein, a recently reported polyfluoroalkenyl imidazolium salt is shown to react with nitrogen-, oxygen- and sulfur-based nucleophiles at the C_β position in a stereoselective and regioselective fashion, without the use of a transition metal. In contrast, reactivity with 1-methylimidazole demonstrates net substitution at C_α. This product reacts quantitatively with water, affording clean transformation of a difluoromethylene group to give an α,β-unsaturated trifluoromethyl ketone. Further reactivity studies demonstrate that the difluoromethyl fragment of an N-heterocyclic fluoroalkene is capable of direct C–C bond formation with NaCp through loss of sodium fluoride and double C–F bond activation (Cp = cyclopentadienide). TD-DFT

calculations of this product indicate that both the HOMO and LUMO are of mixed π/π* character and are delocalized over the N-heterocyclic and Cp fragments, giving rise to a very intense absorption feature in the UV–vis spectrum. Additionally, two carbonylmetalate-substituted fluorovinyl imidazolium complexes featuring Mn and Mo were isolated and fully characterized.

Author contributions: The manuscript was written by MCL. All compounds were synthesized and characterized by MCL. Preliminary experiments involving complexes **10-12** were performed by JGD, under the supervision of MCL. BMG performed the crystallography. SLD, TEI and MLN performed the DFT calculations.

4.2 Transition-Metal-Free Formation of C-E Bonds (E = C, N, O, S) and Formation of C-M Bonds (M = Mn, Mo) from N-Heterocyclic Carbene Mediated Fluoroalkene C-F Bond Activation

4.2.1 Introduction

The introduction of fluorinated groups to organic molecules continues to be a very active field of research, in large part owing to the important physiological and chemical properties that can be imparted upon fluorination.[23,24,26,27] Indeed, many drugs currently being produced contain at least one fluorine atom.[5] Because naturally occurring fluorinated organics are extremely rare, it is vital to develop efficient and general methods for the formation of C–F bonds. Typically, fluorine is inserted into a molecular framework via nucleophilic, electrophilic, or radical methods, often with the help of a transition metal.[23] An alternative pathway is the use of fluorinated synthons as a starting point, such as fluoroform (CF_3H), trifluoroiodomethane (CF_3I), NFSI, NFOBS, Selectfluor, the Rupert–Prakash reagent (Me_3SiCF_3), and Umemoto's reagent, among others.[300]

Fluoroalkanes are generally less reactive than their unsaturated counterparts, owing in part to the increased kinetic shielding arising from the lone pairs on each fluorine atom and also to the remarkable strength of the sp^3 C–F bond.[130] As an important class of electrophilic reagents, unsaturated fluoroalkenes have found widespread use as precursors within the context of polymerization,[17] but their direct reactivity with organic molecules, without the need for a transition metal, is much less common.[1] Typically, such examples involve their reactivity with nucleophiles[127,137,301] or via difficult to control radical pathways.[302–306] In certain systems, fluoroalkenes participate in Diels–Alder cycloadditions.[138–140] Although fluoroalkenes containing perfluoroalkyl substituents are especially resistant to electrophilic conditions, those bearing

hydrogen or halogen groups have been involved in reactions with various electrophiles; although this type of reactivity often involves toxic HF as a reagent, and the reactivity scope is not very general.[307,308]

Scheme 4.1. Previously reported routes to 1 (top) and 2 (bottom)

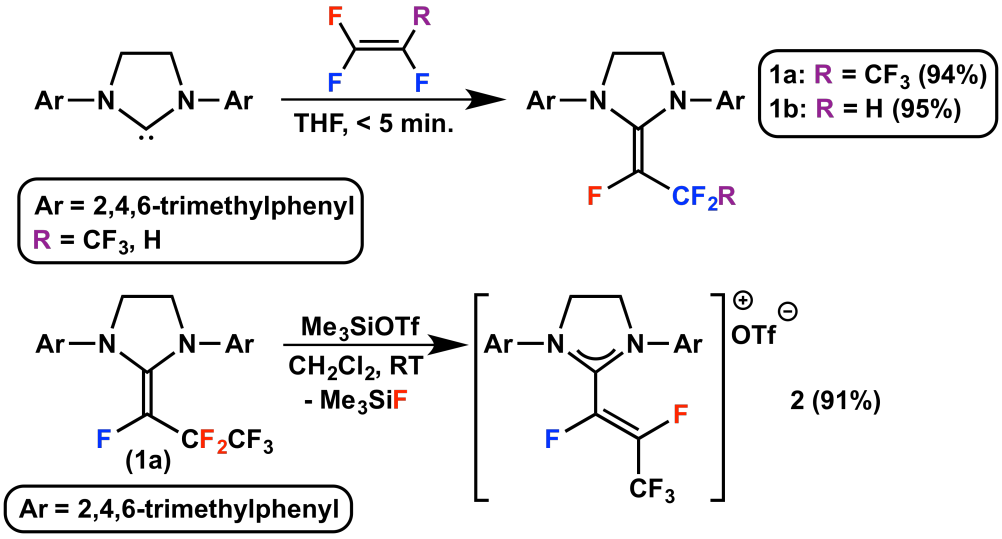

We recently reported a series of N-heterocyclic fluoroalkenes such as **1a**, along with their subsequent transformation to N-heterocyclic polyfluoroalkenyl imidazolium salts (including **2**) via fluoride abstraction with Lewis acids (Scheme 4.1).[268] The latter compounds were shown to undergo efficient and selective substitution of a terminal alkenyl fluorine on C_β by pyrrolidine through loss of HF. Alternatively, reactivity with 4-dimethylaminopyridine (DMAP) afforded a product arising from net C_α substitution. In order to expand on the surprising reactivity of this class of compounds, carbon-, nitrogen-, oxygen-, and sulfur-based nucleophiles were employed to form single isomers of substituted alkenyl compounds and to demonstrate how an N-heterocyclic carbene (NHC) can be used to control the reactivity of fluoroalkenes.

4.2.2 Results and discussion

4.2.2.1 Reactivity with sulfur-based nucleophiles

To simplify these nucleophilic substitution reactions, and to avoid generating HF, sodium salts of several common nucleophilic reagents were prepared, allowing for facile extraction of the desired product from NaF. When **2** is treated with NaSPh in dichloromethane, a single isomer (**3**) is obtained wherein the CF_3 remains oriented trans with respect to the N-heterocyclic fragment (Scheme 4.2).

Scheme 4.2. Synthetic scheme 3

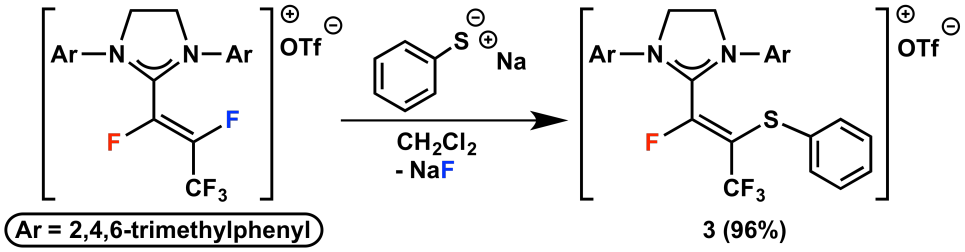

The $R_2C{=}C(CF_3)(SR')$ motif is fairly uncommon in the literature; however, a representative example was recently reported by Volgraf et al.[309] The C–S (1.740(2) Å) and C=C (1.347(3) Å) bond lengths in the molecule of interest, GNE-0723 (Figure 4.1), are comparable to the analogous bonds in **3** (C25–S1 = 1.753(3) Å, C24–C25 = 1.314(4) Å) (Figure 4.2).

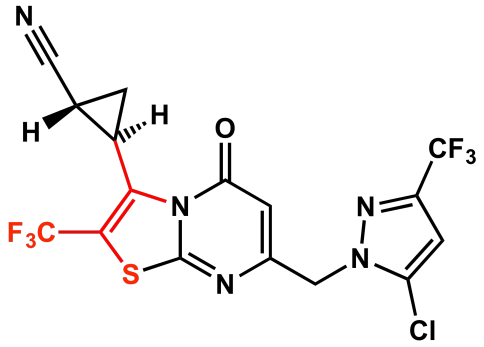

Figure 4.1. Example of the $R_2C{=}C(CF_3)(SR')$ motif in GNE-0723.

Interestingly, the average C–F bond distance of the trifluoromethyl group in **3** (C26–F_{avg} = 1.292 Å) is slightly shorter than that in GNE-0723 (1.336 Å). It is possible that delocalization of the positive charge over the imidazolium and sulfur fragments renders the trifluoromethyl group fairly electron deficient. As such, the fluorine substituents can act as π donors toward this carbon via their lone pairs, decreasing the electronic demand on carbon, while also effectively shortening the C–F bonds.

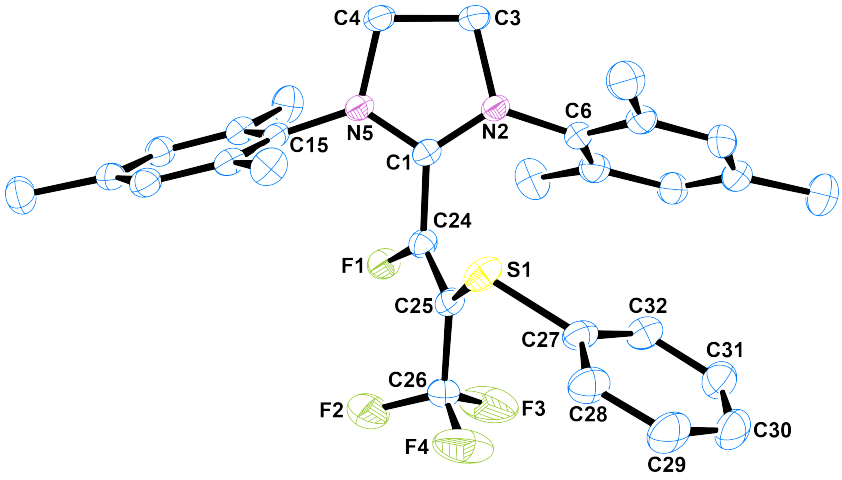

Figure 4.2. Crystallographic representation of **3** with 30% thermal probability ellipsoids. H atoms, the triflate anion, and a molecule of toluene are omitted for clarity. Selected bond lengths and angles are presented in the Supporting Information of the original publication.[310]

4.2.2.2 Reactivity with oxygen-based nucleophiles

I next investigated the reactivity of oxygen-based nucleophiles with **2**. Alkenyl aryl ether **4** is obtained in good yield as small yellow needles from **2** and [Na][8-oxyquinoline] in DMF (Scheme 4.3, top). This reaction provides a single isomer, and no reactivity from the pyridine fragment of the molecule is observed. Treatment of **2** with [Na][L-proline] in EtOH affords alkenyl ester **5** in excellent yield as a pale yellow crystalline solid (Scheme 4.3, bottom). In contrast to the reactivity observed when **3** and **4** are formed, the sole isomer observed for **5** has the CF_3 group cis with respect to the NHC fragment. The *J* coupling observed via ^{19}F NMR between the fluorine and trifluoromethyl groups is significantly different when the two groups are cis to each other (**4**, $^4J_{FF} \approx 15$ Hz), as opposed to trans (**5**, $^4J_{FF} \approx 4$ Hz), which provides a useful handle in support of the observed stereoselectivity.

Scheme 4.3. Synthetic scheme for 4 (top) and 5 (bottom)

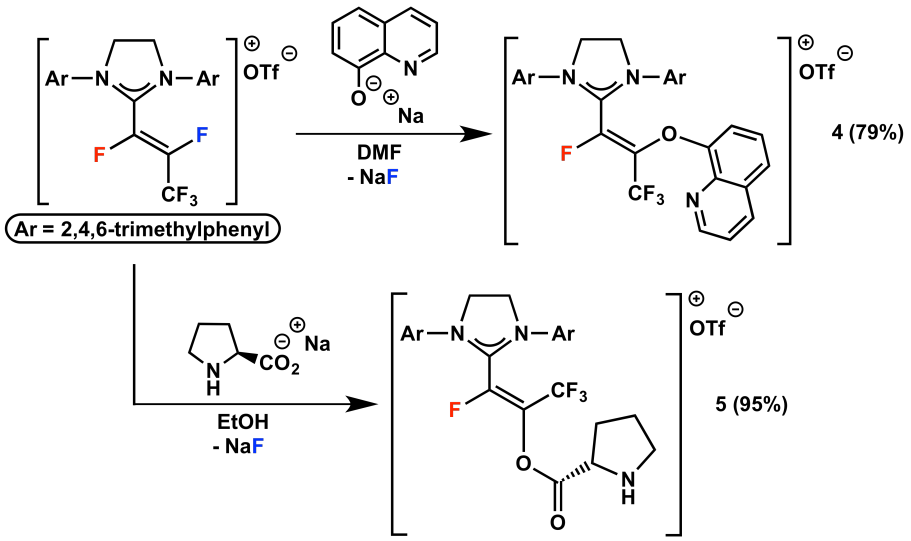

4.2.2.3 Reactivity with nitrogen-based nucleophiles

Our previous report of the reactivity between **2** and pyrrolidine or 4-dimethylaminopyridine (DMAP)[268] prompted us to investigate additional nitrogen-based nucleophiles. The reactivity with pyrrolidine can be viewed as the amination of an alkenyl fluoride via direct C–F activation, resulting in the clean formation of an enamine through overall loss of HF. The formation of sp^2 C–N bonds, including the amination of alkenyl halides, is typically enabled by either Pd-[311–314] or Cu-based[315–319] catalysts.[320] Although transition metals have provided unparalleled chemo- and regioselectivity in this regard, toxicity and cost concerns provide sufficient motivation for the development of metal-free systems capable of these transformations.

Scheme 4.4. Synthetic scheme for 6 (top) and 7 (bottom)

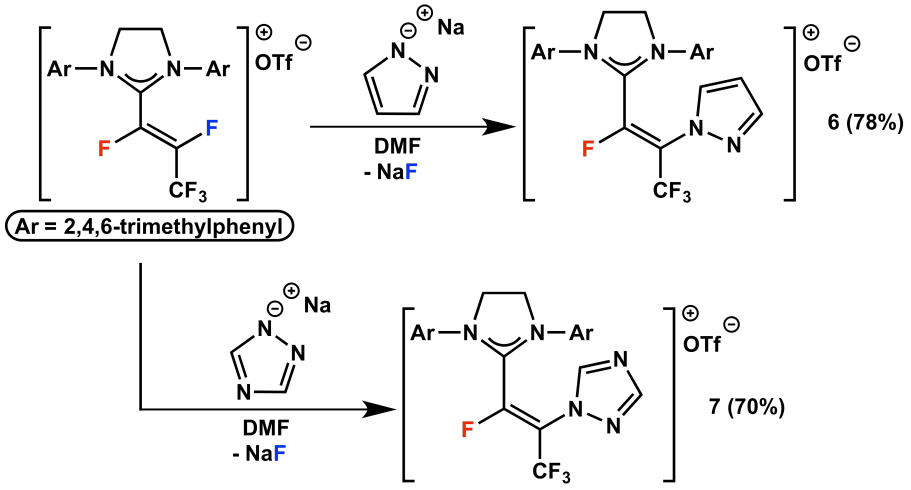

Indeed, this type of alkenyl fluoride substitution could be expanded to include pyrazolate and 1,2,4-triazolate nucleophiles (Scheme 4.4), leading to the formation of N-alkenyl-azole compounds **6** and **7**. Both products were easily isolated in good yields as pale crystalline solids

comprising the alternative stereoisomer ($^4J_{FF} \approx 27$ Hz for **6** and 25 Hz for **7**) of that observed with pyrrolidine.

4.2.2.4 Reactivity with 1-methylimidazole and formal Cα substitution

The unique C_α reactivity observed with DMAP has been expanded to include 1-methylimidazole as the nucleophile, affording N-imidazolium product **8** (Scheme 4.5). In contrast, reactions with analogous reagents such as imidazole, 1,2-dimethylimidazole, and 1-methylbenzimidazole led to a multitude of unidentified products. Additionally, benzothiazole demonstrated no reactivity with our perfluoroalkenyl imidazolium salts. A crystallographic comparison between **8** (Figure 4.3, top) and **1a**[268] demonstrates a surprising lack of change in the average C–F bond lengths of the analogous difluoromethylene fragments (both 1.37 Å). As previously reported,[268] and with the support from DFT studies, we believe that DMAP and 1-methylimidazole initially attack the C_β position and the inability to eliminate HF/NaF leads to a [1,2]-F shift, followed by another attack of the newly released DMAP or 1-methylimidazole at C_α to form the observed products. However, we have not ruled out the possibility of nucleophilic attack at C_β being reversible, and direct attack at C_α is still being considered as a potential reaction pathway for these transformations.

Scheme 4.5. Synthetic scheme for 8

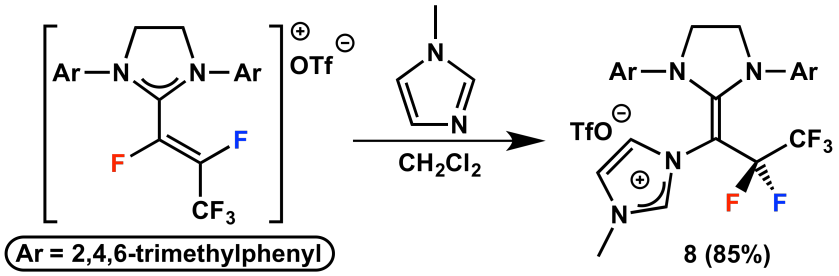

The substitution reactions leading to C_β products **3**–**7** and C_α product **8** were found to occur cleanly in various dry solvents, such as DCM, EtOH, DMF, THF, DEE, and toluene. However, solubility issues and long reaction times with less polar solvents, as well as varying yields and purity of products, obtained have led us to focus on the specific solvents presented in the Experimental Section. Importantly, the chosen solvent was not shown to affect the regioselectivity of the various substitution reactions. Furthermore, initial reactivity studies with previously reported polyfluoroalkenyl imidazolium salts derived from tetrafluoroethylene and trifluoroethylene[268] have demonstrated that the regioselectivity of these substitutions is thus far not dependent on the nature of the fluoroalkene derivative. However, **2** generally provides cleaner products with higher yields. Additionally, when neutral pyrazole was used as a reagent instead of anionic [Na][pyrazolate], the ammonium fluoride analogue of **6** is obtained and treatment with DBU afforded the desired product. The same type of reactivity was observed with the previously reported pyrrolidine substitution, and I have thus far been unable to observe any differences in regioselectivity on the basis of the use of neutral or anionic reagents. However, the removal of HF by a base does lead to a few minor byproducts, which must be removed with some amount of workup. This, coupled with the potential inability of certain reagents to support the formation of a fluoride salt, makes the use of anionic reagents more appealing.

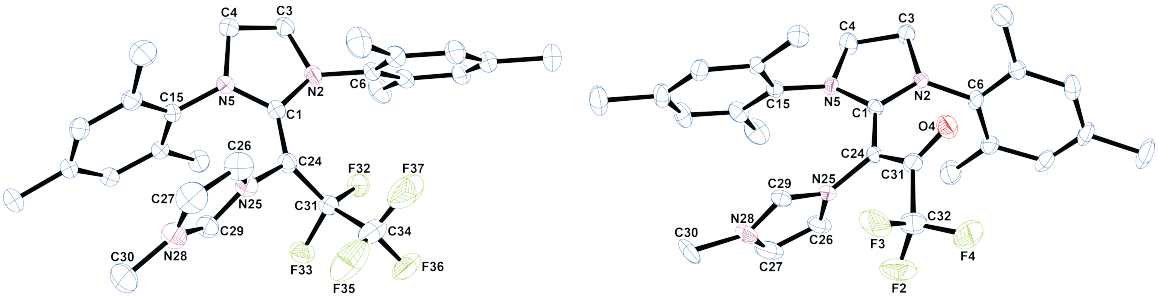

Figure 4.3. Crystallographic representations of **8** (top) and **9** (bottom) with 30% thermal probability ellipsoids. H atoms and the triflate anions are omitted for clarity. Selected bond lengths and angles for **8** and **9** are presented in the Supporting Information of the original publication.[310]

When compound **8** is exposed to water (10 equiv), an immediate clean transformation to the α,β-unsaturated trifluoromethyl ketone compound **9** is observed, along with 2 equiv of HF (Scheme 4.6). Presumably, the fluorine atoms on the difluoromethylene fragment are activated by the presence of two adjacent N-heterocyclic fragments and thus an initial deprotonation of water by a fluoride anion is possible, leading to the formation of an electrophilic alkenyl fragment. Nucleophilic attack on this fragment by hydroxide, followed by expulsion of the second fluoride and formation of the α,β-unsaturated trifluoromethyl ketone, could then occur. To the best of our knowledge, there has been no similar report for the formation of an α,β-unsaturated trifluoromethyl ketone via successive defluorination of a difluoromethylene group.

Scheme 4.6. Reaction of 8 with water to form 9

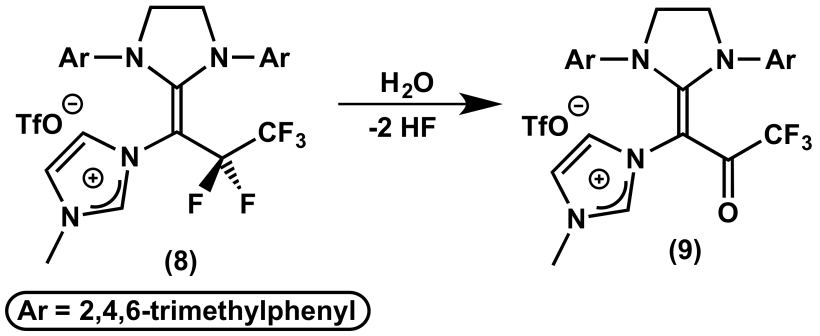

As a functional group, α,β-unsaturated trifluoromethyl ketones have found several important uses in synthesis, particularly in the formation of CF_3-containing heterocycles.[321–324] As such, these types of starting reagents are often mentioned as useful fluorinated synthons, and several methods for their synthesis have been developed, including trifluoroacylation[325,326] and condensation.[327,328] The ability to directly transform a perfluoroethyl group to a desirable fragment such as this one could prove to be a useful tool for organic chemists looking to expand on this area.

Crystallographic studies of the structurally related compounds **8** and **9** (Figure 4.3) reveal notable changes in bond lengths following carbonyl formation. Specifically, the C1═C24 bond length in **8** (1.387(2) Å) elongates in **9** (1.412(6) Å). Additionally, the C24–C31 bond length **8** (1.516(6) Å) shortens significantly in **9** (1.415(7) Å). As these bonds are similar in length, it appears that significant electronic delocalization is present within this fragment in **9**.

4.2.2.5 Double C-F bond activation with sodium cyclopentadienide

Attempts to elaborate on analogous reactivity with carbon-based nucleophiles proved more difficult, as several products were often observed, with most of these remaining

unidentified. However, facile C–C bond formation was observed with the N-heterocyclic fluoroalkene **1b**.[268] The two fluorine atoms in the difluoromethyl fragment of this adduct appear to be especially activated, presumably due to participation of the zwitterionic imidazolium resonance form. In fact, treatment with NaCp (2 equiv, Cp = cyclopentadienide) in THF leads to an immediate colour change from pale orange to a very bright orange-yellow, along with formation of solid NaF (Scheme 4.7). Following substitution at C_β by the Cp anion, the remaining Cp anion acts as a base to abstract the proton remaining on the substituted Cp fragment, giving the fluoroalkenyl-substituted product **10**. When an equimolar amount of NaCp is allowed to react with **1b**, a 50% conversion to **10** is observed, while 50% of **1b** remains unconverted, and no unique reaction intermediates could be observed.

Scheme 4.7. Synthetic scheme for 10

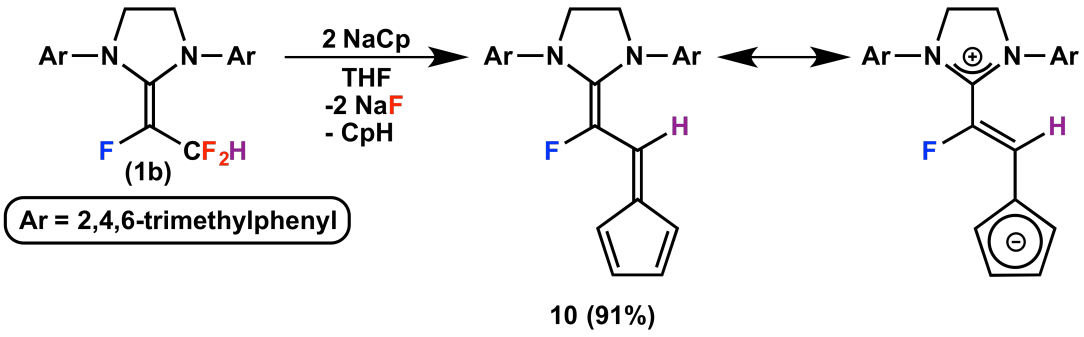

A characteristic coupling constant ($^3J_{FH} \approx 41$ Hz) and crystallography (Figure 4.4) serve to confirm the orientation of the substituents in **10**. The bond lengths point to significant resonance contributions from the zwitterionic form, which can be viewed as the combination of an imidazolium fragment and an aromatic Cp anion. Specifically, the C–N (N1–C5 = 1.360(2) Å, N4–C5 = 1.361(2) Å) and C–C bond lengths (C5–C6 = 1.383(3) Å, C6–C8 = 1.378(3) Å, C8–C9

= 1.379 (3) Å) support the contribution from this form. This is further exemplified by the relative insolubility of **10** in nonpolar solvents.

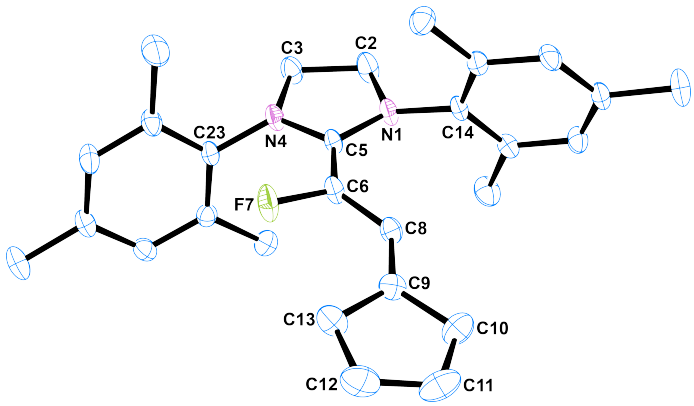

Figure 4.4. Crystallographic representation of **10** with 30% thermal probability ellipsoids. H atoms and a molecule of dichloromethane are omitted for clarity. Selected bond lengths and angles are presented in the Supporting Information of the original publication.[310]

Finally, the electronic absorption spectrum of **10** in DCM (see Annex D) displays an intense absorption feature at ~22150 cm^{-1} (ε = 13150 M^{-1} cm^{-1}) corresponding to the HOMO to LUMO transition on the basis of TD-DFT calculations (see Annex D). It is noteworthy that both the HOMO and LUMO orbitals (Figure 4.5) of **10** are delocalized over both the NHC and Cp fragments and are of mixed π/π^* character.

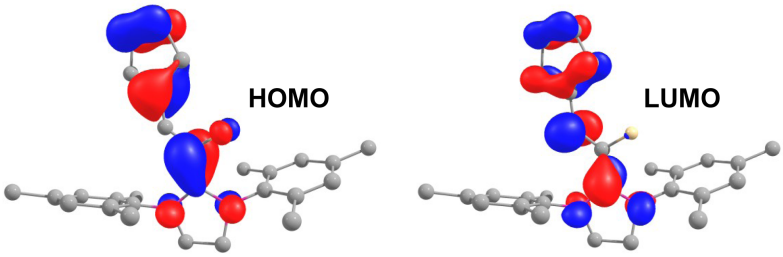

Figure 4.5. Calculated HOMO and LUMO orbitals for **10**.

4.2.2.6 Reactivity with transition metal-based nucleophiles

In expanding this reactivity to include transition metal-based nucleophiles, a variety of carbonylmetalate complexes, as their sodium salts, were allowed to react with **1a**. Namely, in order of decreasing nucleophilicity, $[CpFe(CO)_2]$, $[CpW(CO)_3]$, $[Mn(CO)_5]$, $[CpMo(CO)_3]$, $[CpCr(CO)_3]$, and $[Co(CO)_4]$ were tested. No reactivity was observed with cobalt, presumably due to insufficient nucleophilicity.[329] Reactions with chromium led to multiple paramagnetic products, while tungsten gave rise to unstable complexes that readily decomposed upon forming. Similarly, iron did not react cleanly and provided a multitude of products. However, treatment of **1a** with the manganate nucleophile in THF gave an immediate colour change from pale yellow to deep orange with formation of the Mn-substituted fluorovinyl-imidazolium complex **11** (Scheme 4.8, top) confirmed by ^{19}F NMR ($^4J_{FF} \approx 7$ Hz). Mo-substituted complex **12** (Scheme 4.8, bottom) was obtained by an analogous synthesis, wherein an immediate colour change from pale yellow to a very deep red was observed upon reaction. Although this complex could be formed relatively cleanly at room temperature, formation of unwanted byproducts was eliminated when the addition was performed at −78 °C. Once again, ^{19}F NMR ($^4J_{FF} \approx 6$ Hz) is a helpful handle for determining the relative orientation of the fluorinated substituents. We note that the fluorovinyl-imidazolium fragments on **11** and **12** can be viewed as a unique ligand scaffold and might prove to possess interesting properties within the context of push–pull alkenes,[330] with the potential to vary the imidazolium and metal fragments to obtain the desired electronic density at the double bond.

Scheme 4.8. Synthetic scheme for 11 (top) and 12 (bottom)

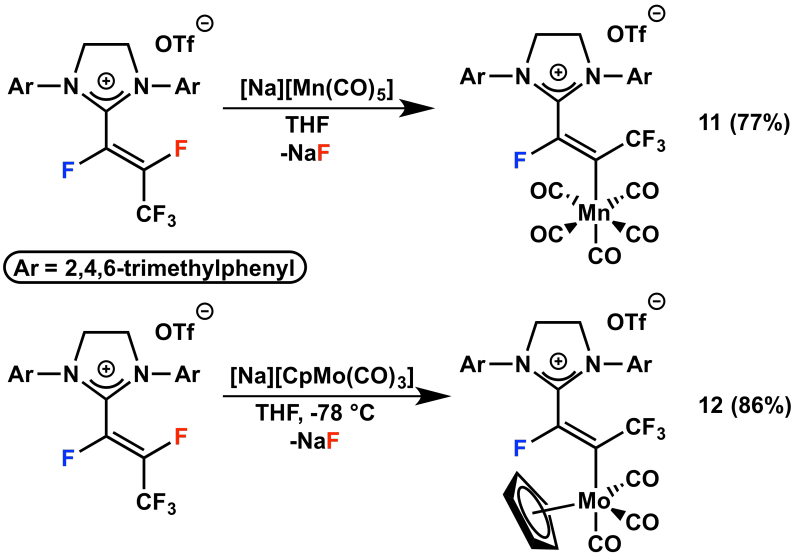

Crystallographic studies of **11** (Figure 4.6) confirm the proposed stereochemistry and reveal that the C═C bond (C24–C26 = 1.314(6) Å) is very similar to analogous bonds in the previously reported **2** (1.316(2) Å)[268] and **3** (1.314(4) Å) and in the previously reported pyrrolidine-substituted product (1.355(3) Å).[268] There are several examples of transition-metal complexes bearing [M]–C(F)═C(F)(CF_3) perfluorovinyl ligands,[94,97,331–337] but there have been fewer reports on the [M]–C(CF_3)═CF_2 form, wherein the trifluoromethyl substituent is on the carbon bound directly to the metal.[334,338–340] In this work, the terminal F trans to the metal in traditional fluorovinyl complexes has effectively been replaced by an imidazolium fragment. Consequently, the C═C bond length in **11** is comparable to that in an analogous Ni-based[338] (1.318(6) Å) perfluorovinyl complex but longer than that in an Ir-based complex[339] (1.22(3) Å) reported by Hughes et al. Replacement of a terminal F by this imidazolium fragment forms what can be viewed as a push–pull alkene type of

system.[341] Unfortunately, comparisons to reports on Rh[334] and Fe examples[340] cannot be made due to the lack of X-ray crystal structure data.

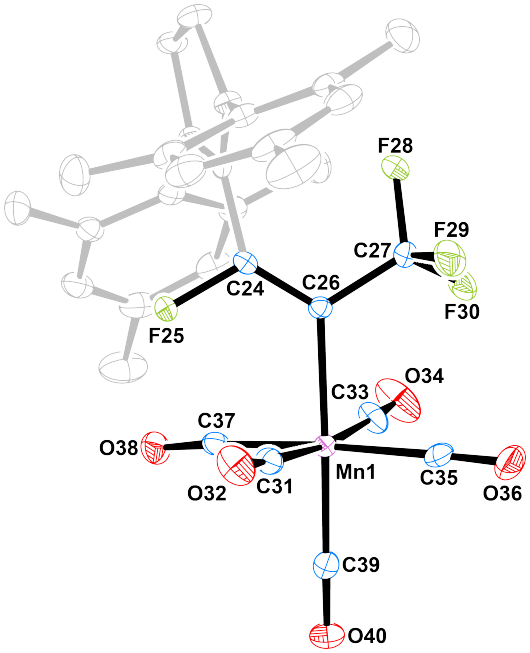

Figure 4.6. Crystallographic representation of **11** with 30% thermal probability ellipsoids. H atoms and the triflate anion are omitted for clarity. Selected bond lengths and angles are presented in the Supporting Information of the original publication.[310]

Transition-metal fluorovinyl complexes[342] have been reported for Mn,[343] Re,[344] Fe,[344–346] Ru,[345–347] Rh,[347] Ni,[348–352] Pd,[332,348,352–355] and Pt.[348,353,354,356–360] Further reactivity of these complexes is often scarce, but a relevant example by Ogoshi et al. has recently been published, wherein a palladium trifluorovinyl complex derived from TFE formed trifluorostyrene derivatives via a base-free Hiyama coupling reaction with a wide variety of aryl groups.[361] Further reactivity studies of complexes **11** and **12** are currently underway in our laboratory.

As a building block, small fluoroalkenes are often overlooked due to the handling difficulties associated with gases. However, I have shown that the isolation of N-heterocyclic

fluoroalkene adducts is facile and gives rise to stable, well-behaved solids. These have been shown to be good platforms for substitution chemistry with a variety of simple reagents. It has become apparent that, although the reactivity of fluoroalkenes is sometimes difficult to control, the presence of an N-heterocyclic/imidazolium fragment has a great effect on governing the selectivity of such substitutions.

4.2.3 Conclusions

In summary, polyfluoroalkenyl imidazolium salts have been shown to be active toward substitution with various sulfur-, oxygen-, and nitrogen-based nucleophiles via direct C–F bond activation, the last of which includes the amination of an alkenyl halide. Such formation of sp^2 C–N bonds is typically enabled by either Pd- or Cu-based catalysts but has been shown in this work to proceed cleanly at room temperature without the need for a catalyst. Rendering this transformation general could provide an indispensable tool to synthetic chemists, and the key potentially lies in utilizing the correct N-heterocyclic fragment. Additional reactivity of this system further illustrates that, although fluoroalkenes are not typically involved in reactions with organic reagents and do not ordinarily react cleanly with nucleophiles, the use of stable and convenient NHC fluoroalkene adducts enables various important transformations with good control. Our group is currently researching methods of extruding the N-heterocyclic fragment post substitution, potentially leading to an organocatalytic system involving fluoroalkenes as fluorinated synthons. Additionally, viewing fluorovinyl-imidazolium fragments as ligand scaffolds offers an opportunity to explore new push–pull alkenes featuring metal complexes, potentially taking advantage of the numerous oxidation states available to transition metals.

4.2.4 Experimental

4.2.4.1 General considerations

All manipulations were carried out using standard Schlenk techniques or in an MBraun glovebox. All glassware was oven-dried at >150 °C for a minimum of 2 h prior to use or flame-dried using a torch. Toluene, hexanes, tetrahydrofuran (THF), diethyl ether (DEE), and *N,N*-dimethylformamide (DMF) were dried on columns of activated alumina using a J. C. Meyer (formerly Glass Contour) solvent purification system. Dichloromethane (DCM) and chloroform-*d* ($CDCl_3$) were dried by refluxing over calcium hydride under a nitrogen flow, followed by distillation and filtration through a column of activated alumina (ca. 10 wt %). Benzene-d_6 (C_6D_6) was dried by standing over activated alumina (ca. 10 wt %) overnight, followed by filtration. Ethanol (EtOH) was dried by refluxing over Mg/I_2 under nitrogen, followed by distillation. All solvents were stored over activated (heated at 250 °C for >6 h under vacuum) 4 Å molecular sieves, except for EtOH (stored over activated 3 Å molecular sieves). The following chemicals were used as purchased, without further purification: trimethylsilyl trifluoromethanesulfonate (Sigma-Aldrich, 98+%), sodium thiophenolate (Sigma-Aldrich, 90%), 1-methylimidazole (Sigma-Aldrich, 99%), L-proline (Sigma-Aldrich, 99+%), 8-hydroxyquinoline (Sigma-Aldrich, 99%), 1,2,4-triazole (TCI America, 99+%), pyrazole (Sigma-Aldrich, 98%), sodium hydroxide (Sigma-Aldrich, 97+%), sodium cyclopentadienide (Sigma-Aldrich, 2.0 M in THF), sodium metal (Alfar Aesar, 99%), mercury (Strem, >99%), $Mn_2(CO)_{10}$(Strem, 98%), and $Mo(CO)_6$ (Strem, 98%). The following salts were prepared according to literature procedures: sodium 1,2,4-triazolate,[362] sodium pyrazolate,[362] sodium (2*S*)-2-pyrrolidinecarboxylate ([Na][L-proline]),[363] sodium 8-oxyquinoline,[364] [Na][$Mn(CO)_5$],[329] and [Na][$CpMo(CO)_3$].[329] The synthesis of SIMes═$CF(CF_2CF_3)$ (**1a**), SIMes═$CF(CF_2H)$ (**1b**), and [SIMes-CF═$CF(CF_3)$][OTf]

(**2**) has been previously described.[268] ^{1}H, ^{19}F, and $^{19}F\{^{1}H\}$ NMR spectra were recorded on either a Bruker Avance 300 or a Bruker Avance II 300 spectrometer at room temperature. $^{13}C\{^{1}H\}$ NMR spectra were recorded on a Bruker Avance 400 spectrometer at room temperature. ^{1}H NMR spectra were referenced to the residual proton peaks associated with the deuterated solvents (C_6D_6 7.16 ppm, $CDCl_3$ 7.26 ppm). ^{13}C NMR spectra were referenced to the signal associated with $CDCl_3$ (77.16 ppm). It is important to note that ^{13}C NMR signals coupled to ^{19}F nuclei are broadened out significantly, and although coupling constant values and multiplicity can sometimes be extracted, it is often impossible to do so. As such, the data are presented to the best of our ability and all efforts have been made to avoid any ambiguity in their presentation. ^{19}F and $^{19}F\{^{1}H\}$ NMR spectra were referenced to internal 1,3-bis(trifluoromethyl)benzene (BTB) (Aldrich, 99%, deoxygenated by purging with nitrogen and stored over 4 Å molecular sieves), set to −63.5 ppm. ^{1}H NMR data for BTB (300 MHz, C_6D_6): δ 6.60 (m, 1H, Ar-5-H), 7.12 (m, 2H, Ar-4,6-H), 7.76 (m, 1H, Ar-2-H). A Micromass Q-ToF 1 instrument (positive mode) was used for electrospray ionization (ESI), with samples diluted to ca. 5 μg/mL in acetonitrile. A Mel-Temp II instrument was used for the determination of melting points. UV–vis spectra were recorded on a Cary 100 instrument, using sealable quartz cuvettes (1.0 cm pathlengths). IR spectra were recorded on a Thermo Nicolet Nexus 670 FT-IR E.S.P. instrument, using KBr plates. Elemental analyses were performed by the Laboratoire d'Analyse Élémentaire de l'Université de Montréal (Montréal, Québec, Canada).

4.2.4.2 Synthesis and characterization

Synthesis of [SIMes-CF═C(CF_3)(SPh)][OTf] (3). In a glovebox, [SIMes-CF═CF(CF_3)][OTf] (**2**; 200 mg, 0.34 mmol) was placed in a vial with a stir bar and dissolved in DCM (~5 mL). To

this stirred solution was added sodium thiophenolate (45 mg, 0.34 mmol), causing an immediate colour change from red to dark orange. Additionally, the formation of a small amount of precipitate could be observed, corresponding to sodium fluoride. After it was stirred for 1 h, the reaction mixture was filtered through Celite with DCM washings (2 × 2 mL), and hexanes (ca. 10 mL) was added to the filtrate, causing precipitation of the product. The suspension was placed in the freezer (−35 °C) for 30 min, and the product was isolated by filtration on a frit and washed with toluene and DEE (ca. 5 mL each). The product was isolated as an off-white solid. Yield: 221 mg, 96% based on [SIMes-CF═CF(CF_3)][OTf]. mp: 171 °C. ^{1}H NMR (300 MHz, $CDCl_3$): δ 2.25–2.49 (ov m, 18H, Ar-CH_3), 4.79 (dm, 4H, N-CH_2CH_2-N), 6.34 (dm, 2H, Ar-*H*), 6.65–7.25 (ov m, 7H, Ar-*H*). ^{13}C{^{1}H} NMR (101 MHz, $CDCl_3$): δ 17.91, 21.18, 53.04, 127.39, 128.21, 128.35, 129.16, 129.26, 129.29 (ov s), 129.39, 130.74 (br m), 135.24 (br m), 141.56, 157.55 (d, $^2J_{CF}$ ≈ 29 Hz, SIMes(*C*)-CF═C(CF_3)(SPh)). ^{19}F NMR (282 MHz, $CDCl_3$): δ −59.3 (d, $^4J_{FF}$ ≈ 16 Hz, 3F, SIMes-CF═C(C*F*$_3$)(SPh), trans), −78.8 (s, 3F, $SO_3CF_3^-$), −85.3 (q, $^4J_{FF}$≈ 16 Hz, 1F, SIMes-C*F*═C(CF_3)(SPh)). MS [ESI (positive mode), solvent MeCN] calcd *m*/*z* (% intensity) for [SIMes-CF═C(CF_3)(SPh)$^+$, $C_{30}H_{31}F_4N_2S^+$] 527.21 (100), 528.22 (32), 529.21 (5); found *m*/*z* (% intensity) 527.2141 (100), 528.2245 (35), 529.2326 (8).

Synthesis of [SIMes-CF═C(CF_3)(8-oxyquinoline)][OTf] (4). In a glovebox, [SIMes-CF═CF(CF_3)][OTf] (**2**; 200 mg, 0.34 mmol) was placed in a vial with a stir bar and dissolved in DMF (~5 mL). To this stirred solution was added sodium 8-oxyquinoline (57 mg, 0.34 mmol), causing a gradual colour change from red to dark orange-yellow over a period of 15 min. After the mixture was stirred for 1 h, the volatiles were removed in vacuo. The product was extracted with DCM and filtered through Celite with DCM washings (2 × 4 mL), and hexanes (ca. 10 mL) was added to the filtrate, causing precipitation of the product. The suspension was placed in the

freezer (−35 °C) for 30 min, and the product was isolated by filtration on a frit and washed with toluene and DEE (ca. 5 mL each). The product was isolated as small yellow needles. Yield: 191 mg, 79% based on [SIMes-CF═CF(CF_3)][OTf]. mp: 145 °C dec. See the Supporting Information of the original publication for the labeling scheme of 8-oxyquinoline.[310] ^{1}H NMR (300 MHz, $CDCl_3$): δ 2.08 (s, 6H, Ar-*p*-C*H*$_3$), 2.29 (s, 12H, Ar-*o*-C*H*$_3$), 4.66 (s, 4H, N-C*H*$_2$C*H*$_2$-N), 6.59 (s, 4H, Ar-*H*), 7.10 (dd, 1H, $^4J_{H^F H^D} \approx$ 7.7 Hz, $^3J_{H^F H^C} \approx$ 1.2 Hz, H^F), 7.36 (dd, 1H, $^3J_{H^E H^B} \approx$ 8.3 Hz, $^3J_{H^E H^A} \approx$ 4.3 Hz, H^E), 7.42 (ov dd, 1H, $^3J_{H^D H^C} \approx$ 8.3 Hz, $^4J_{H^D H^F} \approx$ 7.7 Hz, H^D), 7.58 (dd, 1H, $^3J_{H^C H^D} \approx$ 8.3 Hz, $^3J_{H^C H^F} \approx$ 1.2 Hz, H^C), 8.10 (dd, 1H, $^3J_{H^B H^E} \approx$ 8.3 Hz, $^3J_{H^B H^A} \approx$ 1.6 Hz, H^B), 8.45 (dd, 1H, $^3J_{H^A H^E} \approx$ 4.3 Hz, $^3J_{H^A H^B} \approx$ 1.6 Hz, H^A). ^{13}C{^{1}H} NMR (101 MHz, C_6D_6): δ 17.65, 21.03, 52.83, 115.65, 122.06, 124.33, 126.34, 128.95, 129.99, 130.39, 134.66, 135.62, 137.69, 140.42, 148.52, 149.59, 158.26 (d, $^2J_{CF} \approx$ 25 Hz, SIMes(*C*)-CF═C(CF_3)(8-oxyquinoline)). ^{19}F NMR (282 MHz, $CDCl_3$): δ −65.9 (d, $^4J_{FF} \approx$ 15 Hz, 3F, SIMes-CF═C(C*F*$_3$)(8-oxyquinoline), trans), −78.8 (s, 3F, $SO_3CF_3^-$), −152.7 (q, $^4J_{FF} \approx$ 15 Hz, 1F, SIMes-C*F*═C(CF_3)(8-oxyquinoline)). MS [ESI (positive mode), solvent MeCN]: calcd *m*/*z* (% intensity) for [SIMes-CF═C(CF_3)(8-oxyquinoline)$^+$, $C_{33}H_{32}F_4N_3O^+$] 562.25 (100), 563.25 (36), 564.25 (6); found *m*/*z* (% intensity) 562.2495 (100), 563.2737 (40), 564.2933 (8).

Synthesis of [SIMes-CF═C(CF_3)(L-proline)][OTf] (5). In a glovebox, [SIMes-CF═CF(CF_3)][OTf] (**2**; 200 mg, 0.34 mmol) was placed in a vial with a stir bar and dissolved in EtOH (~5 mL). To this stirred solution was added sodium (2*S*)-2-pyrrolidinecarboxylate ([Na][L-proline]; 47 mg, 0.34 mmol), causing an immediate colour change from red to dark orange. After the mixture was stirred for 1 h, the volatiles were removed in vacuo. The product was extracted with DCM and filtered through Celite with DCM washings (2 × 4 mL), and hexanes (ca. 10 mL) was added to the filtrate, causing precipitation of the product. The suspension was placed in the

freezer (−35 °C) for 30 min, and the product was isolated by filtration on a frit and washed with hexanes (ca. 5 mL). The product was isolated as a yellow-orange powder. Yield: 220 mg, 95% based on [SIMes-CF═CF(CF_3)][OTf]. mp: 140 °C. ^{1}H NMR (300 MHz, $CDCl_3$): δ 1.65–1.98 (m, 2H, L-proline(CH_2)), 2.00–2.16 (m, 1H, L-proline(CH_2)), 2.23–2.39 (m, 18H, Ar-CH_3), 3.05 (m, 1H, L-proline(CH_2)), 3.46 (m, 1H, L-proline(CH_2)), 4.15 (m, 1H, L-proline(CH_2)), 4.34–4.79 (ov m, 5H, N-CH_2-CH_2-N and C*H*-C(O)), 6.92, 7.05 (m, 4H, Ar-*H*). ^{13}C{^{1}H} NMR (101 MHz, $CDCl_3$): δ 14.23, 17.92, 21.09, 22.77, 23.34, 29.17, 30.32, 31.71, 34.79, 52.23, 51.75, 62.82 (m), 119.15, 122.38, 130.35, 130.43, 130.53, 130.56, 130.71, 130.80, 134.55, 134.71, 134.86, 135.02, 135.45, 135.51, 140.79, 161.25 (d, $^2J_{CF} \approx$ 28 Hz, SIMes(*C*)-CF═C(CF_3)(L-proline)) 172.25 (br m, *C*═O). ^{19}F NMR (282 MHz, $CDCl_3$): δ −62.9 (d, $^4J_{FF} \approx$ 3 Hz, 3F, SIMes-CF═C(CF_3)(L-proline), trans), −78.9 (s, 3F, $SO_3CF_3^-$), −145.2 (br q, $^4J_{FF} \approx$ 3 Hz, 1F, SIMes-C*F*═C(CF_3)(L-proline)). MS [ESI (positive mode), solvent MeCN]: calcd *m*/*z* (% intensity) for [SIMes-CF═C(CF_3)(H)$^+$, $C_{24}H_{27}F_4N_2^+$] 419.21 (100), 420.21 (26), 421.22 (3); found *m*/*z* (% intensity) 419.2119 (100), 420.2496 (51), 421.2760 (8); calcd *m*/*z* (% intensity) for [SIMes-CF═C(L-proline)$^+$, $C_{28}H_{34}FN_3O_2^+$] 463.26 (100), 464.27 (30), 465.27 (3); found *m*/*z* (% intensity) 463.2635 (100), 464.2667 (32), 465.2697 (5).

Synthesis of [SIMes-CF═C(CF_3)(pyrazole)][OTf] (6). In a glovebox, [SIMes-CF═CF(CF_3)][OTf] (**2**; 200 mg, 0.34 mmol) was placed in a vial with a stir bar and dissolved in DMF (~5 mL). To this stirred solution was added sodium pyrazolate (31 mg, 0.34 mmol), causing an immediate colour change from red to dark orange. After the mixture was stirred for 1 h, the volatiles were removed in vacuo. The product was extracted with DCM and filtered through Celite with DCM washings (2 × 4 mL), and hexanes (ca. 10 mL) was added to the filtrate, causing precipitation of the product. The suspension was placed in the freezer (−35 °C) for 30

min, and the product was isolated by filtration on a frit and washed with hexanes (ca. 5 mL). The product was isolated as a yellow crystalline solid. Yield: 84 mg, 78% based on [SIMes-CF═CF(CF_3)][OTf]. mp: 101 °C. ^{1}H NMR (300 MHz, $CDCl_3$): δ 2.17 (ov m, 18H, Ar-CH_3), 4.63–4.96 (ov m, 4H, N-CH_2CH_2-N), 6.49 (ov dd, 1H, N-CH═C*H*-CH═N), 6.75 (ov dd, 1H, N-CH═CH-C*H*═N), 6.87–7.04 (br m, 4H, Ar-*H*), 7.86 (ov dd, 1H, N-C*H*═C*H*-CH═N). ^{13}C{^{1}H} NMR (101 MHz, $CDCl_3$): δ 18.02, 21.21, 53.47, 129.09, 130.71, 131.14, 134.85, 135.16, 141.89, 145.26, 154.70. ^{19}F NMR (282 MHz, $CDCl_3$): δ −63.3 (d, $^4J_{FF} \approx$ 27 Hz, 3F, SIMes-CF═C(CF_3)(pyrazole), trans), −78.9 (s, 3F, $SO_3CF_3^-$), −119.0 (q, $^4J_{FF} \approx$ 27 Hz, 1F, SIMes-CF═C(CF_3)(pyrazole)). MS [ESI (positive mode), solvent MeCN]: calcd *m*/*z* (% intensity) for [SIMes-CF═C(CF_3)(pyrazole)$^+$, $C_{27}H_{29}F_4N_4^+$] 485.23 (100), 486.24 (29), 487.24 (4); found *m*/*z* (% intensity) 485.2303 (100), 486.2834 (61), 487.3110 (8).

Synthesis of [SIMes-CF═C(CF_3)(1,2,4-triazole)][OTf] (7). In a glovebox, [SIMes-CF═CF(CF_3)][OTf] (**2**; 200 mg, 0.34 mmol) was placed in a vial with a stir bar and dissolved in DMF (~5 mL). To this stirred solution was added sodium 1,2,4-triazolate (31 mg, 0.34 mmol), causing an immediate colour change from red to dark orange. After the mixture was stirred for 1 h, the volatiles were removed in vacuo. The product was extracted with DCM and filtered through Celite with DCM washings (2 × 4 mL), and hexanes (ca. 10 mL) was added to the filtrate, causing precipitation of the product. The suspension was placed in the freezer (−35 °C) for 30 min, and the product was isolated by filtration on a frit and washed with hexanes (ca. 5 mL). The product was isolated as a pale orange powder. Yield: 151 mg, 70% based on [SIMes-CF═CF(CF_3)][OTf]. mp: 108 °C. ^{1}H NMR (300 MHz, $CDCl_3$): δ 2.25–2.49 (ov m, 18H, Ar-CH_3), 4.76 (s, 4H, N-CH_2CH_2-N), 6.34 (dm, 2H, Ar-*H*), 6.98 (s, 4H, Ar-*H*), 7.21 (m, 1H, N═C*H*-N), 8.23 (s, 1H, N-C*H*═N). ^{13}C{^{1}H} NMR (101 MHz, $CDCl_3$): δ 18.14, 21.14, 52.99, 111.44,

119.37, 122.55, 129.37, 130.39, 130.78 (d), 131.47, 135.35, 135.76, 141.36, 144.85, 157.33 (d, $^{2}J_{CF} \approx 27$ Hz, SIMes(*C*)-CF═C(CF_3)(1,2,4-triazole). ^{19}F NMR (282 MHz, $CDCl_3$): δ −63.6 (d, $^{4}J_{FF} \approx 25$ Hz, 3F, SIMes-CF═C(C*F*$_3$)(1,2,4-triazole), trans), −78.8 (s, 3F, $SO_3CF_3^-$), −111.6 (q, $^{4}J_{FF} \approx 25$ Hz, 1F, SIMes-C*F*═C(CF_3)(1,2,4-triazole)). MS [ESI (positive mode), solvent MeCN]: calcd *m*/*z* (% intensity) for [SIMes-CF═C(CF_3)(1,2,4-triazole)$^+$, $C_{26}H_{28}F_4N_5^+$] 486.23 (100), 487.23 (28), 488.23 (3); found *m*/*z* (% intensity) 486.2252 (100), 487.2361 (29), 488.2381 (4).

Synthesis of [SIMes═C(1-methylimidazolium)(CF_2CF_3)][OTf] (8). In a glovebox, [SIMes-CF═CF(CF_3)][OTf] (**2**; 200 mg, 0.34 mmol) was placed in a vial with a stir bar and dissolved in DCM (~5 mL). To this stirred solution was added 1-methylimidazole (28 μL, 0.34 mmol), causing an immediate colour change from red to dark red. After the mixture was stirred for 1 h, hexanes (ca. 10 mL) was added to the reaction mixture, causing precipitation of the product. The suspension was placed in the freezer (−35 °C) for 30 min, and the product was isolated by filtration on a frit and washed with toluene and DEE (ca. 5 mL each). The product was isolated as a crystalline pale red solid. Yield: 193 mg, 85% based on [SIMes-CF═CF(CF_3)][OTf]. mp: 163 °C. ^{1}H NMR (300 MHz, $CDCl_3$): δ 2.17 (s, 3H, Ar-C*H*$_3$), 2.26 (s, 3H, Ar-C*H*$_3$), 2.29 (ov s, 6H, Ar-C*H*$_3$), 2.35 (s, 3H, Ar-C*H*$_3$), 2.39 (s, 3H, Ar-C*H*$_3$), 3.72 (s, 4H, N-C*H*$_2$C*H*$_2$-N), 3.74–4.12 (ov m, 3H, N-C*H*$_3$), 6.63 (br m, 1H, N-C*H*═C*H*-N), 6.85 (br m, 1H, N-C*H*═C*H*-N), 6.92 (s, 1H, Ar-*H*), 6.94 (ov s, 2H, Ar-*H*), 7.09 (m, 1H, Ar-*H*), 7.93 (s, 1H, N═C*H*-N). ^{13}C{^{1}H} NMR (101 MHz, $CDCl_3$): δ 17.82, 18.22, 18.31, 18.38, 20.81, 21.01, 36.32, 49.96, 52.06, 122.30, 127.56, 129.64, 129.84, 130.07, 130.38, 134.52, 135.24, 135.55, 135.88, 136.23, 136.99, 138.07, 138.96, 140.90, 157.44 (t, $^{3}J_{CF} \approx 2$ Hz, SIMes(*C*)═C(1-methylimidazolium)(CF_2CF_3)). ^{19}F NMR (282 MHz, $CDCl_3$): δ −78.9 (s, 3F, $SO_3CF_3^-$), −83.3 (ov dd, $^{3}J_{FF} \approx 5$ Hz, 3F, CF_2CF_3), −99.8 (dq, $^{2}J_{FF} \approx 272$

Hz, $^{3}J_{FF} \approx 5$ Hz, C$F^{A}F^{A'}CF_3$), −103.0 (dq, $^{2}J_{FF} \approx 272$ Hz, $^{3}J_{FF} \approx 5$ Hz, $CF^{A}F^{A'}CF_3$). Note that ESI-MS for this sample could not be acquired due to the immediate and quantitative conversion of **7** to **8** when exposure to any amount of trace moisture in the air occurred.

Synthesis of [SIMes═C(1-methylimidazolium)(C(O)(CF_3))][OTf] (9)

Method A. In a glovebox, **7** (15 mg, 0.022 mmol) was dissolved in $CDCl_3$ and transferred to an NMR tube. The sample was left to sit in air, outside of the glovebox, with the cap off. After standing overnight, NMR analysis of the sample showed clean and quantitative conversion to **8**.

Method B. In a glovebox, **7** (15 mg, 0.022 mmol) was dissolved in CD_3CN and transferred to a septum-capped NMR tube. H_2O (4 μL, 0.22 mmol) was added, and the NMR tube was shaken vigorously. NMR analysis of the sample showed clean and quantitative conversion to **8** within 30 min. With both methods, the sample can be pumped down after the reaction is complete to give a pale yellow solid. mp: 138 °C. ^{1}H NMR (300 MHz, $CDCl_3$): δ 2.27 (s, 6H, Ar-CH_3), 2.34 (br m, 12H, Ar-CH_3), 3.78 (s, 3H, N-CH_3), 4.09 (s, 4H, N-CH_2CH_2-N), 6.61 (m, 1H, N-C*H*═C*H*-N), 6.93 (br m, 4H, Ar-*H*), 7.09 (m, 1H, N-C*H*═C*H*-N), 8.15 (s, 1H, N═C*H*-N). ^{13}C{^{1}H} NMR (101 MHz, $CDCl_3$): δ 18.00, 18.52, 20.94, 36.25, 50.75, 88.57 (SIMes═*C*), 122.69, 127.18, 130.27, 133.98, 134.27, 134.95, 139.24, 140.62, 163.90 (SIMes(*C*)═C(1-methylimidazolium)(C(O)(CF_3))), 166.33 (q, $^{2}J_{CF} \approx 32$ Hz, *C*═O). ^{19}F NMR (282 MHz, $CDCl_3$): δ −78.9 (s, 3F, $SO_3CF_3^-$), −83.3 (ov dd, $^{3}J_{FF} \approx 5$ Hz, 3F, CF_2CF_3), −99.8 (dq, $^{2}J_{FF} \approx 272$ Hz, $^{3}J_{FF} \approx 5$ Hz, C$F^{A}F^{A'}CF_3$), −103.0 (dq, $^{2}J_{FF} \approx 272$ Hz, $^{3}J_{FF} \approx 5$ Hz, $CF^{A}F^{A'}CF_3$). MS [ESI (positive mode), solvent MeCN]: calcd *m*/*z* (% intensity) for [SIMes═C(1-methylimidazolium)(C(O)(CF_3))$^{+}$, $C_{28}H_{32}F_3N_4O^{+}$] 497.25 (100), 498.26 (30), 499.26 (3); found *m*/*z* (% intensity) 497.2492 (100), 498.2767 (37), 499.2959 (6).

Synthesis of SIMes═C(F)C(H)(═Cp) (10). In a glovebox, SIMes═CF(CF_2H) (**1b**; 200 mg, 0.515 mmol) was placed in a vial and dissolved in THF (~5 mL). The pale yellow solution was transferred to a 25 mL tubular Schlenk flask with a stir bar. To this stirred solution was added sodium cyclopentadienide (2.0 M in THF, 0.528 mL, 1.03 mmol), causing an immediate colour change to bright orange-yellow. After the mixture was stirred for 1 h, volatiles were removed in vacuo. The orange residue was extracted with toluene (15 mL) and filtered through Celite with toluene washings (3 × 5 mL). The toluene was removed in vacuo, minimal THF was added to the orange residue, and the resulting suspension was placed in the freezer (−35 °C). The product was isolated by filtration on a frit, followed by a second recrystallization from the filtrate. The product was isolated as a crystalline, bright orange solid. Yield: 195 mg, 91% based on SIMes═CF(CF_2H). mp: 190–194 °C (decomposition). ^{1}H NMR (300 MHz, $CDCl_3$): δ 2.32 (ov s, 18H, Ar-CH_3), 3.93 (s, 4H, N-CH_2CH_2-N), 5.71 (m, 1H, Cp-*H*), 5.99 (dm, 1H, $^3J_{FH} \approx$ 41 Hz, SIMes-CF═C(*H*)(Cp)), 6.11 (m, 1H, Cp-*H*), 6.28 (m, 1H, Cp-*H*), 6.44 (m, 1H, Cp-*H*), 6.96 (br, 4H, Ar-*H*). ^{13}C{^{1}H} NMR (101 MHz, $CDCl_3$): δ 17.87, 21.13, 50.28, 118.27, 118.37, 120.43, 122.15, 123.75 (br), 124.73, 124.77, 125.75, 125.85, 129.97 (br d, $^2J_{CF} \approx$ 88 Hz, SIMes-CF═*C*(H)(Cp)), 130.62, 132.75, 136.07 (br m, SIMes-*C*F═*C*(H)(Cp)), 149.45 (d, $^2J_{CF} \approx$ 21 Hz, SIMes(*C*)-CF═C(H)(Cp)). ^{19}F NMR (282 MHz, $CDCl_3$): δ −163.4 (dd, 1F, $^3J_{FH} \approx$ 41 Hz, $^4J_{FH} \approx$ 5 Hz, SIMes-C*F*═C(H)(Cp)). ^{19}F{^{1}H} NMR (282 MHz, $CDCl_3$): δ −163.4 (s, 1F, SIMes-C*F*═C(H)(Cp)). MS [ESI (positive mode), solvent MeCN]: calcd *m*/*z* (% intensity) for [SIMes═CF-C(H)(═Cp) + H^+, $C_{28}H_{32}FN_2^+$] 415.25 (100), 416.26 (30), 417.26 (3); found *m*/*z* (% intensity) 415.2511 (100), 416.2699 (38), 417.2863 (6). UV–vis (0.06 mM in DCM): λ_{max} (ε) 452 nm (35522 M^{-1} cm^{-1}).

Synthesis of [SIMes-CF═C(CF$_3$){Mn(CO)$_5$}][OTf] (11). In a glovebox, [Na][Mn(CO)$_5$] (75 mg, 0.341 mmol) was placed in a vial and dissolved in THF (~5 mL). To this stirred solution was added [SIMes-CF═CF(CF$_3$)][OTf] (200 mg, 0.341 mmol), causing an immediate colour change from pale yellow to deep orange, along with the formation of solid NaF. After the mixture was stirred for 1 h, the volatiles were removed in vacuo. The dark orange residue was extracted with DCM (5 mL) and filtered through Celite with DCM washings (3 × 2 mL). Hexanes (~10 mL) was added to the filtrate solution, causing immediate precipitation of the product, which was isolated by filtration on a frit and washed with toluene (~2 mL) and hexanes (~5 mL). The product was isolated as a crystalline orange-yellow solid. Yield: 77% based on [SIMes-CF═CF(CF$_3$)][OTf]. mp: 205 °C. ^{1}H NMR (300 MHz, CDCl$_3$): δ 2.27 (s, 6H, Ar-C*H*$_3$), 2.33 (s, 6H, Ar-C*H*$_3$), 2.39 (s, 6H, Ar-C*H*$_3$), 4.75 (m, 4H, N-C*H*$_2$C*H*$_2$-N), 6.93 (br, 2H, Ar-*H*), 6.95 (br, 2H, Ar-*H*). ^{13}C{^{1}H} NMR (101 MHz, CDCl$_3$): δ 17.78 (br), 21.05, 52.45, 129.29, 130.10, 130.30, 135.68, 136.04, 141.08, 160.84 (d, $^1J_{CF}$ ≈ 44 Hz), 205.68 (br). ^{19}F NMR (282 MHz, CDCl$_3$): δ −51.7 (d, 3F, $^4J_{FF}$ ≈ 7 Hz, SIMes-CF═C(C*F*$_3$){Mn(CO)$_5$}), −61.2 (q, 1F, $^4J_{FF}$ ≈ 7 Hz, SIMes-C*F*═C(CF$_3$){Mn(CO)$_5$}), −78.8 (s, 3F, SO$_3$C*F*$_3^-$). MS [ESI (positive mode), solvent: MeCN]: calcd *m*/*z* (% intensity) for [SIMes-CF═C(CF$_3$){Mn(CO)$_5$}$^+$, $C_{29}H_{26}F_4MnN_2O_5^+$] 613.12 (100), 614.12 (31), 615.12 (5); found *m*/*z* (% intensity) 613.1158 (100), 614.1191 (59), 615.1220 (8). IR: 2139 (m, Mn-*CO*), 2087 (m, br, Mn-*CO*), 2048 (s, br, Mn-*CO*), 2036 (s, br, Mn-*CO*), 1950 cm^{-1} (w, br, Mn-*CO*). Anal. Calcd for $C_{30}H_{26}F_7MnN_2O_8S$: C, 47.25; H, 3.44; N, 3.67; S, 4.20. Found: C, 46.86; H, 3.41; N, 3.70; S, 4.33.

Synthesis of [SIMes-CF═C(CF$_3$){CpMo(CO)$_3$}][OTf] (12). In a glovebox, [Na][CpMo(CO)$_3$] (92 mg, 0.341 mmol) was placed in a round-bottom Schlenk flask and dissolved in THF (~5 mL).

Separately, [SIMes-CF═CF(CF_3)][OTf] (200 mg, 0.341 mmol) was dissolved in THF (~5 mL) and transferred to a tubular Schlenk flask. On a Schlenk line, the round-bottom flask containing [Na][$CpMo(CO)_3$] was cooled to −78 °C using a dry ice and acetone bath. The solution containing [SIMes-CF═CF(CF_3)][OTf] was added dropwise via cannula transfer over ~5 min, causing an immediate colour change from pale yellow to a very deep red, along with the formation of solid NaF. Following THF washings (2 × 2 mL) to ensure quantitative transfer, the reaction mixture was stirred at low temperature for 10 min and then warmed to room temperature and stirred for an additional 30 min before removing the volatiles in vacuo. The dark red residue was extracted with DCM (5 mL) and filtered through Celite with DCM washings (3 × 2 mL). Hexanes (~10 mL) was added to the filtrate solution, causing immediate precipitation of the product, which was isolated by filtration on a frit and washed with toluene (~2 mL) and hexanes (~5 mL). The product was isolated as a very crystalline dark red solid. Yield: 86% based on [SIMes-CF═CF(CF_3)][OTf]. mp: 148–150 °C (decomposition). ^{1}H NMR (300 MHz, $CDCl_3$): δ 2.27 (s, 6H, Ar-CH_3), 2.32 (s, 6H, Ar-CH_3), 2.40 (s, 6H, Ar-CH_3), 4.69 (m, 4H, N-CH_2CH_2-N), 5.03 (s, 5H, Cp), 6.95 (s, 4H, Ar-*H*). ^{13}C{^{1}H} NMR (101 MHz, $CDCl_3$): δ 17.71, 17.95, 21.10, 52.33, 93.03, 129.36, 130.20, 130.39, 136.15, 136.25, 141.14, 161.77 (d, $^1J_{CF}$ ≈ 44 Hz), 224.82 (d, $^2J_{CF}$ ≈ 7 Hz), 235.05. ^{19}F NMR (282 MHz, $CDCl_3$): δ −51.7 (d, 3F, $^4J_{FF}$ ≈ 6 Hz, SIMes-CF═C(CF_3){$CpMo(CO)_3$}), −55.5 (q, 1F, $^4J_{FF}$ ≈ 6 Hz, SIMes-C*F*═C(CF_3){$CpMo(CO)_3$}), −78.8 (s, 3F, $SO_3CF_3^-$). MS [ESI (positive mode), solvent: MeCN]: calcd *m*/*z* (% intensity) for [SIMes-CF═CF(CF_3){$CpMo(CO)_3$}$^+$, $C_{32}H_{31}F_4MoN_2O_3^+$] 665.13 (100), 663.13 (69), 662.13 (66), 659.13 (62), 667.13 (40), 664.13 (40), 661.13 (38), 666.14 (35), 660.14 (21), 668.14 (14), 669.14 (2); found *m*/*z* (% intensity): 665.1165 (100), 663.1187 (83), 662.1217 (72), 659.2177 (118), 667.1360 (42), 664.1259 (62), 661.1340 (42), 666.1360 (35), 660.1575 (29), 668.1487 (15),

669.1550 (3). IR: 2049 (s, Mo-*CO*), 1983 (s, Mo-*CO*), 1957 cm^{-1} (br, Mo-*CO*). Anal. Calcd for $C_{33}H_{31}F_7MoN_2O_6S$: C, 48.78; H, 3.85; N, 3.45; S, 3.95. Found: C, 48.36; H, 3.82; N, 3.43; S, 3.95. We note the difference between C(calcd) and C(found) is 0.42%, which, while slightly outside the range viewed as establishing analytical purity (±0.40%), is provided as the best value obtained to date. All other methods of characterization confirm the purity of **12**.

Chapter 5

5.1 Context

The list of N-heterocyclic carbenes (NHCs) available to researchers keeps expanding, and these include many variations with regards to electronic and steric parameters.[141,160,171] Our first report on the reactivity between common NHCs and fluoroalkenes (Chapter 3), and their eventual transformations to polyfluoroalkenyl imidazolium salts, naturally led us to investigate their substitution chemistry further (Chapter 4). However, my lack of success in expanding the scope of NHC fluoroalkene adducts to include smaller carbenes (I^iPr and IM_4) and unsaturated carbenes (except for the previous report between IPr and tetrafluoroethylene (TFE) by Ogoshi *et al.*),[266] seemed to indicate the need for a more thorough understanding of the fundamental reactivity between these species.

To achieve a better understanding of how the various electronic and steric parameters of NHCs affect the formation and stability of fluoroalkene adducts, a total of 15 carbenes were studied for their activity towards TFE, hexafluoropropene (HFP), trifluoroethylene (HTFE) and vinylidene fluoride (VDF). Chapter 5 will demonstrate that my choice of NHCs to form the adducts first reported in Chapter 3 was surprisingly fortunate. Indeed, unsaturated carbenes are shown to be generally too reactive, unless the backbone is substituted with electron withdrawing substituents, such as chlorine. Alkyl-substituted carbenes also proved unsuccessful in these reactions, leading to a variety of uncharacterized products.

Interestingly, six- and seven-membered ring-expanded NHCs were shown to form very clean and stable adducts with TFE, but failed to do so with HFP, HTFE and VDF. In a surprising reaction, a cyclic (alkyl)(amino)carbene (CAAC) was shown to cleanly produce an alternate

isomer when allowed to react with HTFE. The unique steric constraints of the CAAC appear to modify the initial point of nucleophilic attack, prompting it to favor the less sterically hindered =CH(F) end of the fluoroalkene, as opposed to the more electrophilic $=CF_2$ end. This reaction represents the first example of how modifying the nature of the carbene can modify the isomer obtained in an NHC fluoroalkene adduct.

Attempts to correlate the observed reactivity with electronic (TEP) and steric ($\%V_{bur}$) parameters for NHCs were somewhat unsuccessful, as no discernable trend could be established. However, it does appear that a certain amount of steric bulk is required for the formation of stable adducts. Although much remains to be learned about this reactivity, Chapter 5 establishes very important observations and the unique reactivity observed with the CAAC should prompt researchers to explore other carbenes featuring atypical steric environments. It is certainly possible to envision the formation of new NHC fluoroalkene adducts with interesting applications in umpolung or fluoroalkene polymerization chemistry.

5.1.1 Published contributions

(1) **Leclerc, M. C.**; Da Gama, J. G.; Gabidullin, B. M.; Baker, R. T. *J. Fluorine Chem.* **2017**, doi: 10.1016/j.jfluchem.2017.05.012.

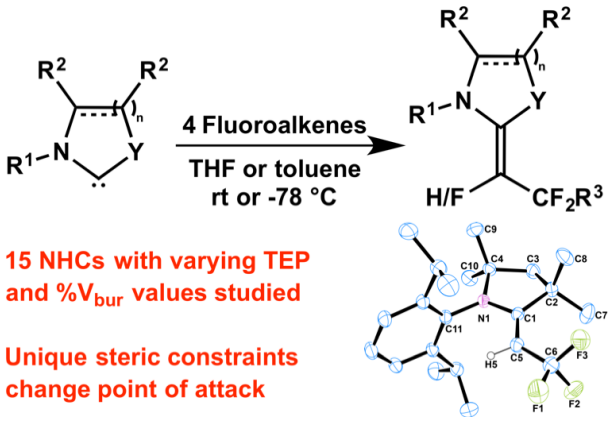

The fundamental reactivity leading to N-heterocyclic fluoroalkene adducts is explored in detail, featuring a total of 15 N-heterocyclic carbenes (NHCs) with various electronic and steric environments. The activity of these carbenes towards tetrafluoroethylene (TFE), hexafluoropropene (HFP), trifluoroethylene (HTFE) and vinylidene fluoride (VDF) is assessed in THF and toluene. Attempts were made to correlate the observed reactivity with electronic (TEP) and steric (%V_{bur}) parameters unique to each NHC, but a trend has yet to be fully determined. However, the unique steric constraints of a cyclic (alkyl)(amino)carbene (CAAC) were shown to modify the initial point of nucleophilic attack on HTFE, providing selective transformation to a different adduct than has been observed to date with all reactions involving this fluoroalkene.

Author contributions: The manuscript was written by MCL. All compounds were synthesized and characterized by MCL. Preliminary experiments involving screening for NHC reactivity with various fluoroalkenes were performed by JGD, under the supervision of MCL. BMG performed the crystallography.

5.2 A Closer Look at the Reactivity Between N-Heterocyclic Carbenes and Fluoroalkenes

5.2.1 Introduction

The incredible diversity of isolable carbenes available to researchers has contributed to these molecules becoming mainstays of transition metal catalysis as ancillary ligands and in main-group chemistry as potent stabilizers for low-valent species.[141,146] More recently, N-heterocyclic carbenes (NHCs) and thiazol-2-ylidenes have also been featured prominently as organocatalysts, with most examples of such reactivity proceeding via the Breslow intermediate and involving a formal umpolung of the carbon in the initially electrophilic substrate.[176,181,189]

Since the pioneering work of Bertrand *et al.*[365] and the seminal isolation of the first persistent carbene by Arduengo *et al.* in 1991,[151] there has been a significant push towards the synthesis of an ever-increasing amount of derivatives and analogues, many of which exhibit marked differences in reactivity from one another. The design of such molecules was greatly aided when it became apparent that the stability of free carbenes was not necessarily governed by sterics, but rather by important σ and π electronic effects, as evidenced by the stability of **IMe$_4$**.[152] The field is largely dominated by N-heterocyclic carbenes, with the possibility of a saturated or unsaturated two-carbon backbone for systems based on imidazoline or imidazole fragments, respectively. The nitrogen atoms in these types of carbenes can possess both aryl or alkyl substituents, and the backbone can also be functionalized. Furthermore, six- and seven-membered expanded ring NHCs are known to be more basic than their five-membered analogues, with the seven-membered species featuring a very twisted ring, which can lead to desirable orientation of the *N*-substituents upon coordination.[172,366] A unique class of carbenes termed cyclic

(alkyl)(amino)carbenes (CAACs), introduced by Bertrand *et al*., has been shown to possess unique steric environments and electronic parameters.[177,178,367]

As powerful nucleophiles, it is somewhat surprising that the reactivity between NHCs and electrophilic alkenes remains relatively unexplored. Arduengo and coworkers have reported on the reactivity of cyanocarbons with imidazole-2-ylidene carbenes, which includes the very electrophilic tetracyanoethylene (TCNE).[368] Following up on this study, they chose to focus on the reactivity between imidazole(in)-2-ylidenes and fluoroalkenes.[267] Closely following the publication of this manuscript, we published our own report examining the reactivity of NHCs with various fluoroalkenes to form several NHC fluoroalkenes.[268] More recently, we have demonstrated that NHCs can promote facile C-F bond activation from NHC fluoroalkene adducts and polyfluoroalkenyl imidazolium salts to form C-E bonds (E = C, N, O, S) and C-M bonds (M = Mn, Mo).[310] Due to the difficulties associated with the formation and manipulation of C-F bonds, the selectivity and ease of activation observed in these systems is somewhat surprising, and herein I aim to gain a better understanding of the fundamental reactivity between various carbenes and fluoroalkenes.

5.2.2 Results and discussion

To probe the limitations and requirements of the reactivity between NHCs and fluoroalkenes, a total of 15 relatively common NHCs (Figure 5.1) were explored. Their reactivity with tetrafluoroethylene (TFE), hexafluoropropene (HFP), trifluoroethylene (HTFE) and vinylidene fluoride (VDF) was examined. Owing to the element's large electronegativity, the presence of more fluorine substituents on an alkene renders it more electrophilic, and thus more reactive (Figure 5.1) towards nucleophilic attack.

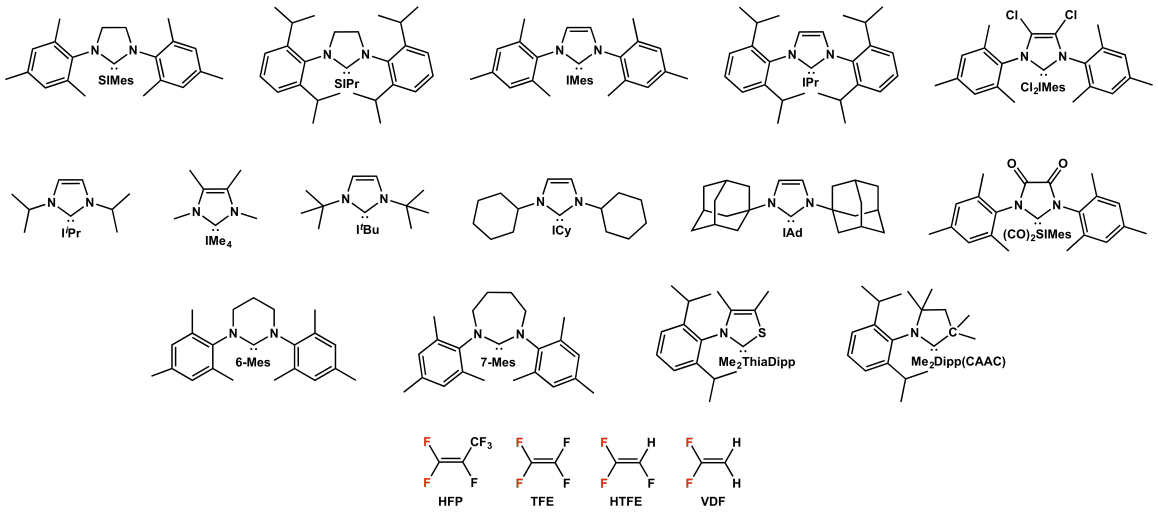

Figure 5.1. Various NHCs (top) and fluoroalkenes (bottom) studied in this work. Terminal $=CF_2$ fragments on fluoroalkenes are highlighted in red, indicating principal point of attack by carbene.

We have previously demonstrated the importance of a sufficiently electron deficient sp^2 carbon center for reactivity with an NHC to occur.[268] Specifically, it was found that *cis*-1,2-difluoroethylene offered no reactivity whatsoever, while seemingly every other fluoroalkene with a terminal $=CF_2$ fragment reacts in some way. The proposed mechanistic pathway for this reaction involves initial attack of the carbene at the $=CF_2$ position of the fluoroalkene, leading to a transient zwitterionic intermediate.[267,268] Expulsion of a fluoride then leads to a polyfluoroalkenyl imidazolium fluoride species, which will rearrange via formal 1,2-F shift to form the observed NHC fluoroalkene adduct. My previous isolation and characterization of the proposed imidazolium fluoride salt lends support for this pathway.

Scheme 5.1. General reaction scheme for the transformation studied in this work

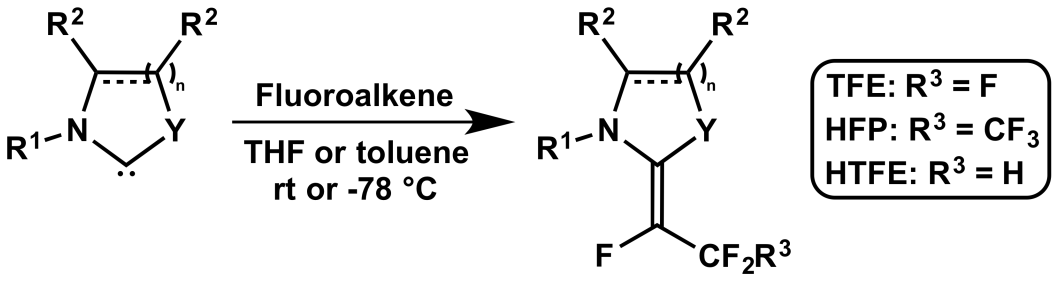

The general reaction studied in this work is presented in Scheme 5.1, and the products shown are those expected from the different fluoroalkenes based on previous work. Due to the extreme reactivity observed between most carbenes and fluoroalkenes in this work, every reaction was performed a minimum of two times, in both polar THF and non-polar toluene. When many different products were observed, the reactions were repeated at -78 °C.

5.2.2.1 Reactivity with N,N'-diaryl NHCs

As have previously reported,[268] both **SIMes** and **SIPr** react cleanly with TFE, HFP and HTFE in THF at room temperature within seconds to afford NHC fluoroalkene adducts, including the **SIMes** adduct with TFE also reported by Arduengo *et al.*[267] The reaction of **IPr** with TFE in C_6D_6 was reported by Ogoshi *et al.* in the Supporting Information of their work as a by-product to their reactions.[266] In my hands, **IPr** was shown to react unfavourably with HFP and HTFE, providing a multitude of unidentified products, even at -78 °C. Additionally, less sterically demanding **IMes** was found to require low temperatures to afford a clean adduct with TFE, and did not provide identifiable products with HFP. When a solution of **IMes** in THF was exposed to HTFE at room temperature, several unidentified products were observed and separation proved difficult. However, when the reaction is performed in toluene or C_6D_6 and HTFE is allowed to

slowly diffuse into the solution a colour change to pale yellow is observed, along with clean formation of **1** (Scheme 5.2). Monitoring the reaction by ^{19}F NMR reveals that the reaction is over within less than 2 minutes, but the product is not stable for more than 10 minutes in solution, decomposing to a mixture of dark brown, almost black products. Attempts to isolate **1** promptly led to decomposition.

Scheme 5.2. Synthetic scheme for 1

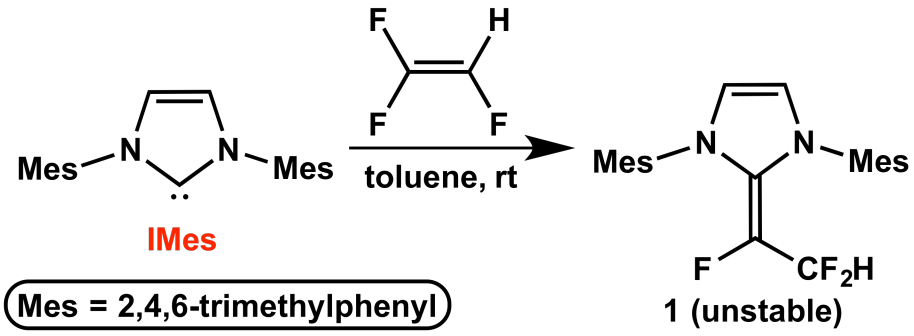

Substitution of the backbone hydrogen atoms with electron withdrawing chlorine atoms lowers the basicity of **IMes** by an appreciable degree.[369] Indeed, **Cl_2IMes** forms **2a** cleanly with TFE without the need for low temperature reaction conditions (Scheme 5.3). Product **2a** can be isolated in very good yield (83%) as a bright yellow crystalline solid. Unfortunately, HFP still proved too reactive at room temperature; however, the expected adduct could be observed via ^{19}F NMR if the reaction was performed at -78 °C. Unfortunately, this product was one of several and was thus not fully characterized. The reactivity between **Cl_2IMes** and HTFE to give **2b** is analogous with **IMes** (Scheme 5.3). The formation of **2b** is noticeably slower, however the stability of the product is only marginally increased. In this case, the reaction is shown to be complete within 5 minutes, and **2b** is stable in solution for approximately 15 minutes, upon which decomposition to dark orange products is observed.

Due to the positive effect of backbone substitution with chloride, I chose to examine **$(CO)_2$SIMes**. This carbene requires deprotonation at low temperatures and immediate *in situ* reactivity due to its thermally accessible triplet state, which leads it to readily dimerize.[370] Unfortunately, generation of the free carbene and injection of fluoroalkenes at low temperature did not provide any reactivity. When the solution was slowly warmed up to room temperature, immediate dimerization was observed and only unreacted fluoroalkene was observed by ^{19}F NMR.

Scheme 5.3. Synthetic scheme for 2

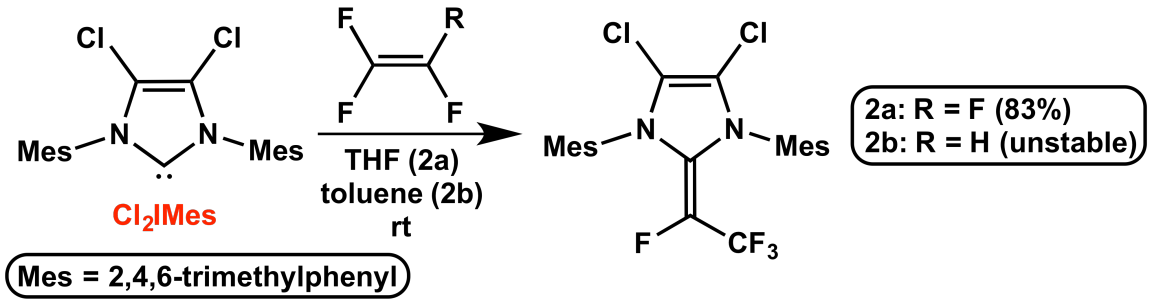

5.2.2.2 Reactivity with N,N'-dialkyl NHCs

We have previously noted that smaller NHCs, **IMe$_4$** and **I^{i}Pr**, do not react cleanly with the fluoroalkenes in our work.[268] Here, I have tried to isolate clean products by performing reactions at -78 °C but no change in reactivity was observed, prompting us to believe that the adducts formed in these reactions are inherently unstable. Attempts to limit further reactivity between the theoretically formed adducts and excess gas by instead utilizing an excess of NHC led to no change in the product distribution. Conversely, **I^{t}Bu** was reported to not react with our studied fluoroalkenes, even upon heating. Unfortunately, we failed to specify that this only applies to TFE and HTFE. Indeed, **I^{t}Bu** reacts with HFP to form a multitude of products, the ^{19}F

NMR spectra of which are difficult to interpret. When reactions with IAd were attempted, analogous reactivity is obtained. A detailed inspection of the ^{19}F NMR spectra obtained using **I^{t}Bu** and **IAd** with HFP reveals that although both reactions produce numerous unidentified products, there is very little overlap between those formed with the two NHCs. Analogously, **ICy** failed to provide any clean or identifiable products with the fluoroalkenes studied herein.

5.2.2.3 Reactivity with ring-expanded NHCs and a thiazol-2-ylidene

Most NHCs feature five-membered core structures, but examples of ring-expanded structures have been reported.[172,366] Due to my lack of success with alkyl-substituted NHCs, I chose to utilize aryl-substituted carbenes **6-Mes** and **7-Mes**. When **6-Mes** is allowed to react with TFE, clean transformation to **3** is observed within seconds at room temperature, and can be isolated in excellent yield (94%) as a pale beige crystalline solid (Scheme 5.4). Conversely, the reactivity with HFP is messy and no distinguishable products were observed.

Scheme 5.4. Synthetic scheme for 3 and 4

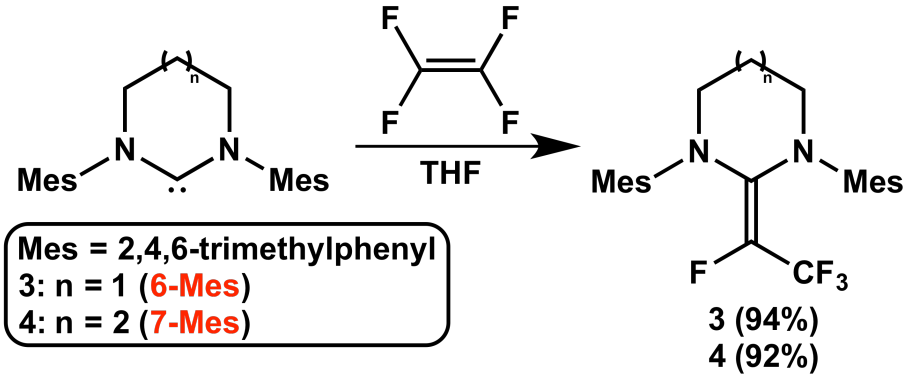

We have previously noted that most of these reactions undergo a vivid, and very short-lived (*ca.* 1-2 seconds), colour change when exposed to fluoroalkenes.[268] This has been proposed to arise from the transient zwitterion and is especially noticeable with TFE and HFP. However, I

have been unable to trap this proposed intermediate despite exploring a large variety of substrates and reaction conditions. When **6-Mes** is exposed to TFE or HFP, an immediate change from colourless to a very bright yellow is observed. Curiously, this colour change persists for approximately 15 seconds before settling on a paler yellow for TFE and a deep red mixture of decomposition products for HFP. When these reactions are performed at -78 °C, the brightly coloured intermediate could be observed and maintained for approximately 2 hours before eventually giving rise to the light yellow or deep red colours of the final reaction mixtures. Unfortunately, limitations pertaining to the introduction of a fluorinated gas into a cooled NMR tube in an NMR probe has prohibited us from visualizing this proposed zwitterionic intermediate by ^{19}F NMR. Attempts to inject the gas and immediately lower the NMR tube into a pre-cooled probe (-50 °C) also proved unsuccessful. Finally, **6-Mes** did not provide clean reactivity with HTFE. The reactivity observed with **7-Mes** was analogous to that of **6-Mes**, giving rise to **4** in very similar yield (92%) (Scheme 5.4).

A thiazol-2-ylidene, which I've termed **Me$_2$ThiaDipp**, failed to provide any adducts with the fluoroalkenes studied in this work. With TFE and HFP, an immediate colour change to deep red was observed, which is indicative of dimerization for this carbene.[371] This was confirmed by ^{1}H NMR and the values matched those reported in the literature. This carbene is known to undergo immediate dimerization in the presence of trace amounts of protic acids, and it is currently unclear what catalyzes this dimerization in the presence of TFE and HFP. No reactivity was observed when HTFE was introduced to **Me$_2$ThiaDipp**.

5.2.2.4 Reactivity with a CAAC

The unique steric constraints imposed by **Me_2Dipp(CAAC)**, wherein the methyl groups on carbon are relatively near the carbene centre and are also in and out of the plane of the heterocyclic fragment, implies these CAACs might react in unique ways with fluoroalkenes. Reactivity with TFE and HFP afforded the expected adducts **5a** and **5b**, respectively (Scheme 5.5). The products are formed in high yields and can be isolated as a pale yellow free-flowing solid (**5a**) or a pale pink-red crystalline solid (**5b**). Although **5b** is stable indefinitely at room temperature in the solid state, it is not stable in solution for more than a few hours.

Scheme 5.5. Synthetic scheme for 5a and 5b

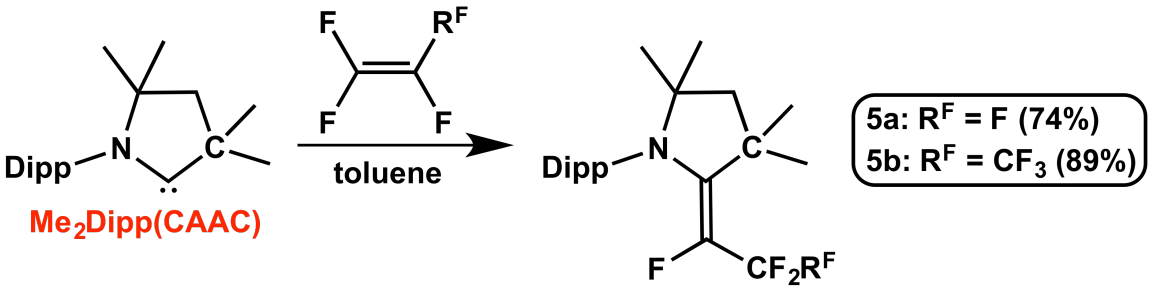

When HTFE was slowly diffused into a solution of **Me_2Dipp(CAAC)** in toluene, a colour change from nearly colourless to dark red and then a very dark green occurred. Surprisingly, a new isomer was identified (**5c**) and characterized for the first time (Scheme 5.6). As opposed to the expected =CF(CF_2H) isomer that has been observed thus far in successful reactions, the =CH(CF_3) isomer is obtained in this case. In fact, this is the only isomer present and there is no evidence for the formation of the =CF(CF_2H) product. The products can be distinguished with ease from their ^{1}H and ^{19}F NMR spectra, due to the different coupling patterns. Thus far, this represents the only isolated example of a fluoroalkene affording a different adduct

in a clean fashion. The isolation of **5c** proceeds in decent yield (67%) and affords bright green-yellow needles. It is probable that this change in reactivity is encouraged by the different steric environment present in **Me_2Dipp(CAAC)**, wherein the nucleophilic attack proceeds at the less sterically demanding =CH(F) carbon instead of the more electrophilic =CF_2 carbon. Following this initial attack, the same rearrangement that forms the other NHC fluoroalkene adducts would lead to **5c**. Evidently, TFE is symmetrical and cannot offer a less hindered site of attack, while the reactivity with HFP already proceeds via the less encumbered site.

Scheme 5.6. Synthetic scheme for 5c

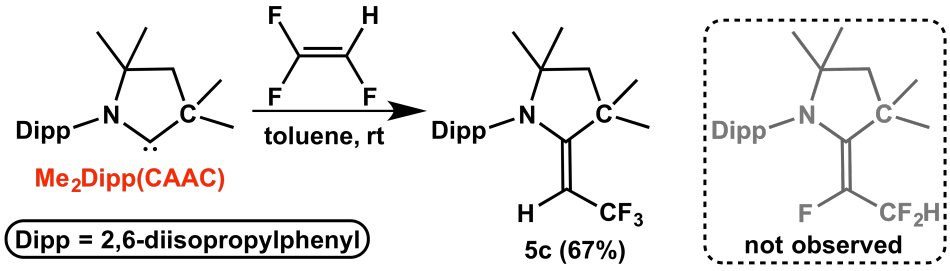

Single crystals of **5c** were grown by cooling (-35 °C) a concentrated solution in pure hexanes, and the proposed structure was confirmed crystallographically (Figure 5.2). The data confirms the orientation of the H and CF_3 substituents with respect to the carbene, wherein H is located closer to the Dipp substituent (Dipp = 2,6-diisopropylphenyl) and CF_3 is oriented towards the side of the two methyl substituents. Analogous to crystallographic data we have previously reported, the Dipp fragment is rotated perpendicular to the plane of the heterocycle. At this time, I do not have any evidence for the formation of the isomer where H and CF_3 would be switched.

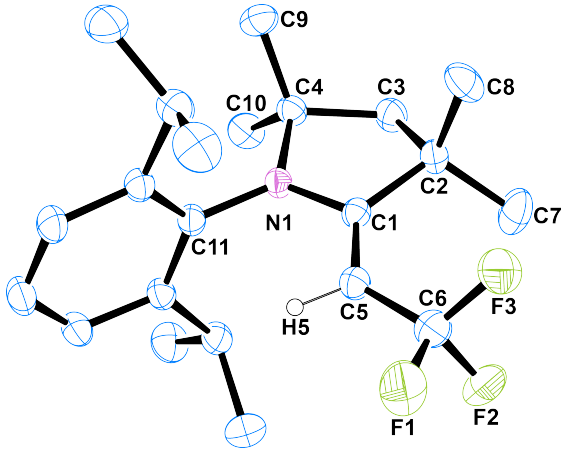

Figure 5.2. Crystallographic representation of 5c with 30% probability thermal ellipsoids. H atoms (except H5) are omitted for clarity. Selected bond lengths and angles are presented in the Supporting Information of the original publication.[372]

5.2.2.5 Reactivity summary

A summary of the reactivity observed between NHCs and fluoroalkenes studied in this work is presented in Table 5.1. Although not discussed until now, VDF has not yet provided any clean or identifiable products. In fact, it leads to decomposition and unstable product mixtures in most cases, except with **I^{t}Bu**, **IAd** and **Me$_2$ThiaDipp**, where no reactivity was observed. It bears mentioning that the ^{19}F NMR shift of the fluorine atom bound directly to the alkene in TFE adducts is very sensitive to the electronic nature of the NHC. Considering data from the **IPr** adduct by Ogoshi *et al*.[266] and our own previous reports with **SIPr** and **SIMes**,[268] as well as the examples with **Cl$_2$IMes**, **6-Mes**, **7-Mes** and **Me$_2$Dipp(CAAC)** reported in this work, this shift was shown to vary between *ca.* $\delta(^{19}F)$ = -170 to -218 ppm.

To attempt and correlate the reactivity observed between the various NHCs and fluoroalkenes with certain structural or electronic characteristics, I have chosen to focus on a few key steric and electronic parameters. The Tolman cone angle[157] is still the most common way of

evaluating the steric impact of a wide variety of phosphines and phosphites, but this model was shown to be an inefficient metric to evaluate NHCs and related carbenes. Instead, the percent buried volume ($\%V_{bur}$) is commonly employed as a more accurate representation of this effect.[166–170] Briefly, the $\%V_{bur}$ is described as the percentage of a sphere with r = 3.5 Å around a metal centre being occupied by a chosen ligand. Typically, the metal-ligand bond length is set to either 2.00 Å or 2.28 Å, and for the purposes of consistency the $\%V_{bur}$ values for a value of 2.00 Å will be utilized throughout this work. A recent review by Nolan *et al*. explores this subject in depth, and offers an extensive collection of values reported to date.[171] A large number of values have been reported for gold complexes of the type (NHC)AuCl, including most NHCs studied here. Unfortunately, I was unable to find **Me_2Dipp(CAAC)** data with gold, and had to rely on results obtained with $Ni(CO)_3$(NHC). Additionally, values for **Me_2ThiaDipp** were obtained from the perchlorate salt as opposed to the free carbene, and data for **Cl_2IMes** was obtained from its $Rh(Cl)(CO)_2$(NHC) complex.

Defining the electronic parameters of an NHC is somewhat less straightforward than its steric effects. However, the Tolman electronic parameter (TEP)[157] remains the most widely utilized method to accomplish this, as elaborated upon in a useful review by Nolan *et al*.[160] Historically, $Ni(CO)_3$(L) complexes were prepared and their corresponding IR spectra were recorded. A strong electron donating ligand will increase the electronic density at the metal, and in turn increase the M-C bond strength. Consequently, the C-O bond weakens and the stretching frequency effectively decreases, as observed by IR spectroscopy. Over the years, researchers have largely moved away from nickel and instead focus on $M(Cl)(CO)_2$(L) complexes (M = Ir, Rh), primarily due to the ease of handling and decreased safety concerns involved in using iridium and rhodium. Linear regression analysis has allowed these systems to be compared to the original

nickel scale, which makes for easier comparisons.[158,159] For consistency, the values utilized in this work are all derived from Ir(Cl)$(CO)_2$(NHC), except for **Cl_2IMes**, **6-Mes** and **7-Mes**, which were derived from the analogous Rh complexes. Additionally, **Me_2Dipp(CAAC)** data was obtained from Ni$(CO)_3$(NHC) and **IMe_4** data was obtained via DFT calculations.

Although the values between different systems do vary slightly for both $\%V_{bur}$ and the TEP, there is sufficient work supporting the general trends observed for these series of values to feel confident in comparing these relative values.[160,171] Finally, it is important to note that TEP values fail to provide any accurate information about the π-acidity of NHCs. For many years, these species were viewed solely as σ-donors, but it is now known that a more accurate depiction of NHC bonding must involve at least some amount of π-backbonding.[161–165] The two primary methods of establishing or quantifying the degree of π-acidity of NHCs involve the formation of carbene-phosphinidene[161,163] and carbene-selenium[162,164] complexes. By recording the ^{31}P and ^{77}Se NMR spectra of these complexes, a clear relationship was observed between the chemical shift and the degree of backbonding from P or Se into the carbene fragment, allowing for a relative ranking of various carbenes and their abilities to participate in π-backbonding.

As evidenced in Table 5.1, **SIPr** and **SIMes** remain the best candidates for reactivity with electrophilic fluoroalkenes. They are the only NHCs thus far that have proven capable of affording clean adducts, at room temperature and in various solvents, with TFE, HFP and HTFE. Generally, HFP has proven to be too reactive, while HTFE appears to often give rise to unstable products that are prone to decomposition. The cleaner reactivity obtained with TFE when utilizing **Cl_2IMes** as opposed to **IMes**, and the complete lack of reactivity observed with **$(CO)_2$SIMes**, does appear to be indicative of a system that is sensitive to the electronic parameters of the NHC. However, the isolation of clean adducts with carbenes that are more

nucleophilic than **IMes**, i.e., **Me$_2$Dipp(CAAC)**, **6-Mes** and **7-Mes**, suggests that there are several other factors at play. To correlate the reactivity presented in this work with key electronic and steric parameters of NHCs, the relative TEP and %V_{bur} values of these carbenes were plotted and are presented in Figure 5.3.

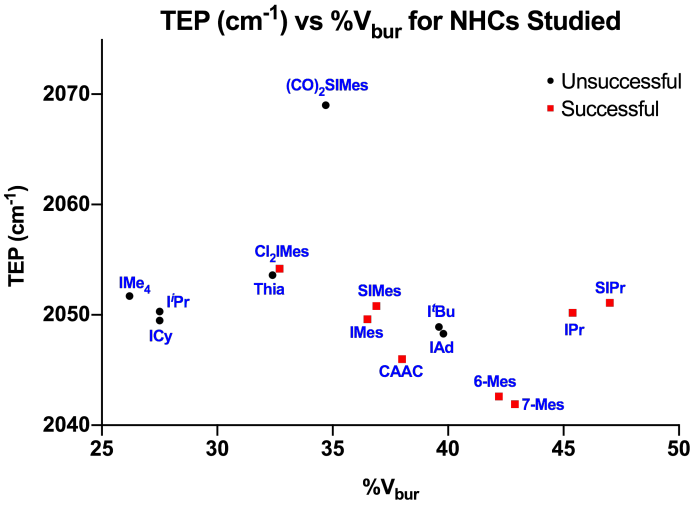

Figure 5.3. Graphical representation of TEP (cm^{-1}) and %V_{bur} values for the NHCs studied in this work, demonstrating a relative lack of correlation between steric and electronic factors and the observed.

Table 5.1. Summary of the reactivity observed between NHCs and fluoroalkenes, as well as TEP (cm^{-1}) and $\%V_{bur}$ values

NHC	TFE	HFP	HTFE	VDF	TEP (cm^{-1})[a]	$\%V_{bur}$[b]
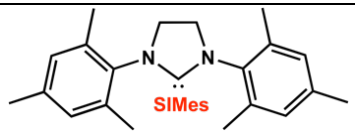 SIMes	✓	✓	✓	decomp.	2050.8[160]	36.9[171]
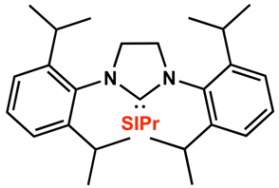 SIPr	✓	✓	✓	decomp.	2051.1[160]	47.0[171]
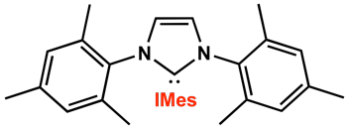 IMes	✓ (-78 °C)	decomp.	✓ (unstable)	decomp.	2049.6[160]	36.5[171]
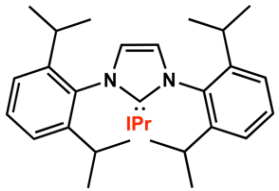 IPr	✓	decomp.	decomp.	decomp.	2050.2[160]	45.4[171]
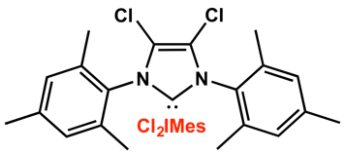 Cl_2IMes	✓	decomp.	✓ (unstable)	decomp.	2054.2[159]	32.7[373,d]

NHC	TFE	HFP	HTFE	VDF	TEP (cm^{-1})[a]	%V_{bur}[b]
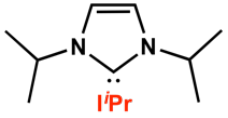 I^iPr	decomp.	decomp.	decomp.	decomp.	2050.3[160]	27.5[171]
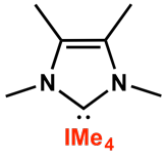 IMe_4	decomp.	decomp.	decomp.	decomp.	2051.7[374,c]	26.2[171]
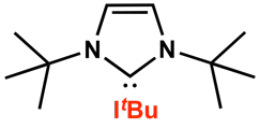 I^tBu	n/r	decomp.	n/r	n/r	2048.9[160]	39.6[171]
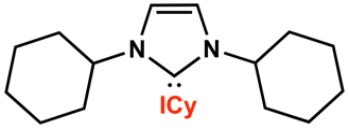 ICy	decomp.	decomp.	decomp.	decomp.	2049.5[160]	27.5[171]
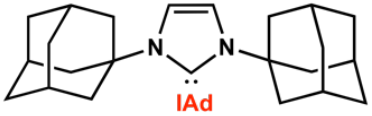 IAd	n/r	decomp.	n/r	n/r	2048.3[160]	39.8[171]

NHC	TFE	HFP	HTFE	VDF	TEP (cm^{-1})[a]	%V_{bur}[b]
	dimerization	dimerization	dimerization	dimerization	2069.0[160]	34.7[375]
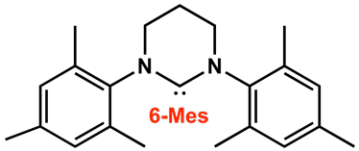	✓	decomp.	✓ (unstable)	decomp.	2042.6[160,d]	42.2[366]
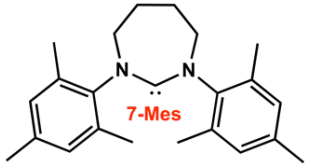	✓	decomp.	✓ (unstable)	decomp.	2041.9[160,d]	42.9[366]
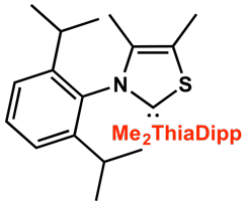	dimerization	dimerization	n/r	n/r	2053.6[160]	32.4[176,f]
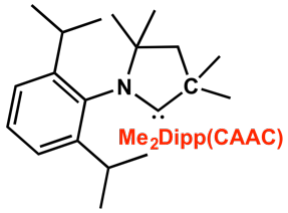	✓	✓	✓ (alternate isomer)	decomp.	2046.0[376,e]	38.0[376,e]

[a]Obtained from $Ir(Cl)(CO)_2(NHC)$ complexes. [b]Obtained (NHC)AuCl complexes. [c]Obtained from DFT calculations. [d]Obtained from $Rh(Cl)(CO)_2(NHC)$ complexes. [e]Obtained from $Ni(CO)_3(NHC)$ complexes. [f]Obtained from the corresponding $HClO_4$ salt.

Although it would be appealing to draw sweeping conclusions from this data, it is still unclear if a correlation can be made between the observed reactivity and the NHC parameters presented in this work. In particular, **I^{t}Bu** and **IAd** stand out as exceptions. It is thus somewhat curious that no clean reactivity with these carbenes has been observed yet, with various solvents and reaction conditions. Finally, attempts to incorporate the relative π-acidity of these carbenes when looking at the TEP values to perhaps obtain a more complete picture of the electronic effects of these carbenes have been inconclusive. In fact, **IAd** has been shown to be a significant π-acceptor, along with **I^{t}Bu**. As with the other factors, it appears that the desired NHCs are spread out over the π-acidity scale and it is difficult to draw any significant conclusions from these values. It does appear, however, that a moderate amount of steric bulk is required for the successful formation and isolation of NHC fluoroalkene adducts. Thus far, no adducts have been isolated with carbenes having a $\%V_{bur}$ below *ca.* 32%. However, it is important to note that although a generous cross-section of carbenes have been studied herein, the incredible amounts of these species having been reported in the literature means that there are possibly other classes that might provide clean adducts. Indeed, the isolation of **5c** should encourage studies involving the use of carbenes with unique or atypical steric arrangements, perhaps aiming towards the formation of other novel isomers or of more labile systems, perhaps capable of effecting organocatalysis or controlled fluoroalkene polymerization.

5.2.3 Conclusions

In summary, a combination of 15 NHCs with various electronic and steric environments and 4 fluoroalkenes were studied to obtain a better understanding of their reactivity to form NHC fluoroalkene adducts. To date, a stable adduct with VDF has not been isolated. Reactivity

between a cyclic (alkyl)(amino)carbene and HTFE provided an alternate isomer than is typically observed with this fluoroalkene, the first time this switch in reactivity has been demonstrated. Unfortunately, I was unable to discern any clear correlations between electronic (TEP) or steric ($\%V_{bur}$) factors, and carbenes providing positive reactivity. However, the unexpected result obtained by using **Me_2Dipp(CAAC)** is encouraging, and should prompt further studies into carbenes featuring atypical steric demands. By employing flexible steric bulk and varying the initial point of attack of the carbene on a fluoroalkene, it is interesting to envision forming novel adducts that could potentially be involved in exciting umpolung chemistry or polymerization reactions with other fluoroalkenes.

5.2.4 Experimental

5.2.4.1 General considerations

All manipulations were carried out using standard Schlenk techniques or in an MBraun glove box. All glassware was oven-dried at >150 °C for a minimum of 2 hours prior to use, or flame-dried using a torch. Toluene, tetrahydrofuran (THF), diethyl ether (DEE) and hexanes were dried on columns of activated alumina using a J. C. Meyer (formerly Glass Contour®) solvent purification system. Dichloromethane (DCM), chloroform ($CHCl_3$), chloroform-d ($CDCl_3$) and acetonitrile (MeCN) were dried by refluxing over calcium hydride under a nitrogen flow, followed by distillation and filtration through a column of activated alumina (ca. 10 wt. %). Methanol (MeOH) and ethanol (EtOH) were dried by refluxing over Mg/I_2 under nitrogen, followed by distillation. Benzene-d_6 (C_6D_6) was dried by standing over activated alumina (ca. 10 wt. %) overnight, followed by filtration. All solvents were stored over activated (heated at 250 °C for >6 h under vacuum) 4Å molecular sieves, except EtOH (stored over activated 3Å molecular

sieves). Acetone (Sigma Aldrich, 99.5+%) and dimethylsulfoxide (DMSO) (Sigma Aldrich, 99.9+%) were used as purchased, without further drying. The following chemicals were used as purchased, without further purification: 2,6-diisopropylaniline (Alfa Aesar, 90+%), 2,4,6-trimethylaniline (Alfa Aesar, 98%), triethyl orthoformate (Alfa Aesar, 98%), glacial acetic acid (Alfa Aesar, 99+%), *N,N*-diisopropylethylamine (Alfa Aesar, 99%), formic acid (Alfa Aesar, 97%), ethyl acetate (Alfa Aesar, 99+%), trimethylsilyl chloride (Sigma Aldrich, 99+%), sodium tetrafluoroborate (Strem Chemicals, 98%), potassium bis(trimethylsilyl)amide (Sigma Aldrich, 95%), carbon tetrachloride (Sigma Aldrich, anhydrous, 99,5+%), 1,3-diisopropylimidazolium chloride (**I^{i}Pr**) (Strem Chemicals, 97%), 1,3-di-*tert*-butylimidazol-2-ylidene (**I^{t}Bu**) (Strem Chemicals, 98%), 1-hexanol (Sigma Aldrich, 98%), 3-hydroxy-2-butanone (Sigma Aldrich, 98+%), *N,N*'-dimethylthiourea (Sigma Aldrich, 99%), potassium (Sigma Aldrich, 98%), cyclohexylamine (Alfa Aesar, 98+%), tetrafluoroboric acid (Strem Chemicals, 48% aqueous solution), oxalyl chloride (Sigma Aldrich, 98%), sodium bis(trimethylsilyl)amide (Sigma Aldrich, 95%), potassium carbonate (Sigma Aldrich, 99+%), 1,3-dibromopropane (Alfa Aesar, 98%), 1,4-diiodobutane (Alfa Aesar, 99%), sodium hydroxide (Sigma Aldrich, 97+%), carbon disulfide (Sigma Aldrich, anhydrous, 99+%), 3-chlorobutan-2-one (Sigma Aldrich, 97%), sodium perchlorate (Sigma Aldrich, 98+%), isobutyraldehyde (Oakwood Chemicals, 99%), lithium diisopropylamide (Sigma Aldrich, 1.0 M in THF/hexanes), isobutylene oxide (Oakwood Chemicals, 97%), trifluoromethanesulfonic anhydride (Oakwood Chemicals, 98%), sodium hydride (Strem Chemicals, 60% in oil), hexafluoropropene (HFP) (SynQuest Labs, 98.5%), trifluoroethylene (HTFE) (SynQuest Labs, 98%) and 1,1-difluoroethylene (VDF) (SynQuest Labs, 99%). Tetrafluoroethylene (TFE) was made by pyrolysis of polytetrafluoroethylene (PTFE) (Scientific Polymer Products, powdered) under vacuum, using a slightly modified literature

procedure [10-20 mTorr, 650 °C, 15 g scale, product stabilized with (*R*)-(+)-limonene (Aldrich, 97%), giving TFE of ≥ 97% purity].[377] The synthesis of [SIMes][HCl],[298] [SIPr][HCl],[299] [IMes][HBF_4],[378] [IPr][HBF_4],[378] **Cl_2IMes**,[369] **IMe_4**,[299] [ICy][HBF_4],[378] [IAd][HBF_4],[379] (CO_2)SIMes(H)(Cl),[370] [6-Mes][HBF_4],[172] [7-Mes][HBF_4],[172] [Me_2ThiaDipp][$HClO_4$][371] and [Me_2Dipp(CAAC)][HOTf][177] have been previously described. Free **SIMes**, **SIPr** and **Me_2ThiaDipp** carbenes were synthesized from the appropriate imidazolium chloride salts by reaction with sodium hydride (2 equiv.) and catalytic potassium *tert*-butoxide (5 mol%) in THF overnight with vigorous stirring. The resulting solution was filtered through Celite with THF washings and the solvent removed *in vacuo* to afford flaky white solid of pure free N-heterocyclic carbene. Following an analogous procedure, but using KHMDS as the base, free **IMes**, **IPr**, **$(CO)_2$SIMes** (at -78 °C), **6-Mes** and **7-Mes** carbenes were prepared from their respective salts. Free **ICy** and **IAd** carbenes were similarly prepared by using KO^{t}Bu as the base. Finally, free **Me_2Dipp(CAAC)** carbene was prepared by deprotonation with LDA at -78 °C. All the carbenes utilized in this work were recrystallized according to their respective literature procedures prior to being screened for reactivity and stored in the freezer at -35 °C. ^{1}H, ^{19}F and ^{19}F{^{1}H} NMR spectra were recorded on either a Bruker Avance 300 or Bruker Avance II 300 spectrometer at room temperature. ^{13}C{^{1}H} NMR spectra were recorded on a Bruker Avance 400 spectrometer at room temperature. ^{1}H NMR spectra were referenced to the residual proton peaks associated with the deuterated solvents (C_6D_6 = 7.16 ppm, $CDCl_3$ = 7.26 ppm). ^{13}C NMR spectra were referenced to the signal associated with $CDCl_3$ (77.16 ppm). It is important to note that ^{13}C NMR signals coupled to ^{19}F nuclei are broadened out significantly, and although coupling constant values and multiplicity can sometimes be extracted it is often impossible to do so. As such, the data is presented to the best of our ability and all efforts are made to avoid any ambiguity in the

presentation of the data. ^{19}F and $^{19}F\{^{1}H\}$ NMR spectra were referenced to internal 1,3-bis(trifluoromethyl)benzene (BTB) (Aldrich, 99%, deoxygenated by purging with nitrogen and stored over 4Å molecular sieves), set to - 63.5 ppm. ^{1}H NMR data for BTB: (300 MHz, C_6D_6) δ 6.60 (m, 1H, Ar-5-H), 7.12 (m, 2H, Ar-4,6-H), 7.76 (m, 1H, Ar-2-H). A Micromass Q-ToF 1 (positive mode) was used for electrospray ionization (ESI), with samples diluted to *ca.* 5 μg/mL in acetonitrile. A Mel-Temp II was used for the determination of melting points.

5.2.4.2 Synthesis and characterization

Synthesis of IMes=CF(CF_2H) (1). In a glove box, **IMes** (20 mg, 0.07 mmol) was placed in a vial with a stir bar and dissolved in C_6D_6 (~ 0.6 mL). The solution was transferred to a screw-cap septum NMR tube. Outside of the glove box, a 3 mL plastic syringe was filled with HTFE and purged, before an additional 3 mL were added and slowly injected into the NMR tube. The gas was allowed to slowly diffuse through the solution to avoid the formation of unwanted, unidentified products. A colour change from nearly colourless to pale yellow could be observed within a few minutes of gas addition. The product is formed quickly and decomposes to a mixture of dark brown, almost black products within *ca*. 10 minutes if left in solution or if attempts are made to isolate it (see main text for more details). The product was thus not isolated, and characterized to the best of our ability using ^{19}F NMR spectroscopy. ^{19}F NMR (282 MHz, C_6D_6) δ -107.6 (dd, $^{2}J_{FH} \approx 52$ Hz, $^{3}J_{FF} \approx 15$ Hz, 1F, IMes=CF(CF_2H)), -221.1 (dt, $^{3}J_{FH} \approx 22$ Hz, $^{3}J_{FF} \approx 16$ Hz, 1F, IMes=CF(CF_2H)). $^{19}F\{^{1}H\}$ NMR (282 MHz, C_6D_6) δ -107.6 (d, $^{3}J_{FF} \approx 15$ Hz, 1F, IMes=CF(CF_2H)), -221.1 (t, $^{3}J_{FF} \approx 16$ Hz, 1F, IMes=CF(CF_2H)).

Synthesis of Cl_2IMes=CF(CF_3) (2a). In a glove box, **Cl_2IMes** (100 mg, 0.27 mmol) was placed in a 50 mL round bottom Schlenk flask with a stir bar and dissolved in THF (~ 4 mL). The flask was sealed with a septum and hooked up to a Schlenk line outside of the glove box. A 10 mL plastic syringe was filled with nitrogen and purged, before being filled with 10 mL of TFE. The gas was quickly injected into the flask, and an additional 5 mL were added immediately after. Immediately upon addition of TFE, a colour change from nearly colourless to bright yellow could be observed. After stirring for 30 minutes, the septum was replaced with a glass stopper, and all volatiles were removed *in vacuo*, affording an off-white residue. The flask was returned to the glove box, and the product was extracted with hexanes (~ 4 mL) and filtered through Celite® with hexanes washings (2 x 1 mL). The solution was concentrated under reduced pressure until the formation of solid could be observed, and then recrystallized from this cloudy solution at -35 °C. The product was isolated by filtration on a frit and dried under vacuum, affording bright yellow crystalline solid. Yield: 105 mg, 83% based on Cl_2IMes. mp: 162-163 °C. ^{1}H NMR (300 MHz, $CDCl_3$) δ 2.22 (br s, 12H, Ar-CH_3), 2.32 (s, 6H, Ar-CH_3), 6.94 (br, 4H, Ar-*H*). ^{13}C{^{1}H} NMR (101 MHz, $CDCl_3$) δ 17.86, 21.31, 112.94 (ov s), 118.79 (m), 123.95 (m), 129.06, 129.39, 131.38, 132.33, 137.20, 137.83, 139.20, 139.60, 139.73, 139.93. ^{19}F NMR (282 MHz, $CDCl_3$) δ -60.1 (d, $^3J_{FF}$ ≈ 16 Hz, 3F, Cl_2IMes=CF(CF_3)), -213.1 (q, $^3J_{FF}$ ≈ 16 Hz, 1F, Cl_2IMes=C*F*(CF_3)). MS [ESI (positive mode), solvent: MeCN] Calc. *m/z* (% intensity) for [Cl_2IMes=CF(CF_3) + H^+, $C_{23}H_{23}Cl_2F_4N_2^+$]: 473.12 (100), 475.11 (64), 476.12 (16). Found *m/z* (% intensity): 473.1174 (100), 475.1247 (60), 476.1349 (14).

Synthesis of Cl_2IMes=CF(CF_2H) (2b). In a glove box, **Cl_2IMes** (20 mg, 0.05 mmol) was placed in a vial with a stir bar and dissolved in C_6D_6 (~ 0.6 mL). The solution was transferred to a screw-cap septum NMR tube. Outside of the glove box, a 3 mL plastic syringe was filled with HTFE

and purged, before an additional 3 mL were added and slowly injected into the NMR tube. The gas was allowed to slowly diffuse through the solution to avoid the formation of unwanted, unidentified products. A colour change from nearly colourless to pale yellow could be observed within a few minutes of gas addition. The product is formed quickly and decomposes to a mixture of dark orange products within *ca*. 15 minutes if left in solution or if attempts are made to isolate it (see main text for more details). The product was thus not isolated, and characterized to the best of our ability using ^{19}F NMR spectroscopy. ^{19}F NMR (282 MHz, C_6D_6) δ -111.1 (dd, $^2J_{FH} \approx 52$ Hz, $^3J_{FF} \approx 17$ Hz, 1F, Cl_2IMes=CF(C*F*$_2$H)), -215.8 (dt, $^3J_{FH} \approx 21$ Hz, $^3J_{FF} \approx 17$ Hz, 1F, Cl_2IMes=C*F*(CF_2H)). ^{19}F{^{1}H} NMR (282 MHz, C_6D_6) δ -111.1 (d, $^3J_{FF} \approx 17$ Hz, 1F, Cl_2IMes=CF(C*F*$_2$H)), -215.8 (t, $^3J_{FF} \approx 17$ Hz, 1F, Cl_2IMes=C*F*(CF_2H)).

Synthesis of 6-Mes=CF(CF$_3$) (3). In a glove box, **6-Mes** (100 mg, 0.31 mmol) was placed in a 50 mL round bottom Schlenk flask with a stir bar and dissolved in THF (~ 4 mL). The flask was sealed with a septum and hooked up to a Schlenk line outside of the glove box. A 10 mL plastic syringe was filled with nitrogen and purged, before being filled with 10 mL of TFE. The gas was quickly injected into the flask, and an additional 5 mL were added immediately after. Immediately upon addition of TFE, a colour change from nearly colourless to very bright yellow could be observed, which persisted for a few seconds before settling on yellow-orange. After stirring for 30 minutes, the septum was replaced with a glass stopper, and all volatiles were removed *in vacuo*, affording an off-white residue. The flask was returned to the glove box, and the product was extracted with THF (~ 4 mL) and filtered through Celite® with THF washings (2 x 1 mL). The solution was concentrated under reduced pressure until the formation of solid could be observed, and then recrystallized from this cloudy solution at -35 °C. The product was isolated by filtration on a frit and dried under vacuum, affording a pale beige crystalline solid. Yield: 123

mg, 94% based on 6-Mes. mp: 175-177 °C. ^{1}H NMR (300 MHz, C_6D_6) δ 1.41 (ov m, 2H, N-$CH_2CH_2CH_2$-N), 2.11 (s, 6H, Ar-CH_3), 2.12 (s, 6H, Ar-CH_3), 2.29 (s, 6H, Ar-CH_3), 2.99 (ov m, 4H, N-$CH_2CH_2CH_2$-N), 6.78 (ov m, 4H, Ar-*H*). ^{13}C{^{1}H} NMR (101 MHz, $CDCl_3$) δ 18.66, 19.26, 20.86, 21.03, 25.28, 47.67, 48.42, 119.63 (m), 123.47 (m), 129.82, 130.02, 133.84, 134.77, 134.80, 134.96, 136.12, 141.78, 141.82, 142.64, 143.62 (dq, $^{2}J_{CF}$ ≈ 15 Hz, $^{3}J_{CF}$ ≈ 2 Hz, 6-Mes(*C*)=CF(CF_3). ^{19}F NMR (282 MHz, C_6D_6) δ -63.4 (d, $^{3}J_{FF}$ ≈ 16 Hz, 3F, 6-Mes=CF(CF_3)), -198.0 (q, $^{3}J_{FF}$ ≈ 16 Hz, 1F, 6-Mes=C*F*(CF_3)). MS [ESI (positive mode), solvent: MeCN] Calc. *m/z* (% intensity) for [6-Mes=CF(CF_3) + H^+, $C_{24}H_{29}F_4N_2^+$]: 421.23 (100), 422.23 (26), 423.23 (3). Found *m/z* (% intensity): 421.2201 (100), 422.2305 (26), 423.2442 (3).

Synthesis of 7-Mes=CF(CF_3) (4). In a glove box, **7-Mes** (100 mg, 0.30 mmol) was placed in a 50 mL round bottom Schlenk flask with a stir bar and dissolved in THF (~ 4 mL). The flask was sealed with a septum and hooked up to a Schlenk line outside of the glove box. A 10 mL plastic syringe was filled with nitrogen and purged, before being filled with 10 mL of TFE. The gas was quickly injected into the flask, and an additional 5 mL were added immediately after. Immediately upon addition of TFE, a colour change from nearly colourless to yellow could be observed. After stirring for 30 minutes, the septum was replaced with a glass stopper, and all volatiles were removed *in vacuo*, affording an off-white residue. The flask was returned to the glove box, and the product was extracted with THF (~ 4 mL) and filtered through Celite® with THF washings (2 x 1 mL). The solution was concentrated under reduced pressure until the formation of solid could be observed, and then recrystallized from this cloudy solution at -35 °C. The product was isolated by filtration on a frit and dried under vacuum, affording a pale beige crystalline solid. Yield: 120 mg, 92% based on 7-Mes. mp: 150-153 °C. ^{1}H NMR (300 MHz, C_6D_6) δ 1.03 (ov m, 4H, N-$CH_2CH_2CH_2$-N), 2.11 (s, 6H, Ar-CH_3), 2.12 (s, 6H, Ar-CH_3), 2.30 (s,

6H, Ar-CH_3), 3.12-3.66 (ov m, 4H, N-CH_2CH$_2$CH_2-N), 6.80 (ov m, 4H, Ar-*H*). ^{13}C{^{1}H} NMR (101 MHz, $CDCl_3$) δ 18.42, 19.92, 20.67, 20.75, 20.89, 21.16, 28.58, 28.68 (br), 30.51, 54.03, 55.07, 101.03, 118.83, 121.32 (m), 123.69 (m), 126.44, 129.71 (ov s), 130.38 (ov m), 134.72, 135.20, 142.30, 143.45 (ov s), 143.53, 144.00. ^{19}F NMR (282 MHz, C_6D_6) δ -63.7 (d, $^3J_{FF}$ ≈ 14 Hz, 3F, 7-Mes=CF(CF_3)), -184.4 (q, $^3J_{FF}$ ≈ 14 Hz, 1F, 7-Mes=C*F*(CF_3)). MS [ESI (positive mode), solvent: MeCN] Calc. *m/z* (% intensity) for [7-Mes=CF(CF_3) + H^+, $C_{25}H_{31}F_4N_2^+$]: 435.24 (100), 436.25 (27), 437.25 (3). Found *m/z* (% intensity): 435.2572 (100), 436.2694 (11), 437.2495 (6).

Synthesis of (Me$_2$Dipp(CAAC))=CF(CF$_3$) (5a). In a glove box, **Me$_2$Dipp(CAAC)** (100 mg, 0.35 mmol) was placed in a 50 mL round bottom Schlenk flask without a stir bar and dissolved in toluene (~ 4 mL). The flask was sealed with a septum and hooked up to a Schlenk line outside of the glove box. A 10 mL plastic syringe was filled with nitrogen and purged, before being half-filled with 5 mL of TFE. The gas was slowly injected into the flask, and allowed to slowly diffuse through the solution to avoid the formation of unwanted, unidentified products. This process was repeated twice with 5 mL portions of TFE. Soon after the addition of TFE, a colour change from nearly colourless to yellow-green could be observed. Following the final gas addition, and after allowing the gas to diffuse through the solution for 1 hour, the septum was replaced with a glass stopper, and all volatiles were removed *in vacuo*, affording a pale yellow residue. The flask was returned to the glove box, and the product was extracted with hexanes (~ 4 mL) and filtered through Celite® with hexanes washings (2 x 1 mL). The solution was concentrated under reduced pressure until the formation of solid could be observed, and then recrystallized from this cloudy solution at -35 °C. The product was isolated by filtration on a frit and dried under vacuum, affording a pale yellow, free-flowing solid. Yield: 99 mg, 74% based on Me$_2$Dipp(CAAC). mp:

87-90 °C (decomposition). ^{1}H NMR (300 MHz, $CDCl_3$) δ 1.11 (d, $^{3}J_{HH}$ ≈ 6.6 Hz, 6H, CH(CH_3)$_2$), 1.17 (s, 6H, C(CH_3)$_2$), 1.28 (d, $^{3}J_{HH}$ ≈ 6.6 Hz, 6H, CH(CH_3)$_2$), 1.51 (s, 6H, C(CH_3)$_2$), 2.12 (s, 2H, CH_2), 3.13 (sept, $^{3}J_{HH}$ ≈ 6.6 Hz, 2H, C*H*(CH$_3$)$_2$), 7.09-7.29 (ov m, 3H, Ar-*H*). ^{13}C{^{1}H} NMR (101 MHz, $CDCl_3$) δ 23.93, 25.19, 25.22, 28.94, 29.22, 29.80 (br m), 57.80, 65.37, 123.86, 127.83, 148.51 (d, $^{2}J_{CF}$ ≈ 4 Hz, Me_2Dipp(CAAC)(*C*)=CF(CF$_3$)). ^{19}F NMR (282 MHz, $CDCl_3$) δ -60.9 (d, $^{3}J_{FF}$ ≈ 13 Hz, 3F, Me_2Dipp(CAAC)=CF(C*F*$_3$)), -170.98 (q, $^{3}J_{FF}$ ≈ 13 Hz, 1F, Me_2Dipp(CAAC)=C*F*(CF$_3$)). MS [ESI (positive mode), solvent: MeCN] Calc. *m/z* (% intensity) for [Me_2Dipp(CAAC)=CF(CF$_3$) + H$^+$, $C_{22}H_{32}F_4N^+$]: 386.25 (100), 387.25 (24), 388.25 (3). Found *m/z* (% intensity): 386.2356 (100), 387.2316 (35), 388.2249 (5).

Synthesis of (Me_2Dipp(CAAC))=CF(CF$_2$CF$_3$) (5b). In a glove box, **Me_2Dipp(CAAC)** (100 mg, 0.35 mmol) was placed in a 50 mL round bottom Schlenk flask without a stir bar and dissolved in toluene (~ 4 mL). The flask was sealed with a septum and hooked up to a Schlenk line outside of the glove box. A 10 mL plastic syringe was filled with nitrogen and purged, before being half-filled with 5 mL of HFP. The gas was slowly injected into the flask, and allowed to slowly diffuse through the solution to avoid the formation of unwanted, unidentified products. This process was repeated twice with 5 mL portions of HFP. Soon after the addition of HFP, a colour change from nearly colourless to pale pink could be observed. Following the final gas addition, and after allowing the gas to diffuse through the solution for 1 hour, the septum was replaced with a glass stopper, and all volatiles were removed *in vacuo*, affording a pale pink, almost white residue. The flask was returned to the glove box, and the product was extracted with hexanes (~ 4 mL) and filtered through Celite® with hexanes washings (2 x 1 mL). The solution was concentrated under reduced pressure until the formation of solid could be observed, and then recrystallized from this cloudy solution at -35 °C. The product was isolated by filtration on a frit and dried under vacuum,

affording a pale pink-red crystalline solid. The product is stable in the solid state, but decomposes in solution over several hours, and I was thus unable to characterize it cleanly by $^{13}C\{^{1}H\}$ NMR. Yield: 135 mg, 89% based on Me_2Dipp(CAAC). mp: 82-83 °C. ^{1}H NMR (300 MHz, $CDCl_3$) δ 1.10 (d, $^{3}J_{HH} \approx 6.7$ Hz, 6H, $CH(CH_3)_2$), 1.17 (s, 6H, $C(CH_3)_2$), 1.29 (d, $^{3}J_{HH} \approx 6.7$ Hz, 6H, $CH(CH_3)_2$), 1.52 (s, 6H, $C(CH_3)_2$), 2.12 (s, 2H, CH_2), 3.12 (sept, $^{3}J_{HH} \approx 6.7$ Hz, 2H, $CH(CH_3)_2$), 7.07-7.30 (ov m, 3H, Ar-*H*). ^{19}F NMR (282 MHz, $CDCl_3$) δ -83.0 (dt, $^{3}J_{FF} \approx 3$ Hz, $^{4}J_{FF} \approx 13$ Hz, 3F, Me_2Dipp(CAAC)=CF(CF_2CF_3)), -108.6 (dq, $^{3}J_{FF} \approx 13$ Hz, $^{3}J_{FF} \approx 18$ Hz, 2F, Me_2Dipp(CAAC)=CF(CF_2CF_3)), -171.8 (tq, $^{3}J_{FF} \approx 18$ Hz, $^{4}J_{FF} \approx 13$ Hz, 1F, Me_2Dipp(CAAC)=C*F*(CF_2CF_3)). MS [ESI (positive mode), solvent: MeCN] Calc. *m/z* (% intensity) for [Me_2Dipp(CAAC)=CF(CF_2CF_3) + H^+, $C_{23}H_{32}F_6N^+$]: 436.24 (100), 437.25 (25), 438.25 (3). Found *m/z* (% intensity): 436.2459 (100), 437.2626 (33), 438.2620 (6).

Synthesis of (Me_2Dipp(CAAC))=CH(CF_3) (5c). In a glove box, **Me_2Dipp(CAAC)** (100 mg, 0.35 mmol) was placed in a 50 mL round bottom Schlenk flask without a stir bar and dissolved in toluene (~ 4 mL). The flask was sealed with a septum and hooked up to a Schlenk line outside of the glove box. A 10 mL plastic syringe was filled with nitrogen and purged, before being half-filled with 5 mL of HTFE. The gas was slowly injected into the flask, and allowed to slowly diffuse through the solution to avoid the formation of unwanted, unidentified products. This process was repeated twice with 5 mL portions of HTFE. Soon after the addition of TFE, a colour change from nearly colourless to dark red could be observed, which eventually turned into a very dark green. Following the final gas addition, and after allowing the gas to diffuse through the solution for 1 hour, the septum was replaced with a glass stopper, and all volatiles were removed *in vacuo*, affording a dark red-green residue. The flask was returned to the glove box, and the product was extracted with hexanes (~ 12 mL) and filtered through Celite® with hexanes

washings (2 x 3 mL), leaving behind the dark red-green residue and affording a bright green-yellow solution. The solution was concentrated under reduced pressure until the formation of solid could be observed, and then recrystallized from this cloudy solution at -35 °C. The product was isolated by filtration on a frit and dried under vacuum, affording bright green-yellow needles. Yield: 86 mg, 67% based on Me_2Dipp(CAAC). mp: 92-93 °C. ^{1}H NMR (300 MHz, $CDCl_3$) δ 1.15 (d, $^3J_{HH}$ ≈ 6.7 Hz, 6H, CH(CH_3)$_2$), 1.22 (s, 6H, C(CH_3)$_2$), 1.28 (d, $^3J_{HH}$ ≈ 6.7 Hz, 6H, CH(CH_3)$_2$), 1.55 (m, 6H, C(CH_3)$_2$), 2.10 (s, 2H, CH_2), 2.99 (sept, $^3J_{HH}$ ≈ 6.7 Hz, 2H, CH(CH$_3$)$_2$), 3.44 (q, $^3J_{HF}$ ≈ 10 Hz, 1H, Me_2Dipp(CAAC)=CH(CF_3)), 7.22-7.40 (ov m, 3H, Ar-H). ^{13}C{^{1}H} NMR (101 MHz, $CDCl_3$) δ 23.74, 26.33, 28.67, 29.47 (br m), 42.39, 56.39, 64.36, 79.36 (q, $^3J_{CF}$ ≈ 38 Hz, Me_2Dipp(CAAC)=CH(CF$_3$)), 124.99, 128.76, 132.58, 149.48, 165.53 (q, $^3J_{CF}$ ≈ 5 Hz, Me_2Dipp(CAAC)(C)=CH(CF_3)). ^{19}F NMR (282 MHz, C_6D_6) δ -46.9 (d, $^3J_{FH}$ ≈ 10 Hz, 3F, Me_2Dipp(CAAC)=CH(CF_3)). ^{19}F{^{1}H} NMR (282 MHz, C_6D_6) δ -46.9 (s, 3F, Me_2Dipp(CAAC)=CH(CF_3)).MS [ESI (positive mode), solvent: MeCN] Calc. *m/z* (% intensity) for [Me_2Dipp(CAAC)=CH(CF_3) + H^+, $C_{22}H_{33}F_3N^+$]: 368.26 (100), 369.26 (24), 370.26 (3). Found *m/z* (% intensity): 368.2135 (100), 369.2284 (27), 370.2165 (5).

Chapter 6

Summary and Outlook

6.1 Overview

Much remains to be understood about fluoroorganometallic chemistry and the direct reactivity of fluoroalkenes with N-heterocyclic carbenes (NHCs). However, the work presented in this thesis represents an important step forward for fluorine chemistry, and it is likely to be expanded upon in future research. This chapter will attempt to summarize the original research introduced herein, and to provide an outlook for the future of these projects.

6.2 Chapter 2

Transition metal complexes bearing two fluorinated ligands, i.e., one fluorine and one perfluoroalkyl or two perfluoroalkyls, are very uncommon. In this chapter, the synthesis and characterization of four perfluoroalkyl Co(III) fluoride complexes was presented. These were demonstrated to be active fluorination catalysts for the transformation of *p*-toluoyl chloride. Although this reaction does not necessarily represent a highly-desired transformation, it represents the first example of a Co(III) fluorination catalyst. Furthermore, these fluoride complexes have demonstrated the most upfield ^{19}F NMR shifts reported to date, the nature of which was studied computationally.

Additionally, two Co(III) bis(perfluoroalkyl) complexes were synthesized and characterized; the first of their kind. From these unique complexes, Co(III) difluorocarbenes were selectively formed and characterized by ^{19}F NMR. These decidedly electrophilic species

underwent an important reaction; namely, insertion into the remaining perfluoroalkyl fragment, leading to a formal elongation of the perfluoroalkyl fragment by one carbon. Aside from previous work by Burton *et al*. on copper, this chain-growth had yet to be demonstrated within the coordination sphere of a transition metal.

The work in this chapter represents an important step forward for transition metal-catalyzed polymerization involving perfluoroalkyl groups. Progress in this area has primarily been stunted by difficulties associated with the preparation of transition metal complexes bearing perfluorinated ligands, as well as the inherent strength of metal perfluoroalkyl bonds. Here, the synthesis of such complexes from readily accessible materials, such as cyclopentadienylcobalt dicarbonyl, perfluoroalkyl iodides, silver fluoride and the Ruppert-Prakash reagent is established. Furthermore, the perfluoroalkyl bonds in these electrophilic Co(III) difluorocarbene systems is shown to be sufficiently labile to accommodate the insertion of a difluoromethylene fragment.

6.3 Chapter 3

Aside from a partially characterized report in the Supporting Information of work performed by Ogoshi *et al*.,[266] and preliminary work by Arduengo *et al*. published during the preparation of our manuscript detailed in Chapter 3,[267] the work presented herein represents the most thorough investigation of NHC fluoroalkene adducts. The synthesis of these novel compounds is shown to be direct and simple, and the products are isolated as pure solids in high yields. Furthermore, their transformations to polyfluoroalkenyl imidazolium salts with Lewis acids is facile and provides the platform for the bulk of the work in Chapter 4.

The structural similarities of NHC fluoroalkenes with the Breslow intermediate were highlighted, however, special focus was paid on the differences in their reactivity. Specifically,

the fluorine atoms on the carbon directly bound to the alkene fragment are activated. Important insight into the nature of the reactivity between NHCs and fluoroalkenes was gained in reactions with vinylidene fluoride (VDF). Indeed, the isolation of the fluoroalkenyl cation with a fluoride anion supports my proposed reaction pathway, wherein initial nucleophilic attack of the carbene on the fluoroalkene leads to a zwitterion, which extrudes a fluoride capable of another nucleophilic attack on a sufficiently electrophilic terminal alkenyl carbon. In the case of VDF, the terminal CH_2 fragment is presumably not electrophilic enough to accommodate the formation of the expected adduct.

The ability of polyfluoroalkenyl imidazolium salts to undergo facile substitution chemistry with nitrogen-based nucleophiles was established, with pyrrolidine and 4-dimethylaminopyridine (DMAP) providing C_β- and C_α-substituted products, respectively. Based on predictions from TD-DFT studies, nucleophiles are expected to attack C_β preferentially, which has led us to conclude that the Cα reactivity observed with DMAP might proceed via this route. However, the inability to eliminate HF presumably prompts a rearrangement to the observed pyridinium product. Alternatively, a reaction pathway involving direct nucleophilic attack on C_α is still being considered.

The pioneering work in this chapter has led to some insightful discoveries and advancements in the field of fluoroalkene chemistry. Specifically, it was shown that common NHCs, such as SIPr and SIMes, are capable of stabilizing fluoroalkene adducts upon their formation. This stability is important, due to the tendency of fluoroalkenes to react multiple times in a difficult to control fashion upon formation of an unstable anion. However, NHCs can stabilize these species electronically and sterically. The electronic stabilization arises primarily from the imidazole fragment, capable of diffusing excess charge via imidazolium formation.

Sterically, these *N*-aryl type carbenes can provide shielding to the fluoroalkene adducts, but can also importantly rotate out of the plane to accommodate their formation in the first place, especially when larger substituents such as trifluoromethyl groups are involved.

6.4 Chapter 4

Having previously established the ease with which polyfluoroalkenyl imidazolium salts could be prepared from NHC fluoroalkenes, and the unique substitution chemistry that these exhibited, I sought to expand on this reactivity and attempt to see which kinds of bonds could be formed with relatively simple organic nucleophiles. In fact, various C-E (E = C, N, O, S) and C-M bonds (M = Mn, Mo) could be formed by reactions with sodiated nucleophilic salts. In doing so, HF removal could be avoided and a simple extraction from NaF afforded clean and characterized products.

Of interest was the continuing reactivity with nitrogen-based nucleophiles. Pyrazolate and 1,2,4-triazolate nucleophiles, along with the previously reported pyrrolidine, are unique examples of Buchwald-Hartwig-type sp^2 C-N bond formation from direct sp^2 C-F bond activation, a transformation typically only achieved via Pd- or Cu-based catalysts. Herein, these occur at room temperature, without the need for a transition metal catalyst, and a single isomer is obtained in all cases. Attempts to replicate the Cα reactivity previously observed with DMAP led us to explore different nitrogen-based nucleophiles incapable of eliminating HF/NaF, such as 1-methylimidazole. Indeed, an analogous Cα product was obtained, and the difluoromethylene fragment was shown to be even more activated than in the parent adduct compound, as evidenced by its immediate reactivity with trace water. Upon exposure to minimal amounts of water, the difluoromethylene fragment is transformed into an α,β-unsaturated trifluoromethyl ketone

compound, the first transformation of its kind. This type of double C-F bond activation was also demonstrated in the reactivity between the SIMes trifluoroethylene (HTFE) adduct and sodium cyclopentadienide, establishing an important example of C-C bond formation with this system. The relative generality of these substitutions was further established by the formation of manganese- and molybdenum-based fluorovinyl complexes. These complexes are quite unique, and these fluorovinyl imidazolium ligands might offer some interesting properties in systems where push-pull alkene-type scaffolds are desired.

This chapter served to really illustrate the potential of an NHC to not only form stable adducts with fluoroalkenes, but more importantly to help govern its reactivity. During these reactions, several C-F bonds are broken or otherwise modified, and due to the difficulties typically associated with these transformations, it is truly surprising that these substitutions are seemingly so facile. Truly, the imidazole fragment has a unique potential to direct some unexpected reactivity, especially with these polyfluoroalkenyl imidazolium salts.

6.5 Chapter 5

The unique reaction leading to the formation of NHC fluoroalkenes introduced in Chapter 3 was shown to work very well with common SIPr and SIMes. However, we had noted that reactivity with I^{t}Bu, as well as with smaller I^{i}Pr and IMe$_4$, was not as successful. Additionally, although Ogoshi *et al*. had previously mentioned the formation of a TFE adduct with unsaturated IPr, I found that reactivity between this carbene and other fluoroalkenes, such as HFP, HTFE and VDF, was not clean. With this knowledge in mind, I believed it would be beneficial to undertake a large-scale study between a variety of different carbenes and the fluoroalkenes studied to date.

In total, 15 different carbenes featuring various electronic and steric environments were explored, and several new adducts were characterized. Important insight was gained, demonstrating that unsaturated carbenes are generally too reactive, unless the backbone is functionalized with electron withdrawing groups, such as chlorides. Additionally, stable adducts with *N*-alkyl-substituted NHCs have yet to be isolated. Ring-expanded NHCs demonstrated clean reactivity with TFE, but did not form clean adducts with HFP. Although clean adducts could be formed with HTFE, these proved to be unstable and decomposed to a variety of uncharacterized products. In fact, the relative instability of HTFE adducts has been observed for several different carbenes. It is still unclear exactly what causes this instability.

Attempts to correlate the observed reactivity with electronic (TEP) and steric ($\%V_{bur}$) parameters were unsuccessful, as no clear trends could be observed. Although it does appear that a minimal amount of steric bulk is indeed required, it is not yet known what role this effect truly has on the stability of the adducts. A truly surprising result was obtained in the reaction between a cyclic (alkyl)(amino)carbene (CAAC) and HTFE, wherein a different isomer was obtained, relative to the HTFE isomer observed in all other clean reactivity. Presumably, the unique steric constraints of this carbene modify the initial point of nucleophilic attack on the fluoroalkene, providing this isomer cleanly.

Although the formation of stable adducts with VDF has yet to be demonstrated, it is possible that a carbene capable of stabilizing this product has yet to be found. The result obtained with the CAAC strongly encourages further studies with carbene featuring unique steric environments, ideally with a variety of different CAACs to observe if the formation of this unique isomer is consistent with this type of carbene. I believe that the right choice of carbene could provide a system capable of being involved in organocatalysis or polymerization featuring

fluoroalkenes, something that has never been demonstrated in this fashion, nor by utilizing these NHC fluoroalkene adducts.

6.6 Outlook

The work outlined in Chapter 2 demonstrates the significant impact that changing the oxidation state of a transition metal can have on the reactivity of the resulting complexes. While our early work was particularly focused on Co(I) difluorocarbenes and the [2+2] cycloadditions that these underwent with electrophilic tetrafluoroethylene, the Co(III) perfluorometallacyclobutane products demonstrated interesting reactivity that implied an underlying lability between Co(III) and perfluoroalkyl bonds. This was demonstrated by the unique insertion reactivity between the electrophilic fluorocarbenes and the remaining cobalt perfluoroalkyl fragment; the first time this type of reactivity was demonstrated on cobalt. Due to these findings, we believe that further studies involving Co(III) perfluoroalkyl complexes are warranted, potentially involving different cobalt ligand arrangements than the half-sandwich complexes that have been our primary focus to date. The ability to render this insertion chemistry catalytic in some fashion would be particularly interesting. Upon insertion of the difluorocarbene fragment into the remain perfluoroalkyl, a vacant site is formed on the Co(III) center. Filling this vacant site with a new difluorocarbene fragment could feasibly extend this chain-growth to include several carbons and perhaps even lead to polymerization featuring perfluoroalkyls, something that has yet to be achieved on a transition metal center. We were unable to fully characterize these novel difluorocarbene complexes, in part due to their immediate reactivity with trace moisture, but also due to their relatively short lifetimes. We have found that the sterically demanding $FB(C_6F_5)_3$ anion led to more stable difluorocarbene complexes than those featuring

the OTf anion. Thus, increased stability might be gained by exploring different Lewis acids, such as the very sterically encumbered, and affectionately named BArF (tris(3,5-bis(trifluoromethyl)phenyl)borane). This would allow for a more thorough study of the difluorocarbene complexes before they undergo the insertion reaction.

The pioneering work that I have established in Chapters 3, 4 and 5 has been the source of much surprise and excitement over the last several years. It is very fortunate that I initially chose the SIPr and SIMes carbenes, because these appear to form the most stable and well-behaved adducts that I have observed thus far in this work. Unfortunately, although I have explored some truly unique reactions, and have learned a lot about the fundamentals of these transformations, I have not yet been able to perform organocatalytic reactions with these adducts. Perhaps my biggest obstacle is the inability to remove the N-heterocyclic fragment after the desired transformations have been achieved. Ideally, a different carbene might prove more labile, or perhaps an alternate approach is required, wherein the substitution reactions with organic nucleophiles feature an additional tethered nucleophile, capable of forming heterocycles and extruding the carbene fragment. In terms of polymerization involving these systems, initial studies with the IPr adduct of TFE demonstrate that the increased charge separation, driven by the aromaticity of the imidazolium fragment, does significantly increase further reactivity. In fact, when a sample of this adduct is heated under an atmosphere of very electrophilic HFP, several new products are formed. However, the product mixture proves very difficult to characterize, and decomposition is apparent. This finding is nonetheless encouraging, as this behavior indicates that there might be some potential for fluoroalkene polymerization utilizing NHCs. Considering that this type of reactivity has not been observed with transition metals, this would be an incredibly important achievement.

Appendix A

X-Ray Crystallography

Details for X-ray crystallography: Samples were mounted on thin glass fibers using paraffin oil and were cooled to 200 K prior to data collection. Data were collected on a Bruker AXS KAPPA single crystal diffractometer equipped with a sealed Mo tube source (wavelength 0.71073 Å) APEX II CCD detector. Raw data collection and processing were performed with the APEX II software package from BRUKER AXS. Diffraction data were collected with a sequence of 0.5° ω scans at 0, 90, 180, 270° in ϕ. Initial unit cell parameters were determined from 60 data frames collected at the different sections of the Ewald sphere. Semi-empirical absorption corrections based on equivalent reflections were applied. Systematic absences in the diffraction data set and unit-cell parameters were consistent with triclinic systems. Solutions in centrosymmetric space group yielded chemically reasonable and computationally stable results of refinement. The structures were solved by direct methods, completed with difference Fourier synthesis, and refined with full-matrix least-squares procedures based on F^2. In the structure, compound molecules are situated in the general position. All non-hydrogen atoms were refined anisotropically with satisfactory thermal parameters values. To achieve satisfactory thermal parameters, it was not necessary to use constraints. Additional crystallographic data and selected data collection parameters are reported below.

5: Empirical formula: $C_{24.5}H_{20.75}CoF_4N_{0.25}P$; FW = 484.56; Crystal size: 0.170 x 0.120 x 0.110 mm^3; Crystal system: monoclinic; Space group: P $2_1/n$; Z = 4; a = 9.4327(2) Å, b = 18.0240(4) Å, c = 14.5156(3) Å; α = 90°, β = 90.5681(13)°, γ = 90°; Volume = 2467.75(9) $Å^3$; Calculated density = 1.304 Mg/m^3; Absorption coefficient = 0.798 mm^{-1}; F(000) = 990; Θ range for data collection: 2.437 to 24.107°; Limiting indices: -10≤h≤10, -20≤k≤20, -16≤l≤16; Reflections collected: 27072; Independent reflections: 3863 [R(int) = 0.0399]; Completeness to Θ = 25.242° (86.5 %); Max. and min. transmission: 0.7457 and 0.6262; Data / restraints / parameters: 3863 / 3 / 284; Goodness-of-fit on F^2 = 1.067; Final R indices [I>2σ(I)]: R1 = 0.0684, wR2 = 0.1741; R indices (all data): R1 = 0.0829, wR2 = 0.1840; Largest diff. peak and hole: 1.098 and -0.467 e. $Å^3$.

6: Empirical formula: $C_{45}H_{44}Co_2F_8P_2$; FW = 916.60; Crystal size: 0.080 x 0.060 x 0.020 mm^3; Crystal system: triclinic; Space group: P -1; Z = 2; a = 8.9559(10) Å, b = 14.4617(17) Å, c= 17.157(2) Å; α = 108.817(2)°, β = 92.449(2)°, γ = 103.213(2)°; Volume = 2031.3(4) $Å^3$; Calculated density = 1.499 Mg/m^3; Absorption coefficient = 0.965 mm^{-1}; F(000) = 940; Θ range for data collection: 1.539 to 24.759°; Limiting indices: -10≤h≤9, -16≤k≤17, -18≤l≤19; Reflections collected: 12537; Independent reflections: 6742 [R(int) = 0.0383]; Completeness to Θ = 25.242° (91.5 %); Max. and min. transmission: 0.7451 and 0.6124; Data / restraints / parameters: 6742 / 87 / 514; Goodness-of-fit on F^2 = 1.022; Final R indices [I>2σ(I)]: R1 = 0.0548, wR2 = 0.1067; R indices (all data): R1 = 0.1091, wR2 = 0.1257; Largest diff. peak and hole: 0.744 and -0.616 e. $Å^{-3}$.

7: Empirical formula: $C_{25}H_{20}CoF_6P$; FW = 524.31; Crystal size: 0.180 x 0.160 x 0.140 mm^3; Crystal system: triclinic; Space group: P -1; Z = 2; a = 9.5767(2) Å, b = 10.2062(2) Å, c= 11.8202(3) Å; α = 85.8132(11)°, β = 87.6375(11)°, γ = 69.3572(10)°; Volume = 1078.12(4) $Å^3$; Calculated density = 1.615 Mg/m^3; Absorption coefficient = 0.933 mm^{-1}; F(000) = 532; Θ range for data collection: 1.728 to 28.348°; Limiting indices: -12≤h≤12, -13≤k≤13, -15≤l≤15; Reflections collected: 11253; Independent reflections: 5293 [R(int) = 0.0127]; Completeness to Θ = 25.242˚ (98.4 %); Max. and min. transmission: 0.7457 and 0.6486; Data / restraints / parameters: 5293 / 0 / 298; Goodness-of-fit on F^2 = 1.041; Final R indices [I>2σ(I)]: R1 = 0.0247, wR2 = 0.0651; R indices (all data): R1 = 0.0279, wR2 = 0.0671; Largest diff. peak and hole: 0.343 and -0.225 e. $Å^{-3}$.

8: Empirical formula: $C_{20}H_{18}CoF_6P$; FW = 462.24; Crystal size: 0.300 x 0.140 x 0.130 mm^3; Crystal system: tetragonal; Space group: P 4_3; Z = 4; a = 10.7808(3) Å, b = 10.7808(3) Å, c= 16.1975(5) Å; α = 90°, β = 90°, γ = 90°; Volume = 1882.56(12) $Å^3$; Calculated density = 1.631 Mg/m^3; Absorption coefficient = 1.056 mm^{-1}; F(000) = 936; Θ range for data collection: 1.889 to 28.294°; Limiting indices: -14≤h≤14, -13≤k≤14, -20≤l≤20; Reflections collected: 20243; Independent reflections: 4591 [R(int) = 0.0187]; Completeness to Θ = 25.242˚ (98.9 %); Max. and min. transmission: 0.7457 and 0.6135; Data / restraints / parameters: 4591 / 1 / 253; Goodness-of-fit on F^2 = 1.033; Final R indices [I>2σ(I)]: R1 = 0.0186, wR2 = 0.0454; R indices (all data): R1 = 0.0194, wR2 = 0.0456; Largest diff. peak and hole: 0.277 and -0.201 e. $Å^{-3}$.

9: Empirical formula: $C_{27}H_{26}CoF_6P$; FW = 554.38; Crystal size: 0.210 x 0.1200 x 0.110 mm^3; Crystal system: triclinic; Space group: P -1; Z = 2; a = 9.0221(6) Å, b = 10.5657(6) Å, c= 13.7403(9) Å; α = 74.820(3)°, β = 77.450(3)°, γ = 79.209(3)°; Volume = 1222.02(14) $Å^3$;

Calculated density = 1.507 Mg/m^3; Absorption coefficient = 0.827 mm^{-1}; F(000) = 568; Θ range for data collection: 2.017 to 28.374°; Limiting indices: -12≤h≤8, -14≤k≤13, -18≤l≤16; Reflections collected: 10914; Independent reflections: 5962 [R(int) = 0.0115]; Completeness to Θ = 25.242 984° (98.3%); Max. and min. transmission: 0.7457 and 0.6641; Data / restraints / parameters: 5962 / 72 / 316; Goodness-of-fit on F^2 = 1.044; Final R indices [I>2σ(I)]: R1 = 0.0320, wR2 = 0.0880; R indices (all data): R1 = 0.0351, wR2 = 0.0908; Largest diff. peak and hole: 1.003 and -0.407 e. $Å^{-3}$.

10: Empirical formula: $C_{24.5}H_{22}CoF_8P$; FW = 558.32; Crystal size: 0.180 x 0.100 x 0.010 mm^3; Crystal system: monoclinic; Space group: C 2/c; Z = 8; a = 32.1741(19) Å, b = 7.6991(5) Å, c= 20.4220(13) Å; α = 90°, β = 110.029(2)°, γ = 90°; Volume = 4752.8(5) $Å^3$; Calculated density = 1.561 Mg/m^3; Absorption coefficient = 0.863 mm^{-1}; F(000) = 2264; Θ range for data collection: 1.347 to 24.750°; Limiting indices: -36≤h≤37, -9≤k≤9, -24≤l≤24; Reflections collected: 17390; Independent reflections: 3984 [R(int) = 0.0674]; Completeness to Θ = 25.242° (92.7); Max. and min. transmission: 0.7451 and 0.6199; Data / restraints / parameters: 984 / 77 / 290; Goodness-of-fit on F^2 = 1.018; Final R indices [I>2σ(I)]: R1 = 0.0625, wR2 = 0.1382; R indices (all data): R1 = 0.1029, wR2 = 0.1547; Largest diff. peak and hole: 0.598 and -0.721 e. $Å^{-3}$.

Chapter 3

1b: Empirical formula: $C_{30}H_{38}F_6N_2$; FW = 540.62; Crystal size: 0.726 x 0.717 x 0.599 mm^3; Crystal system: orthorhombic; Space group: P c a 2_1; Z = 8; a = 24.722(7) Å, b = 9.896(3) Å, c= 23.989(7) Å; α = 90°, β = 90°, γ = 90°; Volume = 5869(3) $Å^3$; Calculated density = 1.224 Mg/m^3; Absorption coefficient = 0.098 mm^{-1}; F(000) = 2288; Θ range for data collection: 1.853 to 27.979°; Limiting indices: -23≤h≤32, -13≤k≤13, -31≤l≤31; Reflections collected: 36587; Independent reflections: 13511 [R(int) = 0.0398]; Completeness to Θ = 25.242˚ (99.8 %); Data / restraints / parameters: 13511 / 184 / 751; Goodness-of-fit on F^2 = 1.024; Final R indices [I>2σ(I)]: R1 = 0.0788, wR2 = 0.2012; R indices (all data): R1 = 0.1434, wR2 = 0.2457; Largest diff. peak and hole: 0.375 and -0.215 e. $Å^{-3}$.

3b: Empirical formula: $C_{30}H_{38}BF_9N_2$; FW = 608.43; Crystal size: 0.260 x 0.180 x 0.030 mm^3; Crystal system: triclinic; Space group: P -1; Z = 2; a = 10.3017(10) Å, b = 10.9000(11) Å, c= 14.8633(14) Å; α = 77.465(2)°, β = 75.393(2)°, γ = 77.049(2)°; Volume = 1551.0(3) $Å^3$; Calculated density = 1.303 Mg/m^3; Absorption coefficient = 0.113 mm^{-1}; F(000) = 636; Θ range for data collection: 1.945 to 28.261°; Limiting indices: -13≤h≤9, -14≤k≤14, -19≤l≤16; Reflections collected: 13728; Independent reflections: 7538 [R(int) = 0.0250]; Completeness to Θ = 25.242˚ (99.6 %); Max. and min. transmission: 0.7457 and 0.6797; Data / restraints / parameters: 7538 / 403 / 442; Goodness-of-fit on F^2 = 1.023; Final R indices [I>2σ(I)]: R1 = 0.0538, wR2 = 0.1279; R indices (all data): R1 = 0.0969, wR2 = 0.1529; Largest diff. peak and hole: 0.318 and -0.268 e. $Å^{-3}$.

6: Empirical formula: $C_{42}H_{56}BCl_2F_8N_3$; FW = 836.60; Crystal size: 0.740 x 0.399 x 0.1760 mm^3; Crystal system: monoclinic; Space group: C 2/c; Z = 8; a = 18.9452(10) Å, b = 16.0008(7) Å, c=

30.0179(14) Å; α = 90°, β = 106.275(2)°, γ = 90°; Volume = 8734.9(7) $Å^3$; Calculated density = 1.272 Mg/m^3; Absorption coefficient = 0.215 mm^{-1}; F(000) = 3520; Θ range for data collection: 1.413 to 27.952°; Limiting indices: -24≤h≤23, -20≤k≤21, -37≤l≤39; Reflections collected: 42519; Independent reflections: 10451 [R(int) = 0.0271]; Completeness to Θ = 25.242˚ (100.0 %); Data / restraints / parameters: 10451 / 64 / 551; Goodness-of-fit on F^2 = 1.054; Final R indices [I>2σ(I)]: R1 = 0.0602, wR2 = 0.1670; R indices (all data): R1 = 0.0969, wR2 = 0.2175; Largest diff. peak and hole: 0.478 and -0.666 e. $Å^{-3}$.

Chapter 4

3: Empirical formula: $C_{29}H_{32}F_8N_4O_3S$; FW = 668.64; Crystal size: 0.807 x 0.642 x 0.388 mm^3; Crystal system: monoclinic; Space group: P 21/n; Z = 4; a = 8.2558(2) Å, b = 14.4009(3) Å, c= 28.6123(6) Å; α = 90°, β = 90.5060(10)°, γ = 90°; Volume = 3401.61(13) $Å^3$; Calculated density = 1.306 Mg/m^3; Absorption coefficient = 0.173 mm^{-1}; F(000) = 1384; Θ range for data collection: 1.423 to 27.935°; Limiting indices: -10≤h≤10, -16≤k≤18, -33≤l≤37; Reflections collected: 44874; Independent reflections: 8096 [R(int) = 0.0292]; Completeness to Θ = 25.242˚ (100.0 %); Data / restraints / parameters: 8096 / 148 / 550; Goodness-of-fit on F^2 = 1.039; Final R indices [I>2σ(I)]: R1 = 0.0539, wR2 = 0.1466; R indices (all data): R1 = 0.0835, wR2 = 0.1649; Largest diff. peak and hole: 0.269 and -0.219 e.$Å^{-3}$.

8: Empirical formula: $C_{69}H_{70}F_{14}N_4;O_6S_4$ FW = 1445.53; Crystal size: 0.957 x 0.229 x 0.068 mm^3; Crystal system: monoclinic; Space group: P 21/n; Z = 2; a = 11.0398(10) Å, b = 12.0040(10) Å, c= 26.202(2) Å; α = 90°, β = 93.087(4)°, γ = 90°; Volume = 3467.3(5) $Å^3$; Calculated density = 1.385 Mg/m^3; Absorption coefficient = 0.228 mm^{-1}; F(000) = 1500; Θ range for data collection: 1.557 to 27.968°; Limiting indices: -14≤h≤14, -15≤k≤15, -34≤l≤34; Reflections collected: 43510; Independent reflections: 8314 [R(int) = 0.0368]; Completeness to Θ = 25.242˚ (100.0 %); Data / restraints / parameters: 8314 / 235 / 549; Goodness-of-fit on F^2 = 1.022; Final R indices [I>2σ(I)]: R1 = 0.0707, wR2 = 0.1964; R indices (all data): R1 = 0.1103, wR2 = 0.2268; Largest diff. peak and hole: 0.887 and -0.411 e.$Å^{-3}$.

9: Empirical formula: $C_{29}H_{32}F_6N_4O_4S$; FW = 646.64; Crystal size: 0.712 x 0.294 x 0.212 mm^3; Crystal system: monoclinic; Space group: P 21/n; Z = 4; a = 8.2473(9) Å, b = 14.5433(15) Å, c= 28.320(3) Å; α = 90°, β = 90.445(5)°, γ = 90°; Volume = 3396.7(6) $Å^3$; Calculated density =

1.265 Mg/m^3; Absorption coefficient = 0.165 mm^{-1}; F(000) = 1344; Θ range for data collection: 0.719 to 28.009°; Limiting indices: -10≤h≤10, -19≤k≤19, -37≤l≤37; Reflections collected: 50100; Independent reflections: 8127 [R(int) = 0.0594]; Completeness to Θ = 25.242˚ (100.0 %); Data / restraints / parameters: 8127 / 267 / 515; Goodness-of-fit on F^2 = 1.206; Final R indices [I>2σ(I)]: R1 = 0.1102, wR2 = 0.3035; R indices (all data): R1 = 0.1499, wR2 = 0.3305; Largest diff. peak and hole: 0.417 and -0.552 e.Å^{-3}.

10: Empirical formula: $C_{28.50}H_{32}ClFN_2$; FW = 457.01; Crystal size: 0.805 x 0.250 x 0.084 mm^3; Crystal system: monoclinic; Space group: P 21/c; Z = 4; a = 8.4965(3) Å, b = 19.0343(8) Å, c= 15.7697(6) Å; α = 90°, β = 100.069(2)°, γ = 90°; Volume = 2511.07(17) Å^3; Calculated density = 1.209 Mg/m^3; Absorption coefficient = 0.178 mm^{-1}; F(000) = 972; Θ range for data collection: 1.693 to 28.248°; Limiting indices: -11≤h≤11, -19≤k≤25, -20≤l≤20; Reflections collected: 21796; Independent reflections: 6165 [R(int) = 0.0386]; Completeness to Θ = 25.242˚ (100.0 %); Data / restraints / parameters: 6165 / 9 / 313; Goodness-of-fit on F^2 = 1.012; Final R indices [I>2σ(I)]: R1 = 0.0612, wR2 = 0.1465; R indices (all data): R1 = 0.1043, wR2 = 0.1690; Largest diff. peak and hole: 0.382 and -0.332 e.Å^{-3}.

11: Empirical formula: $C_{30}H_{26}F_7MnN_2O_8S$; FW = 762.53; Crystal size: 0.501 x 0.360 x 0.122 mm^3; Crystal system: monoclinic; Space group: P 21/c; Z = 4; a = 13.4991(5) Å, b = 20.9929(9) Å, c= 13.2242(5) Å; α = 90°, β = 118.3560(10)°, γ = 90°; Volume = 3297.9(2) Å^3; Calculated density = 1.536 Mg/m^3; Absorption coefficient = 0.555 mm^{-1}; F(000) = 1552; Θ range for data collection: 1.714 to 27.920°; Limiting indices: -15≤h≤171, -27≤k≤27, -17≤l≤17; Reflections collected: 60503; Independent reflections: 7876 [R(int) = 0.0925]; Completeness to Θ = 25.242˚ (100.0 %); Data / restraints / parameters: 7876 / 125 / 485; Goodness-of-fit on F^2 = 1.124; Final R

indices [I>2σ(I)]: R1 = 0.0750, wR2 = 0.1323; R indices (all data): R1 = 0.1175, wR2 = 0.1465; Largest diff. peak and hole: 0.625 and -0.445 e.Å^{-3}.

5c: Empirical formula: $C_{22}H_{32}F_3N$; FW = 367.48; Crystal size: 0.583 x 0.239 x 0.098 mm^3; Crystal system: orthorhombic; Space group: P 2_1 2_1 2_1; Z = 4; a = 9.2871(9) Å, b = 10.2342(10) Å, c= 22.030(2) Å; α = 90°, β = 90°, γ = 90°; Volume = 2093.9(4) $Å^3$; Calculated density = 1.166 Mg/m^3; Absorption coefficient = 0.085 mm^{-1}; F(000) = 792; Θ range for data collection: 1.849 to 28.245°; Limiting indices: $-12 \leq h \leq 12$, $-13 \leq k \leq 13$, $-28 \leq l \leq 29$; Reflections collected: 24751; Independent reflections: 5078 [R(int) = 0.0444]; Completeness to Θ = 25.242˚ (100.0 %); Data / restraints / parameters: 5078 / 0 / 243; Goodness-of-fit on F^2 = 1.022; Final R indices [$I>2\sigma(I)$]: R1 = 0.0470, wR2 = 0.1144; R indices (all data): R1 = 0.0978, wR2 = 0.1463; Largest diff. peak and hole: 0.173 and -0.234 e. $Å^{-3}$.

Appendix B

Appendix to Chapter 2

TD-DFT and Frontier Orbital Studies. The geometries were taken from the X-ray structures, with C-H bond distances adjusted to the length of 1.09 Å. Calculations were performed at the B3LYP[209,210]/TZVP[297] level with the SMD solvent model[221] and CH_2Cl_2 as a solvent using the Gaussian 09 package.[380] Calculations of orbital compositions, Mayer bond orders, and convolution of TD-DFT spectra were performed using the AOMix software package (www.sg-chem.net). The convolution was performed using Gaussian functions with the half bandwidths of 3000 cm^{-1} as previously described.[381]

The electronic structures of **5** and **9** can be discussed in more detail owing to the very good agreement between the experimental and calculated absorption spectra for these two complexes (Figure B.1). Both complexes contain a d^6 Co^{III} metal center. These can be grouped in the class of $CpML_3$ complexes, which can be seen as pseudo-octahedral complexes. The only difference in coordination between **5** and **9** is the replacement of a fluoride ligand in **5** with a trifluoromethyl group in **9**. This ligand change has important implications considering the fluoride ligand can act as both a σ and π donor. Conversely, the trifluoromethyl ligand does not act as π donor and, thus, the Co-CF_3 bond can only feature σ covalent contribution. The HOMO (-6.36 eV) of **5** (Table B.1) has 43% Co character and 25% contribution from the π orbital of the C_5H_5 ligand. This orbital has also 14% contribution from the F ligand (due to an antibonding π-interaction between the ligand and the d_π orbital on the metal). HOMO-1 (-6.76 eV) is fairly delocalized, with 36% contribution from PPh_3, 30% contribution from Co and 26% contribution from C_5H_5. The LUMO (-2.02 eV) is an antibonding orbital, with contributions from the Co d_σ orbital (51%), PPh_3 (20%), C_5H_5 (25%), and F (4%). π-donation of the fluoride ligand to the

metal ion in **5** leads to a destabilization of the occupied Co d_π orbitals, effectively raising the energy of the HOMO and reducing the HOMO-LUMO gap of 4.34 eV for **5** versus 4.89 eV for **9**. This difference of 0.55 eV is expressed as a significant blue shift of the principal absorption bands going from **5** to **9**. Selected frontier orbitals for **5** and **9** are presented in Figure B.2 and Figure B.3, respectively.

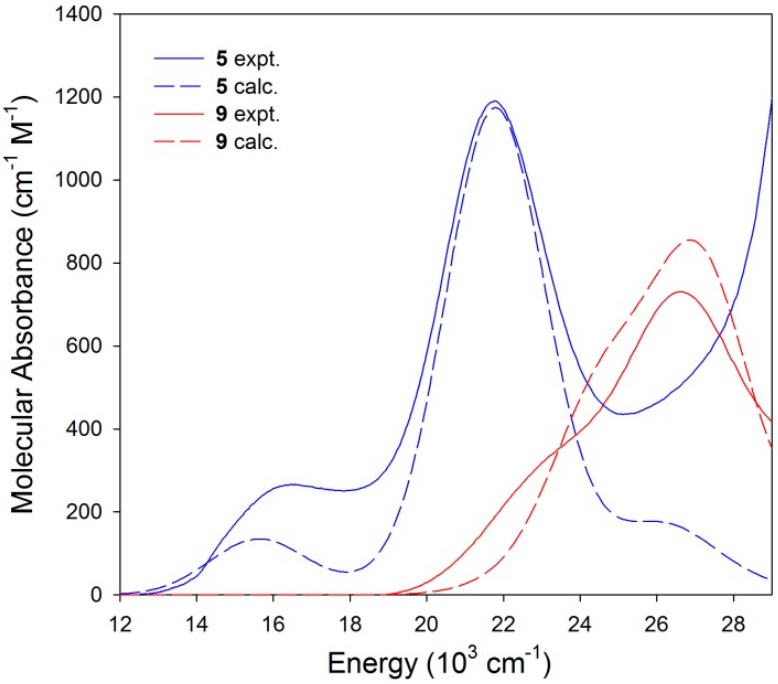

Figure B.1. Experimental (solid lines) and calculated (dashed lines) UV-vis absorption spectra of $CpCo(CF_3)(F)(PPh_3)$ (**5**, blue lines) and $CpCo(CF_3)_2(PPh_2Me)$ (**9**, red lines) in CH_2Cl_2.

The HOMO (-6.62 eV) of **9** (Table B.2) is composed of Co (36%), C_5H_5 (35%), PPh_2Me (22%), and CF_3 (10%) orbital contributions. The HOMO-1 (-6.80 eV) of **9** has the 39% Co character, with additional contributions from C_5H_5 (32%) and PPh_2Me (22%). The LUMO (-1.73 eV) is an antibonding orbital, with contributions from Co d_σ orbital (42%), PPh_2Me (29%), and both CF_3 (7%) ligands. The LUMO+1 (-1.12 eV) is also an antibonding orbital and is a mixture

of a Co d_σ orbital (48% contribution) and the ligand orbitals of C_5H_5 (21%) and both CF_3 (27%) ligands.

Table B.1. Energies and Mulliken population analysis (MPA)-derived compositions (%) for frontier orbitals of $CpCo(CF_3)(F)(PPh_3)$ (5)

	Orbital energy (eV)	MPA-derived fragment contributions (%)				
		Co	C_5H_5	F	CF_3	PPh_3
LUMO+1	-1.48	51	20	3	16	11
LUMO	-2.02	51	25	4	0	20
HOMO	-6.36	43	25	14	5	12
HOMO-1	-6.76	30	26	3	5	36

Table B.2. Energies and Mulliken population analysis (MPA)-derived compositions (%) for frontier orbitals of $CpCo(CF_3)_2(PPh_2Me)$ (9)

	Orbital energy (eV)	MPA-derived fragment contributions (%)			
		Co	C_5H_5	$(CF_3)_2$	PPh_2Me
LUMO+1	-1.12	48	21	27	4
LUMO	-1.73	42	22	7	29
HOMO	-6.62	36	35	10	22
HOMO-1	-6.80	39	32	8	22
HOMO-6	-7.79	78	6	7	9

In a solution of dichloromethane, the absorption spectrum of **5** (Figure B.1) shows two bands in the visible region, at 16 300 cm^{-1} (263 $M^{-1}cm^{-1}$) and 21 800 cm^{-1} (1190 $M^{-1}cm^{-1}$). The calculated UV-vis spectrum (see Supporting Information of original publication)[95] also shows two major electronic bands in the visible region, at 15 600 cm^{-1} (oscillator strength f of 0.0037) and 21 700 cm^{-1} (f = 0.031). The first band in the spectrum of **5** is mostly comprised of the HOMO →→ LUMO electron excitation (contributing 63% to the wave function of the excited state). This transition involves some ligand-to-metal charge transfer (LMCT) character from both the fluoride ligand and the trifluoromethyl ligand to the cobalt ion and some LLCT from the same ligands towards the phosphine, the latter's orbital contributions augmenting by 8%.

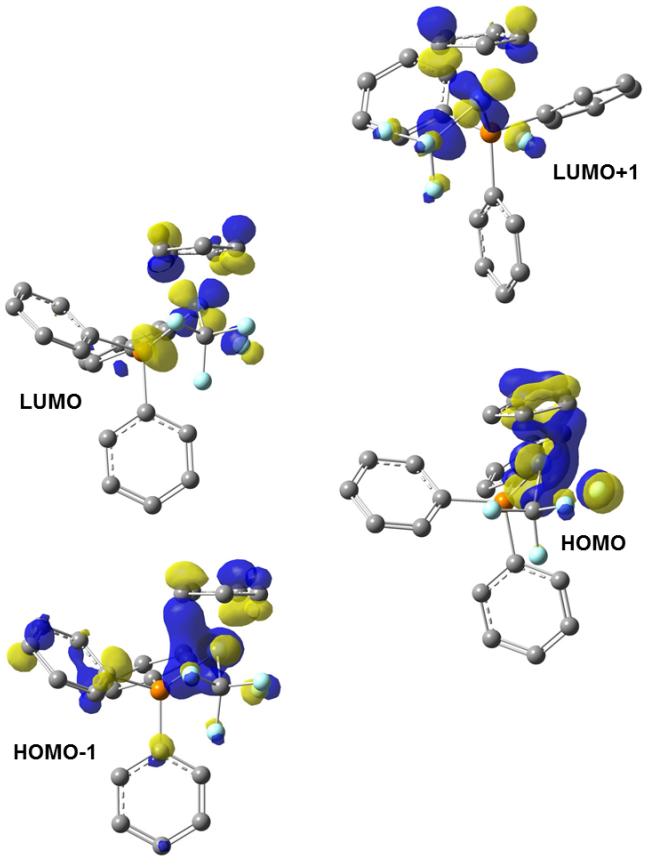

Figure B.2. Selected frontier orbitals of $CpCo(CF_3)(F)(PPh_3)$ (**5**). Hydrogen atoms are omitted for clarity. Isosurface contour value is 0.05 a.u.

The second band has contributions from at least two excitations, namely HOMO → LUMO+1 (25%) and HOMO-1 → LUMO (22%). The HOMO → LUMO+1 transition involves some LMCT from the fluoride ligand to the cobalt ion, as LUMO+1 contains almost 10% more cobalt character than the HOMO. Additionally, the transition involves some ligand-to-ligand charge transfer (LLCT) from the fluoride ligand to the trifluoromethyl ligand, with the LUMO+1 containing 11% more trifluoromethyl character as compared to the HOMO. The second transition related to this band is mostly comprised of LMCT character from the phosphine to the cobalt

metal center, as the LUMO contains approximately 16% less phosphine character and 21% more cobalt character.

The UV-vis spectrum of **9** shows two absorption bands, however, they are blue-shifted relative to the bands of **5**. The first band appears as a shoulder (23 000 cm^{-1}) of the principal band at 25 800 cm^{-1} (730 $M^{-1}cm^{-1}$). The calculated UV-vis spectrum also shows two major electronic bands in the visible region, at 24 500 cm^{-1} (f = 0.013) and 27 100 cm^{-1} (f = 0.021). The band at 27 100 cm^{-1} is due to several excitations, with a largest being HOMO → LUMO+1 (28%). This excitation involves significant amounts of LMCT and LLCT character.

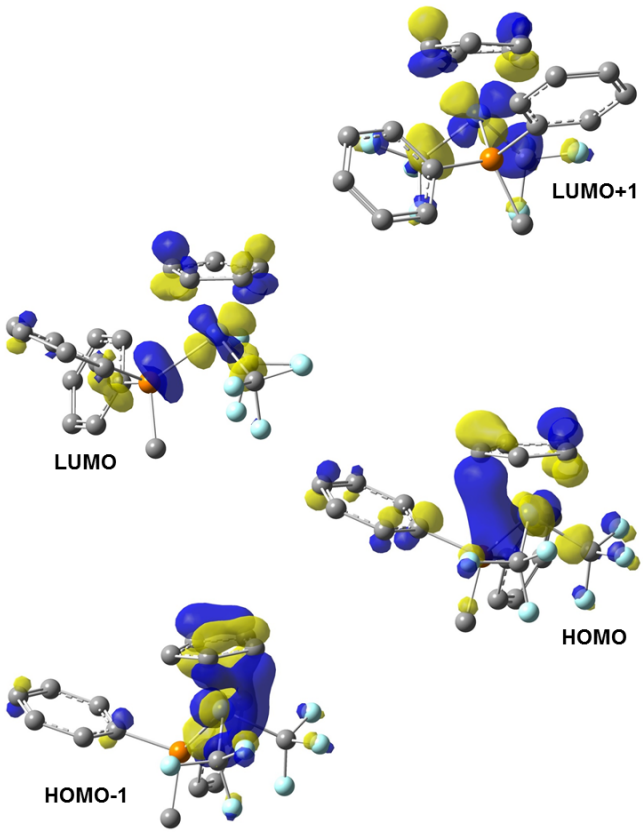

Figure B.3. Selected frontier orbitals of $CpCo(CF_3)_2(PPh_2Me)$ (**9**). Hydrogen atoms are omitted for clarity. Isosurface contour value is 0.05 a.u.

The LMCT comes from the cyclopentadienyl and phosphine ligands whose orbital characters in the LUMO+1 diminish by 14% and 18% respectively, while the cobalt's character is augmented by 12%. The LLCT is directed towards the electron-withdrawing trifluoromethyl ligand, which contains 17% more orbital character in the LUMO+1. The band at 24 500 cm^{-1} involves two major excitations, namely HOMO-1 → LUMO (35%) and HOMO-6 → LUMO (33%). The first of these, HOMO-1 → LUMO, is mostly comprised of LMCT and LLCT from the cyclopentadienyl ligand to the cobalt and the phosphine, respectively. In this excitation, the

cobalt's orbital character augments by approximately 3%, while the phosphine's grows by 7%, along with a corresponding diminishment in the cyclopentadienyl orbital character of 10%.

The second excitation (HOMO-6 → LUMO) is mostly comprised of LMCT from all three ligands to the cobalt. The orbital character of the cobalt increases by 6%, while the cyclopentadienyl diminishes by 12%, the trifluoromethyl by 3% and the phosphine by 7%. The calculated Mayer bond orders of cobalt-ligand bonds in these complexes shed further insight into the electronic nature of these complexes. In **5**, the large bond order for the cyclopentadienyl ligand (2.37) is expected as this type of ligand coordinates in an η^5 fashion and corresponds to an XL_2 type of bonding.

Calculation of ^{19}F NMR shifts. The geometries were initially optimized at the density functional theory (DFT)[208] level with the hybrid B3LYP[209,210] and then with Perdew and Wang's 1991 gradient-corrected correlation functional,[211,212] the DFT-optimized DZVP2 basis set[382] for H, C, F and P atoms and cc-pVDZ-PP (D-PP)[383,384] basis sets for Co using the Gaussian09 program system.[380] Vibrational frequencies were calculated to show that the structures were minima. The PW91/DZVP2/D-PP geometries were used to predict the NMR chemical shifts for F (^{19}F-NMR), P (^{31}P-NMR) and H (^{1}H-NMR) at the BLYP[385] and PW91 level with a valence triple-ζ basis set with polarization functions (VTZP) from Ahlrichs and coworkers.[386] The nuclear magnetic shielding tensors were calculated using the gauge-independent atomic orbital (GIAO)[387,388] approach implemented by Gaussian09. To compare the chemical shifts calculated using Gassian09, PW91/DZVP2/D-PP optimized geometries were used to predict the same NMR chemical shifts calculated with the ADF program system[389,390] with the BLYP[385] functional and the TZ2P basis set in ADF.[390] Scalar relativistic effects were included at the two-component zero-order regular approximation (ZORA) level for the NMR calculations using ADF.[391,392] The ^{19}F-

NMR, ^{31}P-NMR and ^{1}H-NMR chemical shifts are reported relative to their specific standard calculated at the same level: $CFCl_3$, H_3PO_4 and TMS, respectively. The shift is calculated as $\delta = \sigma(\text{standard}) - \sigma(\text{compound})$ where σ is an absolute shift. There are two terms in the calculation of the absolute shift, the diamagnetic component and the paramagnetic component, both of which are tensors. The diamagnetic component (shielding) is mostly an atomic one which goes as r^{-3} and is positive. In most cases, the paramagnetic component is negative (deshielding) and thus cancels out a portion of the diamagnetic component. The paramagnetic component to first order is due to mixing of higher occupied orbitals such as the HOMO with low lying unoccupied orbitals such as the LUMO in the presence of a magnetic field, which can be considered as a perturbation on the ground state wave function giving rise to the first order induced electronic current density.

The chemical shifts in ppm and Co-F bond distances in Å are reported in Table B.3. Co-F Tensors from G09 (BLYP/Alhrich-TZVP), experimental data and the Cartesian coordinates at the PW91/DZVP2/D-PP level for the optimized geometries are reported in the Supporting Information of the original publication.[95] Orbital diagrams for $CpCo(CF_3)(F)(PH_3)$ and $CpCo(CF_3)(F)(PPh_3)$ (**5**) are reported in Figure B.4, Figure B.5 and Figure B.6.

The calculations were performed on a Xeon-based Dell Linux cluster at The University of Alabama, and a local AMD Opteron-based and Intel Xeon-based Linux cluster from Penguin Computing.

Table B.3. **Predicted chemical shifts in ppm and Co-F bond distances in Å**

Chemical shift (ppm)	r(Co-F) (Å)	ADF (BLYP/TZ2P)	G09 (PW91/Alhrich-TZVP)	G09 (BLYP/Alhrich-TZVP)
$CpCo(CF_3)(F)(PH_3)$				
F (Co-**F**)	1.871	-776.4	-807.8	-782.7
F_{avg} ($C\mathbf{F}_3$)		-24.5	-22.3	-24.7
P ($\mathbf{P}H_3$)		-81.4	-108.5	-98.8
H_{avg} (Cp)		+4.9	+4.8	+4.7
$CpCo(CF_3)(F)(PPh_3)$ (5)				
F (Co-**F**)	1.878	-798.2	-841.3	-811.9
F_{avg} ($C\mathbf{F}_3$)		-21.2	-18.3	-21.2
P ($\mathbf{P}Ph_3$)		+79.9	+54.1	+65.5
H_{avg} (Cp)		+4.6	+4.4	+4.3
$CpCo(CF_3)(F)(PPh_2Me)$ (6)				
F (Co-**F**)	1.873	-762.0	-800.3	-774.9
F_{avg} ($C\mathbf{F}_3$)		-24.7	-22.6	-25.0
P ($\mathbf{P}Ph_2Me$)		+86.6	+61.0	+72.2
H_{avg} (Cp)		+4.5	+4.4	+4.4
$CpCo(CF_2CF_3)(F)(PPh_3)$ (7)				
F (Co-**F**)	1.877	-819.9	-868.7	-837.6
F_{avg} ($C\mathbf{F}_3$)		-110.3	-112.0	-112.2
F_{avg} ($C\mathbf{F}_2$)		-91.2	-88.8	-91.5
P ($\mathbf{P}Ph_3$)		+78.0	+52.9	+64.4
H_{avg} (Cp)		+4.4	+4.4	+4.4
$CpCo(CF_2CF_3)(F)(PPh_2Me)$ (8)				
F (Co-**F**)	1.872	-767.5	-808.9	-782.1
F_{avg} ($C\mathbf{F}_3$)		-110.3	-111.8	-111.1
F_{avg} ($C\mathbf{F}_2$)		-101.8	-100.7	-102.5
P ($\mathbf{P}Ph_2Me$)		+88.1	+62.0	+73.3
H_{avg} (Cp)		+4.5	+4.4	+4.4

Standards:
^{19}F-NMR: $CFCl_3$
^{31}P-NMR: H_3PO_4
^{1}H-NMR: TMS

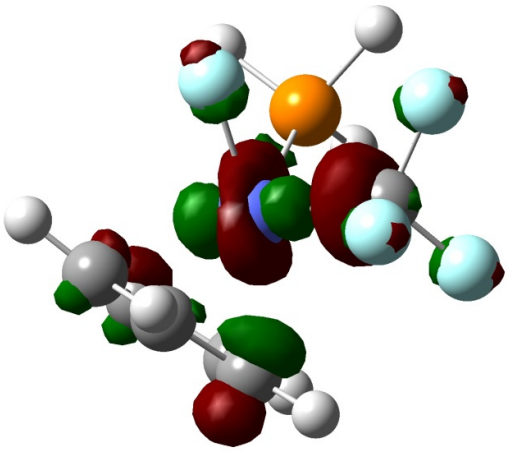

LUMO+1 (58) (-2.61 eV)

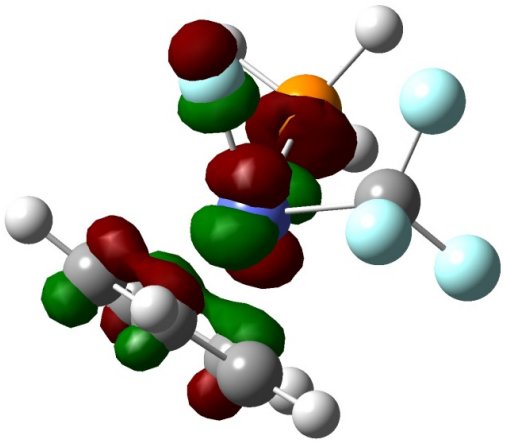

LUMO (57) (-3.28 eV)

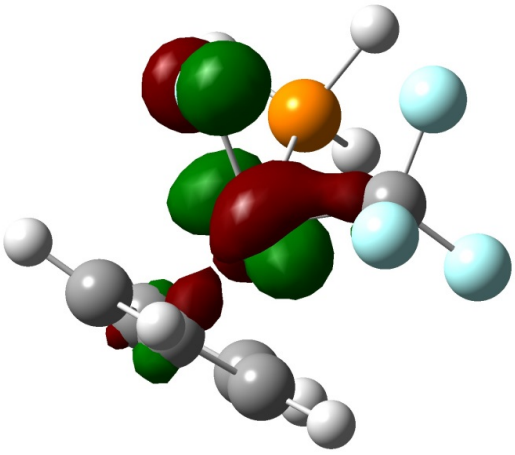

HOMO (56) (-5.20 eV)

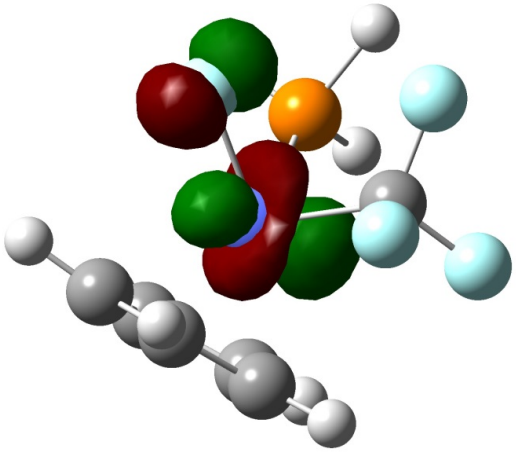

HOMO-1 (55) (-5.63 eV)

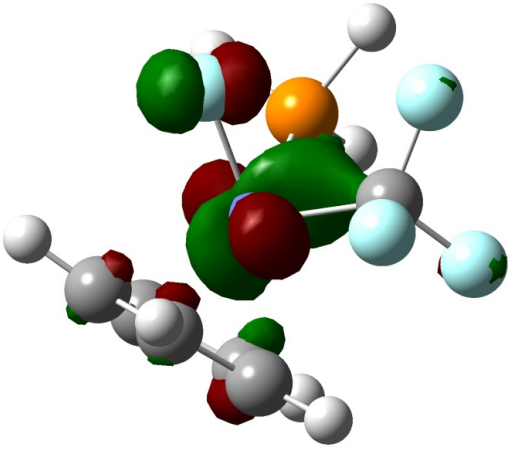

HOMO-2 (54) (-5.99 eV)

Figure B.4. Orbital diagrams for $CpCo(CF_3)(F)(PH_3)$ using PW91/DZVP2/D-PP.

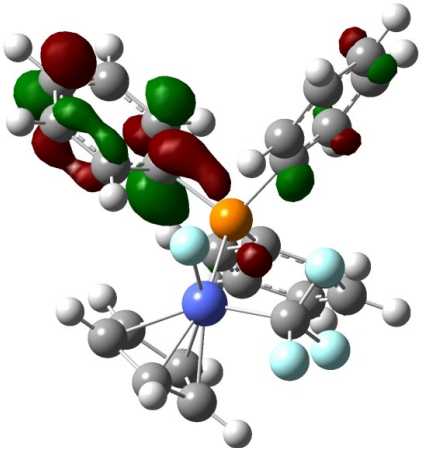

LUMO+2 (-1.90 eV)

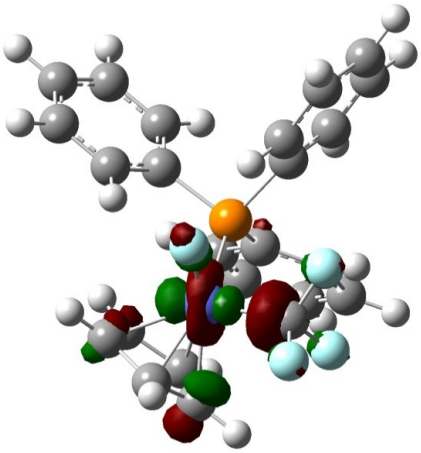

LUMO+1 (-2.27 eV)

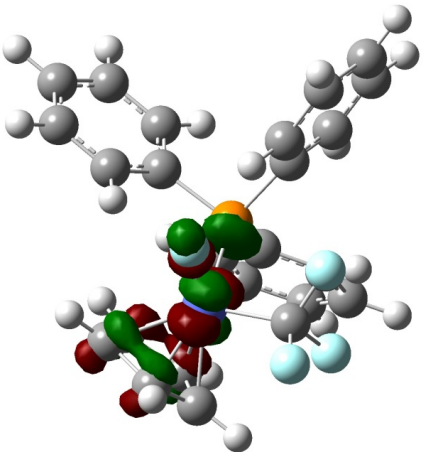

LUMO (-2.88 eV)

Figure B.5. Orbital diagrams for $CpCo(CF_3)(F)(PPh_3)$ (**5**) using PW91/DZVP2/D-PP.

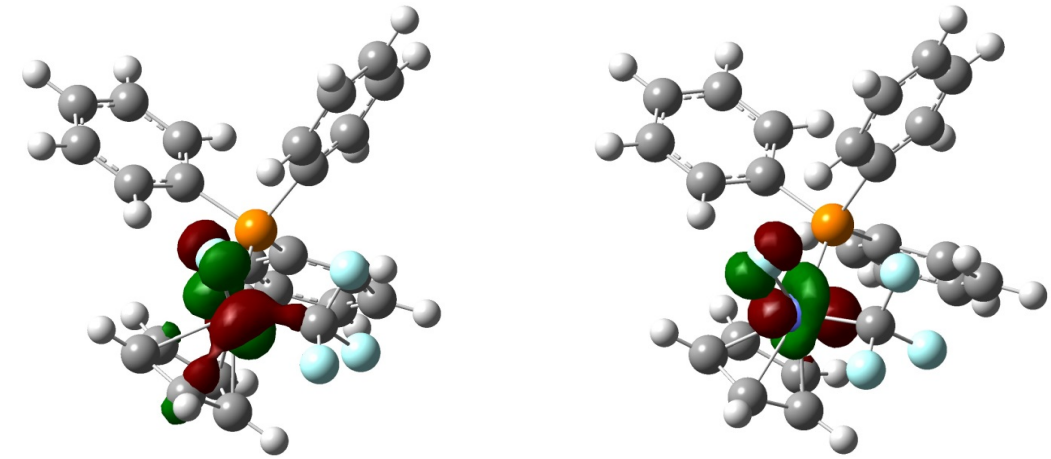

HOMO (-4.65 eV) **HOMO-1 (-5.06 eV)**

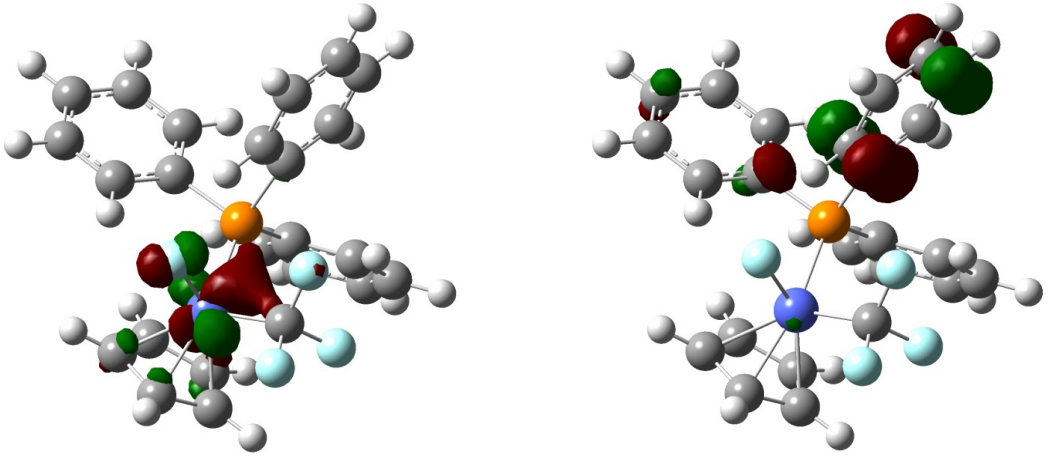

HOMO-2 (-5.34 eV) **HOMO-3 (-5.98 eV)**

Figure B.6. Orbital diagrams for $CpCo(CF_3)(F)(PPh_3)$ (**5**) using PW91/DZVP2/D-PP.

Table B.4. Catalytic fluorination reactions

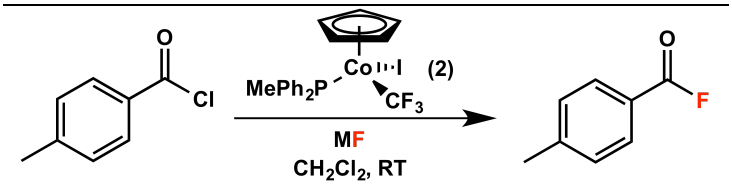

Entry	MF (eq)	Catalyst Loading (mol%)	t (h)	Yield (%)
1	AgF (1.0)	-	16	2
2	CsF (1.0)	-	16	5
3	KF (1.0)	-	16	<1
4	CoF_3	-	16	2
5	KF (3.0)	10	4	3
6	CsF (3.0)	10	4	34
7	AgF (3.0)	10	1	44
8	AgF (3.0)	10	2	52
9	AgF (3.0)	10	3	86
10	AgF (3.0)	10	4	99
11	AgF (2.5)	10	4	48
12	AgF (2.0)	10	4	44
13	AgF (1.5)	10	4	22
14	AgF (3.0)	5	4	99
15	AgF (3.0)	1	4	47
16	AgF (3.0)	0.1	4	26

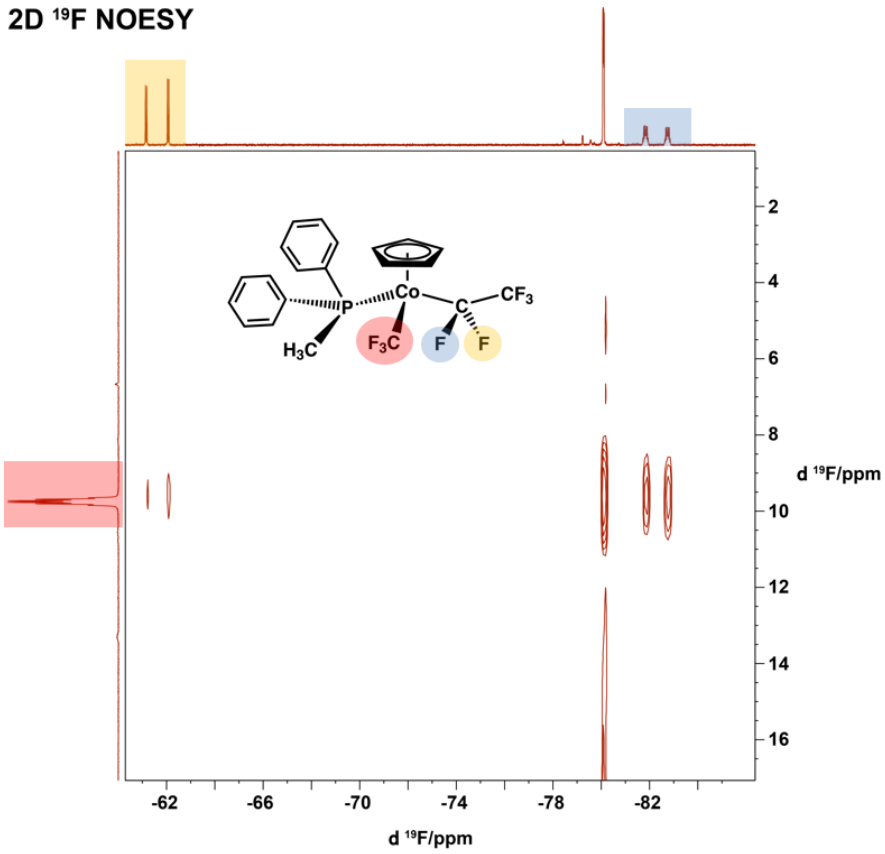

Figure B.7. Two-dimensional ^{19}F NOESY experiment in C_6D_6 to help in the assignment of the two [Co]-CF_2CF_3 fluorine signals is shown. The through-space interaction between the trifluoromethyl ligand on the cobalt and the downfield fluorine signal on the methylene carbon is shown to be weaker than the one with the upfield fluorine signal.

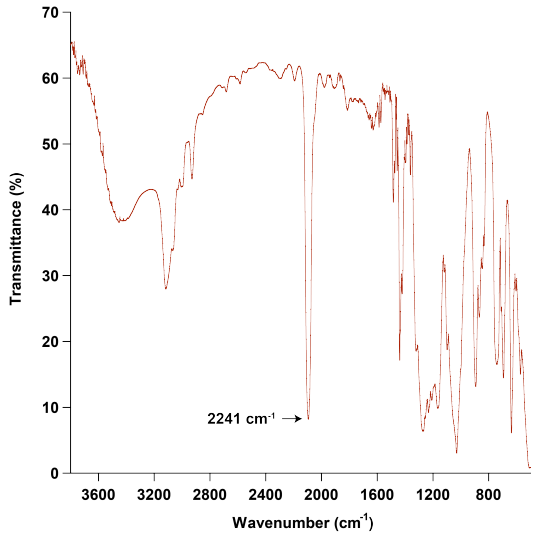

Figure B.8. Infrared spectrum of the reaction between $CpCo(CF_3)_2(PPh_2Me)$ (**9**) and Me_3SiOTf after 1 hour. The cobalt carbonyl stretch is indicated as a product of the reaction of the cobalt difluorocarbene fragment with trace water.

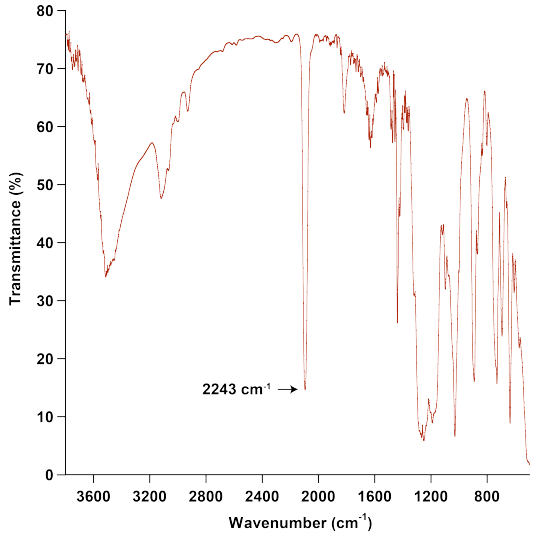

Figure B.9. Infrared spectrum of the reaction between $CpCo(CF_2CF_3)(CF_3)(PPh_2Me)$ (**10**) and Me_3SiOTf after 1 hour. The cobalt carbonyl stretch is indicated as a product of the reaction of the cobalt difluorocarbene fragment with trace water.

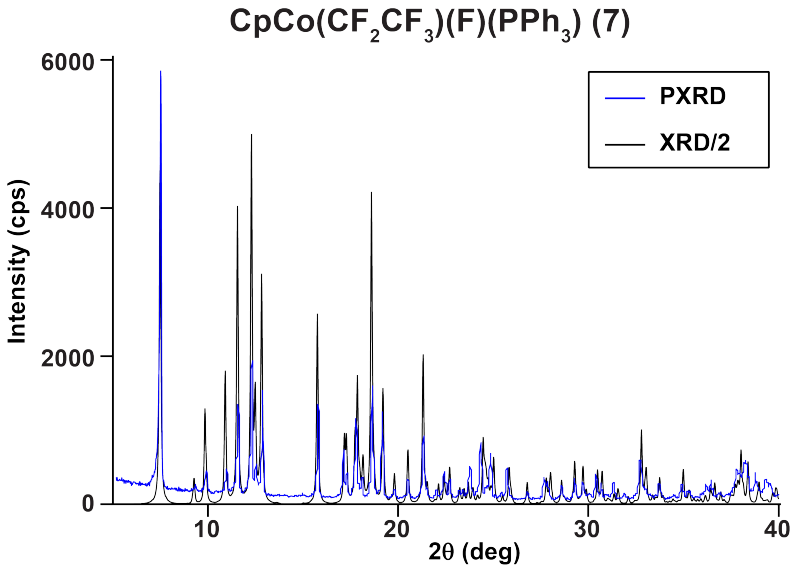

Figure B.10. Powder X-ray diffraction spectrum of $CpCo(CF_2CF_3)(F)(PPh_3)$ (**7**) for single crystals (blue trace) in the 5-40° 2θ region compared with the calculated pattern (black trace) from single crystal X-ray data.

Appendix C

Appendix to Chapter 3

Computational Details. Density functional theory (DFT)[208] calculations have been performed using the B3LYP[209,210] exchange-correlation functional, the TZVP[297] basis set, and the Gaussian 03 package.[393] The single-point calculations of the geometries corresponding to the X-ray structures with C-H bond distances adjusted to 1.08 Å were conducted. Tight SCF convergence criteria (10^{-8} au) were used for all calculations. The AOMix package (www.sg-chem.net) was used for the analysis of MO compositions in terms of contributions from atoms and fragment orbitals, and for the calculation of Mayer bond orders.[223]

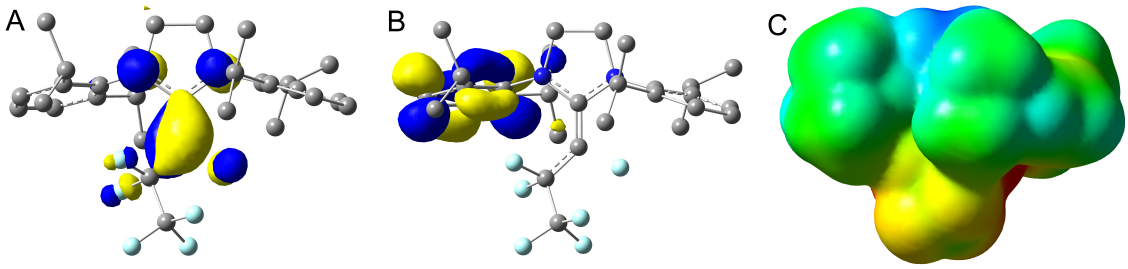

Figure C.1. a) the HOMO of **1b** (shown with the isosurface value of 0.05 a.u.); b) the LUMO of **1b** (shown with the isosurface value of 0.05 a.u.); and c) the total electronic density (isosurface value of 0.0004 a.u.) mapped with the electrostatic potential (ESP; the red, yellow, green and blue colours correspond to the increasing ESP values from negative to neutral to positive) of **1b**.

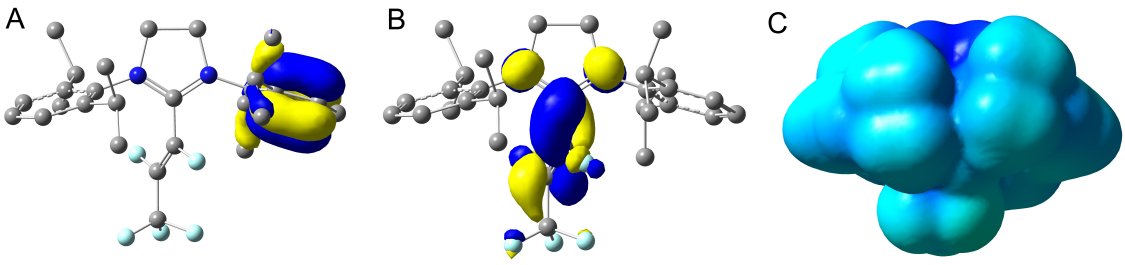

Figure C.2. a) the HOMO of **3b** (shown with the isosurface value of 0.05 a.u.); b) the LUMO of **3b** (shown with the isosurface value of 0.05 a.u.); and c) the total electronic density (isosurface value of 0.0004 a.u.) mapped with the electrostatic potential (ESP; the red, yellow, green and blue colours correspond to the increasing ESP values from negative to neutral to positive) of **3b**.

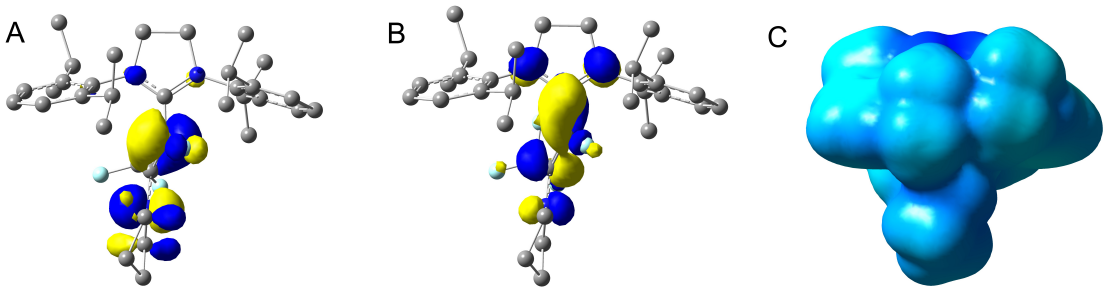

Figure C.3. a) the HOMO of **6** (shown with the isosurface value of 0.05 a.u.); b) the LUMO of **6** (shown with the isosurface value of 0.05 a.u.); and c) the total electronic density (isosurface value of 0.0004 a.u.) mapped with the electrostatic potential (ESP; the red, yellow, green and blue colours correspond to the increasing ESP values from the negative to neutral to positive) of **6**.

Appendix D

Appendix to Chapter 4

DFT Studies. Density functional theory (DFT) calculations were performed with the Gaussian 09 package.[380] Geometry optimization calculations were performed with the PBEPBE[394] exchange-correlation functional with the TZVP[297] basis set on all atoms and inclusion of solvation effects using the polarized continuum model (PCM) with DCM as the solvent. The geometries of all complexes were fully optimized starting from X-ray crystal structures. All optimized geometries had frequencies found to be real. Further calculations of MOs and TD-DFT used the B3LYP functional with the TZVP basis set on all atoms. Orbitals from the Gaussian calculations were plotted with the ChemCraft program. TD-DFT was used to calculate the electronic transition energies for the 40 lowest energy transitions.

Table D.1. Comparison of experimental and calculated structural parameters of 10

	Exp.	Calc.
N1-C5 (Å)	1.361(2)	1.372
N4-C5 (Å)	1.361(2)	1.370
C5-C6 (Å)	1.383(3)	1.409
C6-F7 (Å)	1.376(2)	1.382
C6-C8 (Å)	1.378(3)	1.391
C8-C9 (Å)	1.379(3)	1.396
C9-C10 (Å)	1.436(3)	1.454
C9-C13 (Å)	1.444(3)	1.452
C10-C11 (Å)	1.349(4)	1.381
C11-C12 (Å)	1.426(4)	1.449
C12-C13 (Å)	1.353(4)	1.383
N1-C5-N4 (°)	109.1(2)	109.45
C5-C6-C8 (°)	129.4(2)	127.50
C6-C8-C9 (°)	129.4(2)	129.56

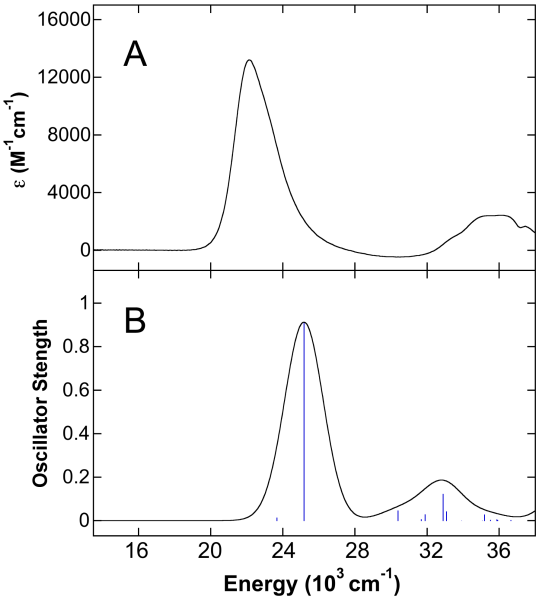

Figure D.1. Electronic absorption spectrum of **10**. (A) The experimental electronic absorption spectrum of **10** collected in DCM and (B) the TD-DFT calculated electronic spectrum of **10** using B3LYP/TZVP (DCM solvent model). From TD-DFT, the high intensity, lowest energy transition is assigned to the HOMO to LUMO transition of **10**. Analogous shifts of the energy of the lowest energy transition calculated by TD-DFT are observed across multiple functionals (Table S8).

Table D.2. TD-DFT predicted energies of the lowest energy intense transition of 10

Functional / basis set	Energy (cm^{-1})
B3LYP / TZVP	25184
CAM-B3LYP / TZVP	25428
M06L / TZVP	24988
PBE1PBE / TZVP	25495

References

(1) Chambers, R. D. In *Fluorine in Organic Chemistry*; CRC Press, 2004.
(2) Böhm, H.-J.; Banner, D.; Bendels, S.; Kansy, M.; Kuhn, B.; Müller, K.; Obst-Sander, U.; Stahl, M. *ChemBioChem* **2004**, *5*, 637–643.
(3) Hagmann, W. K. *J. Med. Chem.* **2008**, *51*, 4359–4369.
(4) O'Hagan, D. *J. Fluorine Chem.* **2010**, *131*, 1071–1081.
(5) Wang, J.; Sánchez-Roselló, M.; Aceña, J. L.; del Pozo, C.; Sorochinsky, A. E.; Fustero, S.; Soloshonok, V. A.; Liu, H. *Chem. Rev.* **2014**, *114*, 2432–2506.
(6) Zhou, Y.; Wang, J.; Gu, Z.; Wang, S.; Zhu, W.; Aceña, J. L.; Soloshonok, V. A.; Izawa, K.; Liu, H. *Chem. Rev.* **2016**, *116*, 422–518.
(7) Lemal, D. M. *J. Org. Chem.* **2004**, *69*, 1–11.
(8) Olah, G. A.; Surya Prakash, G. K.; Molnár, Á.; Sommer, J. In *Superacid Chemistry*; John Wiley & Sons, Inc., 2009.
(9) Riedel, S.; Kaupp, M. *Coord. Chem. Rev.* **2009**, *253*, 606–624.
(10) O'Hagan, D.; B. Harper, D. *J. Fluorine Chem.* **1999**, *100*, 127–133.
(11) Aigueperse, J.; Mollard, P.; Devilliers, D.; Chemla, M.; Faron, R.; Romano, R.; Cuer, J. P. In *Ullmann's Encyclopedia of Industrial Chemistry*; John Wiley & Sons, Inc., 2000.
(12) Harsanyi, A.; Sandford, G. *Green Chem.* **2015**, *17*, 2081–2086.
(13) Braun, J.; Stöß, H.; Zober, A. *Arch. Toxicol.* **1984**, *56*, 50–54.
(14) Amii, H.; Uneyama, K. *Chem. Rev.* **2009**, *109*, 2119–2183.
(15) O'Hagan, D. *Chem. Soc. Rev.* **2008**, *37*, 308–319.
(16) John Scheirs, ed. In *Modern Fluoropolymers: High Performance Polymers for Diverse Applications*; John Wiley & Sons, Inc., 1997.
(17) Ameduri, B.; Boutevin, B. In *Well-Architectured Fluoropolymers: Synthesis, Properties and Applications*; Elsevier, Ltd., 2004.
(18) Ertl, G.; Knozinger, H.; Schüth, F.; Weitkamp, J., eds. In *Handbook of Heterogeneous Catalysis, 2nd edition*; John Wiley & Sons, Inc., 2008.
(19) Beller, M.; Renken, A.; van Santen, R. A., eds. In *Catalysis: From Principles to Applications*; John Wiley & Sons, Inc., 2012.
(20) Ross, J. R. H. In *Heterogeneous Catalysis*; Elsevier, Ltd., 2012.
(21) Hagen, J. In *Industrial Catalysis: A Practical Approach, 2nd Edition*; John Wiley & Sons, Inc., 2005.
(22) Braun, T.; Hughes, R. P., eds. In *Organometallic Fluorine Chemistry*; Springer International Publishing, 2015.
(23) Liang, T.; Neumann, C. N.; Ritter, T. *Angew. Chem. Int. Ed.* **2013**, *52*, 8214–8264.
(24) Champagne, P. A.; Desroches, J.; Hamel, J.-D.; Vandamme, M.; Paquin, J.-F. *Chem. Rev.* **2015**, *115*, 9073–9174.
(25) Wu, J. *Tetrahedron Lett.* **2014**, *55*, 4289–4294.
(26) Furuya, T.; Kamlet, A. S.; Ritter, T. *Nature* **2011**, *473*, 470–477.
(27) Hollingworth, C.; Gouverneur, V. *Chem. Commun.* **2012**, *48*, 2929–2942.
(28) Liu, W.; Huang, X.; Cheng, M.-J.; Nielsen, R. J.; Goddard, W. A.; Groves, J. T. *Science* **2012**, *337*, 1322–1325.
(29) Fier, P. S.; Hartwig, J. F. *Science* **2013**, *342*, 956–960.
(30) West, J. G.; Bedell, T. A.; Sorensen, E. J. *Angew. Chem. Int. Ed.* **2016**, *55*, 8923–8927.
(31) Lou, S.-J.; Xu, D.-Q.; Xu, Z.-Y. *Angew. Chem. Int. Ed.* **2014**, *53*, 10330–10335.

(32) Winfield, J. M. *J. Fluorine Chem.* **1986**, *33*, 159–178.
(33) Thrasher, J. S.; Strauss, S. H., eds. In *Inorganic Fluorine Chemistry - Toward the 21st Century*; ACS Symposium Series, Vol. 555; American Chemical Society, 1994.
(34) Murphy, E. F.; Murugavel, R.; Roesky, H. W. *Chem. Rev.* **1997**, *97*, 3425–3468.
(35) Ahrens, T.; Kohlmann, J.; Ahrens, M.; Braun, T. *Chem. Rev.* **2015**, *115*, 931–972.
(36) Beagley, B.; Young, G. G. *J. Mol. Struct.* **1977**, *40*, 295–297.
(37) García-Monforte, M. A.; Martínez-Salvador, S.; Menjón, B. *Eur. J. Inorg. Chem.* **2012**, *2012*, 4945–4966.
(38) Stone, F. G. A. *J. Fluorine Chem.* **1999**, *100*, 227–234.
(39) Emeléus, H. J. *Angew. Chem. Int. Ed.* **1962**, *1*, 129–133.
(40) King, R. B.; Treichel, P. M.; Stone, F. G. A. *J. Am. Chem. Soc.* **1961**, *83*, 3593–3597.
(41) King, R. B.; Stafford, S. L.; Treichel, P. M.; Stone, F. G. A. *J. Am. Chem. Soc.* **1961**, *83*, 3604–3608.
(42) Lange, H.; Naumann, D. *J. Fluorine Chem.* **1984**, *26*, 435–444.
(43) Burton, D. J.; Wiemers, D. M. *J. Am. Chem. Soc.* **1985**, *107*, 5014–5015.
(44) Guerra, M. A.; Bierschenk, T. R.; Lagow, R. J. *J. Am. Chem. Soc.* **1986**, *108*, 4103–4105.
(45) Aikawa, K.; Toya, W.; Nakamura, Y.; Mikami, K. *Org. Lett.* **2015**, *17*, 4996–4999.
(46) Krause, L. J.; Morrison, J. A. *J. Chem. Soc., Chem. Commun.* **1980**, *14*, 671–672.
(47) Nair, H. K.; Morrison, J. A. *J. Organomet. Chem.* **1989**, *376*, 149–164.
(48) Emeléus, H. J.; Haszeldine, R. N. *J. Chem. Soc.* **1949**, 2953–2956.
(49) Eujen, R.; Lagow, R. J. *J. Chem. Soc., Dalton Trans.* **1978**, *6*, 541–544.
(50) Lagow, R. J.; Eujen, R.; Gerchman, L. L.; Morrison, J. A. *J. Am. Chem. Soc.* **1978**, *100*, 1722–1726.
(51) Chu, L.; Qing, F.-L. *Acc. Chem. Res.* **2014**, *47*, 1513–1522.
(52) Liu, X.; Xu, C.; Wang, M.; Liu, Q. *Chem. Rev.* **2014**, *115*, 683–730.
(53) Prakash, G. K. S.; Yudin, A. K. *Chem. Rev.* **1997**, *97*, 757–786.
(54) Lippert, E. *Angew. Chem.* **1960**, *72*, 602–602.
(55) Campbell, M. G.; Ritter, T. *Chem. Rev.* **2015**, *115*, 612–633.
(56) Ma, J.-A.; Cahard, D. *Chem. Rev.* **2004**, *104*, 6119–6146.
(57) Baudoux, J.; Cahard, D. In *Electrophilic Fluorination with N-F Reagents;* Organic Reactions, Vol. 69; John Wiley & Sons, Inc., 2004.
(58) Chernick, C. L.; Claassen, H. H.; Fields, P. R.; Hyman, H. H.; Malm, J. G.; Manning, W. M.; Matheson, M. S.; Quarterman, L. A.; Schreiner, F.; Selig, H. H.; Sheft, I.; Siegel, S.; Sloth, E. N.; Stein, L.; Studier, M. H.; Weeks, J. L.; Zirin, M. H. *Science* **1962**, *138*, 136–138.
(59) Differding, E.; Ofner, H. *Synlett* **1991**, *1991*, 187–189.
(60) Banks, R. E.; Mohialdin-Khaffaf, S. N.; Lal, G. S.; Sharif, I.; Syvret, R. G. *J. Chem. Soc., Chem. Commun.* **1992**, *8*, 595–596.
(61) Gambhir, S. S. *Nat. Rev. Cancer* **2002**, *2*, 683–693.
(62) Cossee, P. *J. Catal.* **1964**, *3*, 80–88.
(63) Arlman, E. J.; Cossee, P. *J. Catal.* **1964**, *3*, 99–104.
(64) Brookhart, M.; Green, M. L. H. *J. Organomet. Chem.* **1983**, *250*, 395–408.
(65) Xu, Z.; Vanka, K.; Ziegler, T. *Organometallics* **2004**, *23*, 104–116.
(66) Piers, W. E.; Bercaw, J. E. *J. Am. Chem. Soc.* **1990**, *112*, 9406–9407.
(67) Clawson, L.; Soto, J.; Buchwald, S. L.; Steigerwald, M. L.; Grubbs, R. H. *J. Am. Chem. Soc.* **1985**, *107*, 3377–3378.

(68) Hughes, R. P. *Eur. J. Inorg. Chem.* **2009**, *2009*, 4591–4606.
(69) Ivin, K. J.; Rooney, J. J.; Stewart, C. D.; Green, M. L. H.; Mahtab, R. *J. Chem. Soc., Chem. Commun.* **1978**, *14*, 604–606.
(70) Crabtree, R. H., ed. In *The Organometallic Chemistry of the Transition Metals, 6th Edition*; John Wiley & Sons, Inc., 2014.
(71) Bertrand, G. In *Carbene Chemistry: From Fleeting Intermediates to Powerful Reagents*; CRC Press, 2002.
(72) de Frémont, P.; Marion, N.; Nolan, S. P. *Coord. Chem. Rev.* **2009**, *253*, 862–892.
(73) Schrock, R. R. *Chem. Rev.* **2002**, *102*, 145–180.
(74) Brothers, P. J.; Roper, W. R. *Chem. Rev.* **1988**, *88*, 1293–1326.
(75) Cotton, F. A.; McCleverty, J. A. *J. Organomet. Chem.* **1965**, *4*, 490.
(76) Reger, D. L.; Dukes, M. D. *J. Organomet. Chem.* **1978**, *153*, 67–72.
(77) Koola, J. D.; Roddick, D. M. *Organometallics* **1991**, *10*, 591–597.
(78) Halle, L. F.; Armentrout, P. B.; Beauchamp, J. L. *Organometallics* **1983**, *2*, 1829–1833.
(79) Richmond, T. G.; Crespi, A. M.; Shriver, D. F. *Organometallics* **1984**, *3*, 314–319.
(80) Crespi, A. M.; Sabat, M.; Shriver, D. F. *Inorg. Chem.* **1988**, *27*, 812–816.
(81) Crespi, A. M.; Shriver, D. F. *Organometallics* **1985**, *4*, 1830–1835.
(82) Huang, D.; Koren, P. R.; Folting, K.; Davidson, E. R.; Caulton, K. G. *J. Am. Chem. Soc.* **2000**, *122*, 8916–8931.
(83) Clark, G. R.; Hoskins, S. V.; Roper, W. R. *J. Organomet. Chem.* **1982**, *234*, C9–C12.
(84) Clark, G. R.; Hoskins, S. V.; Jones, T. C.; Roper, W. R. *J. Chem. Soc. Chem. Commun.* **1983**, *13*, 719–721.
(85) Trnka, T. M.; Day, M. W.; Grubbs, R. H. *Angew. Chem. Int. Ed.* **2001**, *40*, 3441–3444.
(86) Brothers, P. J.; Burrell, A. K.; Clark, G. R.; Rickard, C. E. F.; Roper, W. R. *J. Organomet. Chem.* **1990**, *394*, 615–642.
(87) Bourgeois, C. J.; Hughes, R. P.; Yuan, J.; DiPasquale, A. G.; Rheingold, A. L. *Organometallics* **2006**, *25*, 2908–2910.
(88) Hughes, R. P.; Laritchev, R. B.; Yuan, J.; Golen, J. A.; Rucker, A. N.; Rheingold, A. L. *J. Am. Chem. Soc.* **2005**, *127*, 15020–15021.
(89) Yuan, J.; Hughes, R. P.; Golen, J. A.; Rheingold, A. L. *Organometallics* **2010**, *29*, 1942–1947.
(90) Goodman, J.; Grushin, V. V.; Larichev, R. B.; Macgregor, S. A.; Marshall, W. J.; Roe, D. C. *J. Am. Chem. Soc.* **2009**, *131*, 4236–4238.
(91) Pell, C. J.; Zhu, Y.; Huacuja, R.; Herbert, D. E.; Hughes, R. P.; Ozerov, O. V. *Chem. Sci.* **2017**.
(92) Harrison, D. J.; Gorelsky, S. I.; Lee, G. M.; Korobkov, I.; Baker, R. T. *Organometallics* **2012**, *32*, 12–15.
(93) Lee, G. M.; Harrison, D. J.; Korobkov, I.; Baker, R. T. *Chem. Commun.* **2013**, *50*, 1128–1130.
(94) Harrison, D. J.; Lee, G. M.; Leclerc, M. C.; Korobkov, I.; Baker, R. T. *J. Am. Chem. Soc.* **2013**, *135*, 18296–18299.
(95) Leclerc, M. C.; Bayne, J. M.; Lee, G. M.; Gorelsky, S. I.; Vasiliu, M.; Korobkov, I.; Harrison, D. J.; Dixon, D. A.; Baker, R. T. *J. Am. Chem. Soc.* **2015**, *137*, 16064–16073.
(96) Harrison, D. J.; Daniels, A. L.; Korobkov, I.; Baker, R. T. *Organometallics* **2015**, *34*, 4598–4604.

(97) Harrison, D. J.; Daniels, A. L.; Korobkov, I.; Baker, R. T. *Organometallics* **2015**, *34*, 5683–5686.
(98) Michelin, R. A.; Ros, R.; Guadalupi, G.; Bombieri, G.; Benetollo, F.; Chapuis, G. *Inorg. Chem.* **1989**, *28*, 840–846.
(99) Karel, K. J.; Tulip, T. H.; Ittel, S. D. *Organometallics* **1990**, *9*, 1276–1282.
(100) Xu, L.; Solowey, D. P.; Vicic, D. A. *Organometallics* **2015**, *34*, 3474–3479.
(101) Wu, E.-C.; Rodgers, A. S. *J. Am. Chem. Soc.* **1976**, *98*, 6112–6115.
(102) Bourgeois, C. J.; Garratt, S. A.; Hughes, R. P.; Larichev, R. B.; Smith, J. M.; Ward, A. J.; Willemsen, S.; Zhang, D.; DiPasquale, A. G.; Zakharov, L. N.; Rheingold, A. L. *Organometallics* **2006**, *25*, 3474–3480.
(103) Torrens, H. *Coord. Chem. Rev.* **2005**, *249*, 1957–1985.
(104) Burch, R. R.; Calabrese, J. C.; Ittel, S. D. *Organometallics* **1988**, *7*, 1642–1648.
(105) Carl, R. T.; Hughes, R. P.; Johnson, J. A.; Davis, R. E.; Kashyap, R. P. *J. Am. Chem. Soc.* **1987**, *109*, 6875–6876.
(106) Swan, G. A.; Timmons, P. S.; Nyholm, R. S.; Turco, A.; Smith, T. D.; Feeney, J.; Sutcliffe, L. H.; Buu-Hoï, N. P.; Jacquignon, P.; Marty, M.; Jones, G.; Eaborn, C.; Waters, J. A.; Parshall, G. W.; Wilkinson, G.; Acheson, R. M.; Hands, A. R.; King, L. J.; Holker, J. R.; Honeyman, J. *J. Chem. Soc.* **1962**, 1120–1136.
(107) Fuller, J. T.; Harrison, D. J.; Leclerc, M. C.; Baker, R. T.; Ess, D. H.; Hughes, R. P. *Organometallics* **2015**, *34*, 5210–5213.
(108) Kalnin'sh, K. K. *Russ. J. Appl. Chem.* **2002**, *75*, 589–597.
(109) Buravtsev, N. N.; A. Kolbanovsky, Y. *J. Fluorine Chem.* **1999**, *96*, 35–42.
(110) Getty, S. J.; Borden, W. T. *J. Am. Chem. Soc.* **1991**, *113*, 4334–4335.
(111) Calm, J. M. *Int. J. Refrig.* **2008**, *31*, 1123–1133.
(112) Kim, K.-H.; Shon, Z.-H.; Nguyen, H. T.; Jeon, E.-C. *Atmos. Environ.* **2011**, *45*, 1369–1382.
(113) McLinden, M. O.; Brown, J. S.; Brignoli, R.; Kazakov, A. F.; Domanski, P. A. *Nat. Commun.* **2017**, *8*, 14476.
(114) Nakajima, T.; Groult, H., eds. In *Fluorinated Materials for Energy Conversion*; Elsevier, Ltd., 2005.
(115) Wall, L. A., ed. In *Fluoropolymers*; John Wiley & Sons, Inc., 1972.
(116) Banks, R. E.; Smart, B. E.; Tatlow, J. C., eds. In *Organofluorine Chemistry - Principles and Commercial Applications*; Springer International Publishing, 1994.
(117) Johns, K.; Stead, G. *J. Fluorine Chem.* **2000**, *104*, 5–18.
(118) Améduri, B.; Boutevin, B.; Kostov, G. *Prog. Polym. Sci.* **2001**, *26*, 105–187.
(119) Vecellio, M. *Prog. Org. Coat.* **2000**, *40*, 225–242.
(120) Wood, K. *Macromol. Symp.* **2002**, *187*, 469–480.
(121) Castelvetro, V.; Aglietto, M.; Ciardelli, F.; Chiantore, O.; Lazzari, M.; Toniolo, L. *J. Coat. Technol.* **2002**, *74*, 57–66.
(122) Bongiovanni, R.; Montefusco, F.; Priola, A.; Macchioni, N.; Lazzeri, S.; Sozzi, L.; Ameduri, B. *Prog. Org. Coat.* **2002**, *45*, 359–363.
(123) Ciardelli, F.; Aglietto, M.; Montagnini di Mirabello, L.; Passaglia, E.; Giancristoforo, S.; Castelvetro, V.; Ruggeri, G. *Prog. Org. Coat.* **1997**, *32*, 43–50.
(124) Arcella, V.; Ghielmi, A.; Tommasi, G. *Ann. N. Y. Acad. Sci.* **2003**, *984* (1), 226–244.
(125) Krebs, F. C.; Jensen, T. *J. Fluorine Chem.* **2003**, *120*, 77–84.
(126) Giesy, J. P.; Kannan, K. *Environ. Sci. Technol.* **2002**, *36*, 146A–152A.

(127) Krespan, C. G.; Van-Catledge, F. A.; Smart, B. E. *J. Am. Chem. Soc.* **1984**, *106*, 5544–5546.
(128) Bruce, M. I.; Stone, F. G. A. *Angew. Chem. Int. Ed.* **1968**, *7*, 747–753.
(129) Buncel, E.; Durst, T. In *Comprehensive Carbanion Chemistry: Structure and Reactivity*; Elsevier, Ltd., 1980.
(130) Chambers, R. D., ed. In *Organofluorine Chemistry - Fluorinated Alkenes and Reactive Intermediates*; Springer International Publishing, 1997.
(131) German, L. S.; Knunyantz, I. L. *Angew. Chem. Int. Ed.* **1969**, *8*, 349–356.
(132) Knunyants, I. L.; German, L. S.; Rozhkov, I. N. *Bull. Acad. Sci. USSR (Div. Chem. Sci.)* **1963**, *12*, 1794–1797.
(133) Martynov, I. V.; Uvarov, V. I.; Brel', V. K.; Anufriev, V. I.; Yarkov, A. V. *Bull. Acad. Sci. USSR (Div. Chem. Sci.)* **1989**, *38*, 2500–2503.
(134) Brace, N. O. *J. Fluorine Chem.* **1999**, *93*, 1–25.
(135) Brace, N. O. *J. Fluorine Chem.* **1999**, *96*, 101–127.
(136) Brace, N. O. *J. Fluorine Chem.* **2001**, *108*, 147–175.
(137) Banks, R. E.; Hitchen, S. M. *J. Chem. Soc., Perkin Trans. 1* **1982**, 1593–1600.
(138) Yamada, S.; Hondo, K.; Konno, T.; Ishihara, T. *RSC Adv.* **2016**, *6*, 28458–28469.
(139) Al'bekov, V. A.; Benda, A. F.; Gontar', A. F.; Sokol'skii, G. A.; Knunyants, I. L. *Bull. Acad. Sci. USSR (Div. Chem. Sci.)* **1988**, *37*, 777–780.
(140) Smart, B. E. *J. Am. Chem. Soc.* **1974**, *96*, 929–929.
(141) Hopkinson, M. N.; Richter, C.; Schedler, M.; Glorius, F. *Nature* **2014**, *510*, 485–496.
(142) Diez-Gonzalez, S., ed. In *N-Heterocyclic Carbenes - From Laboratory Curiosities to Efficient Synthetic Tools, 2nd Edition*; Royal Society of Chemistry, 2016.
(143) Glorius, F., ed. In *N-Heterocyclic Carbenes in Transition Metal Catalysis*; Springer International Publishing, 2007.
(144) Velazquez, H. D.; Verpoort, F. *Chem. Soc. Rev.* **2012**, *41*, 7032–7060.
(145) Cazin, C. S. J., ed. In *N-Heterocyclic Carbenes in Transition Metal Catalysis and Organocatalysis*; Springer International Publishing, 2010.
(146) Nelson, D. J.; Nolan, S. P., eds. In *N-Heterocyclic Carbenes: Effective Tools for Organometallic Synthesis*; John Wiley & Sons, Inc., 2014.
(147) Kuhn, N.; Al-Sheikh, A. *Coord. Chem. Rev.* **2005**, *249*, 829–857.
(148) Fuchter, M. J. *Chem. Eur. J.* **2010**, *16*, 12286–12294.
(149) Martin, D.; Soleilhavoup, M.; Bertrand, G. *Chem. Sci.* **2011**, *2*, 389–399.
(150) Scholl, M.; Ding, S.; Lee, C. W.; Grubbs, R. H. *Org. Lett.* **1999**, *1*, 953–956.
(151) Arduengo III, A. J.; Harlow, R. L.; Kline, M. *J. Am. Chem. Soc.* **1991**, *113*, 361–363.
(152) Arduengo III, A. J.; Dias, H. V. R.; Harlow, R. L.; Kline, M. *J. Am. Chem. Soc.* **1992**, *114*, 5530–5534.
(153) Wanzlick, H. W. *Angew. Chem. Int. Ed.* **1962**, *1*, 75–80.
(154) Dixon, D. A.; Arduengo III, A. J. *J. Phys. Chem.* **1991**, *95*, 4180–4182.
(155) Irikura, K. K.; Goddard, W. A.; Beauchamp, J. L. *J. Am. Chem. Soc.* **1992**, *114*, 48–51.
(156) Arduengo III, A. J.; Goerlich, J. R.; Marshall, W. J. *J. Am. Chem. Soc.* **1995**, *117*, 11027–11028.
(157) Tolman, C. A. *Chem. Rev.* **1977**, *77*, 313–348.
(158) Chianese, A. R.; Li, X.; Janzen, M. C.; Faller, J. W.; Crabtree, R. H. *Organometallics* **2003**, *22*, 1663–1667.

(159) Kelly III, R. A.; Clavier, H.; Giudice, S.; Scott, N. M.; Stevens, E. D.; Bordner, J.; Samardjiev, I.; Hoff, C. D.; Cavallo, L.; Nolan, S. P. *Organometallics* **2008**, *27*, 202–210.
(160) Nelson, D. J.; Nolan, S. P. *Chem. Soc. Rev.* **2013**, *42*, 6723–6753.
(161) Back, O.; Henry-Ellinger, M.; Martin, C. D.; Martin, D.; Bertrand, G. *Angew. Chem. Int. Ed.* **2013**, *52*, 2939–2943.
(162) Liske, A.; Verlinden, K.; Buhl, H.; Schaper, K.; Ganter, C. *Organometallics* **2013**, *32*, 5269–5272.
(163) Rodrigues, R. R.; Dorsey, C. L.; Arceneaux, C. A.; Hudnall, T. W. *Chem. Commun.* **2013**, *50*, 162–164.
(164) Weerdenburg, B. J. A. van; Eshuis, N.; Tessari, M.; Rutjes, F. P. J. T.; Feiters, M. C. *Dalton Trans.* **2015**, *44*, 15387–15390.
(165) Vummaleti, S. V. C.; Nelson, D. J.; Poater, A.; Gómez-Suárez, A.; Cordes, D. B.; Slawin, A. M. Z.; Nolan, S. P.; Cavallo, L. *Chem. Sci.* **2015**, *6*, 1895–1904.
(166) Hillier, A. C.; Sommer, W. J.; Yong, B. S.; Petersen, J. L.; Cavallo, L.; Nolan, S. P. *Organometallics* **2003**, *22*, 4322–4326.
(167) Poater, A.; Cosenza, B.; Correa, A.; Giudice, S.; Ragone, F.; Scarano, V.; Cavallo, L. *Eur. J. Inorg. Chem.* **2009**, *2009*, 1759–1766.
(168) Poater, A.; Ragone, F.; Mariz, R.; Dorta, R.; Cavallo, L. *Chem. Eur. J.* **2010**, *16*, 14348–14353.
(169) Falivene, L.; Credendino, R.; Poater, A.; Petta, A.; Serra, L.; Oliva, R.; Scarano, V.; Cavallo, L. *Organometallics* **2016**, *35*, 2286–2293.
(170) Clavier, H.; Nolan, S. P. *Chem. Commun.* **2010**, *46*, 841–861.
(171) Gómez-Suárez, A.; Nelson, D. J.; Nolan, S. P. *Chem. Commun.* **2017**, *53*, 2650–2660.
(172) Iglesias, M.; Beetstra, D. J.; Knight, J. C.; Ooi, L.-L.; Stasch, A.; Coles, S.; Male, L.; Hursthouse, M. B.; Cavell, K. J.; Dervisi, A.; Fallis, I. A. *Organometallics* **2008**, *27*, 3279–3289.
(173) Iglesias, M.; Beetstra, D. J.; Stasch, A.; Horton, P. N.; Hursthouse, M. B.; Coles, S. J.; Cavell, K. J.; Dervisi, A.; Fallis, I. A. *Organometallics* **2007**, *26*, 4800–4809.
(174) Magill, A. M.; Cavell, K. J.; Yates, B. F. *J. Am. Chem. Soc.* **2004**, *126*, 8717–8724.
(175) Alder, R. W.; Blake, M. E.; Oliva, J. M. *J. Phys. Chem. A* **1999**, *103*, 11200–11211.
(176) Piel, I.; Pawelczyk, M. D.; Hirano, K.; Fröhlich, R.; Glorius, F. *Eur. J. Org. Chem.* **2011**, *2011*, 5475–5484.
(177) Lavallo, V.; Canac, Y.; Präsang, C.; Donnadieu, B.; Bertrand, G. *Angew. Chem. Int. Ed.* **2005**, *44*, 5705–5709.
(178) Soleilhavoup, M.; Bertrand, G. *Acc. Chem. Res.* **2015**, *48*, 256–266.
(179) Lavallo, V.; Canac, Y.; DeHope, A.; Donnadieu, B.; Bertrand, G. *Angew. Chem. Int. Ed.* **2005**, *44*, 7236–7239.
(180) Roy, S.; Mondal, K. C.; Roesky, H. W. *Acc. Chem. Res.* **2016**, *49*, 357–369.
(181) Enders, D.; Niemeier, O.; Henseler, A. *Chem. Rev.* **2007**, *107*, 5606–5655.
(182) Bugaut, X.; Glorius, F. *Chem. Soc. Rev.* **2012**, *41*, 3511–3522.
(183) Breslow, R. *J. Am. Chem. Soc.* **1958**, *80*, 3719–3726.
(184) Berkessel, A.; Elfert, S.; Yatham, V. R.; Neudörfl, J.-M.; Schlörer, N. E.; Teles, J. H. *Angew. Chem. Int. Ed.* **2012**, *51*, 12370–12374.
(185) Biju, A. T.; Kuhl, N.; Glorius, F. *Acc. Chem. Res.* **2011**, *44*, 1182–1195.
(186) Schedler, M.; Wang, D.-S.; Glorius, F. *Angew. Chem. Int. Ed.* **2013**, *52*, 2585–2589.

(187) Nair, V.; Menon, R. S.; Biju, A. T.; Sinu, C. R.; Paul, R. R.; Jose, A.; Sreekumar, V. *Chem. Soc. Rev.* **2011**, *40*, 5336–5346.
(188) Fu, Z.; Xu, J.; Zhu, T.; Leong, W. W. Y.; Chi, Y. R. *Nat. Chem.* **2013**, *5*, 835–839.
(189) Fèvre, M.; Pinaud, J.; Gnanou, Y.; Vignolle, J.; Taton, D. *Chem. Soc. Rev.* **2013**, *42*, 2142–2172.
(190) Martínez-Salvador, S.; Falvello, L. R.; Martín, A.; Menjón, B. *Chem. Eur. J.* **2013**, *19*, 14540–14552.
(191) Blaya, M.; Bautista, D.; Gil-Rubio, J.; Vicente, J. *Organometallics* **2014**, *33*, 6358–6368.
(192) Yamaguchi, Y.; Ichioka, H.; Klein, A.; Brennessel, W. W.; Vicic, D. A. *Organometallics* **2012**, *31*, 1477–1483.
(193) Tang, F.; Rath, N. P.; Mirica, L. M. *Chem. Commun.* **2015**, *51*, 3113–3116.
(194) Bour, J. R.; Camasso, N. M.; Sanford, M. S. *J. Am. Chem. Soc.* **2015**, *137*, 8034–8037.
(195) Lee, G. M.; Clément, R.; Baker, R. T. *Catal. Sci. Tech.* **2017**, Submitted.
(196) Wiemers, D. M.; Burton, D. J. *J. Am. Chem. Soc.* **1986**, *108*, 832–834.
(197) Yang, Z. Y.; Wiemers, D. M.; Burton, D. J. *J. Am. Chem. Soc.* **1992**, *114*, 4402–4403.
(198) Taw, F. L.; Clark, A. E.; Mueller, A. H.; Janicke, M. T.; Cantat, T.; Scott, B. L.; Hay, P. J.; Hughes, R. P.; Kiplinger, J. L. *Organometallics* **2012**, *3*, 1484–1499.
(199) Bourgeois, C. J.; Hughes, R. P.; Husebo, T. L.; Smith, J. M.; Guzei, I. M.; Liable-Sands, L. M.; Zakharov, L. N.; Rheingold, A. L. *Organometallics* **2005**, *24*, 6431–6439.
(200) Hughes, R. P.; Lindner, D. C.; Smith, J. M.; Zhang, D.; Incarvito, C. D.; Lam, K.-C.; Liable-Sands, L. M.; Sommer, R. D.; Rheingold, A. L. *J. Chem. Soc. Dalton Trans.* **2001**, *15*, 2270–2278.
(201) Tomashenko, O. A.; Grushin, V. V. *Chem. Rev.* **2011**, *111*, 4475–4521.
(202) Taw, F. L.; Scott, B. L.; Kiplinger, J. L. *J. Am. Chem. Soc.* **2003**, *125*, 14712–14713.
(203) Vabre, B.; Petiot, P.; Declercq, R.; Zargarian, D. *Organometallics* **2014**, *33*, 5173–5184.
(204) Liu, X.; Xu, C.; Wang, M.; Liu, Q. *Chem. Rev.* **2015**, *115*, 683–730.
(205) Huang, D.; Caulton, K. G. *J. Am. Chem. Soc.* **1997**, *119*, 3185–3186.
(206) Vicente, J.; Gil-Rubio, J.; Guerrero-Leal, J.; Bautista, D. *Organometallics* **2004**, *23*, 4871–4881.
(207) Burns, R. J.; Bulkowski, P. B.; Stevens, S. C. V.; Baird, M. C. *J. Chem. Soc. Dalton Trans.* **1974**, *4*, 415–420.
(208) Parr, R. G. In *Density-Functional Theory of Atoms and Molecules*; Springer International Publishing, 1989.
(209) Becke, A. D. *J. Chem. Phys.* **1993**, *98*, 5648–5652.
(210) Lee, C.; Yang, W.; Parr, R. G. *Phys. Rev. B* **1988**, *37*, 785–789.
(211) Perdew, J. P.; Wang, Y. *Phys. Rev. B* **1992**, *45*, 13244–13249.
(212) Dobson, J. F.; Vignale, G.; Das, M. P., eds. In *Electronic Density Functional Theory - Recent Progress and New Directions*; Springer International Publishing, 1998.
(213) Dugan, T. R.; Sun, X.; Rybak-Akimova, E. V.; Olatunji-Ojo, O.; Cundari, T. R.; Holland, P. L. *J. Am. Chem. Soc.* **2011**, *133*, 12418–12421.
(214) Dugan, T. R.; Goldberg, J. M.; Brennessel, W. W.; Holland, P. L. *Organometallics* **2012**, *31*, 1349–1360.
(215) Li, X.; Sun, H.; Yu, F.; Flörke, U.; Klein, H.-F. *Organometallics* **2006**, *25*, 4695–4697.
(216) Bennett, B. K.; Harrison, R. G.; Richmond, T. G. *J. Am. Chem. Soc.* **1994**, *116*, 11165–11166.
(217) Ketelaar, J. J. *Nature* **1931**, *128*, 303.

(218) Hepworth, M. A.; Jack, K. H.; Peacock, R. D.; Westland, G. J. *Acta Crystallogr.* **1957**, *10*, 63–69.
(219) Treichel, P. M.; Stone, F. G. A. *Adv. Organomet. Chem.* **1964**, *1*, 143–220.
(220) Zhang, C.-P.; Wang, H.; Klein, A.; Biewer, C.; Stirnat, K.; Yamaguchi, Y.; Xu, L.; Gomez-Benitez, V.; Vicic, D. A. *J. Am. Chem. Soc.* **2013**, *135*, 8141–8144.
(221) Marenich, A. V.; Cramer, C. J.; Truhlar, D. G. *J. Phys. Chem. B* **2009**, *113*, 6378–6396.
(222) Lever, A. B. P. In *Inorganic Electronic Spectroscopy*; Elsevier, Ltd., 1984.
(223) Mayer, I. *Theor. Chim. Acta* **1985**, *67*, 315–322.
(224) Veltheer, J. E.; Burger, P.; Bergman, R. G. *J. Am. Chem. Soc.* **1995**, *117*, 12478–12488.
(225) Wiberg, K. B.; Hammer, J. D.; Zilm, K. W.; Cheeseman, J. R.; Keith, T. A. *J. Phys. Chem. A* **1998**, *102*, 8766–8773.
(226) Alexakos, L. G.; Cornwell, C. D. *J. Chem. Phys.* **1964**, *41*, 2098–2107.
(227) Cornwell, C. D. *J. Chem. Phys.* **1966**, *44*, 874–880.
(228) Maity, A.; Stanek, R. J.; Anderson, B. L.; Zeller, M.; Hunter, A. D.; Moore, C. E.; Rheingold, A. L.; Gray, T. G. *Organometallics* **2015**, *34*, 109–120.
(229) Birrell, J. A.; Desrosiers, J.-N.; Jacobsen, E. N. *J. Am. Chem. Soc.* **2011**, *133*, 13872–13875.
(230) Stavber, S.; Košir, I.; Zupan, M. *J. Org. Chem.* **1997**, *62*, 4916–4920.
(231) Motie, R. E.; Satchell, D. P. N.; Wassef, W. N. *J. Chem. Soc., Perkin Trans. 2* **1993**, 6, 1087–1090.
(232) Lee, I.; Shim, C. S.; Chung, S. Y.; Kim, H. Y.; Lee, H. W. *J. Chem. Soc., Perkin Trans. 2* **1988**, 11, 1919–1923.
(233) Okano, T.; Harada, N.; Kiji, J. *Bull. Chem. Soc. Jpn.* **1992**, *65*, 1741–1743.
(234) Mankad, N. P.; Toste, F. D. *Chem. Sci.* **2011**, *3*, 72–76.
(235) Hull, K. L.; Anani, W. Q.; Sanford, M. S. *J. Am. Chem. Soc.* **2006**, *128*, 7134–7135.
(236) Racowski, J. M.; Gary, J. B.; Sanford, M. S. *Angew. Chem. Int. Ed.* **2012**, *51*, 3414–3417.
(237) Akana, J. A.; Bhattacharyya, K. X.; Müller, P.; Sadighi, J. P. *J. Am. Chem. Soc.* **2007**, *129*, 7736–7737.
(238) Gorske, B. C.; Mbofana, C. T.; Miller, S. J. *Org. Lett.* **2009**, *11*, 4318–4321.
(239) Schuler, M.; Silva, F.; Bobbio, C.; Tessier, A.; Gouverneur, V. *Angew. Chem. Int. Ed.* **2008**, *47*, 7927–7930.
(240) Ball, N. D.; Sanford, M. S. *J. Am. Chem. Soc.* **2009**, *131*, 3796–3797.
(241) Zhao, S.-B.; Wang, R.-Y.; Nguyen, H.; Becker, J. J.; Gagné, M. R. *Chem. Commun.* **2011**, *48*, 443–445.
(242) Furuya, T.; Strom, A. E.; Ritter, T. *J. Am. Chem. Soc.* **2009**, *131*, 1662–1663.
(243) Furuya, T.; Ritter, T. *Org. Lett.* **2009**, *11*, 2860–2863.
(244) Tang, P.; Ritter, T. *Tetrahedron* **2011**, *67*, 4449–4454.
(245) Fier, P. S.; Hartwig, J. F. *J. Am. Chem. Soc.* **2012**, *134*, 10795–10798.
(246) Mu, X.; Liu, G. *Org. Chem.* **2014**, *1*, 430–433.
(247) Casitas, A.; Canta, M.; Solà, M.; Costas, M.; Ribas, X. *J. Am. Chem. Soc.* **2011**, *133*, 19386–19392.
(248) Grushin, V. V. *Acc. Chem. Res.* **2010**, *43*, 160–171.
(249) Grushin, V. V. *Chem. Eur. J.* **2002**, *8*, 1006–1014.
(250) Macgregor, S. A.; Roe, D. C.; Marshall, W. J.; Bloch, K. M.; Bakhmutov, V. I.; Grushin, V. V. *J. Am. Chem. Soc.* **2005**, *127*, 15304–15321.
(251) Wang, X.; Mei, T.-S.; Yu, J.-Q. *J. Am. Chem. Soc.* **2009**, *131*, 7520–7521.

(252) Chan, K. S. L.; Wasa, M.; Wang, X.; Yu, J.-Q. *Angew. Chem. Int. Ed.* **2011**, *50*, 9081–9084.
(253) Doherty, N. M.; Hoffmann, N. W. *Chem. Rev.* **1991**, *91*, 553–573.
(254) Urata, H.; Fuchikami, T. *Tetrahedron Lett.* **1991**, *32*, 91–94.
(255) Maggiarosa, N.; Tyrra, W.; Naumann, D.; Kirij, N. V.; Yagupolskii, Y. L. *Angew. Chem. Int. Ed.* **1999**, *38*, 2252–2253.
(256) Kolomeitsev, A.; Movchun, V.; Rusanov, E.; Bissky, G.; Lork, E.; Röschenthaler, G.-V.; Kirsch, P. *Chem. Commun.* **1999**, *11*, 1017–1018.
(257) Wang, X.; Xu, Y.; Mo, F.; Ji, G.; Qiu, D.; Feng, J.; Ye, Y.; Zhang, S.; Zhang, Y.; Wang, J. *J. Am. Chem. Soc.* **2013**, *135*, 10330–10333.
(258) Combettes, L. E.; Clausen-Thue, P.; King, M. A.; Odell, B.; Thompson, A. L.; Gouverneur, V.; Claridge, T. D. W. *Chem. Eur. J.* **2012**, *18*, 13133–13141.
(259) Jablonski, C. R.; Zhou, Z. *Can. J. Chem.* **1992**, *70*, 2544–2551.
(260) Wilford, J. B.; Forster, A.; Stone, F. G. A. *J. Chem. Soc.* **1965**, 6519–6523.
(261) Dichloromethane was used as a solvent because it is not hygroscopic and because it is one of the easiest to dry to minimal water content. For more information pertaining to the drying of various solvents, see: Williams, D. B. G.; Lawton, M. *J. Org. Chem.* **2010**, *75*, 8351–8354.
(262) Díez-González, S.; Nolan, S. P. *Coord. Chem. Rev.* **2007**, *251*, 874–883.
(263) Jacobsen, H.; Correa, A.; Poater, A.; Costabile, C.; Cavallo, L. *Coord. Chem. Rev.* **2009**, *253*, 687–703.
(264) Flanigan, D. M.; Romanov-Michailidis, F.; White, N. A.; Rovis, T. *Chem. Rev.* **2015**, *115*, 9307–9387.
(265) Ebnesajjad, S. In *Introduction to Fluoropolymers: Materials, Technology, and Applications*; Elsevier, Ltd., 2013.
(266) Ohashi, M.; Saijo, H.; Shibata, M.; Ogoshi, S. *Eur. J. Org. Chem.* **2013**, *2013*, 443–447.
(267) Arduengo III, A. J.; Calabrese, J. C.; Dias, H. V. R.; Davidson, F.; Goerlich, J. R.; Jockisch, A.; Kline, M.; Marshall, W. J.; Runyon, J. W. *Phosphorus Sulfur Silicon Relat. Elem.* **2016**, *191*, 527–534.
(268) Leclerc, M. C.; Gorelsky, S. I.; Gabidullin, B. M.; Korobkov, I.; Baker, R. T. *Chem. Eur. J.* **2016**, *22*, 8063–8067.
(269) Crocker, R. D.; Nguyen, T. V. *Chem. Eur. J.* **2016**, *22*, 2208–2213.
(270) Ponti, P. P.; Baldwin, J. C.; Kaska, W. C. *Inorg. Chem.* **1979**, *18*, 873–875.
(271) Gruseck, U.; Heuschmann, M. *Tetrahedron Lett.* **1987**, *28*, 6027–6030.
(272) Gruseck, U.; Heuschmann, M. *Chem. Ber.* **1987**, *120*, 2065–2074.
(273) Heuschmann, M. *Chem. Ber.* **1988**, *121*, 39–49.
(274) Maji, B.; Horn, M.; Mayr, H. *Angew. Chem. Int. Ed.* **2012**, *51*, 6231–6235.
(275) Wang, Y.-B.; Wang, Y.-M.; Zhang, W.-Z.; Lu, X.-B. *J. Am. Chem. Soc.* **2013**, *135*, 11996–12003.
(276) Jia, Y.-B.; Wang, Y.-B.; Ren, W.-M.; Xu, T.; Wang, J.; Lu, X.-B. *Macromolecules* **2014**, *47*, 1966–1972.
(277) Jia, Y.-B.; Ren, W.-M.; Liu, S.-J.; Xu, T.; Wang, Y.-B.; Lu, X.-B. *ACS Macro Lett.* **2014**, *3*, 896–899.
(278) Naumann, S.; Thomas, A. W.; Dove, A. P. *Angew. Chem. Int. Ed.* **2015**, *54*, 9550–9554.
(279) Kuhn, N.; Bohnen, H.; Kreutzberg, J.; Bläser, D.; Boese, R. *J. Chem. Soc. Chem. Commun.* **1993**, *14*, 1136–1137.

(280) Al-Rafia, S. M. I.; Malcolm, A. C.; Liew, S. K.; Ferguson, M. J.; McDonald, R.; Rivard, E. *Chem. Commun.* **2011**, *47*, 6987–6989.
(281) Ghadwal, R. S.; Reichmann, S. O.; Engelhardt, F.; Andrada, D. M.; Frenking, G. *Chem. Commun.* **2013**, *49*, 9440–9442.
(282) Wang, Y.; Abraham, M. Y.; Gilliard, R. J.; Sexton, D. R.; Wei, P.; Robinson, G. H. *Organometallics* **2013**, *32*, 6639–6642.
(283) Kronig, S.; Jones, P. G.; Tamm, M. *Eur. J. Inorg. Chem.* **2013**, *2013*, 2301–2314.
(284) Fürstner, A.; Alcarazo, M.; Goddard, R.; Lehmann, C. W. *Angew. Chem. Int. Ed.* **2008**, *47*, 3210–3214.
(285) Glöckner, A.; Kronig, S.; Bannenberg, T.; Daniliuc, C. G.; Jones, P. G.; Tamm, M. *J. Organomet. Chem.* **2013**, *723*, 181–187.
(286) Kuhn, N.; Bohnen, H.; Bläser, D.; Boese, R. *Chem. Ber.* **1994**, *127*, 1405–1407.
(287) Schumann, H.; Glanz, M.; Winterfeld, J.; Hemling, H.; Kuhn, N.; Bohnen, H.; Bläser, D.; Boese, R. *J. Organomet. Chem.* **1995**, *493*, C14–C18.
(288) Enders, D.; Breuer, K.; Raabe, G.; Runsink, J.; Teles, J. H.; Melder, J.-P.; Ebel, K.; Brode, S. *Angew. Chem. Int. Ed.* **1995**, *34*, 1021–1023.
(289) Clement, N. D.; Cavell, K. J.; Ooi, L. *Organometallics* **2006**, *25*, 4155–4165.
(290) Hamidi, M.; Azadi, A.; Rafiei, P. *Adv. Drug Deliv. Rev.* **2008**, *60*, 1638–1649.
(291) Araújo, M.; Muñoz Capdevila, I.; Díaz-Oltra, S.; Escuder, B. *Molecules* **2016**, *21*, 744.
(292) Douvris, C.; Ozerov, O. V. *Science* **2008**, *321*, 1188–1190.
(293) Caputo, C. B.; Stephan, D. W. *Organometallics* **2012**, *31*, 27–30.
(294) Gu, W.; Haneline, M. R.; Douvris, C.; Ozerov, O. V. *J. Am. Chem. Soc.* **2009**, *131*, 11203–11212.
(295) The triflate salt (**4b[OTf]**) was found to react more cleanly and in higher yield than the tetrafluoroborate salt (**4b**). See Experimental Section (3.2.4) for details on this compound.
(296) Relative pK_b values for the amines mentioned: triethylamine (11.01), *N,N*-dimethylaniline (8.85), pyridine (5.21), DMAP (4.48).
(297) Schäfer, A.; Horn, H.; Ahlrichs, R. *J. Chem. Phys.* **1992**, *97*, 2571–2577.
(298) Kuhn, K. M.; Grubbs, R. H. *Org. Lett.* **2008**, *10*, 2075–2077.
(299) Kuhn, N.; Kratz, T. *Synthesis* **1993**, *1993*, 561–562.
(300) Soloshonok, V. A., ed. In *Fluorine-Containing Synthons*; ACS Symposium Series, Vol. 911; American Chemical Society, 2005.
(301) Olah, G. A.; Chambers, R. D.; Prakash, G. K. S., eds. In *Synthetic Fluorine Chemistry*; John Wiley & Sons, Inc., 1992.
(302) Chambers, R. D.; Fuss, R. W.; Spink, R. C. H.; Greenhall, M. P.; Kenwright, A. M.; Batsanov, A. S.; Howard, J. A. K. *J. Chem. Soc., Perkin Trans. 1* **2000**, 10, 1623–1638.
(303) LaZerte, J. D.; Koshar, R. J. *J. Am. Chem. Soc.* **1955**, *77*, 910–914.
(304) Haszeldine, R. N.; Rowland, R.; Sheppard, R. P.; Tipping, A. E. *J. Fluorine Chem.* **1985**, *28*, 291–302.
(305) Chambers, R. D.; Diter, P.; Dunn, S. N.; Farren, C.; Sandford, G.; Batsanov, A. S.; Howard, J. A. K. *J. Chem. Soc., Perkin Trans. 1* **2000**, 10, 1639–1649.
(306) Chambers, R. D.; Grievson, B. *J. Chem. Soc., Perkin Trans. 1* **1985**, 2215–2218.
(307) Petrov, V. A.; Davidson, F.; Smart, B. E. *J. Org. Chem.* **1995**, *60*, 3419–3422.
(308) Krespan, C. G.; Petrov, V. A. *Chem. Rev.* **1996**, *96*, 3269–3302.
(309) Volgraf, M.; Sellers, B. D.; Jiang, Y.; Wu, G.; Ly, C. Q.; Villemure, E.; Pastor, R. M.; Yuen, P.; Lu, A.; Luo, X.; Liu, M.; Zhang, S.; Sun, L.; Fu, Y.; Lupardus, P. J.; Wallweber,

H. J. A.; Liederer, B. M.; Deshmukh, G.; Plise, E.; Tay, S.; Reynen, P.; Herrington, J.; Gustafson, A.; Liu, Y.; Dirksen, A.; Dietz, M. G. A.; Liu, Y.; Wang, T.-M.; Hanson, J. E.; Hackos, D.; Scearce-Levie, K.; Schwarz, J. B. *J. Med. Chem.* **2016**, *59*, 2760–2779.
(310) Leclerc, M. C.; Gabidullin, B. M.; Da Gama, J. G.; Daifuku, S. L.; Iannuzzi, T. E.; Neidig, M. L.; Baker, R. T. *Organometallics* **2017**, *36*, 849–857.
(311) Barluenga, J.; Valdés, C. *Chem. Commun.* **2005**, *39*, 4891–4901.
(312) Barluenga, J.; Fernández, M. A.; Aznar, F.; Valdés, C. *Chem. Commun.* **2002**, *20*, 2362–2363.
(313) Barluenga, J.; Fernández, M. A.; Aznar, F.; Valdés, C. *Chem. Eur. J.* **2004**, *10*, 494–507.
(314) Willis, M. C.; Brace, G. N. *Tetraedron Lett.* **2002**, *43*, 9085–9088.
(315) Wang, Y.; Liao, Q.; Xi, C. *Org. Lett.* **2010**, *12*, 2951–2953.
(316) Bao, W.; Liu, Y.; Lv, X. *Synthesis* **2008**, *2008*, 1911–1917.
(317) Liao, Q.; Wang, Y.; Zhang, L.; Xi, C. *J. Org. Chem.* **2009**, *74*, 6371–6373.
(318) Taillefer, M.; Ouali, A.; Renard, B.; Spindler, J.-F. *Chem. Eur. J.* **2006**, *12*, 5301–5313.
(319) Ouali, A.; Laurent, R.; Caminade, A.-M.; Majoral, J.-P.; Taillefer, M. *J. Am. Chem. Soc.* **2006**, *128*, 15990–15991.
(320) Taillefer, M.; Ma, D., eds. In *Amination and Formation of sp^2 C-N Bonds*; Springer International Publishing, 2012.
(321) Kelly, C. B.; Mercadante, M. A.; Leadbeater, N. E. *Chem. Commun.* **2013**, *49*, 11133–11148.
(322) Nenaidenko, V. G.; Druzhinin, S. V.; Balenkova, E. S. *Russ. J. Org. Chem.* **2008**, *44*, 485–488.
(323) Sanin, A. V. *Synthesis* **1998**, *1998*, 842–846.
(324) Gerus, I. I.; Gorbunova, M. G.; Kukhar, V. P. *J. Fluorine Chem.* **1994**, *69*, 195–198.
(325) Colla, A.; Martins, M. A. P.; Clar, G.; Krimmer, S.; Fischer, P. *Synthesis* **1991**, *1991*, 483–486.
(326) Vasil'tsov, A. M.; Shmidt, E. Y.; Mikhaleva, A. I.; Zaitsev, A. B.; Tarasova, O. A.; Afonin, A. V.; Toryashinova, D.-S. D.; Il'icheva, L. N.; Trofimov, B. A. *Russ. J. Org. Chem. 37*, 334–338.
(327) Pryadeina, M. V.; Kuzueva, O. G.; Burgart, Y. V.; Saloutin, V. I.; Lyssenko, K. A.; Antipin, M. Y. *J. Fluorine Chem.* **2002**, *117*, 1–7.
(328) Palacios, F.; Ochoa de Retana, A. M.; Pascual, S.; Oyarzabal, J. *J. Org. Chem.* **2004**, *69*, 8767–8774.
(329) Banerjee, S.; Karunananda, M. K.; Bagherzadeh, S.; Jayarathne, U.; Parmelee, S. R.; Waldhart, G. W.; Mankad, N. P. *Inorg. Chem.* **2014**, *53*, 11307–11315.
(330) Kleinpeter, E. *J. Serbian Chem. Soc.* **2006**, *71*, 1–17.
(331) Ahrens, T.; Ahrens, M.; Braun, T.; Braun, B.; Herrmann, R. *Dalton Trans.* **2016**, *45*, 4716–4728.
(332) Ohashi, M.; Shibata, M.; Ogoshi, S. *Angew. Chem. Int. Ed.* **2014**, *53*, 13578–13582.
(333) Braun, T.; Noveski, D.; Neumann, B.; Stammler, H.-G. *Angew. Chem. Int. Ed.* **2002**, *41*, 2745–2748.
(334) Teltewskoi, M.; Panetier, J. A.; Macgregor, S. A.; Braun, T. *Angew. Chem. Int. Ed.* **2010**, *49*, 3947–3951.
(335) Noveski, D.; Braun, T.; Schulte, M.; Neumann, B.; Stammler, H.-G. *Dalton Trans.* **2003**, *21*, 4075–4083.
(336) Braun, T.; Wehmeier, F.; Altenhöner, K. *Angew. Chem. Int. Ed.* **2007**, *46*, 5321–5324.

(337) McBride, D. W.; Dudek, E.; Stone, F. G. A. *J. Chem. Soc.* **1964**, 1752–1759.
(338) Xu, W.; Sun, H.; Xiong, Z.; Li, X. *Organometallics* **2013**, *32*, 7122–7132.
(339) Hughes, R. P.; Laritchev, R. B.; Zakharov, L. N.; Rheingold, A. L. *J. Am. Chem. Soc.* **2004**, *126*, 2308–2309.
(340) Lentz, D.; Nickelt, N.; Willemsen, S. *Chem. Eur. J.* **2002**, *8*, 1205–1217.
(341) Adhikesavalu, D.; Venkatesan, K. *Acta Crystallogr. C* **1983**, *39*, 1044–1048.
(342) Brisdon, A. K.; Banger, K. K. *J. Fluorine Chem.* **1999**, *100*, 35–43.
(343) Einstein, F. W. B.; Luth, H.; Trotter, J. *J. Chem. Soc. A* **1967**, 89–93.
(344) Jolly, P. W.; Bruce, M. I.; Stone, F. G. A. *J. Chem. Soc.* **1965**, 5830–5837.
(345) Fields, R.; Godwin, G. L.; Haszeldine, R. N. *J. Chem. Soc., Dalton Trans.* **1975**, *18*, 1867–1872.
(346) Burt, R.; Cooke, M.; Green, M. *J. Chem. Soc. A* **1970**, 2975–2981.
(347) Booth, B. L.; Haszeldine, R. N.; Perkins, I. *J. Chem. Soc., Dalton Trans.* **1975**, *18*, 1847–1850.
(348) Rest, A. J.; Rosevear, D. T.; Stone, F. G. A. *J. Chem. Soc. A* **1967**, 66–68.
(349) Ashley-Smith, J.; Green, M.; Stone, F. G. A. *J. Chem. Soc. A* **1969**, 3019–3023.
(350) Browning, J.; Green, M.; Stone, F. G. A. *J. Chem. Soc. A* **1971**, 453–457.
(351) Braun, T.; Blöcker, B.; Schorlemer, V.; Neumann, B.; Stammler, A.; Stammler, H.-G. *J. Chem. Soc., Dalton Trans.* **2002**, *10*, 2213–2218.
(352) Ohashi, M.; Shibata, M.; Saijo, H.; Kambara, T.; Ogoshi, S. *Organometallics* **2013**, *32*, 3631–3639.
(353) Hacker, M. J.; Littlecott, G. W.; Kemmitt, R. D. W. *J. Organomet. Chem.* **1973**, *47*, 189–193.
(354) Mukhedkar, V. A.; Kavathekar, B. J.; Mukhedkar, A. J. *J. Inorg. Nucl. Chem.* **1975**, *37*, 483–485.
(355) Ohashi, M.; Kambara, T.; Hatanaka, T.; Saijo, H.; Doi, R.; Ogoshi, S. *J. Am. Chem. Soc.* **2011**, *133*, 3256–3259.
(356) Forniés, J.; Green, M.; Laguna, A.; Murray, M.; Spencer, J. L.; Stone, F. G. A. *J. Chem. Soc., Dalton Trans.* **1977**, *16*, 1515–1518.
(357) Clark, H. C.; Tsang, W. S. *J. Am. Chem. Soc.* **1967**, *89*, 533–539.
(358) Empsall, H. D.; Green, M.; Shakshooki, S. K.; Stone, F. G. A. *J. Chem. Soc. A* **1971**, 3472–3476.
(359) Green, M.; Parker, G. J. *J. Chem. Soc., Dalton Trans.* **1973**, *20*, 2099–2103.
(360) Green, M.; Osborn, R. B. L.; Rest, A. J.; Stone, F. G. A. *J. Chem. Soc. A* **1968**, 2525–2530.
(361) Saijo, H.; Sakaguchi, H.; Ohashi, M.; Ogoshi, S. *Organometallics* **2014**, *33*, 3669–3672.
(362) Begtrup, M.; Larsen, P.; Edlund, U. *Acta Chem. Scand.* **1990**, *44*, 1050–1057.
(363) Yamaguchi, M.; Shiraishi, T.; Hirama, M. *J. Org. Chem.* **1996**, *61*, 3520–3530.
(364) Sun, X.; Zhou, D.-Y.; Qiu, L.; Liao, L.-S.; Yan, F. *J. Phys. Chem. C* **2011**, *115*, 2433–2438.
(365) Igau, A.; Grutzmacher, H.; Baceiredo, A.; Bertrand, G. *J. Am. Chem. Soc.* **1988**, *110*, 6463–6466.
(366) Dunsford, J. J.; Cavell, K. J.; Kariuki, B. M. *Organometallics* **2012**, *31*, 4118–4121.
(367) Lavallo, V.; Canac, Y.; DeHope, A.; Donnadieu, B.; Bertrand, G. *Angew. Chem. Int. Ed.* **2005**, *44*, 7236–7239.

(368) Arduengo III, A. J.; Calabrese, J. C.; Marshall, W. J.; Runyon, J. W.; Schiel, C.; Schinnen, C.; Tamm, M.; Uchiyama, Y. *Z. Anorg. Allg. Chem.* **2015**, *641*, 2190–2198.
(369) Arduengo III, A. J.; Davidson, F.; Dias, H. V. R.; Goerlich, J. R.; Khasnis, D.; Marshall, W. J.; Prakasha, T. K. *J. Am. Chem. Soc.* **1997**, *119*, 12742–12749.
(370) Braun, M.; Frank, W.; Reiss, G. J.; Ganter, C. *Organometallics* **2010**, *29*, 4418–4420.
(371) Arduengo III, A. J.; Goerlich, J. R.; Marshall, W. J. *Liebigs Ann.* **1997**, *1997*, 365–374.
(372) Leclerc, M. C.; Da Gama, J. G.; Gabidullin, B. M.; Baker, R. T. *J. Fluorine Chem.* **2017** doi: 10.1016/j.jfluchem.2017.05.012.
(373) Urbina-Blanco, C. A.; Bantreil, X.; Clavier, H.; Slawin, A. M. Z.; Nolan, S. P. *Beilstein J. Org. Chem.* **2010**, *6*, 1120–1126.
(374) Gusev, D. G. *Organometallics* **2009**, *28*, 6458–6461.
(375) Blake, G. A.; Moerdyk, J. P.; Bielawski, C. W. *Organometallics* **2012**, *31*, 3373–3378.
(376) Paul, U. S. D.; Sieck, C.; Haehnel, M.; Hammond, K.; Marder, T. B.; Radius, U. *Chem. Eur. J.* **2016**, *22*, 11005–11014.
(377) Hunadi, R. J.; Baum, K. *Synthesis* **1982**, *1982*, 454–454.
(378) Hans, M.; Lorkowski, J.; Demonceau, A.; Delaude, L. *Beilstein J. Org. Chem.* **2015**, *11*, 2318–2325.
(379) Miyazaki, Y.; Yamada, Y.; Nakao, Y.; Hiyama, T. *Chem. Lett.* **2012**, *41*, 298–300.
(380) Frisch, M. J.; Trucks, G. W.; Schlegel, H. B.; Scuseria, G. E.; Robb, M. A.; Cheeseman, J. R.; Scalmani, G.; Barone, V.; Mennucci, B.; Petersson, G. A.;Nakatsuji, H.; Caricato, M.; Li, X.; Hratchian, H. P.; Izmaylov, A. F.; Bloino, J.; Zheng, G.; Sonnenberg, J. L.; Hada, M.; Ehara, M.; Toyota, K.; Fukuda, R.; Hasegawa, J.; Ishida, M.; Nakajima, T.; Honda, Y.; Kitao, O.; Nakai, H.; Vreven, T.; J. A. Montgomery, J.; Peralta, J. E.; Ogliaro, F.; Bearpark, M.; Heyd, J. J.; Brothers, E.; Kudin, K. N.; Staroverov, V. N.; Kobayashi, R.; Normand, J.; Raghavachari, K.; Rendell, A.; Burant, J. C.; Iyengar, S. S.; Tomasi, J.; Cossi, M.; Rega, N.; Millam, J. M.; Klene, M.; Knox, J. E.; Cross, J. B.; Bakken, V.; Adamo, C.; Jaramillo, J.; Gomperts, R.; Stratmann, R. E.; Yazyev, O.; Austin, A. J.; Cammi, R.; Pomelli, C.; Ochterski, J. W.; Martin, R. L.; Morokuma, K.; Zakrzewski, V. G.; Voth, G. A.; Salvador, P.; Dannenberg, J. J.; Dapprich, S.; Daniels, A. D.; Farkas, Ö.; Foresman, J. B.; Ortiz, J. V.; Cioslowski, J.; Fox, D. J., *Gaussian 09, Revision A.2*, Gaussian, Inc: Wallingford, CT, 2009.
(381) Gorelsky, S. I.; Lever, A. B. P. *J. Organomet. Chem.* **2001**, *635*, 187–196.
(382) Godbout, N.; Salahub, D. R.; Andzelm, J.; Wimmer, E. *Can. J. Chem.* **1992**, *70*, 560–571.
(383) Balabanov, N. B.; Peterson, K. A. *J. Chem. Phys.* **2005**, *123*, 064107/1-064107/15.
(384) Balabanov, N. B.; Peterson, K. A. *J. Chem. Phys.* **2006**, *125*, 074110/1-064107/10.
(385) Becke, A. D. *Phys. Rev. A* **1988**, *38*, 3098–3100.
(386) Wolinski, K.; Hinton, J. F.; Pulay, P. *J. Am. Chem. Soc.* **1990**, *112*, 8251–8260.
(387) Cheeseman, J. R.; Trucks, G. W.; Keith, T. A.; Frisch, M. J. *J. Chem. Phys.* **1996**, *104*, 5497–5509.
(388) te Velde, G.; Bickelhaupt, F. M.; Baerends, E. J.; Fonseca Guerra, C.; van Gisbergen, S. J. A.; Snijders, J. G.; Ziegler, T. *J. Comput. Chem.* **2001**, *22*, 931–967.
(389) *ADF 2008.01, ADF Users Guide*, http://www.scm.com, SCM, Theoretical Chemistry, Vrije Universiteit: Amsterdam.
(390) Wolff, S. K.; Ziegler, T.; van Lenthe, E.; Baerends, E. J. *J. Chem. Phys.* **1999**, *110*, 7689–7698.
(391) van Lenthe, E.; Baerends, E. J.; Snijders, J. G. *J. Chem. Phys.* **1993**, *99*, 4597–4610.

(392) Kaupp, M.; Bühl, M.; Malkin, V. G., eds. In *Calculation of NMR and EPR Parameters: Theory and Applications*; John Wiley & Sons, Inc., 2004.
(393) Frisch, M. J.; Trucks, G. W.; Schlegel, H. B.; Scuseria, G. E.; Robb, M. A.; Cheeseman, J. R.; Montgomery, Jr., J. A.; Vreven, T.; Kudin, K. N.; Burant, J. C.; Millam, J. M.; Iyengar, S. S.; Tomasi, J.; Barone, V.; Mennucci, B.; Cossi, M.; Scalmani, G.; Rega, N.; Petersson, G. A.; Nakatsuji, H.; Hada, M.; Ehara, M.; Toyota, K.; Fukuda, R.; Hasegawa, J.; Ishida, M.; Nakajima, T.; Honda, Y.; Kitao, O.; Nakai, H.; Klene, M.; Li, X.; Knox, J. E.; Hratchian, H. P.; Cross, J. B.; Bakken, V.; Adamo, C.; Jaramillo, J.; Gomperts, R.; Stratmann, R. E.; Yazyev, O.; Austin, A. J.; Cammi, R.; Pomelli, C.; Ochterski, J. W.; Ayala, P. Y.; Morokuma, K.; Voth, G. A.; Salvador, P.; Dannenberg, J. J.; Zakrzewski, V. G.; Dapprich, S.; Daniels, A. D.; Strain, M. C.; Farkas, O.; Malick, D. K.; Rabuck, A. D.; Raghavachari, K.; Foresman, J. B.; Ortiz, J. V.; Cui, Q.; Baboul, A. G.; Clifford, S.; Cioslowski, J.; Stefanov, B. B.; Liu, G.; Liashenko, A.; Piskorz, P.; Komaromi, I.; Martin, R. L.; Fox, D. J.; Keith, T.; Al-Laham, M. A.; Peng, C. Y.; Nanayakkara, A.; Challacombe, M.; Gill, P. M. W.; Johnson, B.; Chen, W.; Wong, M. W.; Gonzalez, C.; and Pople, J. A.; Gaussian, Inc., Wallingford CT, 2004.
(394) Perdew, J. P.; Burke, K.; Ernzerhof, M. *Phys. Rev. Lett.* **1996**, *77*, 3865–3868.